Cell Derived Exosomes as a Co-delivery Nanocarrier for Anticancer Small Molecule Drug and Tumor Suppressor MicroRNA

THESIS

Submitted in partial fulfilment

of the requirements for the degree of

DOCTOR OF PHILOSOPHY

by

Moumita Basak

Under the Supervision of

Prof. Anupama Mittal

BIRLA INSTITUTE OF TECHNOLOGY & SCIENCE

PILANI-333031 (RAJASTHAN) INDIA

2024

BIRLA INSTITUTE OF TECHNOLOGY AND SCIENCE, PILANI

CERTIFICATE

This is to certify that the thesis titled **Cell Derived Exosomes as a Co-delivery Nanocarrier for Anticancer Small Molecule Drug and Tumor Suppressor microRNA** submitted by **Moumita Basak** ID No **2018PHXF0043P** for award of Ph.D. of the Institute embodies original work done by her under my supervision.

Signature of the Supervisor:

Name in capital letters: Prof. ANUPAMA MITTAL

Designation: Associate Professor

Date:

Table of Content

Acknowledgement

I would like to express my heartfelt gratitude and sincere thanks to my supervisor, **Prof. Anupama Mittal**, for her constant support, invaluable guidance, constructive criticism, and critical assistance that helped me to successfully complete the thesis. Despite having a very busy schedule, she made care to keep a close eye on the thesis work and encouraged me to follow my dreams without any limitations, which was blissful experience for me. She helped me to develop my research ideas, excitement, and professional abilities. She also helped me to become more resilient, self-assured, and optimistic, which I consider to be my most priceless Ph.D. accomplishment. It was truly an honor to work under her guidance and supervision.

.

I would like to personally thank and appreciate **Prof. Anil Jindal**, Associate Professor, and **Dr. Richa Srivastava**, Assistant Professor, who are members of the Doctoral Advisory Committee (DAC), for taking their priceless time to carefully review my thesis and enrich it with their invaluable comments and insights.

With great pleasure and reverence, I express my debt of profound gratitude to **Prof. Souvik Bhattacharyya**, Hon. Ex-Vice Chancellor, BITS, Pilani, **Prof. V. Ramagopal Rao,** Hon. Vice Chancellor, **Prof. Sudhir kumar Barai**, Director, BITS, Pilani, Pilani Campus, **Col. Soumyabrata Chakraborty**, Director, BITS, Pilani, Pilani Campus for providing the most congenial working atmosphere and excellent laboratory facilities.

I would also like to express my sincerest gratitude to **Prof. S. K. Verma**, Dean, Administration and **Prof. Jitendra Panwar**, former Associate Dean, AGSRD, and **Prof. Shamik Chakrabarty**, Associate Dean, AGSRD for their kind support for perusal of my Ph.D. seamless. My special thanks to **Dr. Shilpi Garg,** AGSRD for her continuous help regarding **INSPIRE** fellowship.

It gives me immense pleasure to express my sincere thanks to all the faculties and non-teaching staffs of Department of Pharmacy, BITS Pilani, Pilani campus. My heartfelt thanks and gratitude for **Prof. R. Mahesh** (Ex. Dean, Faculty affairs division), **Prof. Hemant R. Jadav** (former Head, Department of Pharmacy), **Prof. S. Murugesan, Prof. Anil B. Gaikwad** (Head, Department of

Pharmacy), **Prof. Atish T. Paul**, (Former Head, Department of Pharmacy), and **Prof. Rajdeep Chowdhury** (Head, Department of Biological Sciences, BITS Pilani, Pilani campus) for their constant support and encouragement. My special thanks to the faculty members **Prof. Rajiv Taliyan**, **Prof. Deepak Chitkara**, **Prof. Aniruddha Roy, Prof. Gautam Singhvi**, **Dr. M. M. Pandey**, **Dr. Sandeep Sundriyal**, and **Dr. Sushil K Yadav**, (Sr. Vet. In-charge, Central Animal Facility).

This work would have not been possible without the whole hearted encouragement, guidance, support and cooperation of my beloved BITSian colleagues, friends and well-wishers. With profound appreciation, I acknowledge to all the Research scholars in Department of Pharmacy and Biological Sciences**,** especially my seniors **Dr. Kishan S Italiya, Dr. K.V. Krishna, Dr. Pracheta Sengupta, Dr. Dhanashree Surve, Dr. Samrat Mazumdar, Dr. Deepak K Sahel, Dr. Swati Sharma, Dr. & Dr. Avilasha Srivastava**. I feel fortunate to meet a bunch of bright minds as labmates-cum-juniors of ***Nanomedicine and Gene delivery Lab***, including **Mr. N. Saibhargav**, **Mr. Subham A. Salunkhe**, **Mr. K. Sai Pradhyuth**, and **Mr. Pratik Shinde**. I would also like to thank **Ms. Mrunal Kulkarni**, a post-graduate thesis student, whose presence gave me a tremendous opportunity to explore my leadership potential, which I believe would be useful for my future endeavors. Also, I would like to thank **Mr. Imran Ansari**, **Mr. Prabhjeet Singh**, **Ms. Reena Jatyan**, **Ms. Sonia Guha**, **Mr. G. Giriprasad**, **Mr. Atharva Bhide**, **Ms. M. Kavya Shree**, **Ms. Paramita Saha**, **Mr. Rajesh Pradhan**, **Ms. Nikita Hinge**, **Mrs. Sonia Narwal**, **Ms. Hansa, Mr. Yash Katakia, Mr. Srikant Kirwale**, and, **Ms. Shobha Kumari** for being the valuable part of my BITS journey.

I am thankful to administrative staff, **Mr. Puran Singh Ji**, **Laxman Ji, Tarachand Ji, Abhishek Ji**, **Ram Suthar Ji**, **Naveen Ji**, **Mahender Ji**, **Suman Ji**, **Omprakash Ji, Sandeep Ji, Kuldeep Ji Virendra Ji**, **Mahipal Ji and Nitin Ji** for their continuous support.

I owe my family and friends the deepest love, respect, and thanks for their tolerance of my sweet and sour during BITS journey and for their understandings, support, and sacrifices. I feel delighted and contained for having marvelous parents; **Mr. Ratan Kumar Basak** & **Mrs. Alpana Basak** and the most supportive sibling, **Ms. Eisita Basak,** who has always stood behind me with her

precious courage, belief and love. I want to express my gratitude to **Ms. Swarnali Saha** and **Mrs. Sangeeta Banerjee** for being a vital part of my life and assisting me in clinging to my aspirations. The list got enriched with my three Musketeers, **Mr. Arihant Kumar Singh**, **Dr. Geetika**, and **Dr. Karan K. Banoth**, who deserve my congratulations and best wishes since without them, the voyage would have been much more difficult, confusing, and lacking. I am proud of them all and glad to be able to call them my people. Additionally, I feel fortunate to experience unconditional respect and support for **Mr. Arihant** in this hardest reality as a friend, philosopher, well-wisher, alongwith a lab-mate. I feel happy when I looked back and found both of us struggling together to achieve our wildest dreams. I feel fortunate for us, being the support system for each other, just like a fellow time-traveler. The happy and sad moments I shared with my family and my friends during the BITS journey will always be cherished and becomes irreplaceable memoir for rest of the life. A heartfelt thanks, gratitude and regards for all of them.

Last but not the least, I owe it all to **Almighty God** for providing me health, wisdom and strength to push me beyond my limits and fight back.

Let me conclude with the mighty quote by **Sir Rabindranath Tagore**,

"*Everything comes to us that belongs to us if we create the capacity to receive it*"

Moumita Basak

List of Abbreviations

%	Percentage
% DL	Percentage drug loading
% EE	Percentage entrapment efficiency
% RSD	Percentage relative standard deviation
% v/v	Percentage volume by volume
% w/v	Percentage weight by volume
λ_{max}	Wavelength of maximum absorbance
<	Less than
>	More than
≤	Less than or equal to
≥	More than or equal to
=	Equal to
~	Approximately equal to
±	Plus or minus
^{o} C	Degree centigrade
mg	Milligram
mg/mL	Milligram per milliliter
µg/mL	Microgram per milliliter
ng/mL	Nanogram per milliliter
g	Gram
ACN	Acetonitrile
AI	Absolute intensity
APS	Ammonium Persulphate
ANOVA	Analysis of variance
AUC	Area under curve
AUMC	Area under first moment curve
BCS	Biopharmaceutical classification system
BSA	Bovine serum albumin
BCA	Bicinchoninic acid
CAF	Central animal Facility
C3	Caspase 3
CC3	Cleaved Caspase 3
CC	Calibration curve
Cl	Clearance
CL	Cell Lysate
C_{max}	Maximum concentration
CPCSEA	Committee for the purpose of control and supervision of experiments on animals
CD	Cluster of differentiation
DLS	Dynamic light scattering
DMEM	Dulbecco's Modified Eagle Medium
DMSO	Dimethyl sulfoxide
DEPC	Diethylpyrocarbonate

DTX	Docetaxel
EDTA	Ethylene diamine tetra acetic acid
ELISA	Enzyme linked immunosorbent assay
EV	Extracellular Vesicle
EF	Exosomal fragment
Exo_{TC}	Ghost exosomes
Exo	Exosomes
Exo-DTX	DTX encapsulated exosomes
FAM	Fluorescein amidites
FBS	Fetal bovine serum
FESEM	Field emission scanning electron microscopy
h	Hour
HCl	Hydrochloric acid
HPLC	High performance liquid chromatography
HRP	Horseradish peroxidase
HSP 70	Heat shock protein 70
i.v.	Intravenous
IAEC	Institutional animal ethical committee
ICH	International council for harmonization
IFN-γ	Interferon gamma
IPA	Isopropyl alcohol
IS	Internal standard
ISEV	International society of extracellular vesicles
IU	International Unit
LOD	Limit of detection
LOQ	Limit of quantification
MRT	Mean residence time
hUCBMSC	Human umbilical cord blood derived mesenchymal stem cell
MTT	3-(4,5-dimethylthiazol-2-yl)-2,5 diphenyltetrazolium bromide
mV	Millivolt
MWCO	Molecular weight cut off
miRNA	microRNA
mAb	Monoclonal antibody
NPs	Nanoparticles
OD	Optical density
PAH	Polyallylamine hydrochloride
PAN	Polyamine nanoparticles
PAGE	Polyacrylamine gel electrophoresis
PB	Phosphate Buffer
PBS	Phosphate buffer saline
PDI	Polydispersity Index
PFA	Paraformaldehyde
PK	Pharmacokinetics

PI	Protease inhibitor
PTX	Paclitaxel
QC	Quality control
QbD	Quality by Design
R^2	Regression coefficient
RNAi	Interference RNA
rpm	Rotations per minute
RIPA	Radio immunoprecipitation assay
Rt	Retention time
RT	Room temperature
SD	Standard deviation
SDS	Sodium dodecyl sulphate
sec	Second
siRNA	Small interfering RNA
$t_{1/2}$	Half-life
T_{max}	Time to reach maximum concentration
TEMED	N,N,N′,N′ -Tetramethylethylenediamine
TNF-α	Tumour necrosis factor-α
TNBC	Triple negative breast cancer
TSG 101	Tumor susceptibility gene 101
UC	Ultracentrifuge
V_d	Apparent volume of distribution
WB	Western blot
ZP	Zeta potential

LIST OF TABLES

LIST OF FIGURES

ABSTRACT

'Cancer' is a dreadful immune-pathological condition that is characterized by tumorigenic responses, elicited by the infiltrated immune cells in the vicinity of uncontrollably proliferative cancer cells in the tumor microenvironment (TME). TME offers a conducive micro-environment that confers cancer cell survival by modulating the host immune defense. Recent advancement in exosomal research has shown exosomes, originating from both the immune cells as well as the cancer cells, have immense potential of inducing or suppressing cancer progression and its survival in TME. A recent proteomic study revealed the tumorigenic contribution of tumor-associated macrophages (TAM) derived exosomes wherein, the TAM model was established by conditioning murine macrophages (Ana-1 cells) with conditioned media (CM) of colon carcinoma cells (CT-26) for 48 h. As reported, TAM-derived exosomes upregulated the expression of tumorigenic proteins (MMP-8/12/13 and cathepsin) and attenuated the expression of pro-inflammatory proteins (Fcer1g, Polr3c and Prkdc. Among the 115 proteins found expressed in Ana-1 CM derived exosomes, 84 were uniquely expressed in TAM exosomes with a fold change >1.5. Hence, close contact between cancer and the immune cell in the TME seems to be the prerequisite criterion for predominance of tumorigenic responses. In a comparative macrophage expansion study, breast cancer cells (MDA-MB 231) derived exosomes were able to induce expansion and proliferation of the macrophage cells (RAW 264.7) enormously as indicated by almost 350-fold increment in IL-6 expression in comparison to the non-tumorigenic exosomes, isolated from MCF10a cells CM.[5] Further, another hallmark of tumor "ECM remodeling and invasion of cancer cells" was also proved in a study wherein, the macrophages (PMA treated THP-1) were treated with apoptotic breast cancer cells derived exosomes. This treatment particularly increased the release of pro-tumorigenic mediators like IL-6, MMP 2 and 9 and STAT3 in TME, which are well known to cause ECM degradation and invasion of the cancer cells.[6] On the contrary, interesting outcomes have been demonstrated by the macrophage derived exosomes as a nanocarrier of chemotherapeutics as well as immunomodulatory vesicles in their naive and polarized forms without any additional chemo or immunotherapeutic payload. Phorbol-12- myristate-13- acetate (PMA) induced differentiation of THP-1 cells (human monocyte cells) into macrophages, released A Disintegrin and metalloproteinase 15 (ADAM 15) expressing exosomes; DTX loading capacity of 8.86$\pm$1.97 ng DTX/μg exosomes and miRNA retention capacity of these 12.31$\pm$5.73%. This characteristic formulation was able to lower the IC_{50} by 2.36 folds' than the free DTX IC_{50}, and

showed prominent anti-migratory potential through *in vitro* wound healing, transwell assay and F-actin degradation assay in TNBC 4T1. Additionally, exosomes, irrespective of their diverse sources, have been well-reported as efficient nano-carriers for cancer therapeutics and their ability for targeted delivery due to their biogenic nature, ease of cellular uptake, and scope of functionalizing exosomes with biomolecules like peptides, aptamers, targeting ligands, etc. A new strategy has been explored to effectively deliver RAW 264.7 derived exosomes more efficiently in HeLa cells wherein, the exosomes were mixed with self-assembling ethylenediamine modified cholesteryl pullulan (cationic CHP, cCHP) to form a stable exosome-cCHP nanogel hybrid by both electrostatic and hydrophobic interactions. This cCHP nanogel has already been well reported for the delivery of the proteins and peptides.[7] The hybrid nanogel thus formed showed prompter uptake (only 30 min to get adsorbed onto the cell surface followed by an efficient uptake by 4h) in comparison to the free exosomes which is considered to be an advancement in the field of exosomes being explored as a drug delivery system and can eventually be further utilized for development of cancer vaccine.

In light of existing literature support, exosomes are well established and better nanocarrier system than the synthetic polymeric / lipidic / or hybrid nanocarriers. Liposomes, being the closest synthetic nanocarrier to exosomes have been tested and reported less efficient in terms of uptake, release and in-vivo efficiency as compared to exosomes. Yet, exosomes in drug delivery faces odds, including the low %yield, scale-up challenges, lack of unified drug entrapment capacity and %drug loading (DL) with inevitable biological implications carried by the naïve exosomes from different sources[12,13]. The biological implications of exosomes vary greatly depending on their source, such as whether these are isolated from immune cells, cancer cells, stem cells, or other cells. In fact, same cells under different experimental conditions have exhibited significant changes in their omics level, which must be addressed and emphasized before projecting them as the therapeutic nanocarrier candidate for any disease treatment. Exosomal integrity must also be ensured, as well as thorough characterization of exosomal formulations (with loading efficiency or entrapment efficiency) is important to facilitate dose escalation, toxicokinetics, pharmacokinetics, and in-vitro and in vivo correlation (IVIVC).

In the present work, we aimed to explore the strategic advancement of exosomal formulation development under the thesis entitled, "***Cell-derived exosomes as the nanocarrier for the co-***

delivery of the anticancer small therapeutic molecules and tumor suppressor miRNA". In this thesis, we have formulated and evaluated two different exosomal formulations, namely ***miR-125a-Exo-DTX*** and ***Exo(PAN$_{34a+DTX}$)*** to co-deliver TS-miRNA and docetaxel (DTX). In both the cases, exosomes have been utilized to co-load the small molecule drug and miRNA wherein, these exosomes have been obtained from two different sources and two different strategies been adopted for preparation of these formulations.

For the development of the first exosomal formulation ***miR-125a-Exo-DTX***, we isolated the **miR-125a exosomes** from the miR-125a transfected human umbilical cord blood derived mesenchymal stem cells (hUCBMSCs) and utilized them to load DTX by an optimized mild-sonication/incubation method to achieve miR-125a Exo-DTX with DTX loading capacity of 8.86±1.97 ng DTX/μg exosomes and miRNA retention capacity of 12.31±5.73%. This formulation was able to lower the IC_{50} by 2.36 folds' than the free DTX IC_{50} and showed prominent anti-migratory activity in *in vitro* wound healing, transwell assay and F-actin degradation study in TNBC 4T1 cells. In fact, miR-125a Exo-DTX treatment caused wound broadening upto 6.14±0.38% while treatment with free DTX and miR-125a exosomes alone caused 18.71±4.5% and 77.36±10.4% of wound closure respectively in 36 h. miR-125a Exo-DTX treatment further exhibited significantly reduced invasiveness of 4T1 cells (by 3.5±1.8%) along with prominent cytoskeletal degradation and nuclear deformation as compared to the miR-125a exosomes treated group. Another interesting observation during this work was the impact of miR-125a transfection on the proliferative indication of hUCBMSC derived exosomes wherein, miR-125a exosomes demonstrated lesser cell proliferation (% cell viability= 143±25.03) at a concentration of 25 μg/mL equivalent protein in comparison to the hUCBMSC exosomes (% cell viability= 183±24.1) attributed to the presence of transfected TS miR-125a in them. Despite of this, DTX encapsulation in both hUCBMSC exosomes and miR-125a exosomes demonstrated better cytotoxic effect than the free DTX, which clearly signified the potential role of exosomes as a nanocarrier for the cancer therapeutics.

For the development of the second exosomal formulation, ***Exo(PAN$_{34a+DTX}$)***, a novel exosomal membrane enclosed core/shell nanoformulation was fabricated for both DTX and miR-34a wherein, the exosomes isolated from the murine macrophage cells RAW 264.7 were used. This segment was broadly divided into three objectives, (1) isolation, characterization and biological

role of exosomes and exosomal fragments, (2) statistical optimization and development of the Exo-DTX formulation and, (3) development of exosomal fragment enclosed polyamine-phosphate nanocomplex (PAN) of DTX and miR-34a as a co-delivery nanocarrier and evaluation in TNBC 4T1 cells.

In our initial investigation, we found an immune-stimulant role of RAW 264.7 exosomes and exosomal fragments in a concentration dependent manner in 4T1 cells. Herein, we also explored the immune triggering role of RAW 264.7 cell derived exosomes and exosomal fragments with prominent antiproliferative and anti-migratory effect on 4T1 cells in a concentration dependent manner. Also, a correlation was established between exosomal integrity and external mechanical stress to guide us during the optimization of the process parameters for formulation development.

Further next, we methodologically optimized the process parameters to develop and validate the exosomal formulation (RAW Exo-DTX) by applying Quality by Design (QbD) approach to ensure an optimum loading capacity of the exosomes. The statistical optimization of exosomes (~200 µg protein) with Exo: DTX ratio 4:1 provided an encapsulation of 23.60±1.54 ng DTX/ µg exosomes. **Exo-DTX** (~189 nm, -11.03 mV) with 100 ng/ml DTX as payload exhibited ~5 folds' improvement in IC_{50} of DTX and distinct cytoskeletal deformation in TNBC 4T1 cells without any additional payload of TS miRNA. It also showed enormous Filamentous actin (F-actin) degradation and triggered apoptosis signifying effective anti-migratory impact of Exo-DTX with just 2.6±6.33% wound closure and 4.56±1.38% invasion. Western blot analysis confirmed that Exo-DTX downregulated migratory protein EGFR and β1-integrin but raised cleaved caspase 3/caspase 3 (CC3/C3) ratio and BAX/BCL-2 ratio by about 2-2.9 folds. As emphasized earlier, the naive RAW 264.7 exosomes also contributed positively towards the effect of Exo-DTX formulation by suppressing β1-integrin expression and increasing the CC3/C3 ratio in TNBC 4T1 cells. Additionally, significant improvement in PK parameters of Exo-DTX was observed in comparison to Taxotere, 6-folds' and 3.04-folds' improved $t_{1/2}$ and V_d, proving the translational value of Exo-DTX formulation.

As concluded from the work done till this stage, exosomes have the limited loading capacity and enormous biological possibilities. We further investigated RAW 264.7 exosomal fragments to layer the DTX and miR-34a co-loaded polymeric nanoparticles, Exo($P_{34a+DTX}$). This pH-dependent delivery system exhibited ~77.5% DTX encapsulating capacity and efficient complexation

capacity for 3.5μM miRNA which get dissembled at pH<6 found in TME along with undergoing a high cellular uptake attributed to the exosomal layering onto the nanoparticles. Additionally, layering of the PAN particles with exosomal fragments reduced the toxicity of free PAN particles attributed to their surface cationic charge (27.51±2.63% cell death) to 13.76±11.28 % in case of exosomal fragment layered PAN-DTX. It further induced ~48% cytotoxicity in the cells even at a 50% lesser dose of RAW Exo-DTX. Additionally, the inflammatory cytokine release study indicated that Exo($PAN_{34a+DTX}$) induced 4T1 to release significantly higher IFN-γ, (11.8±1.84 ng/Ml) in comparison to free DTX and PAN-DTX.

XXXXXXX

Chapter I

Introduction

1.1 Exosomes

1.1.1 The New-Age biogenic nanocarrier

International Society of Extracellular vesicles (**ISEV**) has defined Extracellular Vesicles (**EV**) as the "*particles naturally released from the cell that are delimited by a lipid bilayer and cannot replicate, i.e. do not contain a functional nucleus*" and broadly categorized them as "*Ectosome*, originating by external budding of plasma membrane" and "*Exosome*, originating by double-invagination and formation of intraluminal vesicles (ILVs)- plasma membrane fusion before exocytosis"[1,2]. *Ectosomes* are characterized by size in the range of 50 nm -1µm, and comprise of microvesicles, microparticles and large vesicles *while exosomes* are well known for their nanosized structure 40-160 nm. The minimal information for studies of extracellular vesicles (**MISEV**) is a major initiative to guide researches with experimental guidelines while working on the EV isolation, characterization and functional exploration. A biogenic particle could only be claimed as EV if, it has been isolated from the extracellular fluid (applicable for cellular and biological fluids), and could be characterized by at least two EV marker proteins including transmembrane proteins, cytosolic proteins, along with a non-EV co-isolated protein, and by electron microscopy and particle size analysis [2]. If the EV population is not found positive for specific markers, these are then termed as small extracellular vesicles (**sEVs**), having particle size <200nm. Depending upon source, size, content, and biological responses, exosomes are heterogeneous in nature and need *in-depth* exploration for their therapeutic application. While, size and content heterogeneity originates due to uneven invagination of the limiting membrane and the variable microenvironment, functional heterogeneity is attributed to the receptors or proteins present on either source or effector cells. While one set of exosomes can induce protective effect in a disorder, another set can initiate apoptotic milieu and may also act as a biomarker of the diseased state [3].

Recent trend in pharmaceutical industry has already witnessed a paradigm shift of interest towards biologicals as therapeutics, including exosomes as a promising therapeutic and nanocarrier system. In the year of 2020, several companies including Mantra Bio, Takeda, Carmine Therapeutics, ReNeuron, EVOX, Eli Lily and many more have invested heavily in the "exosome business" for RNA therapeutics, gene silencing, gene editing, RNAi delivery, and targeted therapy [4]. Additionally, literature supported the relevance and upsurge of exosome research in recent years,

where several phase 1 and phase 2 trials are being conducted especially on mesenchymal stem cell (MSC) derived exosomes for the treatment of Alzheimer's disease (NCT04388982), SARS-Cov2 associated Pneumonia (NCT04491240), Periodontitis (NCT04270006), and colon carcinoma (NCT01294072).[5]The World Intellectual Property Organization (WIPO) also received the highest patent applications in the domain of the exosome research, which is 49.8%, substantially greater than the patents filed in other domains (18%), this surely indicates the trend of the research, technology and business interest towards research in EV. From publication view-point, an exponential growth of documentation was observed since 2014, considering only universities and institutes from United states of America (USA) including NIH funded projects. The key concept that got highlighted in these publications is 'exosomes' in 'disease targeting', as 'biomarkers', in 'drug delivery' and many more[6].

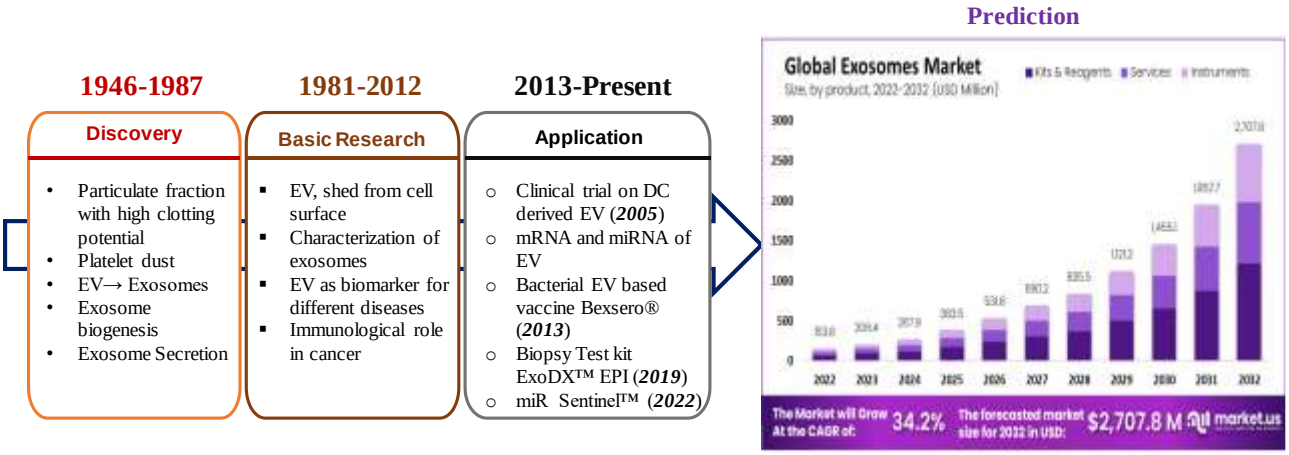

Figure 1.1. Past, present and future of Exosomes in global health market.

C***ourtesy:*** *Market news live, dated 30th Oct, 2023 (https://www.linkedin.com/pulse/exosomes-market-sales-top-usd-2707-billion-revenues-2033-aboli-more)*

1.1.2 Biogenesis, secretion and uptake

All eukaryotic and prokaryotic cells generate EV as a physiological phenomenon. Exosome biogenesis is carried out by both endosomal sorting complex required for transport (**ESCRT**) dependent and independent pathway[7–9]. In conventional ESCRT pathway, the cellular membrane forms a cup-shaped invagination which encloses the cell surface protein, and soluble extracellular matrix (ECM) components and forms the early-sorting endosome (ESE). These ESEs further mature into late sorting endosomes (LSEs). These endosomal limiting membranes of LSEs would

again invaginate to generate ILVs within multi-vesicular bodies (MVBs). These MVBs would either fuse with the lysosomal membrane and undergo degradation or with plasma membrane to expel out the ILVs as exosomes [10]. The whole process of exosomes release is monitored by ESCRT specific proteins[7]. The ESCRT machinery is composed of four complexes wherein, ESCRT-0 is responsible for cargo clustering in an ubiquitin dependent manner and ESCRT-I/II and its accessory protein tumor susceptibility gene 101 (TSG 101) promote bud formation [11]. While, ESCRT-III is irreplaceable for ILV formation, its accessory proteins, i.e., ALIX, and VPS4 are responsible for scission of the membrane and dissociation of the ESCRT-III complex before releasing the exosomes. Also, syndecan-syntenin interaction recruits ALIX, which plays an important role in collaboration with ESCRT-III to promote inward budding of ILVs[12]. In ESCRT-independent manner, MLVs are formed depending upon the presence of lipids, tetraspanin, and heat shock proteins. Ceramide, CD63, CD81 and HSP 70 are well reported for their important role in exosomes biogenesis but CD63 is indispensable in ESCRT-dependent pathway as well [13]. While, Ceramide helps in forming the inward curvature of the MLVs, HSP 70 acts as an aid to recruit transferrin (Tfr) receptors on exosomes [14,15]. Further, the intracellular trafficking of the MVBs and their fusion with the cellular membrane are monitored by Rab GTPase, In Rab GTPase protein family, depletion of Rab 27a showed altered MVBs generation, whereas inhibition of Rab11a/35/7 resulted in reduced sEV recovery. Further, Rab11a and 27a interaction has been proved to occur through Ca^{+2} dependent secretion of exosomes [16]. Apart from exosome biogenesis, Rab27a is responsible for soluble functional protein (matrix metalloproteinase, MMP-9) secretion as well. Apart from Rab protein family, SNARE (soluble *N*-ethylmaleimide-sensitive fusion attachment protein receptor) complexes are specifically required for MVB fusion with the plasma membrane before exocytosis. Syntaxin-1A, a neuron-specific SNARE involved in synaptic vesicle secretion from neuron has proved its role in exosome secretion [17]. Further, the secretion of EV require altered actin polymerization followed by contraction of the acto-myosin cytoskeleton. De-polymerization of cortical actin might also be necessary to allow docking of MVBs to the plasma membrane for subsequent exosome secretion[18]. Certain molecules associated with exosome docking, i.e., tetraspanins, integrins, proteoglycans and lectins are found helpful in guiding the exosomes to their receptor cells. The recruitment of TSPAN 8 (CD 8) in pancreatic adeno-carcinoma exosomes was reported to be beneficial for exosomal docking with additional support

of ECM proteins, i.e., vascular cell adhesion protein 1 (VCAM-1) and integrin α_4[19]. In fact, the presence of certain integrins in exosomal leaflets facilitate the exosomes to carry out some important biological functions, like metastasis. This was supported by an observation wherein, the exosomes secreted by breast cancer cells, 4175-LuT showed higher tendency to accumulate in the lung and liver. Later on, it was discovered that $\alpha_6\beta_1$ and $\alpha_6\beta_4$ integrin expressed in the exosomes enabled this organotropic feature leading to induction of metastasis[19]. The cellular uptake of the exosomes is reported through clathrin and caveolae dependent endocytosis, micropinocytosis, and phagocytic pathways[18–21]. An interesting observation has been made recently wherein, cellular uptake of exosomes was found to be dependent on the %purity of the exosomes as well as their size distribution[22]. This underscores the significance of understanding the biogenesis, secretion and uptake of the exosomes along with exploring exosomes for therapeutic application.

1.1.3. Structural features and natural payload of exosomes

Exosomal structure could be broadly categorized into, exosomal membrane and exosomal payload. Both these structural components are greatly influenced by their source cell and cellular micro-environment. Like other plasma membranes, exosome also have phospholipidic bilayer with varying amount of proteins present within the membrane leaflets. Various studies reveal that exosomes contain several parent cell or tissue derived surface bound, cytosolic proteins, some ribonucleoproteins and tissue-specific proteins that are unique to them. Recently, researchers have also been exploring the use of CAR-T cell-derived exosomes as a potential alternative to CAR-T cell therapy. These exosomes are thought to retain some of the therapeutic properties of the CAR-T cells, such as the ability to target and kill cancer cells, but are devoid of potential drawbacks of using live cells in therapy[23].

Exosomes are exact blueprint of their source cells which sometimes carries the RNA cargo (miRNA, mRNA, tRNA, and snRNA, etc) and nonfunctional DNA (mtDNA, dsDNA, and etc.) that are responsible for their paracrine signaling behaviour in many instances[24]. The exosomal bi-layer is composed of zwitter-ionic, anionic phospholipids and cholesterol which play a crucial role in enabling exosomes to regain their integrity after external mechanical stress. Among zwitter-ionic lipids, phosphatidylcholine (PC) and sphingomyelin (SM) accounted for 16.3% of total lipid and anionic lipids including phosphatidylserine (PS) represented 11.7% of total lipid in prostate

cancer cell PC-3 derived exosomes. Interestingly, PC-3 exosomes showed 43.5% cholesterol (CHOL) which is greater than the cholesterol found in the cellular membrane[25]. Zwitterionic lipids having both positive and a negative charge within the same molecule, allow them to form stable bilayers within aqueous microenvironment and provide leakage-proof barrier for its contents. Additionally, the higher % of CHOL in exosomal membrane helps to maintain liquid order phase (l_0) in lipid bilayer which reduces the fluidity of the membrane, and results in the maintenance of the exosomal integrity even after thermal or mechanical stress applied[26,27]. The protein cargo of exosomes is well explored and in many instances has been related to the exosomal biogenesis and secretion pathway as mentioned above. Recently, a reassessment study on exosomal cargo components has reported the absence of a well-known cargo component in the highly purified exosomal fragment, isolated by high resolution density gradient fractionation and direct immunoaffinity capture (DIC) technique. Although, exosomes thus prepared expressed CD 63, CD 81 and CD9, but were devoid of proteins namely, GAPDH, Ago 1-4, Annexin A2 and many more, that were reported previously to be co-isolated with the exosomes[28]. Hence, a direct link exists between the exact cargo composition and purity of exosomes and efficiency of the method employed to isolate exosomes from their parent cells.

1.2 Exosomes in Cancer Pathology

'Cancer' is a dreadful immune-pathological condition that is characterized by anti-inflammatory and tumorigenic responses that are elicited by the infiltrated immune cells in the vicinity of uncontrollably proliferative tumor in the tumor microenvironment (TME)[29]. TME offers a conducive micro-environment that confers cancer cell survival by modulating the host immune defense. TME contains immunocytes, cancer cells, stem cell and fibrobasts, and each of these cell types release their characteristic exosomes with functionally distinct cargos[30–34]. Recent proteomic and transcriptomic studies reported the involvement of these exosomes in different immune-pathological conditions[35–38].

1.2.1 Immune cell derived exosomes in cancer

A recent proteomic study revealed the tumorigenic contribution of tumor-associated macrophages (TAM) derived exosomes wherein, the TAM model was established by conditioning murine macrophages (Ana-1 cells) with conditioned media (CM) of colon carcinoma cells (CT-26) for 48

h. As reported, TAM-derived exosomes upregulated the expression of tumorigenic proteins (MMP-8/12/13, cathepsin) and attenuated the expression of pro-inflammatory proteins (Fcer1g, Polr3c, Prkdc, etc.). Distinctly, 84 out of 115 proteins were found uniquely expressed in TAM exosomes with a fold change >1.5 in comparison to only Ana-1 CM derived exosomes. Hence, a close contact between cancer and the immune cells in the TME seems to be the prerequisite criterion for predominance of tumorigenic responses.[39] Also, DC-derived exosomes have shown differential immunological cargo depending upon their microenvironment. DC when exposed to two opposite environments i.e. LPS treated immune-stimulatory (LPS_DC) and $VitD_3$ induced immune-inhibitory (Vit D_DC) conditions, exhibited alteration in both the nature and the content of RNAs present in the DC-derived exosomes. Under immune-stimulant conditions, the LPS_DC derived exosomes demonstrated upregulated expression of miR-155-5p, miR-9-5p, and miR-7a-5p, well known to induce DC maturation and monocyte activation whilst the immunosuppressive condition resulted in upregulated levels of miR-10a-5p and miR-223-5p, well known for repression of the pro-inflammatory cascade.[40] The abundance of T_{reg} ($CD4^+CD25^+FoxP3^+$) cells in TME is also responsible for apoptosis of the cytotoxic $CD8^+$ T-cells which further hinders programmed cell death of cancer cells.[41–43] The exosomes derived from T_{reg} cells exhibit anti-inflammatory nature and modulate the DC function. A seven-day long co-culture of T_{reg}-derived exosomes with bone marrow-derived DC (BM-DC) proved that the DC under influence of T_{reg}-derived exosomes can generate T_h cells lacking MHCII. The absence of MHCII on these T_h cells helps in immune evasion by the cancer cells by suppressing the $CD4^+$T cell-mediated responses.[44] Also, in an *in-vivo* study on the induced B16 melanoma model, T_{reg} exosomes were able to kill 37.5% of DC_{OVA} (ovalbumin-treated DC) immunized animals wherein, the DC_{OVA} immunization resulted in the reduction of tumor load with 100% of survival. Most interestingly, MDSC-derived exosomes were reported to cause the "acquired chemo-resistance" in a study wherein, the MDSC-derived exosomes containing miR-126a induced doxorubicin (DOX) chemo-resistance in 4T1 breast cancer *in vivo* model with lung metastasis.[45] All the above mentioned examples highlight how the immune cells contribute towards the modulation of the immunological responses, which are in turn responsible for achieving the cancer hallmarks. Concluding from the limited reports available, it can be stated that exosomes from either immune cells or cancer cells can modulate the host immune defense significantly to maintain the TME and absence of any one of these types of

exosomes could inhibit tumorigenesis. Also, it can be said that exosomes from immune cells and cancer cells in TME have a strongly regulated response, and easy acceptance as a paracrine mediator by both cells. This particular attribute of the exosomes (with or without external payload) could be clinically utilized to modulate the TME.

1.2.2 Cancer cell derived exosomes and cancer

Similar to the immune cells, cancer cells also send signaling cues through the exosomes expelled by them to modulate the immune cells present in their vicinity. These tumor-derived exosomes (TEX) contribute towards cancer hallmarks by interacting with other cellular components in TME. Among the typical hallmarks of cancer progression, "the immunocytes infiltration" is the stepping stone for cancer initiation. In a macrophage expansion study, breast cancer cells (MDA-MB 231) derived exosomes were able to induce expansion and proliferation of the macrophage cells (RAW 264.7) enormously as indicated by almost 350-fold increment in IL-6 expression in comparison to the non-tumorigenic exosomes, isolated from MCF10a cells CM.[46] Further, another hallmark "ECM remodeling and invasion of cancer cells" was also proved in a study wherein, the macrophages (PMA treated monocyte cell THP-1) were treated with apoptotic breast cancer cells derived exosomes. This treatment particularly increased the release of pro-tumorigenic mediators like IL-6, MMP 2 and 9, STAT3, etc. in TME, which are well known to cause ECM degradation and invasion of the cancer cells.[47] The predominant cancer hallmark "persistent hypoxia within TME"is also contributed by an interplay between immunocytes and tumor cells. This was proven by another study wherein, TAM-derived exosomes transferred HISLA (HIF-1α- stabilizing long non-coding RNA) to cancer cells and TEX transferred gp130 to macrophages in a bidirectional crosstalk. This resulted in the dominant expression of tumorigenic cytokines, IL-6/10, CXC4 and CCL2 thus revealing the reason behind the polarization of macrophages into M2 type TAM in this study.[48] In another study, The TAM-derived exosomes and their cargo miRNAs (miR-29a-3p and miR-21-5p) were found to upregulate the T_{reg} and Th17 (anergic) T-cell population, the prevalence of which can be related to another cancer hallmark, i.e. the "evasion of immune responses" by the cancer cells[49].

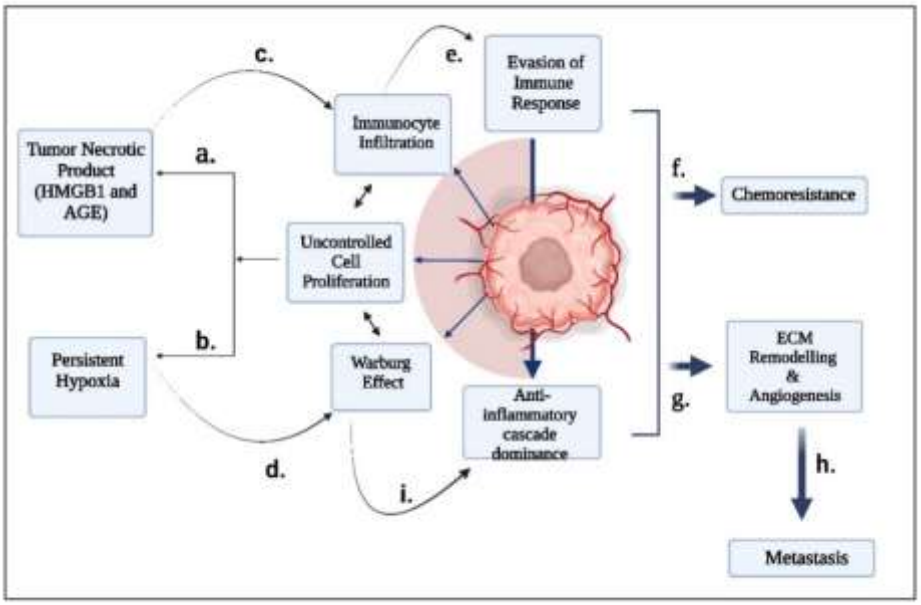

Figure 1.2. Interaction between immune cells and cancer cells essential for the survival of the cancer in the vicinity of host immune microenvironment. Immune cell manipulation by cancer cells plays a vital role in progression of cancer and attaining its hallmarks. (*Reprinted (**Figure 1**) with permission from doi.org/10.1021/acsbiomaterials.2c00893. Copyright 2023 American Chemical Society)*

1.2.3 Stem cell derived exosomes in cancer

Currently the field of MSC exosomes is undergoing extensive research to explore their application in cancer therapeutics, especially the regulatory role of MSC derived exosomes. In one study, bone marrow (BM) MSC derived exosomes, enriched with miR-100 showed tumor suppression by down regulating VEGFR-I expression via HIF-I/mTOR mediated pathway in breast cancer cells, MCF-7 and MDA MB-231, at the dose of 80 µg/mL. Another study however reported BM MSC exosomes (200 µg/mL) inducing angiogenesis by upregulating VEGF in both *in vivo* models of gastric carcinoma (SGC-7901) and colon carcinoma (SW-480)[50,51]. These observations highlight the conflicting role of MSC exosomes in cancer pathophysiology inspite of being derived from the same source. Among the different sources explored for procuring MSCs, human umbilical cord blood (hUCB) derived MSCs (hUCBMSC) have been found functionally anti-inflammatory and anti-tumorigenic in different cancers. They have already been reported to suppress cancer stemness in breast cancer, tumorigenesis in Kaposi sarcoma, and also induce cytotoxicity in U87 glioma cells[52–54]. Several reports have claimed that human umbilical cord MSC derived exosomes are anti-tumorigenic due to presence of miR-375, miR-451a, miR-181 etc., which suppressed the

expression of enabled homolog (ENAH) in squamous cell carcinoma, downregulated a Disintegrin and metalloprotease 10 (ADAM 10) mediated epithelial-mesenchymal transition (EMT) in hepatocellular carcinoma and retarded lysine-specific demethylase 5C (KDM5C) in nasopharyngeal carcinoma [55–57]. Recently, it has been reported that the hUCBMSCs derived exosomes inherently carry miR-503-3p which significantly down regulates the mesoderm specific transcript (MEST) and suppresses the cellular growth in endometrial carcinoma[58].

TME also contain circulating tumor cells (CTC) and cancer stem cells (CSCs), which actually contribute towards in the chemotherapeutic resistance, immune evasion and metastatic aggressiveness. Specifically, circulating tumor cells (CTCs) seem to separate from the primary tumor and circulate throughout the body as single cells or clusters whereas, CSCs are a specialized population of cancer cells inside tumors with the ability of self-renewal, maturation, and tumorigenesis. The CSCs are of massive concern as they can induce the metastasis by metamorphic change from epithelial to mesenchymal phenotype, and remain insensitive towards the existing therapies[59]. The interaction of CSC with their microenvironment (including immune cells, cancer cells and fibroblasts) is also carried through both exosome dependent and independent manner. While M2 macrophages derived exosomes, carrying miR-27a-3p potentiate the stemness marker SOX-2 and Oct-4 expression significantly in hepatic carcinoma cell SMMC-7721, cancer associated fibroblasts (CAFs) enhance renal cancer stemness in RCC cells with exosomal miR-181d-5p[34,60,61]. Also, cancer derived exosomes carrying specific protein, S100A9 were revealed to contribute to the stemness of CSC, required for the survival of cancer.[62] Alongside, CSC derived exosomes are reported to enhance the colon cancer aggressiveness by exosomal transfer of long intergenic non-coding RNA (LINC 01315) [63].

Hence, it can be concluded that the survival of cancer cells depends on a highly decorated mutual interplay between the cellular components of TME wherein exosomes act as the mediator between all the cells.

1.3 Exosomes as Nanocarrier for cancer therapy: Strategies employed

Exosomes are considered as an efficient biogenic nanocarrier with specialized cell-cell communication ability which can be utilized for efficient and targeted cellular uptake of the

payload. Additionally, the inherited biological properties demonstrated by the exosomes isolated from different source cells also become beneficial for desired therapeutic effect. Alongwith, the membrane structure of exosomes could also be semi-synthetically functionalized for targeted therapy [64]. It is invariably safe, devoid of allogenic rejections, non-immunogenic, and biocompatible with superior cellular uptake efficiency. Overall, exosomes combine benefits of both synthetic nanocarrier and cell-mediated drug delivery systems while bypassing their limitations.

1.3.1. Active Loading

Active loading of the therapeutics in the exosomes is a strategy wherein, the cells are either primed with the desired payload or transfected by viral and non-viral vectors carrying genetic material prior to the isolation of the characteristic exosomes. It is also known as the **pre-loading before exosome formation** [65].

1.3.1.1. Cell priming before exosome biogenesis

In the year of 2014, cell priming before isolating the exosomes with desired payload was reported by Pessina *et al*. Mesenchymal stromal cells, SR4987 (10×10^6) were exposed to 2000 ng/ml paclitaxel (PTX) for 24 h and CM was collected for isolation of the exosomes. This PTX loaded exosomal formulation (2.54 ng/mL PTX) demonstrated 50% tumor growth inhibition [66]. Almost similar observation was also reported in 2012 wherein, hepatic carcinoma cells (HepG2, 3×10^5 cells) pretreated with different anticancer drugs, i.e., PTX, carboplatin, irinotecan and etoposide generated HSP bearing exosomes and activated NK mediated immunogenicity against hepatic carcinoma[67].

1.3.1.2 Viral and non-viral vector mediated transfection of cells before exosome biogenesis

For the treatment of Duchenne muscular dystrophy (DMD), a dreadful disease caused by dystropin loss and over-activation of the mycostatin, murine mycostatin propeptide inhibitory domain was cloned in lentivirus expressing vector pCDH-CMV-puro, digested with *Xho 1* and *EcoR1*. These viral vectors were further utilized to infect NIH3T3 fibroblasts for 12h at every 24 h interval for 2 weeks. The exosomes produced from NIH3T3 were utilized for the treatment of DMD animal model and were found to accelerate muscle regeneration and growth, resulting in significantly increased muscle mass by inhibiting the mycostatin[68].

Under non-viral vector mediated transfection of the genetic material, we come across a study wherein, hyaluronic acid-poly(ethyleneimine) and hyaluronic acid-poly (ethylene glycol) nanoparticles were prepared for the plasmid DNA encoding for wild type p53 (wt-p53) and miR-125b respectively with 93.46% and 95.23% entrapment efficiency. Later on, theses nanoparticles were utilized to transfect the lung cancer cells, SK-LU1 and the isolated exosomes from the CM of these transfected cells showed significant repolarization effect in the M2 macrophages[69].

These studies exemplify the versatility of the exosomes for the delivery of genetic materials by modulating the source cell itself. Yet, the mechanism of drug encapsulation during exosome biogenesis needs deeper investigation. Additionally, parameters like cellular growth, impact of the treatment on cell survival and experimental conditions would also drastically impact the yield of the exosomes and its loading efficiency dictating the cost effectiveness of the therapy.

1.3.2. Passive Loading

In this process, the exosomes are isolated from the biological fluids, purified and quantified before being utilized to entrap the payload by means of external stimuli or by density gradient across the exosomal membrane. The strategies explored so far are categorized into ***co-incubation***, ***sonication***, ***sonication and incubation***, ***electroporation***, ***extrusion***, ***freeze-thaw*** *and,* ***permeabilization***.

Milk derived exosomes have been reported to load PTX by simple incubation method to formulate ExoPTX with 7.9±1.0% practical loading capacity to treat A549 xenograft lung tumor orally wherein, ExoPTX (~ 4 mg/kg body weight PTX and exosomes 60 mg/kg) showed nearly 60% tumor growth inhibition compared to vehicle treatment[70]. The drawback of this method was low loading efficiency and its applicability to small hydrophobic molecules only. The exosomal membrane integrity limits the passage of moderate to high molecular weight molecules through its bi-layer even if concentration gradient is maintained. Also the overall ionization state of the molecule at experimental pH plays an important role as exosomes themselves are negatively charged [71].

In comparison to the incubation, mild sonication overcomes the issue providing significantly higher loading capacity (LC) as reported by Kim *et al*. Their study on RAW 264.7 cell derived

exosomes reported PTX loading capacity 20 times higher by mild sonication and 5.4 times more by electroporation than incubation. Although an additional incubation for 1h post sonication was recommended for the attainment of exosomal integrity as well[72]. Another study, reported pancreatic cancer cell, PANC-1 derived exosomes as a nanocarrier for the hydrophilic drug gemcitabine wherein LC was 11.68 ± 3.6% by sonication and 2.79 ± 0.72% by incubation[73]. Comparatively, gemcitabine loading capacity was found 50% more than that of the hydrophobic PTX as mentioned before. Yet, this method also faces several odds, including the exosomal membrane integrity, exosomal agglomeration, effect of the process parameters on the LC, and influence of the experimental variables which would eventually result in non-uniformity in LC from lab to lab. Considering the fact that exosomes are preformed vesicles with a defined volume to accommodate the payload, the optimum exosomal LC of the API needs to be identified which could be monitored by the process parameters that can alter the exosomal integrity and entrapment efficiency [5]. The applicability of all the methods mentioned above could be compared by a study reported by Batrakova *et.al*. In this study, RAW 264.7 cell derived exosomes were explored to encapsulate a macromolecule (an enzyme), named catalase to treat Parkinson's disease. For this, all five techniques (incubation, sonication, freeze thaw, extrusion and saponin mediated permeabilization) were screened to formulate catalase loaded exosomes (ExoCAT). The maximum and equivalent loading capacity was reported with sonication and extrusion, whereas freeze/thaw technique was able to encapsulate catalase moderately and negligible LC was obtained by only incubation method[74]. While, electroporation was applied to incorporate siRNA, extrusion was able to load porphyrin with 28%LC in the exosomes [75,76]. The major drawback of the usage of electroporation for siRNA loading is the metal ions contributed by the electrodes, that may precipitate siRNA by complexation and, extrusion involves extensive mechanical stress that could alter the physicochemical characteristics of exosomes and might adversely affect its inherent therapeutic activity[65].

1.3.3 Exosome-liposome hybrid

Liposomes are synthetic congener of the exosomes and well reported for their biocompatibility, versatility for carrying both hydrophilic and hydrophobic molecules, and passive targeting. Surface decoration or functionalization with the targeting molecules further help the liposomes to target the tumor actively. The major disadvantage of the liposomes is limited loading capacity, leaching,

stability issue and immune activation. Considering the immunogenic aspects, exosomes can evade the immune system and exhibit high cellular uptake efficiency but cannot accommodate large therapeutic molecules like CRISPR/CAS9 expression vector or plasmids[77,78]. Hence, the hybrid of exosomes and liposomes has been proposed as a single nanoparticle system. In a recent study, the exosome-liposome hybrid system was prepared by simple incubation technique, and the encapsulated CRISPR/CAS9 was successfully delivered in MSC cells to modulate the target gene (hCTNNB1) expression[78]. Recently, a CD47 expressing exosome-thermosensitive liposome (gETL) has been reported to deliver DTX and GM-CSF as the part of hyperthermic intraperitoneal chemotherapy in metastatic peritoneal carcinoma (mPC). Herein, the hybrid nanoparticle was prepared by sequential extrusion of the exosomes and liposomes. The loading of GM-CSF and DTX in hybrid system was reported as 7.2 pg/μg and 4.3% respectively. Mechanistically, treatment with co-loaded NPs induced macrophage polarization, enhanced macrophage-mediated tumor cell phagocytosis, and induced cellular apoptosis[79]. This indicates a wide scope of modulating the application of exosomes in the development and delivery of therapeutics along with modulating the TME.

1.3.4 Exosome mimetic nanovesicles (NV)

Exosome mimetic nanovesicles are the bio-inspired cell derived nanovesicles (CDN) to combine the characteristics of the cells and nanocarrier for targeted delivery of the chemotherapeutic agents, by subjecting the cells to serial extrusion through filters with diminishing pore sizes after the cells have been loaded with chemotherapeutic agents. In one such study, NV were prepared by serial extrusion of the cell suspension (U937 cells) to obtain the NV of a specific size range and then these were isolated by density gradient centrifugation which ultimately increased the exosome yield by 100 folds as compared to the conventional differential centrifugation method without altering the surface integrity. The characterization parameters studied using dynamic light scattering (DLS), cryo-TEM, and western blot of exosomal marker proteins proved that the NVs were identical to the exosomes secreted by U937 cells [80].

Recently, macrophage derived NVs have been projected as a promising anticancer immunotherapy wherein, these repolarized the TME into a tumor hostile environment in a unique way. They converted the M1- macrophage rich TME into M2-macrophage dominant one. Macrophages are

heterogeneous, both the subtypes, M1 and M2 indistinctly co-exist under the physiological conditions, which can polarize and proliferate into either of two types depending on their exposure to different immunological conditions. When exposed to a specific antigen or LPS or cytokines, they follow the classical activation pathway to polarize into the M1 type while the M2 type predominantly proliferates upon exposure to glucocorticoid or IL-10 mediated immune-suppressant conditions[81]. We came across just a single study that explored exosome-like nanovesicles (M1NV; obtained by serial extrusion of M1 macrophages) to target the TME along with tumor (using an antibody for Programmed death-ligand 1; aPDL1). The M1NV inherited the lymphocyte function-associated antigen 1 (LFA-1; adhesion molecule) from their source which enabled their localization into TME (highly rich in LFA-1 binding protein, ICAM-1) resulting in the conversion of the predominant M2 of TME into M1 type. The characteristic cargo of NVs was found to be upregulated miRNAs of M1 subtype i.e. miR-155, miR-125 and miR-132, well known to polarize the macrophages to M1 type [82]. These findings bring forth a tremendous possibility of M1 macrophage-derived exosomes as well as the M1NV to be explored for targeting the tumor by modulating the TME.

1.3.5 Surface functionalization of Exosomes

Surface functionalization (by both covalent and non-covalent modification) is one of strategies to potentiate the specificity of exosomes towards the target tissue [83]. The significance of surface functionalization of exosomes was exemplified in a study wherein, PTX loaded macrophage-derived exosomes were surface-functionalized with aminoethylanisamide-polyethylene glycol (AA-PEG). AA-PEG specifically targets Sigma factor, abundantly expressed in lung cancer. The functionalized exosomes resulted in almost complete eradication of all the pulmonary metastatic nodules in comparison to the non-functionalized formulation; this was attributed to the targeting efficiency of the AA-PEG and also the enhanced circulation time due to PEGylation[84]. Likewise, the RGE peptide has been explored as a targeting ligand for the glioma specific receptor Neurophilin 1(NRP1). RAW 264.7 derived exosomes were functionalized with RGE peptide and co-loaded with curcumin (Cur) and superparamagnetic iron oxide nanoparticles (SPION) to cross the blood-brain barrier (BBB) and target the NRP1 expressing glioma cells. Comparative cytotoxicity study of RGE-Exo-SPION, RGE-Exo-Cur, and RGE-Exo-SPION/Cur in the NRP1 expressing glioma cells U251, revealed that maximum cytotoxicity was rendered by RGE-Exo-

SPION/Cur among all the groups wherein, SPION and Cur produced synergistic effect. The loading of SPION in the exosomes reduced the toxicity of free SPION and the RGE conjugation enabled specific targeting of NRP1, thus resulting in site-specific delivery to glioma[85]. A new strategy has been explored to effectively deliver RAW 264.7 derived exosomes more efficiently in HeLa cells wherein, the exosomes were mixed with self-assembling ethylenediamine modified cholesteryl pullulan (cationic CHP, cCHP) to form a stable exosome-cCHP nanogel hybrid by both electrostatic and hydrophobic interactions. This cCHP nanogel has already been well reported for the delivery of the proteins and peptides[86]. The hybrid nanogel thus formed showed prompter uptake (only 30 min to get adsorbed on the cell surface followed by an efficient uptake within 4h) in comparison to the free exosomes, especially through the caveolae-mediated and macropinocytic pathway as depicted by the internalization assay in presence of endocytosis inhibitors.

1.3.6 Exosomal layering of synthetic nanoparticles

'Camouflaging' synthetic nanovesicles with exosomal bi-layer could be considered as the one of the trending opportunistic strategies that enable the nanoparticles to overcome immune recognition, and undergo prolonged circulation, and homotyping targeting [87]. It is basically a core-shell delivery system wherein, the nanoparticle of the therapeutic would act as the '**core**' and the exosomal membrane, as the '**shell**' of the system. Through this method, the limitation associated with the use of the individual components could be overcome, i.e., the low entrapment of the therapeutics by exosomes and the 'opsonization and serum protein binding' issues with the synthetic nanoparticles[88]. Few such examples are discussed herein. In an interesting study, the use 4T1 derived exosomal layering of cationic Bovine serum albumin (cBSA) nanoparticle carrying siS100A4 (siRNA for metastatic marker protein S100A4) for the treatment of the breast cancer related lung metastasis has been reported. Within 24h, CBSA/siRNA@exosomes were able to distribute in the lungs 2.9-fold more than the CBSA/siRNA@liposome as per the post-operative biodistribution assay in *in vivo* disease model[89]. In another study, the homotypic targeting activity of exosomal membrane enclosed DiR-PLGA nanoparticles was compared with the cancer cell membrane enclosed DiR-labeled PLGA nanoparticles in A549 induced murine lung cancer model. The pharmacokinetic study concluded that the A549 derived exosomal membrane enclosed PLGA nanoparticles (EM-PLGA NP) exhibited greater circulation half-life ($t_{0.5}$= 13.5h) in comparison to the A549 cancer cell membrane enclosed PLGA nanoparticles (CCM-PLGA NP) with a half-life

of 7h. Additionally, the corresponding DiR labeled poly(lactic-co-glycolic acid) or PLGA nanoparticles showed a variable distribution in the A549 tumor. It was observed that the fluorescence intensity of EM-PLGA NP in the A549 tumor was more prominent than the MDA MB-231 tumor and got diminished over extended period of time[90]. This clearly indicated the superiority of the homotyping targeting capacity of exosomes over the cell membrane of same origin.

1.4 Scope of exosomes for co-delivery of miRNA and small molecules

Exosomes have been reported for co-delivery of miRNA and small anticancer therapeutic molecules. Being hydrophilic and anionic in nature, miRNAs are not easily entrapped in the exosomes, which has been overcome by chemically modifying the miRNA to provide hydrophobicity to the molecule. Firstly, THP-1 cells were treated with Phorbol myristate-12 accetate 13 (PMA) to enhance the A disintegrin and metalloproteinase 15 (A15) overexpressing exosomes (A15-Exo) to confer the tumor targeting ability towards the breast cancer cells. miR-159 was hydrophobically modified with cholesterol (Chol) to form Chol-miR159 which enhanced the miRNA loading into exosomes by almost 5 folds in comparison to unmodified miR-159. Doxorubicin was co-delivered with Chol-miR159 using A-15 exosomes; wherein it was entrapped in the exosomes by incubation technique with maximum loading of ~160 ng DOX/μg exosomes. *In vitro* apoptosis assay showed 28.26 % and 47.15% of MDA MB-231 cellular apoptosis in Chol-miR159 and A15-Exo/Chol-miR159 treated groups[91]. In another study, HEK293T cells were stably transduced with lentiviral vector encoding the Her2 binding antibody, LAMP-2 and GFP and utilized to isolated exosomes (THLG-Exo) with homing property. These exosomes were electroporated with 5-fluorouracil (5-FU) and then incubated with miR-21 inhibitor (miR-21i) to specifically target the co-delivery system to the 5-FU resistant colorectal carcinoma cells (HCT-$116^{5\text{-FR}}$) [92]. However, 5-FU and miR-21i LC into exosomes was only 3.1% and 0.5% respectively. Evidently, both the studies exhibited low loading efficiency of miRNA and the small therapeutic molecules in exosomes which needs to be addressed further. Yet these systems produced significant therapeutic efficacy in both cases which might be attributed to the targeting property attained by the modified exosomes along with the co-delivery of small molecule and miRNA.

Although, exosome mediated co-delivery of miRNA and small therapeutic molecules is not much explored, but well reported with synthetic nanoparticles. In a recent study, an amphiphilic tri-block co-polymer, poly (ethylene glycol)-*b*-poly-L-lysine-*b*-poly-L-leucine (PEG-PLL-PLLeu) was utilized to entrap DTX in the micelles with +38.8 ± 2.1 mV surface charge, onto which the siRNA-BCL-2 has been adsorbed to prepare the micelleplex with zeta-potential value of +20.48±1.8 mV[93]. This study indicated that small molecules and siRNAs can be co-delivered with smart designing of the co-delivery system utilizing non-covalent interaction, i.e., hydrophobic interaction and electrostatic interaction as in the case.

Tandem self-assembly delivery system: Leveraging non-covalent interaction

'Tandem self-assembly' or 'Polyamine –salt aggregates' (PSA) are a relatively newer concept of core-shell drug delivery system wherein, the core is composed of ionically cross-linked nanoparticles of cationic polyamine with a multivalent anionic salt, and the PSA thus formed acts as a template for the negatively charged shell material to form the capsular structure. This technique has several advantages namely; a preformed template is not required, rather the template is formed *in situ* by ionic interaction and the size of the template can be fine-tuned by changing process parameters. Additionally, encapsulation is performed by merely adding the cargo before capping the PSAs with the shell-forming material, and the procedure involves simple mixing and mild processing conditions[94,95]. In the year of 2010, Wong et al, reported phosphate driven Polyallylamine hydrochloride (PAH, M_W: 70,000 Da) self-assembled aggregates, encapsulating 56% of indocyanin green (ICG) after aging at 4˚C for 2h. As a negatively charged dye molecule, ICG interacted with the polymer/salt aggregates electrostatically, and stabilized the PAH/phosphate aggregate particulate structure through strong hydrophobic interactions with the PAH backbone as well. These particles were then brought in contact with the negatively charged anti-EGFR antibody to form the shell around the aggregates. The shell formation resulted from charged interactions between the carboxyl groups of anti-EGFR molecule and amine groups of the PAH chains of the uncoated nanocapsules[96]. Recently, Moya lab working on this self-assembled system for delivery of siRNA, reported the Phosphate driven polyamine nanoparticles (PAN) for efficient delivery of the siRNA, along with oleic acid (OA) and PEGylated polyamine, resulting in greater efficacy of the siRNA for cancer therapy[97–100]. However, this system has never been explored for co-delivery of miRNA and small molecules, and exosomal membrane has not been

layered onto these particles as the shell material. Considering this, exosome with its bi-layer structure has a great scope to be considered for exploration of this novel strategy.

1.5 Cargo components: DTX and tumor suppressor (TS) microRNA

1.5.1. Docetaxel Trihydrate (DTX): an anti-cancer small molecule

DTX (M_W: 819.6 Da) is an anti-neoplastic agent, well known for its high hydrophobicity and low solubility (log P-4.2 and pK_a-10.8, BCS IV category). It causes excessive polymerization of microtubule, eventually resulting in dynamic instability and consequently inducing apoptosis. It is well reported that DTX has a biphasic effect especially on TNBC; at considerably lower concentration<4 Nm, it induces aberrant mitosis followed by hypodiploidy while at higher concentration >100 nM, it induces mitotic arrest at G_2/M phase of cell cycle and mitotic slippage, resulting in multi-nucleation and nuclear degradation [101,102]. Apart from inducing apoptosis in aggressive breast cancer cells, DTX is also known to distort the cytoskeletal organization which is otherwise maintained by close co-ordination between microtubule and F-actin [103,104]. Also, the marketed formulation of DTX, i.e., Taxotere® has shown biphasic plasma half-life of 7 min and 1.2 h in both normal and tumor bearing mice [105].

1.5.2. microRNA (miRNA): Mode of action and importance in cancer treatment

miRNA is a single stranded non-coding RNA (with 22 nt) molecule that targets mRNA to modulate the protein expression. Most miRNAs are transcribed from DNA to form primary miRNAs (pri-miRNAs) which are further converted to precursor miRNA. The pre-miRNA is exported to the cytoplasm in an Exportin5/RanGTP-dependent manner and processed to produce the mature miRNA duplex. Argonaute (AGO) family of proteins aid these duplexes to form a miRNA-induced silencing complex (miRISC) which binds to target mRNAs to induce translational modification[106].

Tumor suppressor miR-125a

Among RNAi(s), miRNAs plays a significant role in regulating the gene expression by modulating the target mRNAs either as oncomiRs, stimulating oncogenesis or TS miRNAs, suppressing the tumor [107]. miR-125a is a well-known TS miRNA which specifically targets the HER2/ ErbB2 (EGFR subfamily) mediated signaling pathway that contributes to the migratory nature of aggressive BC cells [108]. Basal level of the miR-125a transcript has been reported to be under-expressed in human BC tissues by 1.75-fold in comparison to the normal breast epithelial cells.

miR-125a-3p has been shown to increase the expression of the ErbB2 which eventually reduces the invasiveness of the cancer cells [109]. Also, miR-125a-5p was reported to suppress BC susceptibility gene 1–associated protein 1 (BAP1) resulting in induction of cancer cell apoptosis [110]. Hence, miR-125a was chosen as one of the therapeutic molecules to be co-loaded with DTX in exosomes in this study.

Tumor suppressor miR-34a

miR-34a is another widely explored tumor suppressor miRNA, which functions through apoptotic TP53 integration pathway[111]. In general, miR-34a level is found downregulated in triple negative breast cancer (TNBC) in comparison to the mesenchymal BC cells and $Her2^+$ cancer cells. In fact, MDA-MB-231 transfected with synthetic miR-34a mimics induced 25.7 ± 4.2 % apoptotic cell death and around 12.5% late phase apoptosis in comparison to MDA MB-435 with 22.5 ± 3.4 % apoptosis including only 6.1% cells in late phase apoptosis cycle[112]. miR-34a has also been well reported to regulate cell proliferation through the suppression of apoptosis related proteins, such as Bcl-2, SIRT-1, E2F3, CDK4 and CDK6. Also, miR-34a directly binds to the 3'-untranslated region of eEF2K and FOXM1 mRNAs and suppresses their expression, leading to inhibition of TNBC proliferation, motility, and invasion[113]. The phase I clinical trial of liposomal formulation of miR-34a mimic (**MRX34**) with dexamethasone premedication in advanced solid tumor patients demonstrated manageable toxicity with some clinical activity. Pharmacodynamics data demonstrated dose dependent modulation of miR34a target genes in the patients and miR34a localization in the tumor as well[114].

1.6 Gaps in Existing Research

Current research in the field of 'Exosomes' is mainly focused upon its clinical application in various diseases either as a potent immunotherapeutic agent or biogenic nanocarrier of the therapeutics[6,115]. It has been observed that most of the research studies are exploring the advantages of exosomes in comparison to the synthetic nanocarriers or the marketed products, while neglecting the limitations associated with exosomes or challenges involved in working with exosomes including optimization and QbD driven formulation development and scale-up. Exosomes have mainly been restricted to the lab scale, but these also need to be projected upto the

manufacturing scale to take complete advantage of the versatility of these tiny vesicles. The challenges associated with exosomal research that need urgent consideration can be stated as:

(1) Lack of unified isolation, purification, characterization technique causing variable results among different research groups.

(2) Cost-effective cell maintenance process to continuously procure the exosomes, which needs proper GMP regulation for cell maintenance, processing, collection and storage guidelines.

(3) Low yield of exosomes compromises the pace of the research work which needs drastic improvement without altering the nature of the naïve exosomes.

(4) Exosomal formulations reported so far, lack systematic development, validation and characterization in terms of the drug potency, stability, and capacity.

(5) In-depth exploration of the effect of the process parameters as well as the distinct physicochemical and biological attributes of the exosomes *per se* on the observed efficacy of the exosomal formulations.

(7) Dose escalation from in-vitro assays to in-vivo efficacy studies of the exosomal formulations also need to be addressed.

(8) Consideration of the alternative strategies wherein, the advantages of the exosomes or exosomal fragments could be explored with the aim of overcoming the limited loading capacity and immunogenicity of synthetic carrier.

(9) Designing of the exosomal formulation with versatile cargos needs to be considered, especially co-delivery of small molecules and RNAi. It is expected that the mechanism of action of the small molecules could be synergistically enhanced by the RNAi inclusion which together would act as "***two edged swords***" for the disease treatment.

The above-mentioned points are not merely ***Gaps in Research*** with exosomes but also the hurdles that could be overcome with the detailed and elaborate research work.

1.7 Outline of Current Research Work

In this current research work, we explored the overall impact of two major attributes on the formulation development strategy for the co-delivery of the DTX and TS miRNA, i.e., physiological behavior of the exosomes inherited from their respective source cells, and the co-delivery strategy to encapsulate the miRNA and DTX to achieve more promising outcome as the anti-cancer therapeutics.

Herein, we explored the active loading of TS miRNA (miR-125a) in the hUCBMSC derived exosomes by plasmid vector mediated transfection of its source cells. After isolating the miR-125a transfected exosomes, these were utilized to load DTX by an optimized sonication/incubation method for development of the final formulation. From this segment of the research work, it was concluded that the biological nature of exosomes relied upon the source cells, which should be evaluated in detail. Also, DTX loading in the miR-125a transfected exosomes by sonication/incubation method compromised the of transfected miRNA payload, which needs to be further enhanced to make the formulation more economical and effective.

The initial observations with the outcomes of the research work led us to redefine exosome research by following the sequential exploration of the biological implications of the macrophage (RAW 264.7 cells) derived exosomes, followed by development of the RAW Exo-DTX in a statistically proven manner to achieve the optimum DTX loading capacity in the exosomes. Further, a strategic concept of PSA has also been introduced in the research work wherein, a phosphate driven polyamine nanoparticle of DTX and TS miR-34a was prepared and optimized to form the core of the core/shell delivery system. For the shell material, we explored RAW exosomal fragments after confirming the biological implication of the same in 4T1 cells. In this method, the prepared formulation was expected to overcome the loss of miRNA and to achieve the profound therapeutic impact of the DTX and TS miRNA in the TNBC 4T1 cells.

1.8 Objectives of Proposed Work

The main aim of the thesis is to explore exosomes as a co-delivery system for DTX and TS miRNA by different strategies. For this purpose, two different formulations were developed using two different strategies using two different source cells for the exosomes.

Objective 1: Development and evaluation of human umbilical cord blood derived mesenchymal stem cell (hUCBMSC) derived exosomal formulation for co-delivery of DTX and miR125a in breast cancer (**miR-125a Exo-DTX**).

Objective 1.A. Isolation and characterization of the exosomes from naïve hUCBMSCs and miR125a transfected hUCBMSCs

Objective 1.B. Development of the hUCBMSC Exo-DTX and miR-125a Exo-DTX formulations

Objective 1.C. Evaluation of the formulations for their anti-cancer effect in cell culture

Objective 2: Development and evaluation of macrophage (RAW264.7) derived exosomal formulation for the co-delivery of DTX and miR-34a **[RAW Exo ($PAN_{34a+DTX}$)]**

Objective 2.A. Isolation, preparation, characterization and *in vitro* evaluation of the RAW 264.7 cell derived exosomes and exosomal fragments

Objective 2.B. Optimization, development and evaluation of the RAW Exo-DTX formulations

Objective 2.C. Exploring exosomal fragment enclosed Polyamine-salt nanocomplex of DTX and miR-34a as a novel co-delivery strategy in breast cancer

1.9 References

(1) Lötvall, J.; Hill, A. F.; Hochberg, F.; Buzás, E. I.; Vizio, D. Di; Gardiner, C.; Gho, Y. S.; Kurochkin, I. V.; Mathivanan, S.; Quesenberry, P.; Sahoo, S.; Tahara, H.; Wauben, M. H.; Witwer, K. W.; Théry, C. Minimal Experimental Requirements for Definition of Extracellular Vesicles and Their Functions: A Position Statement from the International Society for Extracellular Vesicles. *J. Extracell. Vesicles* **2014**, *3* (1), 1–6. https://doi.org/10.3402/jev.v3.26913.

(2) Théry, C.; Witwer, K. W.; Aikawa, E.; Alcaraz, M. J.; Anderson, J. D.; Andriantsitohaina, R.; Antoniou, A.; Arab, T.; Archer, F.; Atkin-smith, G. K.; Ayre, D. C.; Bach, J.; Bachurski, D.; Baharvand, H.; Balaj, L.; Baldacchino, S.; Bauer, N. N.; Baxter, A. A.; Bebawy, M.; Beckham, C.; Zavec, A. B.; Benmoussa, A.; Berardi, A. C.; Bergese, P.; Bielska, E.; Blenkiron, C.; Bobis-wozowicz, S.; Boilard, E.; Brisson, A.; Broekman, M. L. D.; Bromberg, J. F.; Bryl-górecka, P.; Buch, S.; Buck, A. H.; Burger, D.; Busatto, S.; Buschmann, D.; Bussolati, B.; Buzás, E. I.; Byrd, J. B.; Camussi, G.; Carter, D. R. F.; Caruso, S.; Chamley, L. W.; Chang, Y.; Chaudhuri, A. D.; Chen, C.; Chen, S.; Cheng, L.; Chin, A. R.; Clayton, A.; Clerici, S. P.; Cocks, A.; Dominici, M.; Dourado, M. R.; Driedonks, T. A. P.; Duarte, F. V; Erdbrügger, U.; Falcón-pérez, J. M.; Fatima, F.; Fish, J. E.; Flores-, M. Minimal Information for Studies of Extracellular Vesicles 2018 (MISEV2018): A Position Statement of the International Society for Extracellular Vesicles and Update of the MISEV2014 Guidelines. **2018**, *7*.

(3) Kalluri, R.; Lebleu, V. S. The Biology, Function, and Biomedical Applications of Exosomes. **2020**, *367* (6478). https://doi.org/10.1126/science.aau6977.The.

(4) Fougerolles, D.; Therapeutics, C.; Therapeutics, S. Big Pharma Buys into Exosomes for Drug Delivery. **2020**, *38* (November). https://doi.org/10.1038/s41587-020-0724-8.

(5) Silva, A. K. A.; Morille, M.; Piffoux, M.; Arumugam, S.; Mauduit, P.; Larghero, J.; Bianchi, A.; Aubertin, K.; Blanc-brude, O.; Noël, D.; Velot, E.; Ravel, C.; Elie-caille, C.; Sebbagh, A.; Boulanger, C.; Wilhelm, C.; Rahmi, G.; Raymond-letron, I.; Cherukula, K.; Montier, T.; Martinaud, C.; Bach, J.; Favre-bulle, O.; Spadavecchia, J.; Jorgensen, C.; Menasché, P.; Aussel, C.; Chopineau, J.; Mosser, M.; Ullah, M.; Sailliet, N.; Luciani, N.; Mathieu, N.; Rautou, P.; Brouard, S.; Boireau, W.; Jauliac, S.; Dedier, M.; Trouvin, J.; Gazeau, F.; Trouillas, M.; Peltzer, J.; Monsel, A.; Banzet, S. Development of Extracellular Vesicle-Based Medicinal Products : A Position Paper of the Group ‘‘ Extracellular Vesicle TranslatiOn to ClinicaL PerspectiVEs – EVOLVE France ”. **2021**, *179*. https://doi.org/10.1016/j.addr.2021.114001.

(6) Tenchov, R.; Sasso, J. M.; Wang, X.; Liaw, W. S.; Chen, C. A.; Zhou, Q. A. Exosomes Nature’s Lipid Nanoparticles, a Rising Star in Drug Delivery and Diagnostics. *ACS Nano* **2022**, *16* (11), 17802–17846. https://doi.org/10.1021/acsnano.2c08774.

(7) Colombo, M.; Moita, C.; Niel, G. Van; Kowal, J.; Vigneron, J. Analysis of ESCRT Functions in Exosome Biogenesis , Composition and Secretion Highlights the Heterogeneity of Extracellular Vesicles. **2011**. https://doi.org/10.1242/jcs.128868.

(8) Kalluri, R.; LeBleu, V. S. The Biology, Function, and Biomedical Applications of Exosomes. *Science (80-.).* **2020**, *367*, eaau6977. https://doi.org/10.1126/science.aau6977.

(9) Théry, C.; Zitvogel, L.; Amigorena, S.; Roussy, I. G. EXOSOMES : COMPOSITION , BIOGENESIS AND FUNCTION. **2002**, *2* (August). https://doi.org/10.1038/nri855.

(10) Henne, W. M.; Buchkovich, N. J.; Emr, S. D. Review The ESCRT Pathway. *Dev. Cell* **2011**, *21* (1), 77–91. https://doi.org/10.1016/j.devcel.2011.05.015.

(11) Katzmann, D. J.; Babst, M.; Emr, S. D. Ubiquitin-Dependent Sorting into the Multivesicular Body Pathway Requires the Function of a Conserved Endosomal Protein Sorting Complex, ESCRT-I. *Cell* **2001**, *106* (2), 145–155. https://doi.org/10.1016/S0092-8674(01)00434-2.

(12) Baietti, M. F.; Zhang, Z.; Mortier, E.; Melchior, A.; Degeest, G.; Geeraerts, A.; Ivarsson, Y.; Depoortere, F.; Coomans, C.; Vermeiren, E.; Zimmermann, P.; David, G. Syndecan-Syntenin-ALIX Regulates the Biogenesis of Exosomes. *Nat. Cell Biol.* **2012**, *14* (7), 677–685.

https://doi.org/10.1038/ncb2502.

(13) van Niel, G.; Charrin, S.; Simoes, S.; Romao, M.; Rochin, L.; Saftig, P.; Marks, M. S.; Rubinstein, E.; Raposo, G. The Tetraspanin CD63 Regulates ESCRT-Independent and -Dependent Endosomal Sorting during Melanogenesis. *Dev. Cell* **2011**, *21* (4), 708–721. https://doi.org/10.1016/j.devcel.2011.08.019.

(14) Trajkovic, K. Ceramide Triggers Budding of Exosome Vesicles into Multivesicular Endosomes (Science (1244)). *Science (80-.).* **2008**, *320* (5873), 179. https://doi.org/10.1126/science.320.5873.179.

(15) Colombo, M.; Moita, C.; Van Niel, G.; Kowal, J.; Vigneron, J.; Benaroch, P.; Manel, N.; Moita, L. F.; Théry, C.; Raposo, G. Analysis of ESCRT Functions in Exosome Biogenesis, Composition and Secretion Highlights the Heterogeneity of Extracellular Vesicles. *J. Cell Sci.* **2013**, *126* (24), 5553–5565. https://doi.org/10.1242/jcs.128868.

(16) Gurung, S.; Perocheau, D.; Touramanidou, L.; Baruteau, J. The Exosome Journey : From Biogenesis to Uptake and Intracellular Signalling. *Cell Commun. Signal.* **2021**, 1–19. https://doi.org/10.1186/s12964-021-00730-1.

(17) Liu, C.; Liu, D.; Wang, S.; Gan, L.; Yang, X.; Ma, C. Identification of the SNARE Complex That Mediates the Fusion of Multivesicular Bodies with the Plasma Membrane in Exosome Secretion. *J. Extracell. Vesicles* **2023**, *12* (9). https://doi.org/10.1002/jev2.12356.

(18) Mathieu, M.; Martin-Jaular, L.; Lavieu, G.; Théry, C. Specificities of Secretion and Uptake of Exosomes and Other Extracellular Vesicles for Cell-to-Cell Communication. *Nat. Cell Biol.* **2019**, *21* (1), 9–17. https://doi.org/10.1038/s41556-018-0250-9.

(19) Nazarenko, I.; Rana, S.; Baumann, A.; McAlear, J.; Hellwig, A.; Trendelenburg, M.; Lochnit, G.; Preissner, K. T.; Zöller, M. Cell Surface Tetraspanin Tspan8 Contributes to Molecular Pathways of Exosome-Induced Endothelial Cell Activation. *Cancer Res.* **2010**, *70* (4), 1668–1678. https://doi.org/10.1158/0008-5472.CAN-09-2470.

(20) Verdera, H. C.; Gitz-francois, J. J.; Schi, R. M.; Vader, P. Cellular Uptake of Extracellular Vesicles Is Mediated by Clathrin-Independent Endocytosis and Macropinocytosis. **2017**, *266* (July), 100–108. https://doi.org/10.1016/j.jconrel.2017.09.019.

(21) Tkach, M.; Théry, C. Communication by Extracellular Vesicles: Where We Are and Where We Need to Go. *Cell* **2016**, *164* (6), 1226–1232. https://doi.org/10.1016/j.cell.2016.01.043.

(22) Caponnetto, F.; Manini, I.; Skrap, M.; Palmai-pallag, T.; Loreto, C. Di; Beltrami, A. P.; Cesselli, D.; Ferrari, E. Size-Dependent Cellular Uptake of Exosomes. **2017**, *13*, 1011–1020. https://doi.org/10.1016/j.nano.2016.12.009.

(23) Fu, W.; Lei, C.; Liu, S.; Cui, Y.; Wang, C.; Qian, K.; Li, T.; Shen, Y.; Fan, X.; Lin, F.; Ding, M.; Pan, M.; Ye, X.; Yang, Y.; Hu, S. CAR Exosomes Derived from Effector CAR-T Cells Have Potent Antitumour Effects and Low Toxicity. *Nat. Commun.* **2019**, *10* (1), 4355. https://doi.org/10.1038/s41467-019-12321-3.

(24) Valadi, H.; K, E.; A, B.; Lotvall J et al. Exosome-Mediated Transfer of MRNAs and MicroRNAs Is a Novel Mechanism of Genetic Exchange between Cells. *Nat. Cell Biol.* **2008**, *9* (6), 654–659. https://doi.org/10.1038/ncb1596.

(25) Skotland, T.; Hessvik, N. P.; Sandvig, K.; Llorente, A. Exosomal Lipid Composition and the Role of Ether Lipids and Phosphoinositides in Exosome Biology. **2019**, *60*, 9–18.

(26) Suga, K.; Matsui, D.; Watanabe, N.; Okamoto, Y.; Umakoshi, H. Insight into the Exosomal Membrane: From Viewpoints of Membrane Fluidity and Polarity. **2021**. https://doi.org/10.1021/acs.langmuir.1c00687.

(27) Kim, M. S.; Haney, M. J.; Zhao, Y.; Mahajan, V.; Deygen, I.; Klyachko, N. L.; Inskoe, E.; Piroyan, A.; Sokolsky, M.; Okolie, O.; Hingtgen, S. D.; Kabanov, A. V.; Batrakova, E. V. Development of Exosome-Encapsulated Paclitaxel to Overcome MDR in Cancer Cells. *Nanomedicine Nanotechnology, Biol. Med.* **2016**, *12* (3), 655–664. https://doi.org/10.1016/j.nano.2015.10.012.

(28) Jeppesen, D. K.; Fenix, A. M.; Franklin, J. L.; Rome, L. H.; Burnette, D. T.; Coffey, R. J.; Jeppesen,

D. K.; Fenix, A. M.; Franklin, J. L.; Higginbotham, J. N.; Zhang, Q.; Zimmerman, L. J.; Liebler, D. C.; Ping, J.; Liu, Q.; Evans, R.; Fissell, W. H.; Patton, J. G.; Rome, L. H.; Burnette, D. T.; Coffey, R. J. Reassessment of Exosome Composition. *Cell* **2019**, *177* (April 4), 428–445. https://doi.org/10.1016/j.cell.2019.02.029.

(29) Grivennikov, S. I.; Greten, F. R.; Karin, M. Immunity , Inflammation , and Cancer. *Cell* **2010**, *140* (6), 883–899. https://doi.org/10.1016/j.cell.2010.01.025.

(30) Veerman, R. E.; Güçlüler Akpinar, G.; Eldh, M.; Gabrielsson, S. Immune Cell-Derived Extracellular Vesicles – Functions and Therapeutic Applications. *Trends Mol. Med.* **2019**, *25* (5), 382–394. https://doi.org/10.1016/j.molmed.2019.02.003.

(31) Kugeratski, F. G.; Kalluri, R. Exosomes as Mediators of Immune Regulation and Immunotherapy in Cancer. *FEBS J.* **2021**, *288* (1), 10–35. https://doi.org/10.1111/febs.15558.

(32) Rodríguez, M.; Silva, J.; Herrera, A.; Herrera, M.; Peña, C.; Martín, P.; Gil-Calderón, B.; Larriba, M. J.; Coronado, M. J.; Soldevilla, B.; Turrión, V. S.; Provencio, M.; Sánchez, A.; Bonilla, F.; García-Barberán, V. Exosomes Enriched in Stemness/Metastatic-Related MRNAS Promote Oncogenic Potential in Breast Cancer. *Oncotarget* **2015**, *6* (38), 40575–40587. https://doi.org/10.18632/oncotarget.5818.

(33) Ramteke, A.; Ting, H.; Agarwal, C.; Mateen, S.; Somasagara, R.; Hussain, A.; Graner, M.; Frederick, B.; Agarwal, R.; Deep, G. Exosomes Secreted under Hypoxia Enhance Invasiveness and Stemness of Prostate Cancer Cells by Targeting Adherens Junction Molecules. *Mol. Carcinog.* **2015**, *54* (7), 554–565. https://doi.org/10.1002/mc.22124.

(34) Ding, M.; Zhao, X.; Chen, X.; Diao, W.; Kan, Y.; Cao, W.; Chen, W.; Jiang, B.; Qin, H.; Gao, J.; Zhuang, J.; Zhang, Q.; Guo, H. Cancer-Associated Fibroblasts Promote the Stemness and Progression of Renal Cell Carcinoma via Exosomal MiR-181d-5p. *Cell Death Discov.* **2022**, *8* (1). https://doi.org/10.1038/s41420-022-01219-7.

(35) Kaban, K.; Hinterleitner, C.; Zhou, Y.; Salva, E.; Kantarci, A. G.; Salih, H. R.; Märklin, M. Therapeutic Silencing of Bcl-2 Using Nk Cell-Derived Exosomes as a Novel Therapeutic Approach in Breast Cancer. *Cancers (Basel).* **2021**, *13* (2397), 1–16. https://doi.org/10.3390/cancers13102397.

(36) Neviani, P.; Wise, P. M.; Murtadha, M.; Liu, C. W.; Wu, C. H.; Jong, A. Y.; Seeger, R. C.; Fabbri, M. Natural Killer–Derived Exosomal MiR-186 Inhibits Neuroblastoma Growth and Immune Escape Mechanisms. *Cancer Res.* **2019**, *79* (6), 1151–1164. https://doi.org/10.1158/0008-5472.CAN-18-0779.

(37) Cianciaruso, C.; Beltraminelli, T.; Duval, F.; Nassiri, S.; Hamelin, R.; Mozes, A.; Gallart-Ayala, H.; Ceada Torres, G.; Torchia, B.; Ries, C. H.; Ivanisevic, J.; De Palma, M. Molecular Profiling and Functional Analysis of Macrophage-Derived Tumor Extracellular Vesicles. *Cell Rep.* **2019**, *27* (10), 3062–3080. https://doi.org/10.1016/j.celrep.2019.05.008.

(38) Lin, Z.; Wu, Y.; Xu, Y.; Li, G.; Li, Z.; Liu, T. Mesenchymal Stem Cell-Derived Exosomes in Cancer Therapy Resistance: Recent Advances and Therapeutic Potential. *Mol. Cancer* **2022**, *21* (1), 1–17. https://doi.org/10.1186/s12943-022-01650-5.

(39) Zhu, Y.; Chen, X.; Pan, Q.; Wang, Y.; Su, S.; Jiang, C.; Li, Y.; Xu, N.; Wu, L.; Lou, X.; Liu, S. A Comprehensive Proteomics Analysis Reveals a Secretory Path- and Status-Dependent Signature of Exosomes Released from Tumor-Associated Macrophages. *J. Proteome Res.* **2015**, *14* (10), 4319–4331. https://doi.org/10.1021/acs.jproteome.5b00770.

(40) Driedonks, T. A. P.; van der Grein, S. G.; Ariyurek, Y.; Buermans, H. P. J.; Jekel, H.; Chow, F. W. N.; Wauben, M. H. M.; Buck, A. H.; 't Hoen, P. A. C.; Nolte-'t Hoen, E. N. M. Immune Stimuli Shape the Small Non-Coding Transcriptome of Extracellular Vesicles Released by Dendritic Cells. *Cell. Mol. Life Sci.* **2018**, *75* (20), 3857–3875. https://doi.org/10.1007/s00018-018-2842-8.

(41) Xie, Y.; Zhang, X.; Zhao, T.; Li, W.; Xiang, J. Natural CD8+25+ Regulatory T Cell-Secreted Exosomes Capable of Suppressing Cytotoxic T Lymphocyte-Mediated Immunity against B16 Melanoma. *Biochem. Biophys. Res. Commun.* **2013**, *438* (1), 152–155.

https://doi.org/10.1016/j.bbrc.2013.07.044.

(42) Fanini, F.; Fabbri, M. Cancer-Derived Exosomic MicroRNAs Shape the Immune System within the Tumor Microenvironment: State of the Art. *Semin. Cell Dev. Biol.* **2017**, *67*, 23–28. https://doi.org/10.1016/j.semcdb.2016.12.004.

(43) Aiello, S.; Rocchetta, F.; Longaretti, L.; Faravelli, S.; Todeschini, M.; Cassis, L.; Pezzuto, F.; Tomasoni, S.; Azzollini, N.; Mister, M.; Mele, C.; Conti, S.; Breno, M.; Remuzzi, G.; Noris, M.; Benigni, A. Extracellular Vesicles Derived from T Regulatory Cells Suppress T Cell Proliferation and Prolong Allograft Survival. *Sci. Rep.* **2017**, *7* (1), 1–19. https://doi.org/10.1038/s41598-017-08617-3.

(44) Tung, S. L.; Boardman, D. A.; Sen, M.; Letizia, M.; Peng, Q.; Cianci, N.; Dioni, L.; Carlin, L. M.; Lechler, R.; Bollati, V.; Lombardi, G.; Smyth, L. A. Regulatory T Cell-Derived Extracellular Vesicles Modify Dendritic Cell Function. *Sci. Rep.* **2018**, *8* (1), 1–12. https://doi.org/10.1038/s41598-018-24531-8.

(45) Deng, Z.; Rong, Y.; Teng, Y.; Zhuang, X.; Samykutty, A.; Mu, J.; Zhang, L.; Cao, P.; Yan, J.; Miller, D.; Zhang, H. Exosomes MiR-126a Released from MDSC Induced by DOX Treatment Promotes Lung Metastasis. *Oncogene* **2016**, *36* (5), 639–651. https://doi.org/10.1038/onc.2016.229.

(46) Chow, A.; Zhou, W.; Liu, L.; Fong, M. Y.; Champer, J.; Haute, D. Van; Chin, A. R.; Ren, X.; Gugiu, B. G.; Meng, Z.; Huang, W.; Ngo, V.; Kortylewski, M.; Wang, S. E. Macrophage Immunomodulation by Breast Cancer-Derived Exosomes Requires Toll-like Receptor 2-Mediated Activation of NF- k B. *Sci. Rep.* **2014**, *4* (5750), 1–11. https://doi.org/10.1038/srep05750.

(47) Yu, X.; Zhang, Q.; Zhang, X.; Han, Q.; Li, H.; Mao, Y.; Wang, X.; Guo, H. Exosomes from Macrophages Exposed to Apoptotic Breast Cancer Cells Promote Breast Cancer Proliferation and Metastasis. *J. Cancer* **2019**, *10*, 2892–2906. https://doi.org/10.7150/jca.31241.

(48) Chen, F.; Chen, J.; Yang, L.; Liu, J.; Zhang, X.; Zhang, Y.; Tu, Q.; Yin, D.; Lin, D.; Wong, P. P.; Huang, D.; Xing, Y.; Zhao, J.; Li, M.; Liu, Q.; Su, F.; Su, S.; Song, E. Extracellular Vesicle-Packaged HIF-1α-Stabilizing LncRNA from Tumour-Associated Macrophages Regulates Aerobic Glycolysis of Breast Cancer Cells. *Nat. Cell Biol.* **2019**, *21* (4), 498–510. https://doi.org/10.1038/s41556-019-0299-0.

(49) Zhou, J.; Li, X.; Wu, X.; Zhang, T.; Zhu, Q.; Wang, X.; Wang, H.; Wang, K.; Lin, Y.; Wang, X. Exosomes Released from Tumor-Associated Macrophages Transfer MiRNAs That Induce a Treg / Th17 Cell Imbalance in Epithelial Ovarian Cancer. **2018**, *6* (December), 1578–1593. https://doi.org/10.1158/2326-6066.CIR-17-0479.

(50) Pakravan, K.; Babashah, S.; Sadeghizadeh, M.; Mowla, S. J.; Mossahebi-Mohammadi, M.; Ataei, F.; Dana, N.; Javan, M. MicroRNA-100 Shuttled by Mesenchymal Stem Cell-Derived Exosomes Suppresses in Vitro Angiogenesis through Modulating the MTOR/HIF-1α/VEGF Signaling Axis in Breast Cancer Cells. *Cell. Oncol.* **2017**, *40* (5), 457–470. https://doi.org/10.1007/s13402-017-0335-7.

(51) Zhu, W.; Huang, L.; Li, Y.; Zhang, X.; Gu, J.; Yan, Y.; Xu, X. Exosomes Derived from Human Bone Marrow Mesenchymal Stem Cells Promote Tumor Growth in Vivo. *Cancer Lett.* **2012**, *315*, 28–37. https://doi.org/10.1016/j.canlet.2011.10.002.

(52) Katakowski, M.; Buller, B.; Zheng, X.; Lu, Y.; Rogers, T.; Osobamiro, O.; Shu, W.; Jiang, F.; Chopp, M. Exosomes from Marrow Stromal Cells Expressing MiR-146b Inhibit Glioma Growth. *Cancer Lett.* **2013**, *335* (1), 201–204. https://doi.org/10.1016/j.canlet.2013.02.019.

(53) Bruno, S.; Collino, F.; Deregibus, M. C.; Grange, C.; Tetta, C.; Camussi, G. Microvesicles Derived from Human Bone Marrow Mesenchymal Stem Cells Inhibit Tumor Growth. *Stem Cells Dev.* **2013**, *22* (5), 758–771. https://doi.org/10.1089/scd.2012.0304.

(54) Lee, J.; Park, S.; Jung, B.; Jeon, Y.; Lee, Y.; Kim, K.; Kim, Y.; Jang, J.; Kim, C. Exosomes Derived from Mesenchymal Stem Cells Suppress Angiogenesis by Down-Regulating VEGF Expression in Breast Cancer Cells. *PLoS One* **2013**, *8* (12), e84256. https://doi.org/10.1371/journal.pone.0084256.

(55) Liu, J.; Zhu, M.; Tang, Q. Human Umbilical Cord Mesenchymal Stem Cells-Derived Exosomal

MicroRNA-181a Retards Nasopharyngeal Carcinoma Development by Mediating KDM5C. *J. Cancer Res. Clin. Oncol.* **2021**, *147* (10), 2867–2877. https://doi.org/10.1007/s00432-021-03684-6.

(56) He, Z.; Li, W.; Zheng, T.; Liu, D.; Zhao, S. Human Umbilical Cord Mesenchymal Stem Cells-Derived Exosomes Deliver MicroRNA-375 to Downregulate ENAH and Thus Retard Esophageal Squamous Cell Carcinoma Progression. *J. Exp. Clin. Cancer Res.* **2020**, *39* (1), 1–18. https://doi.org/10.1186/s13046-020-01631-w.

(57) Xu, Y.; Lai, Y.; Cao, L.; Li, Y.; Chen, G.; Chen, L.; Weng, H.; Chen, T.; Wang, L.; Ye, Y. Human Umbilical Cord Mesenchymal Stem Cells-Derived Exosomal MicroRNA-451a Represses Epithelial–Mesenchymal Transition of Hepatocellular Carcinoma Cells by Inhibiting ADAM10. *RNA Biol.* **2021**, *18* (10), 1408–1423. https://doi.org/10.1080/15476286.2020.1851540.

(58) Pan, Y.; Wang, X.; Li, Y.; Yan, P.; Zhang, H. Human Umbilical Cord Blood Mesenchymal Stem Cells-Derived Exosomal MicroRNA-503-3p Inhibits Progression of Human Endometrial Cancer Cells through Downregulating MEST. *Cancer Gene Ther.* **2022**, *29* ((8-9)), 1130–1139. https://doi.org/10.1038/s41417-021-00416-3.

(59) Shi, Z.; Pang, K.; Wu, Z.; Dong, Y.; Hao, L.; Qin, J.; Wang, W.; Chen, Z. Tumor Cell Plasticity in Targeted Therapy-Induced Resistance : Mechanisms and New Strategies. **2023**, No. December 2022. https://doi.org/10.1038/s41392-023-01383-x.

(60) Li, W.; Xin, X.; Li, X.; Geng, J.; Sun, Y. Exosomes Secreted by M2 Macrophages Promote Cancer Stemness of Hepatocellular Carcinoma via the MiR-27a-3p/TXNIP Pathways. *Int. Immunopharmacol.* **2021**, *101* (PA), 107585. https://doi.org/10.1016/j.intimp.2021.107585.

(61) Zhan, Y.; Du, J.; Min, Z.; Ma, L.; Zhang, W.; Zhu, W.; Liu, Y. Carcinoma-Associated Fibroblasts Derived Exosomes Modulate Breast Cancer Cell Stemness through Exonic CircHIF1A by MiR-580-5p in Hypoxic Stress. *Cell Death Discov.* **2021**, *7* (1). https://doi.org/10.1038/s41420-021-00506-z.

(62) Wang, Y.; Yin, K.; Tian, J.; Xia, X.; Ma, J.; Tang, X.; Xu, H.; Wang, S. Granulocytic Myeloid-Derived Suppressor Cells Promote the Stemness of Colorectal Cancer Cells through Exosomal S100A9. *Adv. Sci.* **2019**, *6* (18), 1901278. https://doi.org/10.1002/advs.201901278.

(63) Li, Y.; Wu, M.; Xu, S.; Huang, H.; Yan, L.; Gu, Y. Colorectal Cancer Stem Cell-Derived Exosomal Long Intergenic Noncoding RNA 01315 (LINC01315) Promotes Proliferation, Migration, and Stemness of Colorectal Cancer Cells. *Bioengineered* **2022**, *13* (4), 10827–10842. https://doi.org/10.1080/21655979.2022.2065800.

(64) Batrakova, E. V.; Kim, M. S. Using Exosomes, Naturally-Equipped Nanocarriers, for Drug Delivery. *J. Control. Release* **2015**, *219*, 396–405. https://doi.org/10.1016/j.jconrel.2015.07.030.

(65) Wang, J.; Chen, D.; Ho, E. A. Challenges in the Development and Establishment of Exosome-Based Drug Delivery Systems. *J. Control. Release* **2021**, *329* (October 2020), 894–906. https://doi.org/10.1016/j.jconrel.2020.10.020.

(66) Pascucci, L.; Coccè, V.; Bonomi, A.; Ami, D.; Ceccarelli, P.; Ciusani, E.; Viganò, L.; Locatelli, A.; Sisto, F.; Doglia, S. M.; Parati, E.; Bernardo, M. E.; Muraca, M.; Alessandri, G.; Bondiolotti, G.; Pessina, A. Paclitaxel Is Incorporated by Mesenchymal Stromal Cells and Released in Exosomes That Inhibit in Vitro Tumor Growth: A New Approach for Drug Delivery. *J. Control. Release* **2014**, *192*, 262–270. https://doi.org/10.1016/j.jconrel.2014.07.042.

(67) Lv, L. H.; Wan, Y. Le; Lin, Y.; Zhang, W.; Yang, M.; Li, G. N.; Lin, H. M.; Shang, C. Z.; Chen, Y. J.; Min, J. Anticancer Drugs Cause Release of Exosomes with Heat Shock Proteins from Human Hepatocellular Carcinoma Cells That Elicit Effective Natural Killer Cell Antitumor Responses in Vitro. *J. Biol. Chem.* **2012**, *287* (19), 15874–15885. https://doi.org/10.1074/jbc.M112.340588.

(68) Ran, N.; Gao, X.; Dong, X.; Li, J.; Lin, C.; Geng, M.; Yin, H. F. Effects of Exosome-Mediated Delivery of Myostatin Propeptide on Functional Recovery of Mdx Mice. *Biomaterials* **2020**, *236* (December 2019), 119826. https://doi.org/10.1016/j.biomaterials.2020.119826.

(69) Trivedi, M.; Talekar, M.; Shah, P.; Ouyang, Q.; Amiji, M. Modification of Tumor Cell Exosome Content by Transfection with Wt-P53 and MicroRNA-125b Expressing Plasmid DNA and Its Effect on Macrophage Polarization. *Oncogenesis* **2016**, *5* (8), e250-12.

https://doi.org/10.1038/oncsis.2016.52.

(70) Agrawal, A. K.; Aqil, F.; Jeyabalan, J.; Spencer, W. A.; Beck, J.; Gachuki, B. W.; Alhakeem, S. S.; Oben, K.; Munagala, R.; Bondada, S.; Gupta, R. C. Milk-Derived Exosomes for Oral Delivery of Paclitaxel. *Nanomedicine Nanotechnology, Biol. Med.* **2017**, *13* (5), 1627–1636. https://doi.org/10.1016/j.nano.2017.03.001.

(71) Zhang, M.; Zang, X.; Wang, M.; Li, Z.; Qiao, M.; Hu, H.; Chen, D. Exosome-Based Nanocarriers as Bio-Inspired and Versatile Vehicles for Drug Delivery: Recent Advances and Challenges. *J. Mater. Chem. B* **2019**, *7* (15), 2421–2433. https://doi.org/10.1039/C9TB00170K.

(72) Kim, M. S.; Haney, M. J.; Zhao, Y.; Mahajan, V.; Deygen, I.; Klyachko, N. L.; Inskoe, E.; Piroyan, A.; Sokolsky, M.; Okolie, O.; Hingtgen, S. D.; Kabanov, A. V.; Batrakova, E. V. Development of Exosome-Encapsulated Paclitaxel to Overcome MDR in Cancer Cells. *Nanomedicine Nanotechnology, Biol. Med.* **2016**, *12* (3), 655–664. https://doi.org/10.1016/j.nano.2015.10.012.

(73) Li, Y. J.; Wu, J. Y.; Wang, J. M.; Hu, X. Bin; Cai, J. X.; Xiang, D. X. Gemcitabine Loaded Autologous Exosomes for Effective and Safe Chemotherapy of Pancreatic Cancer. *Acta Biomater.* **2020**, *101*, 519–530. https://doi.org/10.1016/j.actbio.2019.10.022.

(74) Haney, M. J.; Klyachko, N. L.; Zhao, Y.; Gupta, R.; Plotnikova, E. G.; He, Z.; Patel, T.; Piroyan, A.; Sokolsky, M.; Kabanov, A. V.; Batrakova, E. V. Exosomes as Drug Delivery Vehicles for Parkinson's Disease Therapy. *J. Control. Release* **2015**, *207*, 18–30. https://doi.org/10.1016/j.jconrel.2015.03.033.

(75) Fuhrmann, G.; Serio, A.; Mazo, M.; Nair, R.; Stevens, M. M. Active Loading into Extracellular Vesicles Significantly Improves the Cellular Uptake and Photodynamic Effect of Porphyrins. *J. Control. Release* **2015**, *205*, 35–44. https://doi.org/10.1016/j.jconrel.2014.11.029.

(76) Kooijmans, S. A. A.; Stremersch, S.; Braeckmans, K.; De Smedt, S. C.; Hendrix, A.; Wood, M. J. A.; Schiffelers, R. M.; Raemdonck, K.; Vader, P. Electroporation-Induced SiRNA Precipitation Obscures the Efficiency of SiRNA Loading into Extracellular Vesicles. *J. Control. Release* **2013**, *172* (1), 229–238. https://doi.org/10.1016/j.jconrel.2013.08.014.

(77) Chan, M. H.; Chang, Z. X.; Huang, C. Y. F.; Lee, L. J.; Liu, R. S.; Hsiao, M. Integrated Therapy Platform of Exosomal System: Hybrid Inorganic/Organic Nanoparticles with Exosomes for Cancer Treatment. *Nanoscale Horizons* **2022**, *7* (4), 352–367. https://doi.org/10.1039/d1nh00637a.

(78) Lin, Y.; Wu, J.; Gu, W.; Huang, Y.; Tong, Z.; Huang, L.; Tan, J. Exosome–Liposome Hybrid Nanoparticles Deliver CRISPR/Cas9 System in MSCs. *Adv. Sci.* **2018**, *5* (4), 1–9. https://doi.org/10.1002/advs.201700611.

(79) Lv, Q.; Cheng, L.; Lu, Y.; Zhang, X.; Wang, Y.; Deng, J.; Zhou, J.; Liu, B.; Liu, J. Thermosensitive Exosome–Liposome Hybrid Nanoparticle-Mediated Chemoimmunotherapy for Improved Treatment of Metastatic Peritoneal Cancer. *Adv. Sci.* **2020**, *7* (18), 1–13. https://doi.org/10.1002/advs.202000515.

(80) Jang, S. C.; Kim, O. Y.; Yoon, C. M.; Choi, D. S.; Roh, T. Y.; Park, J.; Nilsson, J.; Lötvall, J.; Kim, Y. K.; Gho, Y. S. Bioinspired Exosome-Mimetic Nanovesicles for Targeted Delivery of Chemotherapeutics to Malignant Tumors. *ACS Nano* **2013**, *7* (9), 7698–7710. https://doi.org/10.1021/nn402232g.

(81) Mantovani, A.; Sica, A. Macrophages, Innate Immunity and Cancer: Balance, Tolerance, and Diversity. *Curr. Opin. Immunol.* **2010**, *22* (2), 231–237. https://doi.org/10.1016/j.coi.2010.01.009.

(82) Choo, Y. W.; Kang, M.; Kim, H. Y.; Han, J.; Kang, S.; Lee, J. R.; Jeong, G. J.; Kwon, S. P.; Song, S. Y.; Go, S.; Jung, M.; Hong, J.; Kim, B. S. M1 Macrophage-Derived Nanovesicles Potentiate the Anticancer Efficacy of Immune Checkpoint Inhibitors. *ACS Nano* **2018**, *12* (9), 8977–8993. https://doi.org/10.1021/acsnano.8b02446.

(83) Salunkhe, S.; Dheeraj; Basak, M.; Chitkara, D.; Mittal, A. Surface Functionalization of Exosomes for Target-Specific Delivery and in Vivo Imaging & Tracking: Strategies and Significance. *J. Control. Release* **2020**, *326* (May), 599–614. https://doi.org/10.1016/j.jconrel.2020.07.042.

(84) Kim, M. S.; Haney, M. J.; Zhao, Y.; Yuan, D.; Deygen, I.; Klyachko, N. L.; Kabanov, A. V.;

Batrakova, E. V. Engineering Macrophage-Derived Exosomes for Targeted Paclitaxel Delivery to Pulmonary Metastases: In Vitro and in Vivo Evaluations. *Nanomedicine Nanotechnology, Biol. Med.* **2018**, *14* (1), 195–204. https://doi.org/10.1016/j.nano.2017.09.011.

(85) Jia, G.; Han, Y.; An, Y.; Ding, Y.; He, C.; Wang, X.; Tang, Q. NRP-1 Targeted and Cargo-Loaded Exosomes Facilitate Simultaneous Imaging and Therapy of Glioma in Vitro and in Vivo. *Biomaterials* **2018**, *178*, 302–316. https://doi.org/10.1016/j.biomaterials.2018.06.029.

(86) Sawada, S. I.; Sato, Y. T.; Kawasaki, R.; Yasuoka, J. I.; Mizuta, R.; Sasaki, Y.; Akiyoshi, K. Nanogel Hybrid Assembly for Exosome Intracellular Delivery: Effects on Endocytosis and Fusion by Exosome Surface Polymer Engineering. *Biomater. Sci.* **2020**, *8* (2), 619–630. https://doi.org/10.1039/c9bm01232j.

(87) Chen, H. Y.; Deng, J.; Wang, Y.; Wu, C. Q.; Li, X.; Dai, H. W. Hybrid Cell Membrane-Coated Nanoparticles: A Multifunctional Biomimetic Platform for Cancer Diagnosis and Therapy. *Acta Biomater.* **2020**, *112*, 1–13. https://doi.org/10.1016/j.actbio.2020.05.028.

(88) Chen, H.-Y.; Deng, J.; Dai, H.-W.; Al, E. Hybrid Cell Membrane-Camouflaged Nanoparticle: A Novel Multifunctional Biomimetic Drug Delivery Carrier for Cancer Therapy. *Acta Biomater.* **2020**, *112* (1), 1–13. https://doi.org/10.1016/j.actbio.2020.05.028.

(89) Han, J.; Wang, Q.; Zhang, Z.; Gong, T.; Sun, X. Cationic Bovine Serum Albumin Based Self-Assembled Nanoparticles as SiRNA Delivery Vector for Treating Lung Metastatic Cancer. *Small* **2014**, *10* (3), 524–535. https://doi.org/10.1002/smll.201301992.

(90) Liu, C.; Zhang, W.; Li, Y.; Chang, J.; Tian, F.; Zhao, F.; Ma, Y.; Sun, J. Microfluidic Sonication to Assemble Exosome Membrane-Coated Nanoparticles for Immune Evasion-Mediated Targeting. *Nano Lett.* **2019**, *19* (11), 7836–7844. https://doi.org/10.1021/acs.nanolett.9b02841.

(91) Gong, C.; Tian, J.; Wang, Z.; Gao, Y.; Wu, X.; Ding, X.; Qiang, L.; Li, G.; Han, Z.; Yuan, Y.; Gao, S. Functional Exosome-Mediated Co-Delivery of Doxorubicin and Hydrophobically Modified MicroRNA 159 for Triple-Negative Breast Cancer Therapy. *J. Nanobiotechnology* **2019**, *17* (1), 1–18. https://doi.org/10.1186/s12951-019-0526-7.

(92) Liang, G.; Zhu, Y.; Ali, D. J.; Tian, T.; Xu, H.; Si, K.; Sun, B.; Chen, B.; Xiao, Z. Engineered Exosomes for Targeted Co-Delivery of MiR-21 Inhibitor and Chemotherapeutics to Reverse Drug Resistance in Colon Cancer. *J. Nanobiotechnology* **2020**, *18* (1), 1–15. https://doi.org/10.1186/s12951-019-0563-2.

(93) Zheng, C.; Zheng, M.; Gong, P.; Deng, J.; Yi, H. Biomaterials Polypeptide Cationic Micelles Mediated Co-Delivery of Docetaxel and SiRNA for Synergistic Tumor Therapy. *Biomaterials* **2013**, *34* (13), 3431–3438. https://doi.org/10.1016/j.biomaterials.2013.01.053.

(94) Murthy, V. S.; Rana, R. K.; Wong, M. S. Nanoparticle-Assembled Capsule Synthesis: Formation of Colloidal Polyamine-Salt Intermediates. *J. Phys. Chem. B* **2006**, *110* (51), 25619–25627. https://doi.org/10.1021/jp061826b.

(95) Bagaria, H. G.; Wong, M. S. Polyamine-Salt Aggregate Assembly of Capsules as Responsive Drug Delivery Vehicles. *J. Mater. Chem.* **2011**, *21* (26), 9454–9466. https://doi.org/10.1039/c1jm10712g.

(96) Yu, J.; Javier, D.; Yaseen, M. A.; Nitin, N.; Richards-Kortum, R.; Anvari, B.; Wong, M. S. Self-Assembly Synthesis, Tumor Cell Targeting, and Photothermal Capabilities of Antibody-Coated Indocyanine Green Nanocapsules. *J. Am. Chem. Soc.* **2010**, *132* (6), 1929–1938. https://doi.org/10.1021/ja908139y.

(97) Andreozzi, P.; Simó, C.; Moretti, P.; Porcel, J. M.; Lüdtke, T. U.; Ramirez, M. de los A.; Tamberi, L.; Marradi, M.; Amenitsch, H.; Llop, J.; Ortore, M. G.; Moya, S. E. Novel Core–Shell Polyamine Phosphate Nanoparticles Self-Assembled from PEGylated Poly(Allylamine Hydrochloride) with Low Toxicity and Increased In Vivo Circulation Time. *Small* **2021**, *17* (35). https://doi.org/10.1002/smll.202102211.

(98) Salvador, C.; Andreozzi, P.; Romero, G.; Loinaz, I.; Dupin, D.; Moya, S. E. Self-Assembled Oleic Acid-Modified Polyallylamines for Improved SiRNA Transfection Efficiency and Lower Cytotoxicity. *ACS Appl. Bio Mater.* **2023**, *6* (2), 529–542. https://doi.org/10.1021/acsabm.2c00845.

(99) Di Silvio, D.; Martínez-Moro, M.; Salvador, C.; de los Angeles Ramirez, M.; Caceres-Velez, P. R.; Ortore, M. G.; Dupin, D.; Andreozzi, P.; Moya, S. E. Self-Assembly of Poly(Allylamine)/SiRNA Nanoparticles, Their Intracellular Fate and SiRNA Delivery. *J. Colloid Interface Sci.* **2019**, *557*, 757–766. https://doi.org/10.1016/j.jcis.2019.09.082.

(100) Andreozzi, P.; Diamanti, E.; Py-Daniel, K. R.; Cáceres-Vélez, P. R.; Martinelli, C.; Politakos, N.; Escobar, A.; Muzi-Falconi, M.; Azevedo, R.; Moya, S. E. Exploring the PH Sensitivity of Poly(Allylamine) Phosphate Supramolecular Nanocarriers for Intracellular SiRNA Delivery. *ACS Appl. Mater. Interfaces* **2017**, *9* (44), 38242–38254. https://doi.org/10.1021/acsami.7b11132.

(101) Hernández-Vargas, H.; Palacios, J.; Moreno-Bueno, G. Molecular Profiling of Docetaxel Cytotoxicity in Breast Cancer Cells: Uncoupling of Aberrant Mitosis and Apoptosis. *Oncogene* **2007**, *26* (20), 2902–2913. https://doi.org/10.1038/sj.onc.1210102.

(102) Vakili-Ghartavol, R.; Rezayat, S. M.; Faridi-Majidi, R.; Sadri, K.; Jaafari, M. R. Optimization of Docetaxel Loading Conditions in Liposomes: Proposing Potential Products for Metastatic Breast Carcinoma Chemotherapy. *Sci. Rep.* **2020**, *10* (1), 1–14. https://doi.org/10.1038/s41598-020-62501-1.

(103) Liu, Y. L.; Chou, C. K.; Kim, M.; Vasisht, R.; Kuo, Y. A.; Ang, P.; Liu, C.; Perillo, E. P.; Chen, Y. A.; Blocher, K.; Horng, H.; Chen, Y. I.; Nguyen, D. T.; Yankeelov, T. E.; Hung, M. C.; Dunn, A. K.; Yeh, H. C. Assessing Metastatic Potential of Breast Cancer Cells Based on EGFR Dynamics. *Sci. Rep.* **2019**, *9* (1), 1–13. https://doi.org/10.1038/s41598-018-37625-0.

(104) Pimm, M. L.; Henty-Ridilla, J. L. New Twists in Actin-Microtubule Interactions. *Mol. Biol. Cell* **2021**, *32* (3), 211–217. https://doi.org/10.1091/MBC.E19-09-0491.

(105) Clarke, S. J.; Rivory, L. P.; Oncology, M.; Centre, S. C.; Prince, R.; Hospital, A. Clinical Pharmacokinetics of Docetaxel. *Clin. Pharmacokinet.* **1999**, *36* (2), 99–114.

(106) O'Brien, J.; Hayder, H.; Zayed, Y.; Peng, C. Overview of MicroRNA Biogenesis, Mechanisms of Actions, and Circulation. *Front. Endocrinol. (Lausanne).* **2018**, *9* (AUG), 1–12. https://doi.org/10.3389/fendo.2018.00402.

(107) Xin, Y.; Huang, M.; Guo, W. W.; Huang, Q.; Zhang, L. zhen; Jiang, G. Nano-Based Delivery of RNAi in Cancer Therapy. *Mol. Cancer* **2017**, *16(1)* (134), 1–9. https://doi.org/10.1186/s12943-017-0683-y.

(108) El Majzoub, R.; Fayyad-kazan, M.; Nasr El Dine, A.; Makki, R.; Hamade, E.; Grée, R.; Hachem, A.; Talhouk, R.; Fayyad-Kazan, H.; Badran, B. A Thiosemicarbazone Derivative Induces Triple Negative Breast Cancer Cell Apoptosis: Possible Role of MiRNA-125a-5p and MiRNA-181a-5p. *Genes and Genomics* **2019**, *41* (12), 1431–1443. https://doi.org/10.1007/s13258-019-00866-y.

(109) Ninio-many, L.; Hikri, E.; Burg-golani, T.; Stemmer, S. M. MiR-125a Induces HER2 Expression and Sensitivity to Trastuzumab in Triple-Negative Breast Cancer Lines Characterizing the Expression Profile Of. *Front. Oncol.* **2020**, *10* (191), 1–12. https://doi.org/10.3389/fonc.2020.00191.

(110) Yan, L.; Zhang, C. Y.; Wang, Y. B. MiR - 125a - 5p Functions as a Tumour Suppressor in Breast Cancer by Downregulating BAP1. *J. Cell. Biochem.* **2018**, *119* (11), 8773–8783. https://doi.org/10.1002/jcb.27124.

(111) Zhang, L.; Liao, Y.; Tang, L. MicroRNA-34 Family : A Potential Tumor Suppressor and Therapeutic Candidate in Cancer. **2019**, *5*, 1–13.

(112) Li, L.; Yuan, L.; Luo, J. MiR-34a Inhibits Proliferation and Migration of Breast Cancer through down-Regulation of Bcl-2 and SIRT1. **2013**, 109–117. https://doi.org/10.1007/s10238-012-0186-5.

(113) Bayraktar, R.; Ivan, C.; Bayraktar, E.; Kanlikilicer, P.; Kabil, N. N.; Kahraman, N.; Mokhlis, H. A.; Karakas, D.; Rodriguez-aguayo, C.; Arslan, A.; Sheng, J.; Wong, S.; Lopez-berestein, G.; Calin, G. A.; Ozpolat, B. Dual Suppressive Effect of MiR-34a on the FOXM1 / EEF2-Kinase Axis Regulates Triple-Negative Breast Cancer Growth and Invasion. 4225–4241. https://doi.org/10.1158/1078-0432.CCR-17-1959.

(114) Hong, D. S.; Kang, Y.; Borad, M.; Sachdev, J.; Ejadi, S.; Lim, H. Y.; Brenner, A. J.; Park, K.; Lee,

J.; Kim, T.; Shin, S.; Becerra, C. R.; Falchook, G.; Stoudemire, J.; Martin, D. Phase 1 Study of MRX34 , a Liposomal MiR-34a Mimic , in Patients with Advanced Solid Tumours. *Br. J. Cancer* **2020**, No. August 2019, 7–11. https://doi.org/10.1038/s41416-020-0802-1.

(115) Basak, M.; Chaudhary, D. K.; Takahashi, R. U.; Yamamoto, Y.; Tiwari, S.; Tahara, H.; Mittal, A. Immunocyte Derived Exosomes: Insight into the Potential Chemo-Immunotherapeutic Nanocarrier Targeting the Tumor Microenvironment. *ACS Biomater. Sci. Eng.* **2023**, *9* (1), 20–39. https://doi.org/10.1021/acsbiomaterials.2c00893.

XXXXXXX

Analytical and Bioanalytical Method development

Chapter II

2.1 Introduction

The development and validation of the analytical and bioanalytical methods for analyzing active pharmaceutical ingredient (API) is important and irreplaceable for determination of some important parameters including solubility of the API and formulation characteristics like % drug loading (DL), % entrapment efficiency (%EE) and unknown concentration of API in the release samples, stability and dosing measurements[1,2]. On the other hand, bio-analysis is considered as an essential prerequisite for several in vivo studies like pharmacokinetic (PK), toxicokinetics (TK), biodistribution (BD), and pharmacodynamic (PD) studies. The process of quantifying the API in the biological matrices (blood, plasma, serum, tissue, saliva, urine, faeces, etc.) requires high-throughput sample collection, sample cleaning, development of a sensitive method using hyphenated analytical techniques including high performance liquid chromatography (HPLC), liquid chromatography-tandem mass spectroscopy (LC-MS/MS), fluorometry and many more[3]. In this thesis work, DTX has been explored as the API for loading into exosomal formulation. HPLC/PDA and LC-MS/MS techniques were chosen for the development of the analytical and bioanalytical methods respectively. Several reports are already available for estimation of DTX using the above mentioned techniques; based on these reports, methods were developed and validated in lab. The ICH guidelines **Q2(R1)** and **M10** have been referred for the validation of the analytical and bioanalytical method respectively[4,5].

2.1.1 Analytical method development for quantification of DTX

In literature, several analytical methods have shown the suitability of the isocratic mobile phase in efficiently eluting and quantifying DTX under optimized chromatographic conditions. A simultaneous analytical method for quantifying DTX and cabazitaxel has been reported wherein, the mobile phase (water: methanol: acetonitrile ::42:32:26) in isocratic mode at 1.2 mL/min flow rate eluted DTX at 7.4 min which was detected at 232 nm[6]. Our lab has already reported a systematically validated analytical method for simultaneous analysis of DTX and α-lipoic acid. The isocratic mobile phase used was 35% v/v 10mM acetate buffer (pH 3.5) and 65 %v/v acetonitrile at 1mL/min flow rate; it exhibited DTX retention time of 5.82 min, detected at 227 nm. The method was found linear within the concentration range of 1-15 µg/mL and provided 98.26 ± 0.37% accuracy of lower QC sample (LQC) which is considered reliable for detection of DTX[7]. Another study has also reported the application of the mobile phase (0.1% o-phosphoric

acid: acetonitrile::40:60) in isocratic mode at 1mL/min flow rate and retention time of 7.2 min[8]. In another recent study, mobile phase composed of water: acetonitrile::35:65 at a flow rate of 0.8 mL/min retained DTX for 5.5 min and was found linear within the range 1-75 µg/mL with 93.08% accuracy for LQC[9].

2.1.2 Bio-analytical method development for quantification of DTX

In case of bioanalytical method development, sample preparation and method validation, both are equally important. 'Liquid-liquid extraction' (LLE) of DTX from the plasma matrix is well reported. Acetonitrile: n-butylchloride (1:4 v/v) solvent system was used to reconstitute the sample before HPLC analysis. With a mobile phase consisting of water: methanol: tetrahydrofuran: ammonium hydroxide :: 37.5:60.2:2.5:0.1 v/v at a flow rate of 1mL/min, LLOQ of DTX was found to be 88.5-108.6% accurate and extraction recovery was reported to be 84.3±6.8%[10]. In another study, methanol: acetonitrile (1:1 v/v) solvent system was utilized to precipitate the protein and extract DTX in the organic layer, which was further processed to be analyzed by LC-MS/MS method for developing a sensitive bioanalytical method of DTX. The calibration curve for DTX in mouse plasma was linear over the range 25–2500 nM. The LLOD was 8 nM and the LLOQ was 25 nM. With a linear gradient method at a flow rate of 0.25 mL/min, the transition (m→z) for DTX was 808.2→527.05 and 854.2→285.9 for PTX using electrospray ionization. The calibration curve thus plotted showed correlation coefficient >0.997, and ~100% recovery of QC smaples[11]. Another study has reported an isocratic LC method in combination with the mass spectrometric analysis of DTX in a dried blood spot. The mobile phase consisted of water and acetonitrile with 0.1% formic acid (45:55 v/v), eluted at 0.2 ml/min by MRM monitored transitions of DTX (830 → 303) and of PTX (835 → 247). The method was linear in 50- 3000 ng/mL range with an accuracy of 89%-114% and precision within 2.5-10.1%[12].

2.2. Materials and Methods

2.2.1 Materials

DTX (MW 829.9 Da) and PTX (MW 875.9 Da) were provided by Fresenius Kabi and M/s, INTAS Pharmaceuticals Ltd. as gift samples respectively. Acetonitrile (HPLC and LC-MS grade), Methanol (HPLC grade), EDTA disodium salt dehydrate and Formic acid were procured from Merck (Darmstadt, Germany). Ammonium accetate was obtained from CDH (New Delhi, INDIA).

Female swiss albino mice, 20-25 g were procured from the central animal facility (CPCSEA No. 417/PO/be/2001/CPCSEA), BITS Pilani, Pilani campus (India), as per approved animal protocol (IAEC/RES/31/03) and utilized for obtaining the plasma required for the bioanalytical calibration curve and QC sample preparation.

2.2.2. Methods

2.2.2.1 Development of analytical method for DTX

Chromatographic Conditions

DTX analytical method was developed in HPLC system (Shimadzu, Kyoto, Japan) coupled with a photodiode array (PDA) detector. The system was purged and equilibrated for half an hour before analyzing the samples. Chromatographic separation was carried out using Intersil® ODS (C18) column (250 × 4.6 mm, 5 µm) with isocratic flow of mobile phase consisting of acetonitrile: water in a ratio of 70:30 v/v with flow rate at 1 mL/min. The injection volume was kept as 80 µL and DTX was analyzed at a wavelength of 227 nm. The generated data was processed using LC solution software 1.22 SP1.

Preparation of stock solution, calibration solution and quality control samples

A primary DTX stock solution of 1 mg/mL was prepared by dissolving 10 mg of DTX in 10 mL of methanol (HPLC grade). From this main stock solution, secondary DTX stock solution of 10 µg/mL was prepared and utilized for preparation of the calibration samples. Six calibration samples i.e., 1000, 500, 250, 125, 50, and 25 ng/mL and 3 QC samples i.e., 750 ng/mL (High, HQC), 375 ng/mL (Medium, MQC), 62.5 ng/mL (Low, LQC) were prepared in n=6 replicates. For dilution, mobile phase was used as a diluent to prepare the analytical samples.

2.2.2.2 Validation of the analytical method

1. Linearity and Range

Total six calibration curves were prepared and analyzed in consecutive three days and the linearity of the method was established within 25-1000 ng/mL. The calibration curve was plotted between concentration of DTX vs. peak area (mAU). The regression line was also constructed and regression coefficient calculated.

2. Accuracy and Precision

For accuracy and precision analysis, the intra-day and inter-day sample analysis was carried out with HQC, MQC and LQC samples (n=3). As per the ICH guidelines, % bias and %RSD of analytical samples was calculated, these parameters are recommended to be within ±2%.

3. LOD and LOQ

Signal to Noise ratio (S/N) method was utilized to analyze LOD and LOQ. According to the guideline, LOD should have S/N≥3, and LOQ should have S/N≥10.

4. Specificity

Specificity was determined by analyzing the QC sample spiked with exosomes ~ 40 µg/mL. Any interference due to the presence of the exosomes was monitored at 227 nm wavelength.

2.2.2.3 Development of bio-analytical method for DTX using LC-MS/MS

Chromatographic and mass spectrometric conditions

The LC-MS/MS bioanalytical method of the DTX and PTX was developed using Waters Xevo TQD Triple Quadrupole consisting of quaternary solvent manager (Acquity UPLC H-Class), sample manager (Acquity UPLC), nitrogen generator compressor (PEAK Scientific), a triple quadrupole (Xevo TQD) mass analyzer with an ionization source (ZsprayTM). The chromatographic separation was achieved in an Acquity®BEH C18 column (150 × 2.1 mm, 1.7 µm; Waters Milford, USA), maintained at 30°C, while keeping the temperature of the sampler constant (4 °C) throughout the analysis. The mobile phase consisted of 0.01M ammonium acetate buffer (pH 5.5, maintained with 0.1% formic acid) and acetonitrile (10:90 v/v), eluted at 0.18 ml min^{-1}. MRM monitored transitions of DTX were: DTX m/z 829.9 → 304.07 (quantitation); m/z 830 → 303 and 830 → 549.26 (qualification) and IS m/z 875.9 → 308.05 (quantitation); m/z 835 → 308.05 and 835 → 591.21 (qualification). The injection volume was 10.0 µl. The mass spectrometry conditions optimized for analysis are shown in **Table 2.1**.

Table 2.1
Chromatographic parameters of mass spectrometry in LC-MS.

Molecule	Ion fragment Quantitation (m>z)	Capillary Voltage (kV)	Gas desolvation Temperature (˚C)	Flow rate of gas desolvation (L/h)	Cone Voltage (V)	Collision Energy MS (V)
DTX	829.9>304.07	3.75	450	750	42	22
PTX	875.9>308.05				90	28

Preparation of stock and calibration samples

Stock solution of DTX and PTX were prepared in ACN at a concentration of 1mg/ml. One-day prior to the LC-MS/MS analysis, all calibration samples were prepared in mice plasma matrix. Initially, working solutions of 2000-15.62 ng/ml DTX and 500 ng/ml of PTX were prepared in ACN before beginning the sample preparation. In 40 µL of EDTA containing mice plasma, required volume of DTX and PTX (of prepared working solutions) was added to prepare calibration samples (serially diluted) 200, 50, 12.5, 6.25, 3.125 and 1.56 ng/mL and vortexed for 1 min followed by further processing for sample preparation.

Sample preparation

ACN (1 ml) was used to precipitate the plasma proteins to extract out DTX and PTX into the organic layer. The samples were vortexed for 10 min and then centrifuged at 15,000 rpm for 15 min at 4˚C. The organic layer was collected and evaporated at 45˚ overnight under vacuum condition. The dried samples were further redispersed in 60 µl of ACN:water in 1:1 ratio and centrifuged at 15,000 rpm for 15 min at 4˚C prior to analysis in LC-MS/MS. The respective analysis was interpreted as [DTX] vs. $\frac{Area\ of\ [DTX]}{Area\ of\ [PTX\}}$ and the calibration curve (n=6) was used for the quantification of DTX in pharmacokinetic samples.

2.2.2.4 Validation of the bioanalytical method

1. Linearity and Range

Calibration samples i.e., 100, 50, 12.5, 6.25, 3.125 and 1.56 ng/mL were analyzed (n=6). Calibration curves were generated by correlating the nominal concentrations of the calibration samples with the peak area ratios from DTX and IS. While X axis represented [DTX], Y axis was plotted as $\frac{Area\ of\ [DTX]}{Area\ of\ [PTX\}}$. Further, the trend line equation, y=mx+c (m-slope and c-intercept) with correlation coefficient (R^2) was calculated.

2. Accuracy and Precision

For accuracy and precision analysis, the intra-day and inter-day sample analysis was carried out with HQC, MQC and LQC samples (n=3). As per the ICH guidelines, % bias and %RSD of analytical samples was calculated, these parameters are recommended to be within ±15%[3,5]. Although, % bias and %RSD for LLOQ is considered acceptable with ±20% variation from the true value

2.3. Results

2.3.1 Analytical method of DTX by HPLC

The HPLC based analytical method of DTX was successfully developed wherein the DTX showed R_T of 4.93 min (**Fig. 2.1**).

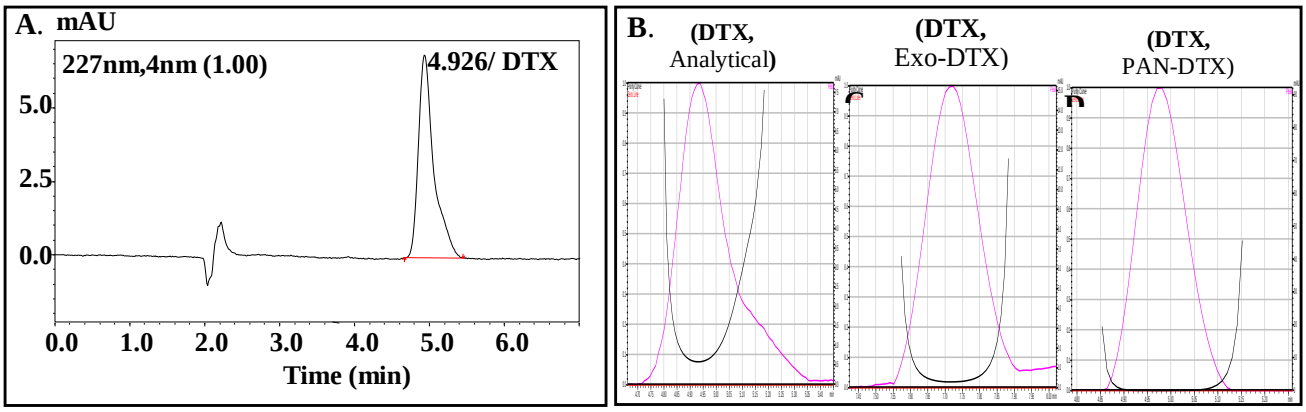

Figure 2.1 Representative chromatogram of (A) DTX (1000 ng/mL) without excipients and, (B-D) Peak purity curves of DTX (B) alone, and in the presence of (C) exosomes and (D) PAN particles

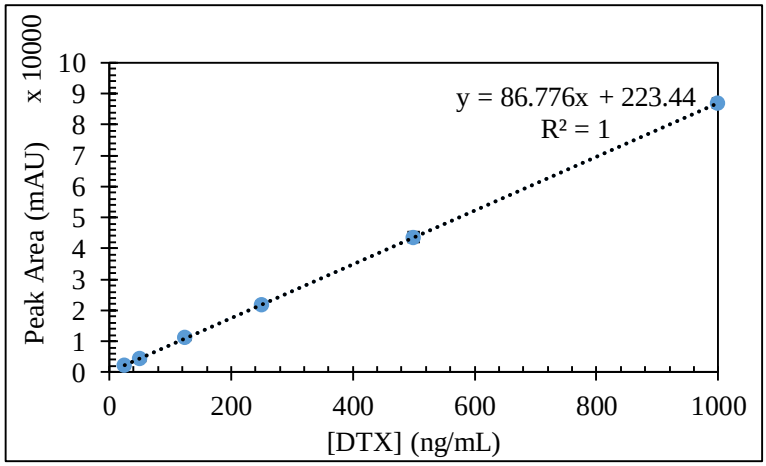

Figure 2.2 Representative calibration curve of DTX in linearity range of 25-1000 ng/mL.

1.Linearity and Range

All the six calibration curves (CC) showed linearity over the range 25-1000 ng/mL with the regression equation y = 86.776x + 223.44 (R^2=1.00) as indicated in **Figure. 2.2**.

Table 2.2

Interday and Intraday precision and accuracy of the QC samples of DTX

Analyte	Level	Nominal conc. (ng/ml)	Precision (%RSD)		Accuracy (%Bias)	
			Interday	Intraday	Interday	Intraday
Docetaxel (DTX)	LQC	62.5	2.04	2.47	4.97	5.42
	MQC	375	2.17	1.67	5.93	6.85
	HQC	750	2.67	1.44	4.58	5.78

2. Accuracy and Precision

The interday and intraday precision (%RSD) for QC samples was found to be 2.19-3.69 % and 1.44-2.96 % respectively (**Table 2.1**) although the recommended limit for precision is within ± 2%. This slight variation could be attributed to the lower concentration range selected within 1000-25 ng/mL for the validation of the method which requires high sensitivity difficult to obtain using HPLC. Likewise, interday and intraday accuracy of HQC and MQC was found within 4.58-5.9 % and 5.78-6.85%, which is ~ ±5%.

3. LOD and LOQ

According to the signal to noise (S/N) ratio, LOD and LOQ were found to be ~28.85 ng/mL and ~87.43 ng/mL respectively as per equation recommended by ICH Q2 (R1).

4. Specificity

The specificity of the method was verified by analyzing the analytical sample (1000 ng/mL) in the presence of excipients (exosomes and blank PAN) that are employed to formulate the drug delivery system of DTX. Interference of any of the excipients was not observed at the retention time of the analyte which confirmed the specificity of the analytical method. Representative chromatogram of the drug and peak purity curves are shown in **Fig 2.1 A and B-D** respectively. Peak purity for DTX in the presence of the exosomes and PAN particles were found to be>0.999.

2.3.2 Bioanalytical method of DTX by LC-MS/MS method

1. Linearity and Range

The developed method was found linear within the range 200-1.56 ng/mL with the calibration curve showing R^2 value of 0.9984. The representative calibration curve is plotted between [DTX] vs. and $\frac{Area\ of\ DTX}{Area\ of\ PTX}$ was generated using 3 replicates for each calibration sample.

2. ***Accuracy and Precision***

As **Table 2.3** shows the interday and intraday precision (%RSD) for biological QC samples, i.e., MQC and HQC samples was found to be 14.95-16.18 % and 12.67-15.28 % respectively, whereas precision is expected within ± 15%. For LQC only, the interday and intraday precision (%RSD) was found to be 19.72% and 17.84% which is acceptable for LLOQ (±20%). This slight variation in precision could be attributed to the very low concentration range selected within 200-1.56 ng/mL for the validation of the bioanalytical method. Likewise, interday and intraday accuracy of HQC and MQC was found within 7.97-9.51 % and 3.70-9.51%, which is ~ ±10%.

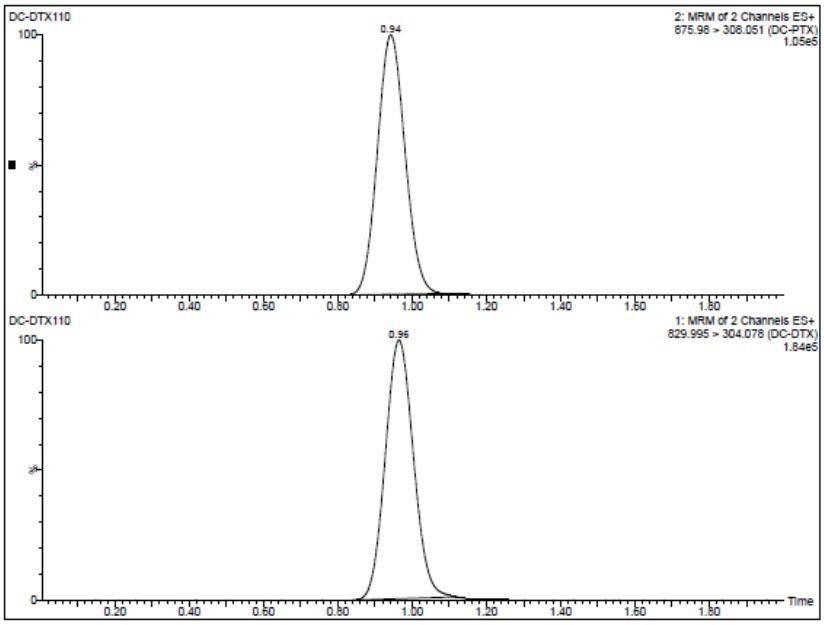

Figure 2.3 Representative chromatograms of DTX (100 ng/mL) and PTX (50 ng/mL) using LC-MS/MS **(**without any excipients) wherein, DTX showed R_T at 0.94 min and PTX at 0.96 min.

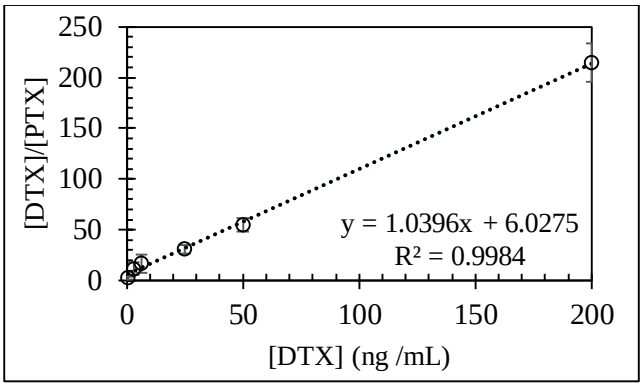

Figure 2.4 Representative CC for detection of DTX in bio-analytical samples using LC-MS/MS method from DTX concentration vs. $\frac{Area\ of\ DTX}{Area\ of\ PTX}$ profile wherein, PTX was used as an internal standard (IS). The CC has been prepared from n=3 sets of the calibration samples and the data is presented here as mean (n=3) ±SD.

Table 2.3
Interday and Intraday precision and accuracy of the bioanalytical QC samples of DTX.

Level	Nominal conc. (ng/ml)	Precision (%RSD)		Accuracy (%Bias)	
		Interday	Intraday	Interday	Intraday
LQC	3.25	19.72	17.84	3.46	4.97
MQC	25	16.18	12.67	7.97	3.70
HQC	100	14.95	15.28	9.51	5.65

2.4 Discussion

A simple and concise analytical method has been developed using RP-HPLC/UV method to detect DTX using binary solvent system (ACN: water = 7:3) at 1.0 mL/min flow rate. The developed method will be utilized to analyze the entrapped drug in the formulation and for *in vitro* release analysis. The optimized method was found reliable to detect DTX upto 87.43 ng/mL whereas LOD was 28.85 ng/mL. As the method was well established by our lab previously, a partial validation was performed for the analytical method of DTX[7]. LC-MS/MS methods are well reported for the establishing a highly sensitive method optimized to detect the drug in both in vitro and in vivo samples. The optimized method was reliable in analyzing the bioanalytical samples containing DTX in the concentration range of 1.56-200 ng/mL wherein, the interday accuracy and precision with LQC sample was achieved with less than 20% and 15% respectively[3,13]. The validated method was utilized to analyze the PK samples wherein, the study has been performed with DTX dose as 1mg/kg body weight of the healthy Swiss albino mice.

2.5 References

(1) Sharma, S.; Goyal, S.; Chauhan, K. A Review on Analytical Method Development and Validation. *Int. J. Appl. Pharm.* **2018**, *10* (6), 8–15. https://doi.org/10.22159/ijap.2018v10i6.28279.

(2) Krull, I. S.; Swartz, M. Analytical Method Development and Validation for the Academic Researcher. *Anal. Lett.* **1999**, *32* (6), 1067–1080. https://doi.org/10.1080/00032719908542878.

(3) Moein, M. M.; El Beqqali, A.; Abdel-Rehim, M. Bioanalytical Method Development and Validation: Critical Concepts and Strategies. *J. Chromatogr. B Anal. Technol. Biomed. Life Sci.* **2017**, *1043*, 3–11. https://doi.org/10.1016/j.jchromb.2016.09.028.

(4) European Medicines Agency ICH. Q2 (R1): Validation of Analytical Procedures: Text and Methodology. *Int. Conf. Harmon.* **2005**, *2* (May 1997), 1–15.

(5) International Conference on Harmonization, I. M10 Bioanalytical Method Validation. **2019**, No. February, Stability studies on rFVIIIFc drug substance. 1–14.

(6) Lazzarini, R.; Salvadori, S.; Trapella, C.; Guerrini, R.; Marzola, E.; Pasini, G.; Dalpiaz, A. Physicochemical Stability of Cabazitaxel and Docetaxel Solutions. *Eur. J. Hosp. Pharm.* **2015**, *22* (3), 150–155. https://doi.org/10.1136/ejhpharm-2014-000558.

(7) Kothari, I. R.; Italiya, K. S.; Sharma, S.; Mittal, A.; Chitkara, D. A Rapid and Precise Liquid Chromatographic Method for Simultaneous Determination of Alpha Lipoic Acid and Docetaxel in Lipid-Based Nanoformulations. *J. Chromatogr. Sci.* **2018**, *56* (10), 888–894. https://doi.org/10.1093/chromsci/bmy064.

(8) Kumbhar, P. S.; Diwate, S. K.; Mali, U. G.; Shinde, T. U.; Disouza, J. I.; Manjappa, A. S. Development and Validation of RP-HPLC Method for Simultaneous Estimation of Docetaxel and Ritonavir in PLGA Nanoparticles. *Ann. Pharm. Fr.* **2020**, *78* (5), 398–407. https://doi.org/10.1016/j.pharma.2020.07.004.

(9) Aires-Fernandes, M.; Eloy, J. O.; Damiani Victorelli, F.; Scanavez Ferreira, P.; Pironi, A. M.; Chorilli, M. Reversed-Phase High-Performance Liquid Chromatography: A Fast and Efficient Analytical Method to Quantify Docetaxel-Loaded Pegylated Liposomes in Release Study. *J. Sep. Sci.* **2021**, *44* (21), 3986–3995. https://doi.org/10.1002/jssc.202100382.

(10) Loos, W. J.; Verweij, J.; Nooter, K.; Stoter, G.; Sparreboom, A. Sensitive Determination of Docetaxel in Human Plasma by Liquid-Liquid Extraction and Reversed-Phase High-Performance Liquid Chromatography. *J. Chromatogr. B Biomed. Appl.* **1997**, *693* (2), 437–441. https://doi.org/10.1016/S0378-4347(97)00089-3.

(11) Hou, W.; Watters, J. W.; McLeod, H. L. Simple and Rapid Docetaxel Assay in Plasma by Protein Precipitation and High-Performance Liquid Chromatography-Tandem Mass Spectrometry. *J. Chromatogr. B Anal. Technol. Biomed. Life Sci.* **2004**, *804* (2), 263–267. https://doi.org/10.1016/j.jchromb.2004.01.021.

(12) Raymundo, S.; Muller, V. V.; Andriguetti, N. B.; Tegner, M.; Artmann, A. C.; Kluck, H. M.; Franzoi, M. A.; Vilela, R. M. M.; Schwartsmann, G.; Linden, R.; Antunes, M. V. Determination of Docetaxel in Dried Blood Spots by LC–MS/MS: Method Development, Validation and Clinical Application. *J. Pharm. Biomed. Anal.* **2018**, *157*, 84–91. https://doi.org/10.1016/j.jpba.2018.05.011.

(13) Kollipara, S.; Bende, G.; Agarwal, N.; Varshney, B.; Paliwal, J. International Guidelines for Bioanalytical Method Validation: A Comparison and Discussion on Current Scenario. *Chromatographia* **2011**, *73* (3–4), 201–217. https://doi.org/10.1007/s10337-010-1869-2.

miR-125a Exo-DTX

Development and Evaluation of Human Umbilical Cord Blood Derived Mesenchymal Stem Cell (hUCBMSC) Derived Exosomal Formulation for Co-Delivery of DTX and mir-125a in Breast Cancer

Chapter III

3.1. Introduction

As discussed in **Chapter I**, the cargo as well as the yield of exosomes may change depending upon physiological stress as well as the pathological conditions[2]. Exosomes, either from bio-fluids (plasma, saliva, urine, amniotic fluid, umbilical cord Wharton's jelly, bovine milk etc.) or conditioned media from cells (grown under *in vitro* conditions) have recently gained tremendous attention as a biogenic nanocarrier of therapeutics for the treatment of different pathological conditions[3]. Among all, MSCs having inherent immunosuppressive properties, produce immunosuppressive exosomes that can easily overcome the allogenic rejection and confer easy acceptance by the target cells[4]. Currently the field of MSC exosomes is undergoing extensive research to explore their application in cancer therapeutics, especially the regulatory role of MSCs derived exosomes. In a recent study, bone marrow (BM) MSC derived exosomes, enriched with miR-100 showed tumor suppression by down regulating VEGFR-I expression via HIF-I/ mTOR mediated pathway in BC cells, MCF-7 and MDA MB-231, at the dose of 80 μg/mL; while another study reported BM MSC exosomes (200 μg/mL) induces angiogenesis by upregulating VEGF in both *in vivo* models of gastric carcinoma (SGC-7901) and colon carcinoma (SW-480)[5,6]. These observations highlight the conflicting role of MSC exosomes in cancer pathophysiology in spite of being derived from the same source.

Among the different sources explored for procuring MSCs, in this thesis work, human umbilical cord blood (hUCB) derived MSCs (hUCBMSC) were chosen as one of the sources of exosomes (*named as* hUCBMSC Exo) considering that the procurement of the hUCB is completely non-invasive, least unethical and safe. Also, the ability to undergo extensive scale-up under *in vitro* conditions makes hUCBMSCs one of the most appropriate source to isolate MSC exosomes[7]. hUCBMSCs have also been functionally characterized to be anti-inflammatory and anti-tumorigenic in different cancers. They have already been reported to suppress cancer stemness in BC, tumorigenesis in Kaposi sarcoma, and also induce cytotoxicity in U87 glioma cells[8–10]. Several reports have claimed that human umbilical cord MSC derived exosomes are anti-tumorigenic due to presence of miR-375, miR-451a and miR-181, which suppresses expression of enabled homolog (ENAH) in squamous cell carcinoma, downregulates a Disintegrin and metalloprotease 10 (ADAM 10) mediated EMT in hepatocellular carcinoma and retards lysine-specific demethylase 5C (KDM5C) in nasopharyngeal carcinoma respectively[11–13]. Recently, it

has been reported that the hUCBMSCs derived exosomes inherently carry miR-503-3p which significantly down regulates the mesoderm specific transcript (MEST) and suppresses the cellular growth in endometrial carcinoma [14]. Thus, hUCBMSCs derived exosomes were selected as the biogenic nanocarrier for DTX and their cargo was further enriched with TS miR-125a by prior transfection of the source cells to obtain DTX and miR-125a co-loaded exosomal formulation.

Among all the biomolecules explored lately, RNAi (interfering RNAs) is one of the most intriguing example as it can regulate physiological functions at transcriptomic level. Among RNAi(s), miRNA plays a significant role in regulating the gene expression by modulating the target mRNAs either as oncomiRs stimulating oncogenesis or TS miRNAs, suppressing the tumor[15]. miR-125a is a well-known TS miRNA which specifically targets the HER2/ ErbB2 (EGFR subfamily) mediated signaling pathway that contributes to the migratory nature of aggressive BC cells [16]. Basal level of the miR-125a transcript has been reported to be under-expressed in human BC tissues by 1.75-fold in comparison to the normal breast epithelial cells. miR-125a-3p has been shown to increase the expression of the ErbB2 which eventually reduces the invasiveness of the cancer cells [17]. Also, miR-125a-5p was reported to suppress BC susceptibility gene 1–associated protein 1 (BAP1) resulting in induction of cancer cell apoptosis [18]. Hence, we chose miR-125a as one of the therapeutic macromolecules to be co-loaded with DTX in hUCBMSC Exo.

Considering the formulation aspect, the co-loading of anti-cancer small molecule with a TS miRNA in exosomes is a concept still in its infancy. Although this kind of co-delivery has been explored with synthetic nano-formulations like core-shell tecto dendrimers, chitosome, PEI-PLGA nanoparticles and hyaluronic acid/chitosan nanoparticles; the exploration of exosomes as a nanocarrier for the simultaneous delivery of both the therapeutic molecules is less explored[19–22]. We came across just a single study reporting the exosomal co-loaded formulation of DOX and hydrophobically modified miR-159 wherein, the loading of the therapeutics was carried out by overnight incubation and produced synergistic effect in terms of cellular apoptosis, uptake and bio distribution in malignant tumors[23].

For this objective, we strategically transfected the source hUCBMSCs with miR-125a using a plasmid vector of the miRNA which conferred around 2 folds' and 1.8 folds' increase in the expression of miR-125a in hUCBMSC and the exosomes isolated from them respectively. Then, DTX was loaded by an optimized formulation technique comprising of mild-sonication and

incubation to develop a miR-125a and DTX co-loaded exosomal formulation (miR-125a Exo-DTX). Further, the formulations (hUCBMSC Exo-DTX and miR-125a Exo-DTX) were assessed for in-vitro efficacy in TNBC 4T1 cells by an anti-proliferative assay, cellular uptake and release study. The anti-migratory effect of the formulations was assessed by wound healing, transwell invasion and morphological deformation assays. The mechanism underlying morphological deformation was also confirmed by morphometric microscopy and F-actin degradation assay.

3.2. Materials and Methods

3.2.1. Chemicals and Cell culture

Dulbecco's modified Eagle's medium (Gibco™ DMEM, high glucose) and Fetal bovine serum (FBS) were purchased from GIBCO (Invitrogen Inc. Gibco BRL, USA). Penicillin plus streptomycin solution, 3-(4,5-dimethylthiazol- 2-yl)-2,5-diphenyltetrazolium bromide (MTT) and Tween 20 were obtained from Sigma-Aldrich (St. Louis, MO, USA). Pierce™ Bicinchoninic acid (BCA) protein assay kit, PKH26 red fluorescent cell linker mini kit (MINI 26-1KT), Pierce® Fast western blot kit and ECL substrate (#35055), StemPro™ Adipogenesis Differentiation Kit (A1007001), StemPro™ Osteogenesis Differentiation Kit (A1033201) and StemPro™ Chondrogenesis Differentiation Kit (A1007101) were obtained from Thermo™ Scientific (Waltham, USA). DTX was kindly donated by Fresenius Kabi (New Delhi, India). Other solvents and reagents were of analytical grade and were obtained from Merck (Darmstadt, Germany). Anti-CD81 mouse mAb [# ab109201], Anti-TSG101 mouse mAb antibody [#ab125011], anti-CD63 mouse mAb [# ab59479] and Rhodamine Phalloidin (# ab235138) were procured from Abcam (Waltham, USA). Anti-CD73, CD90, and CD105 (BioLegend, San Diego, CA, USA), and anti-CD45 and CD34 (BioLegend, San Diego, CA, USA), HLA-DR (BD Biosciences, San Jose, CA, USA) were also procured. 2-well culture inserts were procured from ibdi GmbH (Martinsried, Germany) and Falcon® Transwell inserts with 8 μm PET membrane (for 24-well plate) from Corning (Riverfront Plaza, USA). For transfection purpose, human miR-125a expression plasmid (SC40082) and pCMVMIR vector for miRNA expression cloned with green fluorescent protein (GFP) were designed by OriGene, USA. Also, the transfection efficiency was ascertained by using TaqMan MicroRNA Assays (Applied Biosystems), TaqMan MicroRNA Reverse Transcription Kit (Applied Biosystems, Life Technologies, USA) and miRNeasy® Mini Kit (Qiagen, USA). For isolation and quantification of miRNAs, miRVana™ miRNA isolation kit (Life Technologies) and Quant-iT™ Ribogreen™ RNA assay kit (Invitrogen, Oregon) were also purchased.

For cell culture, murine BC cells (4T1) were obtained as a gift from Professor Avinash Bajaj, Regional Center of Biotechnology, Haryana, India. The hUCBMSC procurement protocol was approved by Institutional Committee for Stem Cell Research (IC-SCR; Code: 2019-03-IMP-08), Sanjay Gandhi Postgraduate Institute of Medical Sciences (SGPGI), Lucknow, Uttar Pradesh, India. This part of the thesis was carried out in collaboration with Prof. Swasti Tiwari, Professor and Head, Division of Molecular Medicine & Biotechnology Sanjay Gandhi Post Graduate Institute of Medical Sciences (SGPGIMS), Lucknow, U.P, India.

3.2.2. Biospecimen collection for isolation and characterization of hUCBMSCs

After isolation of hUCBMSCs from human UCB as per the approved protocol (IC-SCR; Code: 2019-03-IMP-08), the hUCBMSCs were propagated to 3^{rd}-5^{th} passage and were further characterized using MSC positive markers anti-CD73, CD90, CD105, and negative hematopoietic markers anti-CD45 and CD34, HLA-DR by confocal microscopy (Fluo-View F10i confocal microscope, Olympus) and flow cytometry (Becton Dickinson, New Jersey, USA)[24]. To evaluate hUCB-MSCs' ability to undergo trilineage differentiation, StemPro™ Adipogenesis Differentiation KIT, StemPro™ Osteogenesis Differentiation Kit, and StemPro™ Chondrogenesis Differentiation Kit were used.

3.2.3. Transfection and characterization of transfected hUCBMSCs

The hUCBMSCs at the 3^{rd} passage were seeded in a 96-well plate at a density of 1.5×10^5 cells/cm^2 for attachment. After 24 h, the sub-confluent monolayers were transfected with 500 ng/µl, pCMV – MIR vector/miR-125a carrying the GFP gene using Lipofectamine™ RNAiMAX Transfection Reagent (Invitrogen, Oregon) and the green fluorescence signals were observed under a fluorescent microscope 48 h after transfection.

3.2.4. Isolation and Characterization of hUCBMSC and miR-125a transfected hUCBMSCs derived exosomes

3.2.4.1. Isolation of hUCBMSC and miR-125a transfected hUCBMSCs derived exosomes

The following flow chart represents the optimized process for isolation of the exosomes from hUCBMSCs-

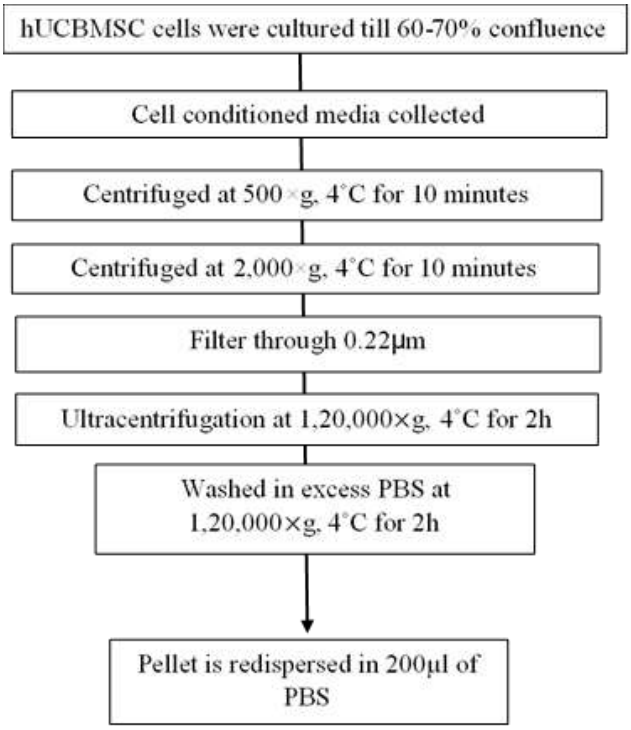

3.2.4.2. Characterization of hUCBMSC and miR-125a hUCBMSC exosomes

Particle size, PDI, zeta-potential and protein quantification

These isolated exosomes were characterized for particle size and zeta-potential by dynamic light scattering by Litesizer™ 500 (Anton Paar, Graz, Austria). Morphology was studied using FESEM by FEI (Apreo-loVac, Hillsboro, USA). The intact exosomes were also quantified by Pierce® BCA Kit (Pierce, BCA Protein Assay Kit, Thermo Scientific, Pittsburg, PA).

Expression of exosomal proteins

The hUCBMSCs cells and their derived exosomes were lysed in RIPA buffer using a freshly prepared protease inhibitor cocktail (Roche Diagnostics, Germany) and protein concentration was determined by the Pierce® BCA Kit. Proteins was denatured and resolved on 15% SDS-PAGE gel and transferred to PVDF membrane. Membrane was incubated overnight with exosomal markers; mouse anti-TSG101, anti-CD63, and anti-CD81 antibody followed by HRP-conjugated secondary antibody. The membrane was visualized by an enhanced chemiluminescence detection system. Images were acquired on a ChemiDoc imaging system (Universal Hood III, Bio-Rad, California, USA).

Quantification of miR-125a expression in transfected exosomes

After 72 h of transfection, media containing exosomes was collected and exosomes were isolated from it as described previously (*section no. 3.2.4.1*). Total RNA including microRNA from exosomes was extracted by using Qiagen miRNeasy Mini Kit according to the manufacturer's instructions. RNA concentrations were measured with NanoDrop (SIMPLINANO™ Spectrophotometer, Biochrom) and subsequently quantified by RT-PCR.

The expression of miR-125a was quantified by the TaqMan MicroRNA Assay (Applied Biosystem) according to the manufacturer's protocol. Briefly, 10 ng of miRNA was converted to cDNA by a TaqMan MicroRNA Reverse Transcription Kit according to the manufacturer's instructions. Then the cDNA products were used to quantify the expression of microRNA. miR-125a expression fold change was calculated by the $2^{-\Delta\Delta CT}$ method. 18S was used as the normalization control.

3.2.5. Development and characterization of exosomal formulations of DTX (hUCBMSC Exo-DTX and miR-125a Exo-DTX)

3.2.5.1. Development of DTX loaded hUCBMSC Exosomes (hUCBMSC Exo-DTX and miR-125a Exo-DTX)

hUCBMSC Exo-DTX was prepared by a combination of mild sonication and incubation technique. hUCBMSC-Exo (200 µg surface protein equivalent) was probe sonicated (Sonics Vibra-Cell™, USA) with 50 µL of DTX (1 mg/mL in methanol) and tween 80 (0.02% v/v in 10 mM PBS) at an amplitude of 15% for 4 cycles; each cycle comprised of 30 sec "on" and 30 sec "off" followed by an intermediate incubation period (IP) of 2 min (on ice) after each cycle. Post-sonication, hUCBMSC Exo-DTX were incubated for 2 h at 37℃ to allow the exosomal membrane to recover and reseal. Excess of unloaded DTX was separated from hUCBMSC Exo-DTX by centrifugation at 10,000 rpm for 10 min at 4℃. To obtain the hUCBMSC Exo-DTX, another cycle of ultra-centrifugation at 1,20,000× g, 4℃, for 90 min was carried out to pellet down the DTX loaded exosomes. Once obtained, these were further redispersed into 200 µL of 1X PBS and stored at -80℃ till further use. miR-125a Exo-DTX was also prepared following the similar procedure and the optimized process parameters and compared for physical properties and loading capacity with the untransfected hUCBMSC Exo-DTX.

3.2.5.2. Optimization of process parameters for formulating hUCBMSC-Exo DTX and miR-125a Exo-DTX

Different process parameters involved in the formulation of hUCBMSC-Exo-DTX were optimized including (a) exosome: drug (Exo: DTX) ratio, (b) number of sonication cycles (carried out during formulation development), (c) percentage of tween 80 used and, (d) batch size i.e., total exosome content (µg protein equivalent). For optimization of exosomal formulations, the above-mentioned process parameters were varied one at a time keeping other parameters constant, to evaluate their effect on drug loading (% DL), particle size and capacity of exosomes [DTX (ng)/exosome (µg)] as depicted in **Table 1.** Also, the effect of the process parameters was determined on the miRNA retention capacity of exosomes by quantifying total miRNA content in miRNA 125a exosomes before and after formulating miR-125a Exo-DTX.

3.2.5.3. Characterization of the formulations

***Size, size distribution and morphology*:** The particle size and polydispersity index (PDI) of unloaded exosomes and their respective Exo-DTX formulations were determined using Litesizer™ 500 (Anton Paar, Graz, Austria) with 173° backscattering, at 25° C, equilibration time (1 min) and 10 runs per sample while zeta-potential (mV) was analysed at 50 runs per sample with maximum 40V beam energy. The samples were used undiluted for the DLS analysis, while for FESEM, DTX loaded exosomes (50 µg equivalent protein) were fixed with 2% paraformaldehyde on cover-slip and dehydrated with ethanol in ascending concentrations (from 30%-90%) followed by analysis by FESEM (FEI, Apreo-loVac, Hillsboro, USA).

***DL, capacity and miRNA retention**:* Analytical method for the quantification of DTX as described in Chapter 2 (*section 2.2.2*) was utilized for estimating the % DL and capacity. DL and capacity were calculated using **Equation 3.1 and 3.2**.

For estimating the amount of miRNA retained into the exosomes after carrying out the drug loading process; miR-125a Exo-DTX formulation was prepared using miR-125a transfected exosomes (100 µg equivalent protein). miRNA was isolated from both naive miR-125a exosomes and miR-125a Exo-DTX using miRVana™ miRNA isolation kit (Life Technologies). The miRNA content in the exosomes before and after loading of DTX was evaluated by Quant-iT™ Ribogreen™ RNA assay kit. The quantification of miRNA thus, provided an insight into the impact of the drug loading process onto the miRNA retention capacity of exosomes (**Equation 3.3**).

$$\text{Drug Loading (\%DL)} = \frac{\text{Amount of drug loaded}}{\text{Total Amount of drug taken and carrier}} \times 100 \ldots\ldots \textbf{Equation 3.1}$$

$$\text{Capacity (ng drug/µg Exosomes)} = \frac{\text{Content of drug loaded in the exosomes (ng)}}{\text{Content of exosomes (µg protein)}} \ldots\ldots \textbf{Equation 3.2}$$

$$\text{\% miRNA retention capacity: } \frac{miRNA\ (ng)\ in\ the\ miR{-}125a\ Exo{-}DTX}{miRNA\ (ng)\ in\ miR{-}125a\ Exosome} \times 100 \ldots\ldots\ldots \textbf{Equation 3.3}$$

3.2.5.4. *In vitro* DTX release and stability study

The in-vitro release of DTX from hUCBMSC Exo-DTX was evaluated by the dialysis method wherein, the formulation was dispersed in PBS (10mM, pH 7.2) containing 0.2% Tween 80 and transferred to a regenerated cellulose dialysis tube bag (Snakeskin™ dialysis tubing, Thermo Fisher, MWCO3500 Da). The dialysis bag was immersed in 5 mL of release media and at each preset time point, release media was withdrawn and replaced with the fresh one to ensure maintenance of the sink conditions. The amount of DTX released from Exo-DTX was estimated and release profiles were plotted. Also, a week long stability study at -20˚C was performed to evaluate the effect of the process parameters on the exosomal integrity of the hUCBMSC Exo-DTX formulations. The response parameters considered here were, particle size (nm), zeta-potential (mV) and Capacity (ng DTX/µg exosomes).

3.2.6. In-vitro functional assays

Cell culture studies

Murine 4T1 cells were cultured in growth medium (DMEM+10% FBS+100 IU/mL penicillin-streptomycin) and incubated at 37 ℃ in a humidified atmosphere with 5% CO_2. Prior to treatment, the cells were seeded and incubated under the above mentioned conditions for 12 h to permit their adherence to the culture plate or flask.

3.2.6.1. Anti-proliferative study

2.5×10^3 cells per well were seeded in a 96 well plate and allowed to attach overnight. The anti-proliferative effect of the both miR-125a Exo-DTX and hUCBMSC Exo-DTX formulations was evaluated in comparison to the free DTX (10-500 ng/ml) on 4T1 cells after 48h. Blank hUCBMSCs exosomes (untransfected and miR-125a transfected) having protein content equivalent to Exo-DTX (containing 250 and 100 ng/mL DTX) were also studied to evaluate the effect of naïve exosomes on cellular viability of 4T1 as well. MTT assay was carried out after 48 h of incubation

following standard protocol. The IC_{50} of the free DTX and the Exo-DTX formulations was reported and compared statistically.

Also, the effect of the free DTX (100 ng/mL), blank exosomes (~10 µg/mL protein) and corresponding Exo-DTX (~100 ng/mL DTX) formulations, i.e. hUCBMSC Exo-DTX and miR-125a Exo-DTX on the cellular morphology and proliferation of 4T1 after 48h of incubation was ascertained by FESEM at 500X magnification.

3.2.6.2. Cellular uptake study

4T1 cells (1.0×10^4 cells/well) were seeded in a 24-well plate on coverslips and allowed to attach and form a monolayer overnight. A time dependent (1h/3h/6h/12h) cellular uptake study was performed in the cells with both naïve PKH26 dye labelled and Coumarin 6 (COU6) loaded untransfected exosomes. At predetermined time-points, the cells were washed twice with PBS followed by fixing the cells with 2.0% paraformaldehyde (PFA). The nuclei of the cells were stained with DAPI and viewed under a fluorescence microscope (AXIOVERT A1, Zeiss).

3.2.6.3. Wound healing assay

4T1 cells were seeded in a culture-insert at a density of 2.1×10^4 cells per well. After allowing the cells to attach overnight, the culture insert was removed and the cells were washed with PBS to remove non-adherent cells. Fresh media containing free DTX, hUCBMSC Exo-DTX, miR-125a Exo-DTX (100 ng/mL) and equivalent untransfected and miR-125a exosomes was replaced and images of different fields (n=3) were captured at 0, 6, 12, 24, 36, 48 h. The area of the wound at 12, 24, 36 h were analysed and the wound area was compared by Image J software and the %wound healing was calculated (**Equation 3.4)**.

$$\%\text{Wound Healing}=\frac{(A_0-A_t)}{A_0}\times 100 \quad \ldots. \textbf{Equation 3.4}$$

($where, A_0$ is the area of the wound at zero time-point andA_t is the area of the wound at time point, t)

3.2.6.4. Transwell invasion assay

For this assay, Corning® Matrigel® Basement Membrane matrix, LDEV free (Product No. 354234), 300 µg/mL in DMEM was cast in the upper chamber of a transwell (8 µm pore filter) in a 24-well plate to mimic the basement membrane. 10×10^4 cells were seeded onto it and incubated

for 12h followed by treatment with blank exosomes and respective Exo-DTX formulations in DMEM+5% FBS. The lower chamber was filled with DMEM+10% FBS (as chemoattractant). After 48h of treatment, the cells remaining on the Matrigel bed of the insert were removed with a cotton swab and the cells which transversed to the lower surface of the transwell were fixed with methanol for 5 min. The fixed cells were stained with 0.1% crystal violet and visualized by microscopy. The average number of cells which migrated per field were counted to determine the comparative %invasion of the cells after different treatments (n=3).

3.2.6.5. Cytoskeletal deformation assay

4T1 cells were grown on the coverslips to form a monolayer of cells for 12 h prior to the treatment. Cells were treated with 100 ng/mL of free DTX, hUCBMSC Exo-DTX, miR-125a Exo-DTX and an equivalent concentration of hUCBMSC exosomes for 48 h followed by fixing them with 4% PFA.

For FESEM, the fixed cells were washed with increasing concentrations of ethanol (30%, 50%, 70% and 90%) to dehydrate them and air dried overnight. The samples were chromium sputtered and visualized using electron beam at a magnification of 3000X.

3.2.6.6. F-actin degradation assay

For confocal microscopy (Carl Zeiss, model no: LSM 880), the cells were grown on the coverslip for 24 h after seeding, the cells were then treated with 100 ng/mL of free DTX, hUCBMSC Exo-DTX, miR-125a Exo-DTX and an equivalent concentration of hUCBMSC exosomes for 48 h. Post 48 h, the cells fixed with 4% PFA followed by staining with Rhodamine phalloidin dye (to stain F-actin) for 1 h at room temperature. The nuclei of the cells were then counter-stained with DAPI followed by washing thrice with chilled PBS. Fluorescence images of the cells were captured using a confocal microscope

3.3. Results

3.3.1. Characterization of hUCBMSC and hUCBMSC derived exosomes

The differentiation of mononuclear cells (MNCs) from the UCB into hUCBMSCs was ascertained by their inherent adhesiveness to the culture flask surface along with rapid fibroblast-like bipolar transformation of cells in the culture media (**Fig. 3.1.A**). Additionally, MSCs were found strongly positive for MSC marker proteins, CD73 (99.77%), CD90 (99.90%), and CD105 (99.36%), almost negative for CD34 (0.11%), CD45 (0.15%) and HLA-DR (0.01%) as revealed by flow cytometry

(**Fig. 3.1.B**) as well as by immunocytochemistry (**Fig. 3.1.C**). The ability of the MSCs to differentiate into osteogenic (21st day from induction), adipogenic (14th day from induction) and chondrogenic cells (28th day from the induction) was also demonstrated by Alizarin Red S, Oil-o-Red and Alcian blue assay (**Fig. 3.1. D**). While, loose clusters of the fibroblast-like shaped cells indicate their osteogenic nature, presence of lipid droplets (adipocyte differentiation indicator of cells) within 14 days of induction and Alcian blue mediated proteoglycan complexation after 28 days clearly indicated the adipogenic and chondrogenic differentiation of the MSCs in the differentiating media.

Further, hUCBMSCs derived exosomes were characterized for the presence of distinct exosomal transmembrane proteins, CD63, CD81 and cytosolic protein, TSG101 in exosome lysate (EL) in comparison to the cell lysate (CL). Also, the absence of the housekeeping protein, β-actin in EL in comparison to CL indicated that these vesicles were not merely cellular membrane enclosed cytosol (**Fig. 3.2.A**). **Table 2** clearly showed that hUCBMSC and miR-125a exosomes exhibited almost same particle size of 185 nm with high polydispersity index (>0.2) and characteristic negative surface charge -6 to -10 mV by DLS. Exosomes demonstrated 60-180 nm of size with spherical morphology and presence of clumps in FESEM images (**Fig. 3.2.B**). After loading of DTX, exosomal size was increased without any alteration in their morphology as indicated in **Table 3 and Figure 3.2.C and D** respectively**.**

.

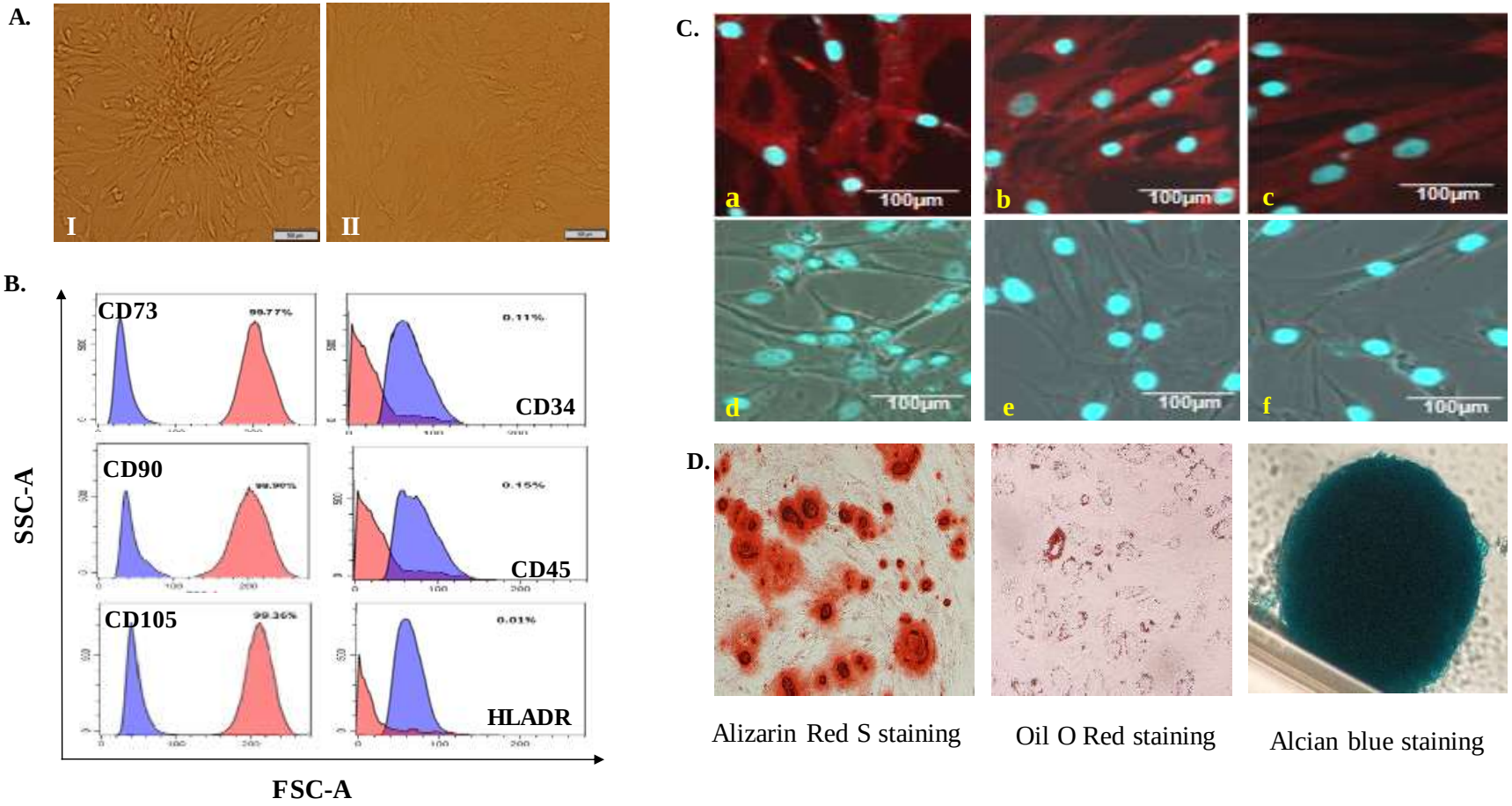

Figure 3.1. Characterization of hUCBMSCs. A. Morphological transformation of MNCs to hUCBMSCs characterized by fibroblastic shape (in passage 1) and bipolar fibroblastic morphology (in passage 3) (II) by light microscopy, scale bar 500 µm B. Flow cytometry expression of positive MSC marker proteins (left panel) CD73, CD90 & CD 105 and lack of expression of negative MSC marker protein (right panel) CD34, CD45 & HLA-DR, C. immunocytochemistry showed that cells were positive for typical MSC markers CD73 (a), CD90 (b) and CD105 (c) & lacked expression of hematopoietic markers CD34 (d), CD45 (e) and HLA-DR (f) D. Representative osteogenic, adipogenic and chondrogenic differentiation of MSCs by Alizarin red S, Oil-o-Red and Alcian blue assay.

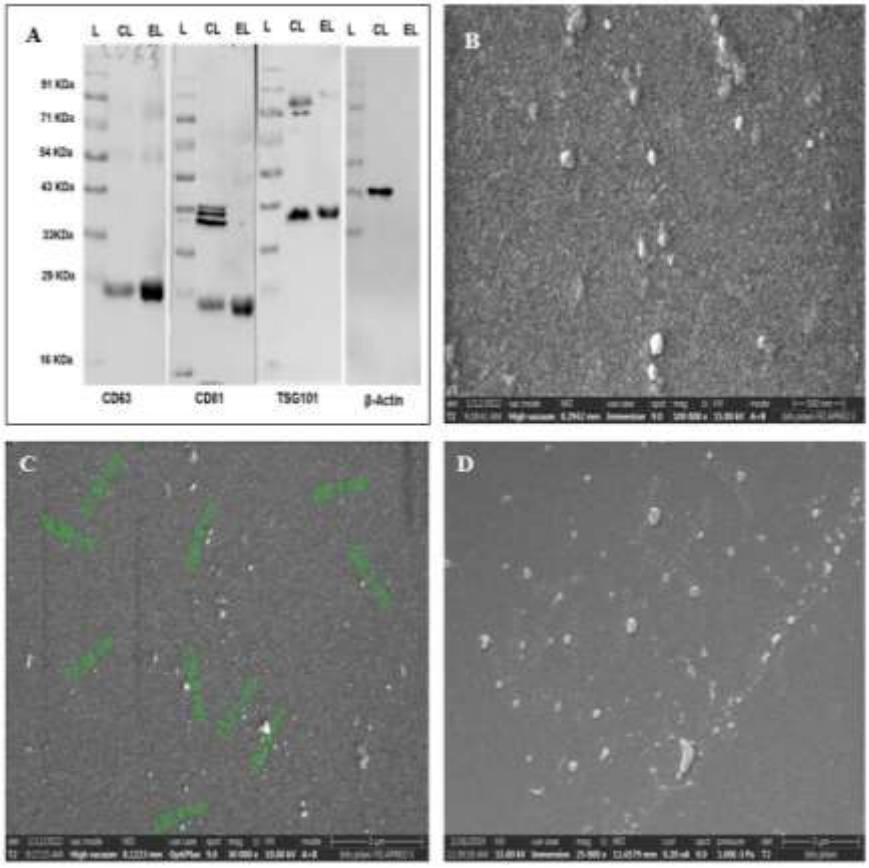

Figure 3.2 Characterization of the hUCBMSCs derived exosomes. A. Comparative expression of the exosomal proteins, CD63, CD81, and TSG 101 and housekeeping β-actin in the naïve hUCBMSCs derived exo-lysate (EL) in comparison to the cell lysate (CL) by western blot analysis. B. The representative FE-SEM image of the unloaded MSC exosomes showing the tendency of forming clumps resulting in the high polydispersity at 1,00,000X magnification, scale bar 500 nm C: Representative FESEM image of the unloaded hUCBMSC exosomes, scale bar 3µm D: Representative FESEM image of the DTX loaded hUCBMSC exosomes, scale bar 3µm.

3.3.2. Characterization of plasmid vector mediated transfection of miR-125a in hUCBMSCs and derived exosomes

hUCBMSCs cells were transfected with the GFP tagged plasmid vectors for 48 h (**Fig. 3.3.A**). The successful transfection (considering at least 70% of the transfection efficiency) of cells, and of the exosomes isolated from them was ascertained by qRT-PCR (**Fig. 3.3.B and C**). Transfection efficiency was found above 80% in all cases, which was ascertained by checking the concentration

and purity of extracted DNA from transfected hUCBMSCs by NanoDrop. Additionally, the respective transfection efficiency of miR-125a in hUCBMSCs and derived

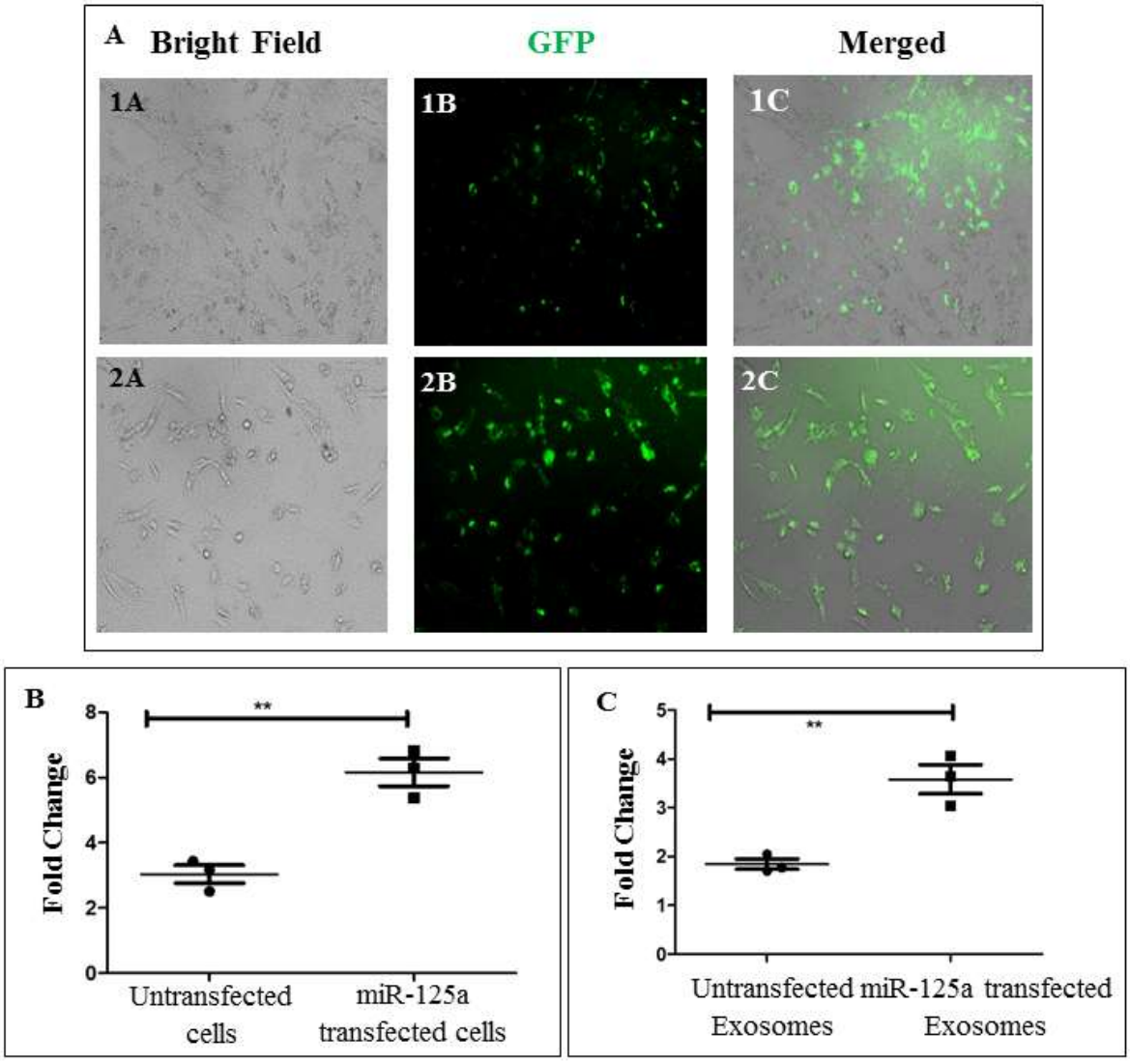

Figure 3.3. Transfection of hUCBMSCs with miR-125a. A. Transfection efficiency of miR-125a by pCMV-miRs in hUCBMSCs observed by fluorescence microscopy wherein, **panel 1** indicates the cells transfected with GFP tagged pCMV vector and panel 2 shows the representative images of the cells transfected with GFP tagged pCMV-miR125a, wherein A, B, and C indicated brightfield image, fluorescence image and their overlay, B. expression of miR-125a showed a 2-fold increase in transfected cells than the untransfected cells and, C. expression of miR-125a in exosomes isolated from the transfected cells exhibited 1.89-fold increase than exosomes from the non-transfected cells.

exosomes was quantified by the qRT-PCR assay wherein, the transfected hUCBMSCs and hUCBMSCs exosomes exhibited almost 2-folds and 1.89 folds' increase in expression of miR-125a in comparison to the untransfected ones (**Fig. 3.3.B and C**).

3.3.3. Optimization and development of the DTX loaded naive hUCBMSC Exo-DTX and miR-125a-Exo-DTX

DTX, being a BCS (IV) drug with poor solubility and permeability is challenging to load into a membrane enclosed structure attributed to the primary negative charge of both DTX and the exosomes in physiological buffer like PBS (10mM PBS, pH 7.2) and relatively high molecular weight of DTX (807.879 Da). While exosomes bear a negative surface charge due to the presence of phospholipids in their surface membrane, DTX is also negatively charged under physiological conditions (pH=7.2). Considering this, mild-sonication in combination with incubation was chosen to formulate DTX into the exosomes without compromising the exosomal integrity. Optimization of critical process parameters involved in the formulation development like number of sonication cycles, sonication pattern, presence of co-solvent and surfactant in the dispersion media (PBS) was carried out. The centrifugation speed and time for expelling out the unloaded DTX prior to pelleting down the DTX loaded exosomes were also optimized. As indicated in **Fig. 3.4.A**, 4 cycles of sonication with 30s on/off pulse at a stretch was found optimal to give maximum % entrapment efficiency (% EE) of DTX in the exosomes wherein, increasing the cycles from 4X to 12X (**Table 1.** B4 vs. B10, capacity) further reduced the capacity considerably. Also, presence of surfactant Tween 80 (0.02 %v/v) and co-solvent methanol (10% v/v) in the dispersion media increased the % EE owing to the increased solubility of DTX in the dispersion media (**Fig. 3.4.B and 3.4.C**). **Table 1** also indicated that increasing content of exosomes from 40 to 200 µg equivalent protein (B9 vs B10) while keeping the other process parameters constant, drastically increased the DTX loading capacity of the exosomes. Another interesting observation was made while formulating batches B3 and B5. While preparing B5, the exosomes were dispersed in the saturated DTX solution in PBS+0.02% Tween 80 (9.93 µg/mL) and processed in the same way as B3. B3 exhibited almost 2-folds increment in capacity in comparison to the B5; clearly proving the fact that presence of DTX beyond the saturation level in the dispersion media is required for higher entrapment of DTX. Lastly, to ensure that the unloaded DTX is completely separated out from the DTX loaded exosomes, an intermediate centrifugation step was incorporated in the formulation

process before proceeding to ultracentrifugation to obtain the final pellet containing DTX loaded exosomes (**Fig. 3.4.D**).

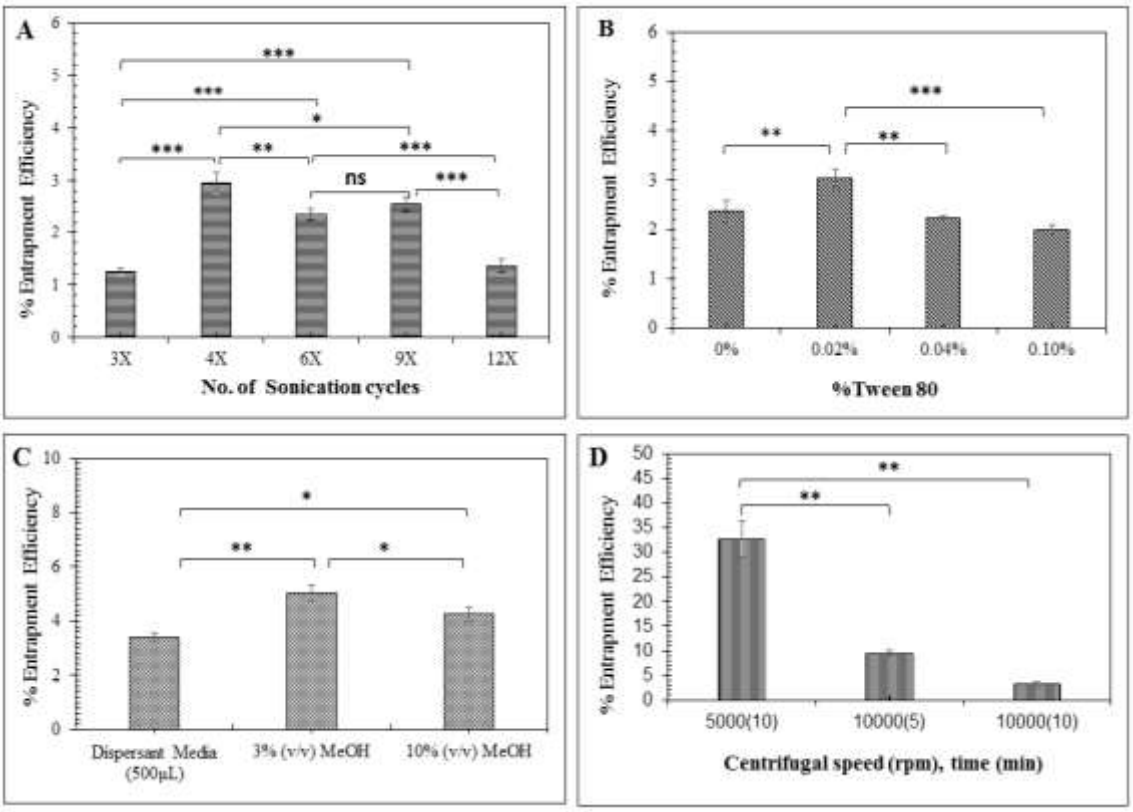

Figure 3.4. Optimization of process parameters for the loading of DTX in hUCBMSCs derived exosomes A: Effect of the number of sonication cycles on the % EE of the formulation, where X denotes one 30sec on/off sonication cycle, B. Effect of % Tween 80 on the % EE, C: Effect of the percentage of co-solvent (methanol, MeOH) considering total volume of dispersant media (PBS) as 500 µL for each batch of formulation. D: Optimization of the centrifugation speed (rpm) and time (min) to expel out the unloaded and insoluble DTX prior to pelleting down the exosomal formulations. All the data is represented as mean (n=3) ±S.D. with statistical significance being ascertained by one-way ANOVA followed by Tukey post-test, *p<0.05, **p<0.01, and ***p<0.001.

In order to evaluate the effect of DTX loading by mild sonication/incubation technique on the miRNA payload of exosomes, total miRNA was isolated from both the naive miR125a Exosomes and miR125a Exo-DTX (≅100µg) and quantified by highly sensitive Quant-iT™ Ribogreen™ assay, using rRNA from E.coli as the standard. While, miR-125a exosomes showed miRNA payload equivalent to 65.66±3.68 ng RNA before the DTX loading, mild sonication/incubation retained 12.31±5.73 % of miRNA after loading DTX in them, as shown in **Table 4**.

Further, the characterization of Exo-DTX formulations (both hUCBMSC and miR-125a Exo-DTX) was carried out by DLS. The comparative changes in the particle size and surface charge are tabulated in **Table 2,** which clearly indicates a slight increment in the size of exosomes (both untransfected and transfected) after loading of DTX wherein, both the types of exosomes showed almost similar initial particle size (~180 nm) and polydispersity before loading DTX. Although hUCBMSC exosomes differed from miR-125a exosomes in zeta-potential values, but in both the cases, loading of DTX increased the zeta-potential slightly within acceptable range. Interestingly, the lowering of PDI after DTX loading clearly indicated that the exosomal clumps might be dissembled during the processing steps without compromising the exosomal integrity. hUCBMSC and miR-125a exosomes demonstrated DTX loading capacity of 9.75±1.84 and 8.86±1.97 ng DTX/ μg exosomes respectively which also proved that transfection of miR-125a in the exosomes did not bring any change in the DTX loading capacity of the exosomes.

3.3.4. *In vitro* release of DTX and stability study of hUCBMSC Exo-DTX formulation

A biphasic release pattern was observed wherein, Exo-DTX formulation released 74±0.52 % and 90.83±3.9 % of DTX within 8 and 12 h respectively (**Fig. 3.5.A**) while free DTX showed 90.1±3.28 % and 98.68±1.56 % release at these time points. A complete release of DTX from Exo-DTX occurred by passive diffusion in almost 50 h while free DTX was completely released within 12h. The release pattern exhibited burst release of DTX from Exo-DTX formulation indicating surface bound drug however, a subsequent decrease in the rate of release proves the sustainability of release from Exo-DTX formulation up to 50 h. Exosomes are phospholipidic bi-layered vesicles, amphiphilic in nature and can accommodate both hydrophobic and hydrophilic drugs. DTX, being highly hydrophobic (BCS class IV) with a high protein binding affinity is expected to adhere onto the surface of the exosomes as well as to get entrapped into the exosomes by mild sonication/incubation method. This surface bound DTX exhibits burst release at initial time points in the in-vitro release study. The release data exhibited best fit in the Higuchi model (**Fig. 3.5.B**) with r^2=0.9922 proving that the drug was entrapped into the exosomes and was released primarily by diffusion.

hUCBMSC Exo-DTX formulations were found stable in a week long stability study at -20˚C which was concluded by negligible variation in particle size and zeta-potential at Day 0 and Day 7 in **Table 5.**

Table 3.1.

Different batches of Exo-DTX (B1-B10) formulated with different process parameters and corresponding response parameters.

	Critical process parameters (CPP)				Response Parameters	
Batch No.	**Exosomes (µg)**	**Exo: DTX**	**%T 80**	**Sonication Pattern**	**%DL**	**Capacity (ng DTX/µg Exo)**
B1	30	4:1	0	4X	0.436	5.11
B2	30	4:1	0	4X-4X	0.381	4.76
B3	40	4:1	0.02	4X-4X	0.654	8.65
B4	200	4:1	0.02	4X-4X-4X	0.532	6.65
*B5	40	4:1	0.02	4X-4X	0.387	4.39
B6	30	8:1	0.02	4X	0.33	3.86
B7	40	4:1	0.04	4X	0.56	7.07
B8	40	2:1	0.02	4X	0.51	6.32
B9	40	4:1	0.02	4X	0.84	8.50
B10	200	4:1	0.02	4X	1.19	14.96

*DTX has been taken in its completely solubilized form in dispersion media (PBS+0.02% Tween 80).

Table 3.2.

Characterization of hUCBMSC and miR-125a exosomes before and after loading DTX.

Specifications	**Particle size (nm)**		**Zeta-Potential (mV)**		**PDI**		**Capacity DTX(ng)/exosomes (µg)**
	Before Loading	After Loading	Before Loading	After Loading	Before Loading	After Loading	
hUCBMSC Exosomes	187.57±4.55	217.60 ±16.88	-10.62±4.05	-9.61±1.07	0.36±0.18	0.28±0.07	9.75±1.84
miR-125a Exosomes	183.64 ±0.33	232.50 ±12.9	-6.65±1.90	-3.6±1.97	0.26±0.03	0.27±0.03	8.86±1.97

*Exosomes ~40µg equivalent protein

Table 3.3.

Comparative particle size analysis of hUCBMSC exosomes before and after loading with DTX by DLS and FESEM assay

	Particle size (nm)	
	DLS	**FESEM**
Before Loading	187.57±4.55	101.187±25.68
After Loading	217.6±16.88	182.21±42.14

Table 3.4.

Representative miRNA retention capacity after the loading of DTX in transfected miR-125a exosomes.

Specification	**miRNA (ng) before DTX loading**	**miRNA (ng) after DTX loading**	**% miRNA retention capacity**
miR-125a Exo-DTX	65.66±3.68	7.9±4.85	12.31±5.73

Table 3.5.

Stability study of hUCBMSC Exo-DTX formulation for 7 days at -20˚C.

	Day 0	**Day 7**
Particle Size (nm)	245.5±1.13	235.9±29.6
ZP (mV)	-11.9± 0.1414	-9.1±0.8475
Capacity (ng DTX/µg Exo)	13.503±2.06	10.56±1.02

The capacity was found decreased to 21.7% on Day 7 in comparison to Day 0 **(Table 5)** which might be attributed to the gradual release of DTX from Exo-DTX under these storage condition.

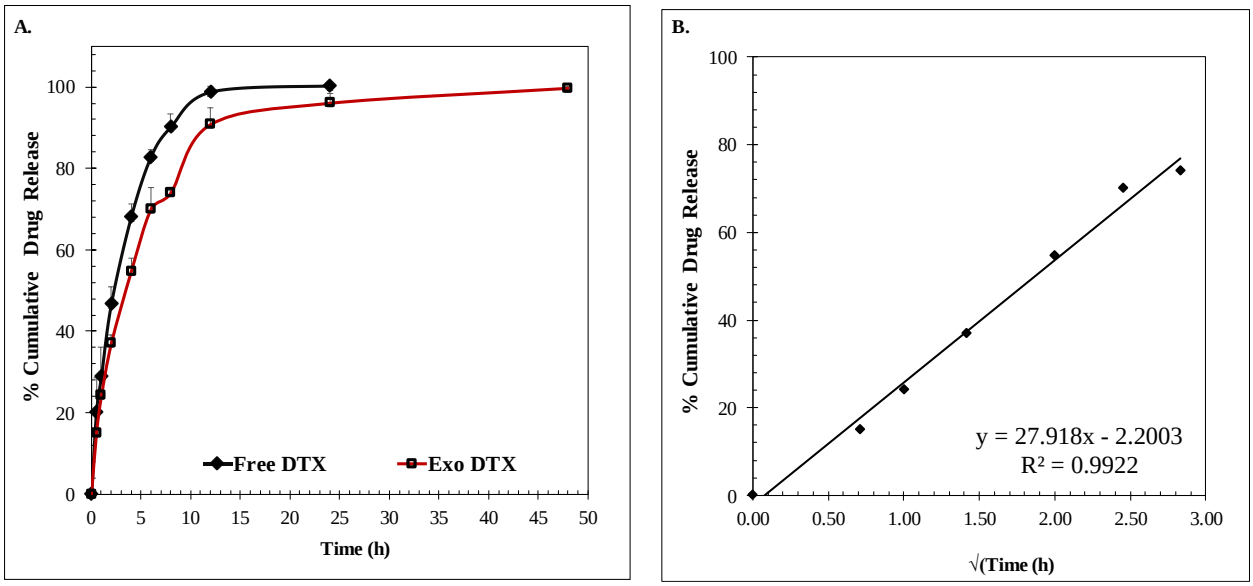

Figure 3.5. In vitro release of DTX from Exo-DTX formulation A: Release profile of DTX from Exo-DTX formulation in 0.01M PBS (pH 7.2) and 37°C and 100 rpm. % Cumulative drug release is expressed as mean (n=3) ± SD, B: Release kinetics of DTX from Exo-DTX followed Higuchi release kinetics.

Cell culture studies

3.3.5. Cytotoxicity assay: MTT and morphometric assay

Herein, the cytotoxic effect of the DTX loaded untransfected and transfected exosomes was determined on the 4T1 cells after 48h of treatment. **Figure 3.6.A.1** shows the cytotoxic effect of the DTX loaded untransfected and transfected exosomes, while **Figure 3.6.A.2** indicated the prominent cytoprotective effect (% cell viability) of the naïve exosomes of both type. In **Figure 3.6.A.2,** both hUCBMSC and miR-125a exosomes (~10 µg/mL equivalent protein, calculated as per the drug loading capacity of exosomes for 200 µg batch) showed almost similar cell viability as the media control. hUCBMSC derived exosomes demonstrated cell proliferative effect owing to the multipotent feature of the source hUCBMSC cells (as indicated in **Figure 3.1.D**). Also, miR-125a exosomes demonstrated lesser cell proliferation (% cell viability= 143±25.03) at increasing concentration (25 µg/mL equivalent protein) in comparison to the hUCBMSC exosomes (% cell viability= 183±24.1) owing to the presence of transfected TS miR-125a in them. In **Figure 3.6.A.1,** free DTX (50-500 ng/mL) showed cytotoxicity in ascending order with increasing concentration and reached IC_{50} at 472.8 ng/mL. As indicated, hUCBMSC Exo-DTX and miR125a Exo-DTX showed 43.09±0.46% and 56.5±1.76% of cell death at 250 ng/mL in comparison to 33.57±5.46% cell death induced by free DTX in 4T1 cells. Interestingly, miR-125a Exo-DTX

exhibited superior cytotoxic activity than hUCBMSC Exo-DTX at both 100 ng/mL and 250 ng/mL, which could be attributed to the presence of transfected miRNA as payload and synergism between the miR-125a and DTX. As indicated, miR-125a Exo-DTX demonstrated significantly superior cytotoxicity in comparison to free DTX as well as hUCBMSC Exo-DTX, especially at 100 ng/mL and 250 ng/mL, which could be correlated with the additional anti-proliferative activity of miRNA-125a as shown in **Figure 3.6.A.2** at 25 µg/mL miR-125a exosomes treated group. Additionally, it was also found that free DTX showed IC_{50} nearly at 472.8 ng/mL, hUCBMSC Exo-DTX and miR-125a Exo-DTX exhibited IC_{50} at 306 ng/mL and 192.8 ng/mL respectively, which is almost 1.5 folds' and 2.36 folds' lower than the free DTX IC_{50}.

Interestingly, the cellular morphology after treatment with the free DTX, and both the exosomal formulations was found to be distorted and cells appeared rounded with increased nucleus size and degraded appendages under the bright field microscopy (**Fig. 3.6.B**) in comparison to the control groups, which clearly indicated the impact of DTX free/ loaded into the exosomes. Also, the effect of the hUCBMSC and miR-125a exosomes on cell viability could be visually ascertained here. Hence, it could concluded that the entrapment into exosomes facilitated the cellular uptake and sustained the effect of DTX prominently in Exo-DTX formulations as well the effect of miR-125a exosomes is also prominent in comparison to the hUCBMSC exosomes treated group.

3.3.6. Cellular internalization assay

Initially, the cellular internalization of PKH-26 stained hUCBMSC exosomes was assessed in a time dependent manner without any forced fusion at 1h/3h/6h/12h post treatment which indicated increased intensity of the PKH26 fluorescence beginning with 3h, and maximum at 6h which was further sustained till 12h. **Figure 3.7.A** clearly revealed that the cellular internalization increased with increasing time of incubation. In order to rule out the possibility of transfer of lipophilic dye PKH26 from exosomes to the cellular membrane, the hUCBMSC exosomes were also loaded with hydrophobic model drug COU6 (MW: 350.4 Da) as a fluorescent substitute of DTX with the same optimized protocol to produce exosomal formulation of COU6 (Exo-COU6, capacity: 21ng COU6/µg exosomes). Subsequently, the time-dependent uptake of Exo-COU6 by 4T1 cells was evaluated, and expectedly with increasing time, the intensity of green fluorescence of COU6 was seen distributed in the cytoplasm of 4T1 cells (**Fig. 3.7.B**). A significant enhancement in the fluorescence was observed 6 h post treatment of the cells with Exo-COU6 (~200 ng/mL loaded

COU6). This study also depicted that the exosomes are internalized by the cells even within 1h and this further continues with time and also, ability of exosomes to release the cargo drug molecule in a controlled way within the cells as indicated by an increase in green fluorescence intensity as a function of time.

3.3.7. In-vitro wound healing assay

The time-dependent wound healing assay after different treatments depicted the anti-proliferative and anti-migratory feature of hUCBMSC Exo-DTX and miR-125a Exo-DTX in comparison to the media control, hUCBMSC exosomes and miR-125a exosomes. **Figure 3.8.A** shows initiation of cellular migration and wound closure beginning from 12h post-treatment followed by extensive migration within 24h in the media control and DTX unloaded exosomes (both transfected and non-transfected) followed by complete wound closure by 48h. In comparison to that, free DTX itself showed 17.09$\pm$0.52% wound closure after 36 h which clearly indicates its anti-migratory effect. In comparison to that, both hUCBMSC Exo-DTX and miR-125a Exo-DTX exhibited more prominent anti-migratory and apoptotic function (5.52$\pm$0.345% and -6.14$\pm$0.38% wound closure respectively). The negative % wound healing in case of miR-125a Exo-DTX clearly stated the synergistic efficiency of the loaded DTX and miR-125a contributing towards broadening of the wound attributed to the induced apoptotic responses in the cells (**Fig. 3.8.B**).

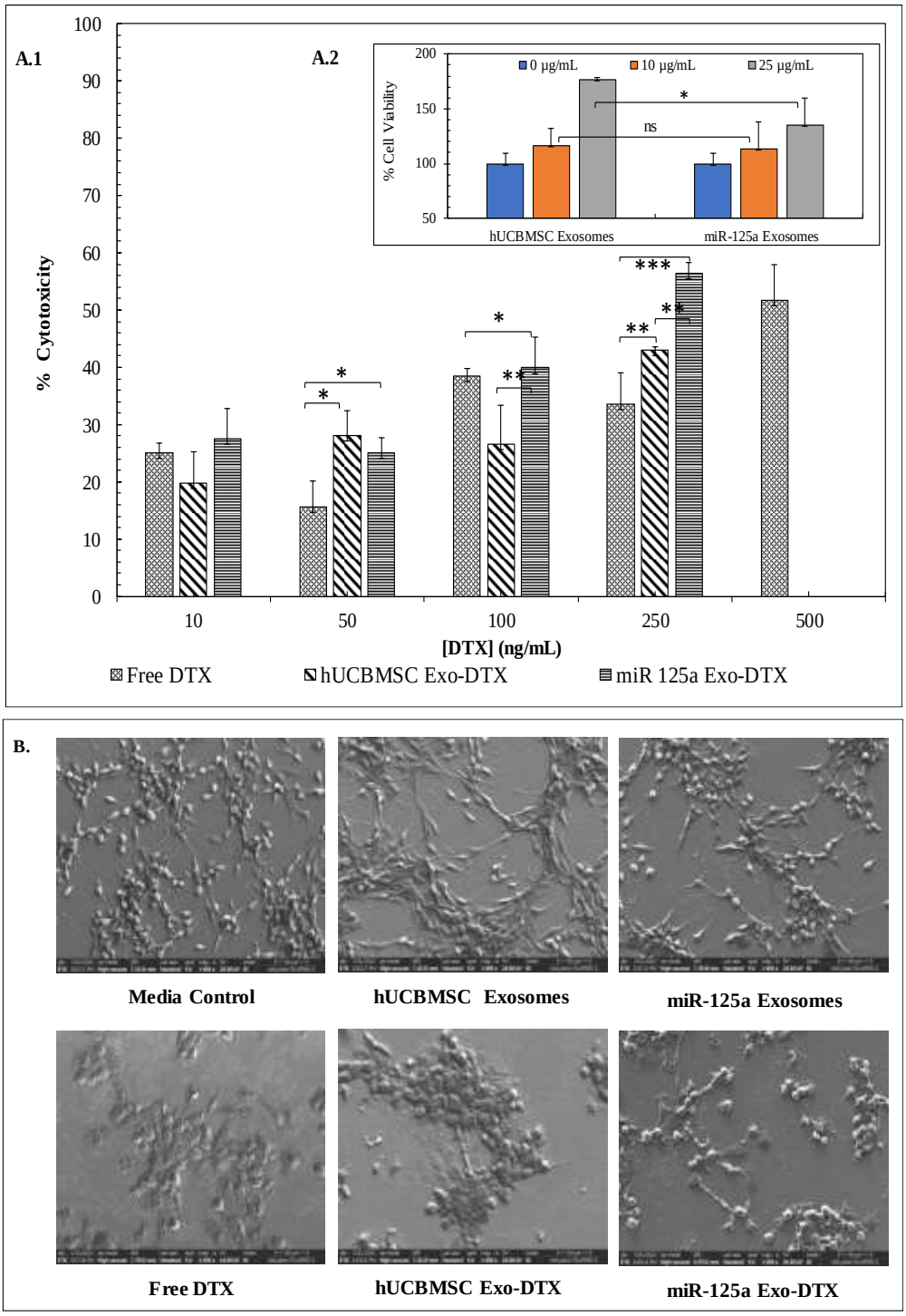

Figure 3.6 Anti-proliferative assay in 4T-1 cells by MTT and microscopy (A.1). In-vitro cytotoxicity assay of free DTX, hUCBMSC Exo-DTX and miR-125a Exo-DTX after 48h, inset shows the corresponding % cell viability of hUCBMSC Exo and miR125a Exo (A.2) with DTX loading capacity of ≈10 ng DTX/µg exosomes. Herein, the data are represented as mean (n=5)±SD. Two-way ANOVA followed by Bonferroni post-test was applied for statistical significance (***p<0.001, **p<0.01) B. Morphological distortment and effect on the cell density after treatment with different Exo-DTX (100 ng/mL) formulations in comparison to the media control and blank exosome control groups by FESEM. Scale bar: 200 µm

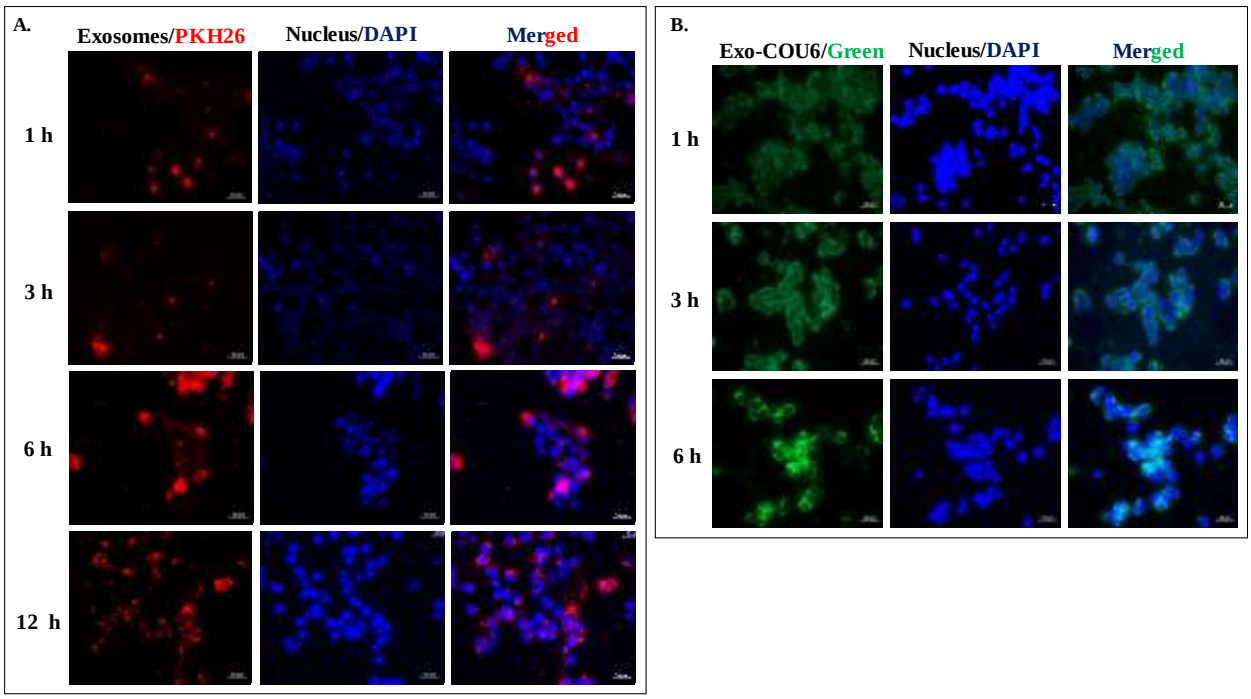

Figure 3.7 Time-dependent *in vitro* cellular internalization assay. A. Time dependent cellular uptake of PKH26-stained unloaded hUCBMSC exosomes (10 µg/mL equivalent protein), by 4T1 cells, wherein nuclei are counterstained with DAPI (n=3), scale bar 20 µm. B: Time dependent cellular uptake of Coumarin 6 loaded hUCBMSC exosomes (Exo-COU6, capacity 21.8 ng COU6 /µg exosomes) at a concentration of 250 ng/mL COU6. n=3, Scale Bar 20 µm.

3.3.8. In-vitro invasion assay

Cellular migration is a three dimensional process wherein, cells need to invade the physiological barriers. Tumor cell invasion is also a multi-step process which is initiated by attachment of cells to the basement membrane, matrix degradation and migration. In order to access the effect of both the non-transfected and transfected Exo-DTX formulation and their respective naive exosomes on invasiveness of 4T1 cells, transwell invasion assay was performed wherein, the Matrigel bed was cast to act as a reconstituted basement membrane. As indicated in **Figures 3.9.A and B**, the invasiveness of the 4T1 was found to be reduced significantly after 48h of treatment; cells treated with miR-125a exosomes exhibited 77.36±5.5% invasion in comparison to the media control (considered as 100% invasion) and hUCBMSC exosomes (116.2±1.6%), proving higher anti-migratory effect of miR-125a exosomes as compared to hUCBMSC exosomes. After loading with DTX, both hUCBMSC Exo-DTX and miR-125a Exo-DTX demonstrated significant lowering of invasion upto 5.5±0.6 % and 3.5±1.8% respectively which is far more

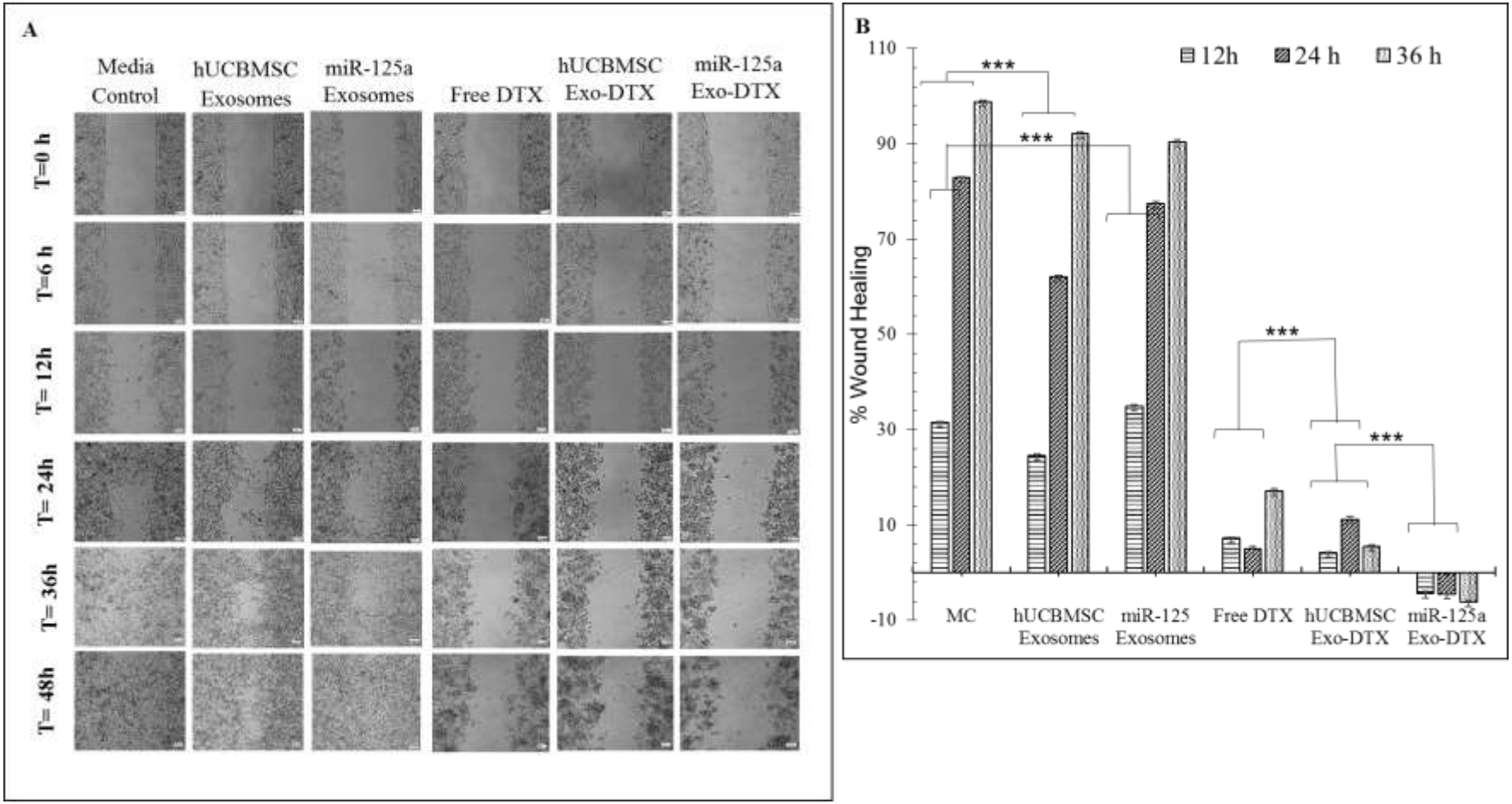

Figure 3.8 In vitro wound healing assay. A. Time-dependent wound healing assay in 4T1 cells at 0/6/12/24/36/48h after being treated with free DTX, hUCBMSC exosomes, miR-125a exosomes, Free DTX, hUCBMSC Exo-DTX and miR-125a Exo-DTX, (n=3), scale bar 100 μm. B. Comparable effect of each treatment on the closure or broadening of the wound (***$p<0.001$).

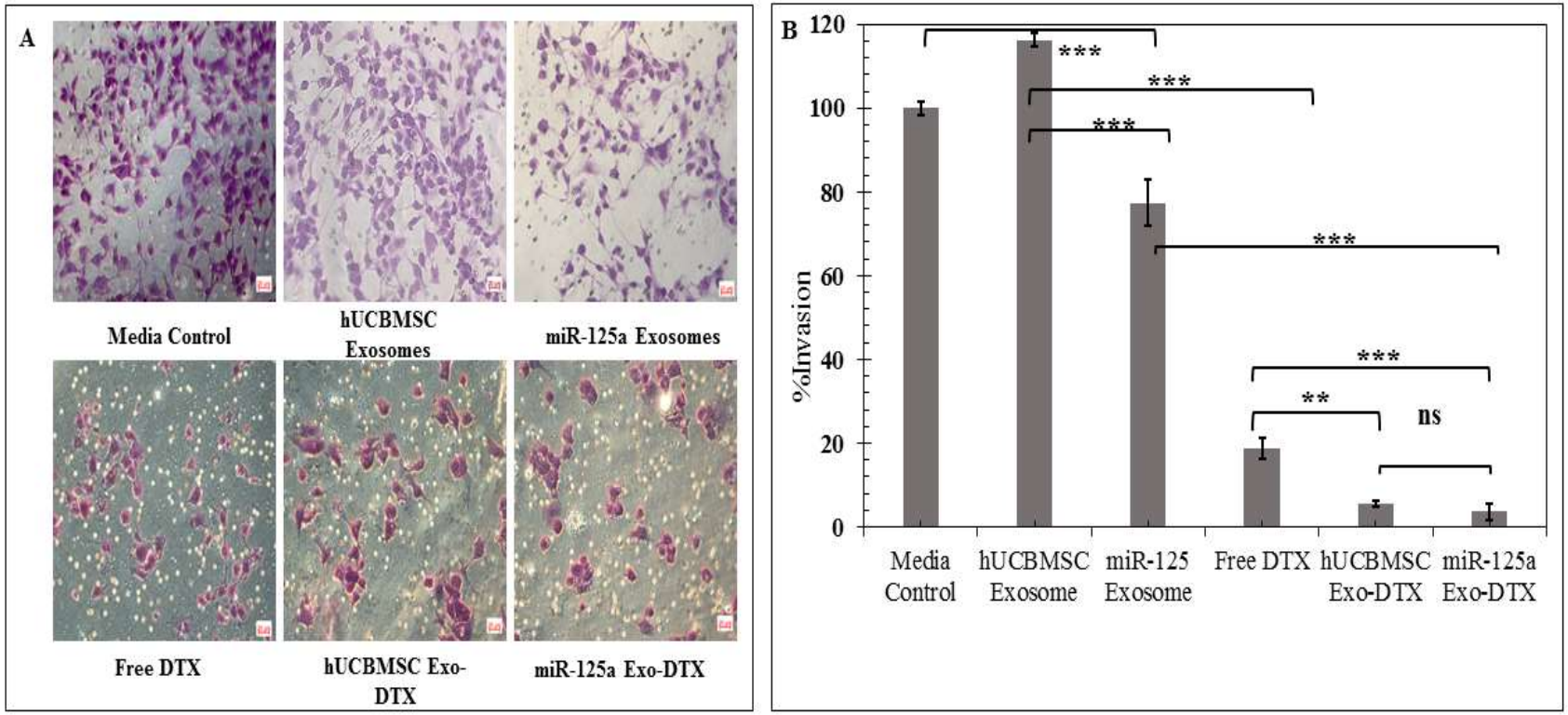

Figure 3.9. **In vitro transwell invasion assay** A: Microscopic evaluation of invasion efficiency of 4T1 cells through Matrigel bed (300 µg/mL) after 48h of treatment of naive hUCBMSC exosomes, miR-125a exosomes and respective Exo-DTX (100 ng/mL) formulations. B. The graphical representation of the invasion efficiency of 4T1 cells in terms of number of migrated cells/field. (***$p<0.001$)

than that of free DTX treated group (18.7±2.4 %). This clearly showed exosomes enabled an easy uptake of DTX resulting in diminished invasion.

3.3.9. Cytoskeletal deformation assay by FESEM

Migration of aggressively metastatic cancer cells is governed by the cytoskeletal dynamics contributed by both F-actin (filopodia, lamellipodial and invadopodia) and microtubules and their mutual interaction conferring the motility, shape change, cellular adhesion and extracellular matrix degradation. The two active components of the formulation are DTX and miR-125a wherein, DTX as a microtubule hyper polymerizing moiety causes "dynamic instability" and miR-125a as a TS miRNA is expected to produce anti-metastatic effect synergistically with DTX when co-loaded in the hUCBMSC exosomes. hUCBMSC exosomes resulted in the formation of excessive appendages in 4T-1 cells (as indicated with **white arrow** in **Fig. 3.10.**) in comparison to the media control and miR-125a exosomes (as indicated by **black arrow** in **Fig. 3.10.**). A massive degradation of filopodial and lamellipodial appendages as well the change in cellular morphology from elongated to rounded was distinctly visible in the presence of hUCBMSC Exo-DTX and miR-125a Exo-DTX attributed to the efficient uptake of exosomal formulations in comparison to the free DTX (100 ng/mL), as indicated by **red arrow** in **Fig. 3.10**. In comparison to the free DTX treated group, hUCBMSC Exo-DTX and miR-125a Exo-DTX treatment demonstrated a more prominent cytoskeletal degradation with massive nuclear damage, particularly the miR-125a Exo-DTX produced a more pronounced apoptotic effect among both the formulations.

3.3.10. F-actin degradation assay by Phalloidin/DAPI counterstaining

The micro-environmental complexity directly acts on the cytoskeletal organization which involves actin polymerization at the leading edge, acto-myosin contraction, producing traction force to form blebs eventually resulting in the morphological change, essential for the motility of the cells. At the same time, the microtubule (MT) formation and its dynamic plasticity at different stages of the cell cycle also contribute towards the cellular survival, motility and proliferation. Hence, to assess the reason behind the morphological changes along with the degradation of appendages, the cells treated with different treatments were further stained with Phalloidin (specific F-actin conjugating molecule) which clearly exhibited F-actin degradation in the free DTX**,** hUCBMSC Exo-DTX and miR-125a Exo-DTX group in comparison to the media control, hUCBMSC exosomes control and miR-125a exosome control group. Also the decreased intensity of DAPI in free DTX, hUCBMSC

Exo-DTX and miR-125a Exo-DTX indicated the DNA degradation. Additionally, multi-nucleation and cellular degradation is evident in **Figure. 9.B** (as indicated by white and red arrow in DAPI panel respectively) attributed to the presence of DTX at 100 ng/mL in both the transfected and non-transfected exosomes treated groups. Evidently, miR-125a Exo-DTX showed superior F-actin degradation and oligo-nucleosomal fragmentation in comparison to the free DTX as well as hUCBMSC Exo-DTX (**Fig. 3.11**).

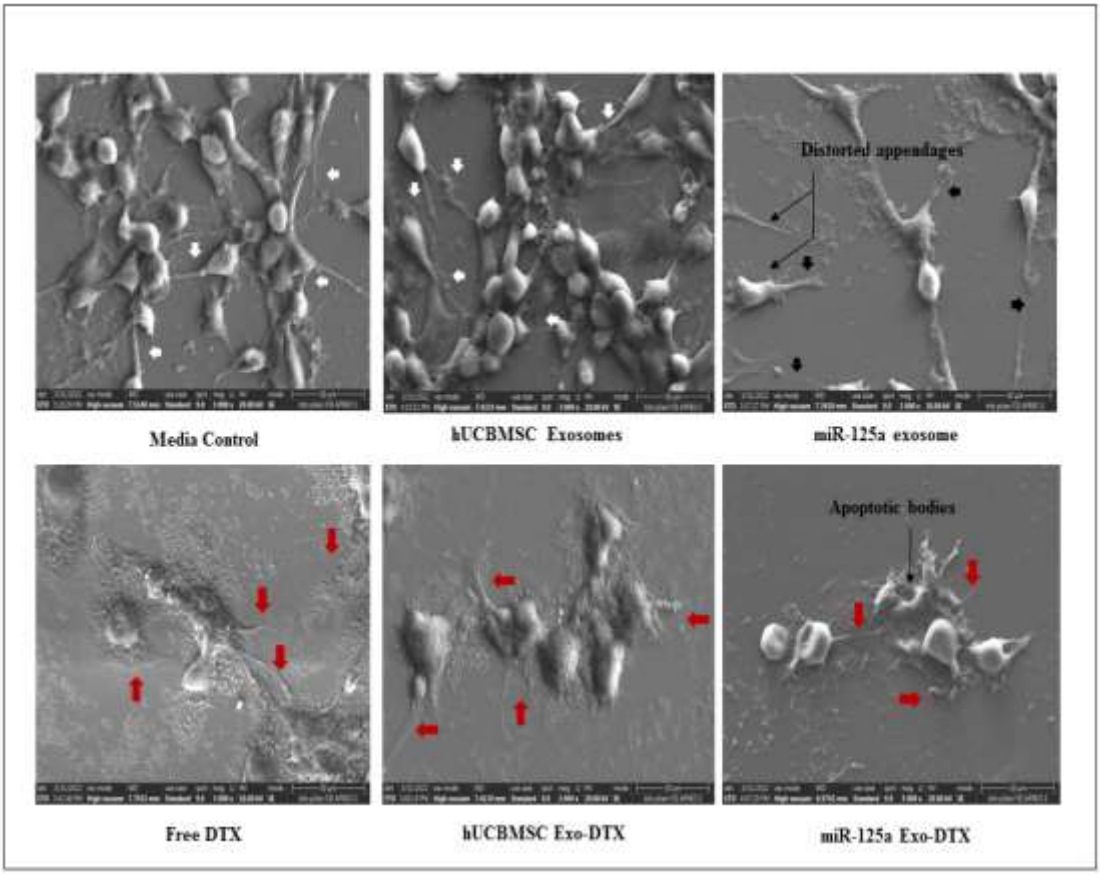

Figure 3.10. In-vitro anti-migratory and apoptotic effect of hUCBMSC-Exo and miR-125a Exo-DTX on 4T1 cells by FESEM. FESEM imaging of the treatment groups clearly indicated the cytoskeletal degradation effect of hUCBMSC Exo-DTX and miR-125a Exo-DTX (at 100 ng/mL) in comparison to the media and blank exosome control groups at a magnification of 5000 X (n=3), Red arrow indicated the F-actin degradation severity in free DTX, hUCBMSC Exo-DTX and miR-125a Exo-DTX treated groups. Scale bar 30 μm.

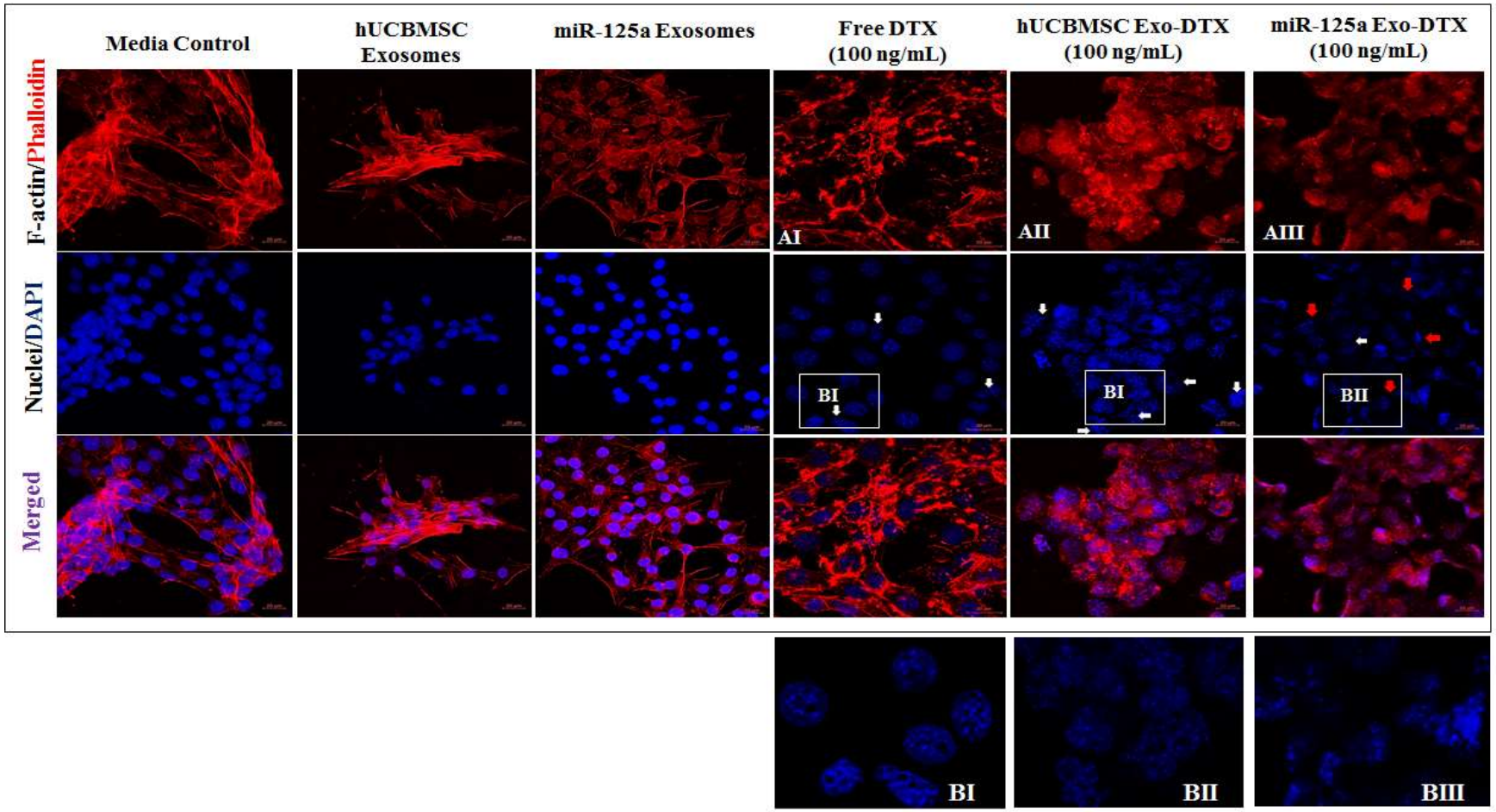

Figure 3.11. In-vitro F-actin and nuclear degradation in 4T1 cells in the presence of hUCBMSC Exo-DTX and miR-125a Exo-DTX by confocal microscopy. The anti-metastatic F-actin degradation by different treatment groups was confirmed by F-actin staining with Rhodamine Phalloidin (red) and counterstaining nuclei with DAPI (blue), which clearly showed the anti-metastatic effect of the formulations in comparison to the free DTX and control groups (630X). Both the studies were performed after 48h treatment of cells with different treatments. White arrows indicated multi-nucleation, red arrow indicated nucleosomal degradation in DAPI in the order BIII>BII>BI panel while, comparing AI, AII and AIII in Phalloidin panel clearly indicated the F-actin degradation in AIII>AII>AI. Scale bar 20 µm.

3.4. Discussion

Herein, we report for the first time hUCBMSC exosomes as a nanocarrier for two therapeutic molecules i.e. anti-tubulin molecule, DTX and TS miRNA-125a. Two exosomal formulations, hUCBMSC Exo-DTX and miR-125a Exo-DTX were formulated using three components, hUCBMSC exosomes, DTX and miRNA 125a, each of these components bear distinctive activity on cancer survival and metastasis.

As per literature, human umbilical cord MSC exosomes (with miR-224-5p) were reported to enhance survival and promote EMT in both MDA-MB 231 and MCF-7 cells, the same study also reported that the MSCs transfected with miR-224-5p inhibitor were able to produce the miR-224-5p inhibitor loaded exosomes which further supressed miR-224-5p expression in BC cells [26]. Several reports also emphasized on direct loading of miRNA mimic or inhibitors in exosomes to suppress the cancer progression and metastasis. A recent study has reported that MDA-MB 231, treated with adipose derived MSC exosomes with electroporated miR-381-3p mimic was able to increase miRNA expression in the cancer cells by several folds that enhanced the apoptotic index as well as suppressed the migration of the cells [27]. Most of the studies in literature have reported exosomes as a nanocarrier for either miRNA or a small molecule, only a few studies have also explored the co-delivery of the anticancer molecule and miRNA. Electroporation mediated loading of miR-21 inhibitor and 5-fluorouracil (5-FU) in the exosomes exhibited enhanced cytotoxicity and reversed the resistance in 5-FU resistant colorectal HCT cells [28]. However, we did not come across any study wherein, the miRNA has been loaded by plasmid mediated transfection and the small molecule by mild sonication/incubation technique with methodologically optimized key process parameters. Henceforth, we designed a miR-125a and DTX co-loaded exosomal formulation and optimized the process parameters for formulation development to obtain highest capacity of the payload per unit weight of the exosomes. The formulation revealed superior anti-migratory and apoptotic effect in BC cells in comparison to the free DTX.

After initial characterization of hUCBMSCs cells for MSC marker proteins and confirming their differentiation into different reported lineages (**Fig. 3.1**), the naïve hUCBMSC exosomes were isolated and characterized for particle size, polydispersity, spherical morphology and negative surface charge and exosomal protein expression (**Fig. 3.2 and Table 2**). The particle size of hUCBMSCs derived exosomes was found ~180 nm through DLS and ~ 150 nm by FESEM with

surface charge of -10 mV in 10mM PBS (pH 7.2), which is in agreement with the available literature [29]. Mild sonication/ incubation method was optimized and used (**Table 1**) to reduce the rigidity of the exosomal membrane and facilitate loading of DTX could not be possibly loaded efficiently, despite its high hydrophobicity because of three reasons, (1) the high molecular weight of DTX providing hindrance for the passive diffusion, (2) its tendency of carrying anionic charge at physiological pH and, (3) poor solubility in physiological buffers in which exosomes are dispersed and stored [30]. Post sonication, the exosomal integrity was restored although an increase in exosomal size and surface potential was observed with same polydispersity (**Table 2**); this is in agreement with the other reports wherein, sustenance of surface charge of the exosomes after loading by mild sonication followed by resealing period at 37℃ for 2h is a marker of restored exosomal membrane sealing.[31]. As indicated in the **Table 5**, the capacity (ng DTX/µg exosomes) was found ~20% reduced within seven days of storage at -20˚C comparatively no change in the particle size of the exosomes. This data clearly indicated that, exosomes were able to retain 80% DTX even after 7 days. As per reported literature the microviscosity of the exosomal membrane was found reduced by sonication which was proved to be regained after one-hour incubation at 37 ˚C by fluorescence polarization assay [32]. Henceforth, it can be said that the post-sonication two hours' incubation at 37 ˚C would be sufficient to regain the exosomal integrity to an extent that it could retain the 80% DTX payload till seven days. Although, DTX loading capacity is not hampered by the transfected miRNA (as indicated by **Table 2**), but the mild sonication/incubation indeed reduced the miRNA payload of the transfected exosomes substantially (**Table 4**)[33]. Along with, DTX loaded exosomes showed size>150nm, which makes them prone to RES mediated removal from the circulation. However, exosomes with efficient cellular uptake with surface negative potential, are found efficient enough even the formulation size >150nm. Despite of all drawbacks, we found miR-125a Exo-DTX profoundly efficient in inducing cytotoxicity and anti-metastatic behaviour in comparison to the hUCBMSC Exo-DTX.

Once the DTX loading protocol was optimized and validated (**Table 1 and Fig. 3.4**) with hUCBMSC exosomes, our main focus shifted towards the transfection of miR-125a into hUCBMSCs to ensure the long term, cost-effective utilization of resources for isolating the transfected exosomes (miR-125a exosomes) (**Fig. 3.3 and 3.4**) which was found beneficial over well reported techniques like electroporation of miRNA mimic or inhibitors directly into the exosomes [26,27]. Our experimental findings indicated that, plasmid mediated transfection of

hUCBMSC cells can increase the miR-125a payload in the exosomes isolated from them by 1.89 folds than the exosomes isolated from the hUCBMSCs (**Fig. 3.3.C**) without significant change in physiological characteristics i.e. particle size (nm), zeta-potential (mV) and PDI of the exosomes (**Table 2**). After confirming efficient transfection efficiency (~80%), the miR-125a Exo-DTX formulations were prepared and compared with the hUCBMSC Exo-DTX for DLS characterization and subsequent in vitro functional assays.

The second component of the formulation is DTX, a well-known anti-neoplastic agent responsible for excessive polymerization of microtubule, eventually resulting in dynamic instability and consequently inducing apoptosis. It is well reported that DTX has a biphasic effect especially on TNBC; at considerably lower concentration (~4 nM) it induces aberrant mitosis followed by hypodiploidy while at higher concentration (100 nM) it induces mitotic arrest at G_2/M phase of cell cycle and mitotic slippage, resulting in multi-nucleation and nuclear degradation [34,35]. Apart from inducing apoptosis in aggressive breast cancer cells, DTX is also known to distort the cytoskeletal organization which is otherwise maintained by close co-ordination between microtubule and F-actin [36,37]. Till now, we came across only two reports, wherein tumor derived exosomes (HELA cells and A549 cells) were utilized to load DTX by electroporation with % EE of 12.2±5.5 % and 65.85±12.43% respectively to enhance apoptosis and exhibit selective cytotoxicity towards cancer cells [38,39]. Our findings of the %DL and DTX loading capacity of exosomes clearly differed from these studies however, no unified loading capacity of exosomes has been reported till date. Here, we are reporting the capacity of miR-125a Exo-DTX, as 8.86±1.97ng DTX/µg exosomes with 12.31±5.730 miRNA retention capacity [40–42].

The third component of the formulation reported here is miR-125a, a well-known tumor suppressor miRNA that induces apoptosis, mitochondrial fission and suppresses EMT and aerobic glycolysis in cancer cells. In general, miR-125a expression is downregulated in Her2 overexpressed BC, wherein miR-125a is responsible for downregulating BAP1 and BRCA1 mediated cancer progression, survival and PI3K/AkT mediated migration[43,44]. Apart from this, miR-125a has also been reported to restrict EMT by downregulating the expression levels of TAFAZZIN, transglutaminase 2-phosphorylated-AKT, N-cadherin, vimentin and upregulating the apoptotic E-cadherin, cleaved caspase-3 and Bax in Adriamycin resistant MCF7, notably Her2 positive breast cancer cells [44]. As indicated by **Fig. 3.6.A and 3.6.B**, naive miR-125a transfected exosomes

exhibited less proliferative and more anti-migratory characteristics in 4T1 cells (**Fig. 3.8 and 3.9**) in comparison to the naive hUCBMSC exosomes, which could be further attributed for the superior anti-cancer effect of the miR-125a Exo-DTX. The morphometric deformation and cytoskeletal degradation observed after treatment with miR-125a Exo-DTX formulations could be correlated with the % wound healed and % invasion in **Figure 3.8.B and 3.9.B**. These findings emphasized the efficiency of miR-125a to sustain the wound by suppressing the 2D-cellular migration as well as invasion through the basement membrane, even at 100 ng/mL DTX payload. Further, F-actin degradation assay (**Fig. 3.10 and 3.11**) emphasized that hUCBMSC exosomes could prove lethal to cancer cells by inducing oligo-nucleosomal degradation and cytoskeletal deformations, only after being loaded with DTX and miR-125a, while naive hUCBMSC exosomes might aid cancer survival.

In conclusion, our data indicated that despite of all odds of hUCBMSC exosomes, it could be utilized as a nanocarrier for anti-cancer therapeutic small molecules by means of optimized sonication/incubation method and transfecting a TS miRNA in their parent cells using a plasmid vector. It was also observed that the transfected formulation was superior in cytotoxicity in comparison to free DTX with almost twice the potency. Eventually the drastic change in cellular and nuclear structure observed upon incubation with the miR-125a Exo-DTX proved that the use of exosomes as nanocarrier facilitated the cellular uptake of the formulation along with eliciting superior nucleosomal and F-actin degradation, and evidently, apoptosis induction and appearance of apoptotic bodies by miR-125a Exo-DTX was also in tandem with the broadening of the wound. Clearly, this study also indicated that of the inherent physiological attributes of the exosomes should be taken into consideration while developing the exosomal formulations.

3.5 Conclusion

This is the first time, we co-delivered a biological molecule (miR-125a) with an anticancer small molecule (DTX) as the payload of MSC exosomes, which further proved to synergistically target the aggressiveness of highly metastatic 4T1 cells. We successfully isolated the exosomes from miR-125a transfected hUCBMSC cells and explored them as nanocarrier for the delivery of small anticancer agent, i.e. DTX. We further screened and optimized the process parameters for developing hUCBMSC Exo-DTX and miR-125a Exo-DTX formulations to ensure the maximum DTX loading capacity without altering the exosomal integrity. The co-delivery of the miR-125a

and DTX eventually resulted in the synergistic anti-metastatic and anti-proliferative effect on the TNBC 4T1 cells. The DTX loading in both the non-transfected and transfected exosomes were able to produce enhanced cytotoxicity by the 1.5 folds' and 2.36 folds' more than the free DTX. The prominent anti-metastatic effect could be confirmed by the broadening of the wound, and reduced invasion through Matrigel layer on the transwell. The F-actin deformation and massive nuclear degradation in TNBC 4T1 cells could be attributed to the synergistic effect of the dual payload of miR-125a Exo-DTX.

3.6. References

(1) Théry, C.; Witwer, K. W.; Aikawa, E.; Alcaraz, M. J.; Anderson, J. D.; Andriantsitohaina, R.; Antoniou, A.; Arab, T.; Archer, F.; Atkin-Smith, G. K.; Ayre, D. C.; Bach, J. M.; Bachurski, D.; Baharvand, H.; Balaj,et al. Minimal Information for Studies of Extracellular Vesicles 2018 (MISEV2018): A Position Statement of the International Society for Extracellular Vesicles and Update of the MISEV2014 Guidelines. *J. Extracell. Vesicles* **2018**, *7* (1). https://doi.org/10.1080/20013078.2018.1535750.

(2) Kalluri, R.; LeBleu, V. S. The Biology, Function, and Biomedical Applications of Exosomes. *Science (80-.).* **2020**, *367*, eaau6977. https://doi.org/10.1126/science.aau6977.

(3) Srivastava, A.; Babu, A.; Filant, J.; Moxley, K. M.; Ruskin, R.; Dhanasekaran, D.; Sood, A. K.; McMeekin, S.; Ramesh, R. Exploitation of Exosomes as Nanocarriers for Gene-, Chemo-, and Immune-Therapy of Cancer. *J. Biomed. Nanotechnol.* **2016**, *12* (6), 1159–1173. https://doi.org/10.1166/jbn.2016.2205.

(4) Qian, X.; An, N.; Ren, Y.; Yang, C.; Zhang, X.; Li, L. Immunosuppressive Effects of Mesenchymal Stem Cells-Derived Exosomes. *Stem Cell Rev. Reports* **2021**, *17*, 411–427. https://doi.org/10.1007/s12015-020-10040-7.

(5) Pakravan, K.; Babashah, S.; Sadeghizadeh, M.; Mowla, S. J.; Mossahebi-Mohammadi, M.; Ataei, F.; Dana, N.; Javan, M. MicroRNA-100 Shuttled by Mesenchymal Stem Cell-Derived Exosomes Suppresses in Vitro Angiogenesis through Modulating the MTOR/HIF-1α/VEGF Signaling Axis in Breast Cancer Cells. *Cell. Oncol.* **2017**, *40* (5), 457–470. https://doi.org/10.1007/s13402-017-0335-7.

(6) Zhu, W.; Huang, L.; Li, Y.; Zhang, X.; Gu, J.; Yan, Y.; Xu, X. Exosomes Derived from Human Bone Marrow Mesenchymal Stem Cells Promote Tumor Growth in Vivo. *Cancer Lett.* **2012**, *315*, 28–37. https://doi.org/10.1016/j.canlet.2011.10.002.

(7) Wei, W.; Ao, Q.; Wang, X.; Cao, Y.; Liu, Y.; Zheng, S. G. Mesenchymal Stem Cell – Derived Exosomes : A Promising Biological Tool in Nanomedicine. *Front. Pharmacol.* **2021**, *11* (January), 590470. https://doi.org/10.3389/fphar.2020.590470.

(8) Katakowski, M.; Buller, B.; Zheng, X.; Lu, Y.; Rogers, T.; Osobamiro, O.; Shu, W.; Jiang, F.; Chopp, M. Exosomes from Marrow Stromal Cells Expressing MiR-146b Inhibit Glioma Growth. *Cancer Lett.* **2013**, *335* (1), 201–204. https://doi.org/10.1016/j.canlet.2013.02.019.

(9) Bruno, S.; Collino, F.; Deregibus, M. C.; Grange, C.; Tetta, C.; Camussi, G. Microvesicles Derived from Human Bone Marrow Mesenchymal Stem Cells Inhibit Tumor Growth. *Stem Cells Dev.* **2013**, *22* (5), 758–771. https://doi.org/10.1089/scd.2012.0304.

(10) Lee, J.; Park, S.; Jung, B.; Jeon, Y.; Lee, Y.; Kim, K.; Kim, Y.; Jang, J.; Kim, C. Exosomes Derived from Mesenchymal Stem Cells Suppress Angiogenesis by Down-Regulating VEGF Expression in Breast Cancer Cells. *PLoS One* **2013**, *8* (12), e84256. https://doi.org/10.1371/journal.pone.0084256.

(11) Liu, J.; Zhu, M.; Tang, Q. Human Umbilical Cord Mesenchymal Stem Cells-Derived Exosomal MicroRNA-181a Retards Nasopharyngeal Carcinoma Development by Mediating KDM5C. *J. Cancer Res. Clin. Oncol.* **2021**, *147* (10), 2867–2877. https://doi.org/10.1007/s00432-021-03684-6.

(12) He, Z.; Li, W.; Zheng, T.; Liu, D.; Zhao, S. Human Umbilical Cord Mesenchymal Stem Cells-Derived Exosomes Deliver MicroRNA-375 to Downregulate ENAH and Thus Retard Esophageal Squamous Cell Carcinoma Progression. *J. Exp. Clin. Cancer Res.* **2020**, *39* (1), 1–18. https://doi.org/10.1186/s13046-020-01631-w.

(13) Xu, Y.; Lai, Y.; Cao, L.; Li, Y.; Chen, G.; Chen, L.; Weng, H.; Chen, T.; Wang, L.; Ye, Y. Human Umbilical Cord Mesenchymal Stem Cells-Derived Exosomal MicroRNA-451a Represses Epithelial–Mesenchymal Transition of Hepatocellular Carcinoma Cells by Inhibiting ADAM10. *RNA Biol.* **2021**, *18* (10), 1408–1423. https://doi.org/10.1080/15476286.2020.1851540.

(14) Pan, Y.; Wang, X.; Li, Y.; Yan, P.; Zhang, H. Human Umbilical Cord Blood Mesenchymal Stem Cells-Derived Exosomal MicroRNA-503-3p Inhibits Progression of Human Endometrial Cancer Cells through Downregulating MEST. *Cancer Gene Ther.* **2022**, *29* ((8-9)), 1130–1139.

https://doi.org/10.1038/s41417-021-00416-3.

(15) Xin, Y.; Huang, M.; Guo, W. W.; Huang, Q.; Zhang, L. zhen; Jiang, G. Nano-Based Delivery of RNAi in Cancer Therapy. *Mol. Cancer* **2017**, *16(1)* (134), 1–9. https://doi.org/10.1186/s12943-017-0683-y.

(16) El Majzoub, R.; Fayyad-kazan, M.; Nasr El Dine, A.; Makki, R.; Hamade, E.; Grée, R.; Hachem, A.; Talhouk, R.; Fayyad-Kazan, H.; Badran, B. A Thiosemicarbazone Derivative Induces Triple Negative Breast Cancer Cell Apoptosis: Possible Role of MiRNA-125a-5p and MiRNA-181a-5p. *Genes and Genomics* **2019**, *41* (12), 1431–1443. https://doi.org/10.1007/s13258-019-00866-y.

(17) Ninio-many, L.; Hikri, E.; Burg-golani, T.; Stemmer, S. M. MiR-125a Induces HER2 Expression and Sensitivity to Trastuzumab in Triple-Negative Breast Cancer Lines Characterizing the Expression Profile Of. *Front. Oncol.* **2020**, *10* (191), 1–12. https://doi.org/10.3389/fonc.2020.00191.

(18) Yan, L.; Zhang, C. Y.; Wang, Y. B. MiR - 125a - 5p Functions as a Tumour Suppressor in Breast Cancer by Downregulating BAP1. *J. Cell. Biochem.* **2018**, *119* (11), 8773–8783. https://doi.org/10.1002/jcb.27124.

(19) Sun, X.; Xu, H.; Huang, T.; Zhang, C.; Wu, J.; Luo, S. Simultaneous Delivery of Anti-MiRNA and Docetaxel with Supramolecular Self-Assembled " Chitosome " for Improving Chemosensitivity of Triple Negative Breast Cancer Cells. **2021**, *21*, 192–204.

(20) Song, C.; Xiao, Y.; Ouyang, Z.; Shen, M.; Shi, X. Efficient Co-Delivery of MicroRNA 21 Inhibitor and Doxorubicin to Cancer Cells Using Core-Shell Tecto Dendrimers Formed via Supramolecular Host-Guest Assembly. *J. Mater. Chem. B* **2020**, *8* (14), 2768–2774. https://doi.org/10.1039/d0tb00346h.

(21) Deng, X.; Cao, M.; Zhang, J.; Hu, K.; Yin, Z.; Zhou, Z.; Xiao, X.; Yang, Y.; Sheng, W.; Wu, Y.; Zeng, Y. Hyaluronic Acid-Chitosan Nanoparticles for Co-Delivery of MiR-34a and Doxorubicin in Therapy against Triple Negative Breast Cancer. *Biomaterials* **2014**, *35* (14), 4333–4344. https://doi.org/10.1016/j.biomaterials.2014.02.006.

(22) Wang, S.; Zhang, J.; Wang, Y.; Chen, M. Hyaluronic Acid-Coated PEI-PLGA Nanoparticles Mediated Co-Delivery of Doxorubicin and MiR-542-3p for Triple Negative Breast Cancer Therapy. *Nanomedicine Nanotechnology, Biol. Med.* **2016**, *12* (2), 411–420. https://doi.org/10.1016/j.nano.2015.09.014.

(23) Gong, C.; Tian, J.; Wang, Z.; Gao, Y.; Wu, X.; Ding, X.; Qiang, L.; Li, G.; Han, Z.; Yuan, Y.; Gao, S. Functional Exosome-Mediated Co-Delivery of Doxorubicin and Hydrophobically Modified MicroRNA 159 for Triple-Negative Breast Cancer Therapy. *J. Nanobiotechnology* **2019**, *17* (1), 1–18. https://doi.org/10.1186/s12951-019-0526-7.

(24) Sharma, R.; Kumari, M.; Mishra, S.; Chaudhary, D. K.; Kumar, A.; Avni, B.; Tiwari, S. Exosomes Secreted by Umbilical Cord Blood-Derived Mesenchymal Stem Cell Attenuate Diabetes in Mice. *J. Diabetes Res.* **2021**, *2021*. https://doi.org/10.1155/2021/9534574.

(25) Théry, C.; Amigorena, S.; Raposo, G.; Clayton, A. Isolation and Characterization of Exosomes from Cell Culture Supernatants and Biological Fluids. *Curr. Protoc. Cell Biol.* **2006**, *30* (1), 1–29. https://doi.org/10.1002/0471143030.cb0322s30.

(26) Wang, Y.; Wang, P.; Zhao, L.; Chen, X.; Lin, Z.; Zhang, L.; Li, Z. MiR-224-5p Carried by Human Umbilical Cord Mesenchymal Stem Cells-Derived Exosomes Regulates Autophagy in Breast Cancer Cells via HOXA5. *Front. Cell Dev. Biol.* **2021**, *9*, 679185. https://doi.org/10.3389/fcell.2021.679185.

(27) Shojaei, S.; Hashemi, S. M.; Ghanbarian, H.; Sharifi, K.; Salehi, M.; Mohammadi-Yeganeh, S. Delivery of MiR-381-3p Mimic by Mesenchymal Stem Cell-Derived Exosomes Inhibits Triple Negative Breast Cancer Aggressiveness; an In Vitro Study. *Stem Cell Rev. Reports* **2021**, *17* (3), 1027–1038. https://doi.org/10.1007/s12015-020-10089-4.

(28) Liang, G.; Zhu, Y.; Ali, D. J.; Tian, T.; Xu, H.; Si, K.; Sun, B.; Chen, B.; Xiao, Z. Engineered Exosomes for Targeted Co-Delivery of MiR-21 Inhibitor and Chemotherapeutics to Reverse Drug Resistance in Colon Cancer. *J. Nanobiotechnology* **2020**, *18* (10), 1–15.

https://doi.org/10.1186/s12951-019-0563-2.

(29) Sancho-Albero, M.; Navascués, N.; Mendoza, G.; Sebastián, V.; Arruebo, M.; Martín-Duque, P.; Santamaría, J. Exosome Origin Determines Cell Targeting and the Transfer of Therapeutic Nanoparticles towards Target Cells. *J. Nanobiotechnology* **2019**, *17(1)* (16), 1–13. https://doi.org/10.1186/s12951-018-0437-z.

(30) Vakili-Ghartavol, R.; Rezayat, S. M.; Faridi-Majidi, R.; Sadri, K.; Jaafari, M. R. Optimization of Docetaxel Loading Conditions in Liposomes: Proposing Potential Products for Metastatic Breast Carcinoma Chemotherapy. *Sci. Rep.* **2020**, *10* (1), 5569. https://doi.org/10.1038/s41598-020-62501-1.

(31) Kim, M. S.; Haney, M. J.; Zhao, Y.; Mahajan, V.; Deygen, I.; Klyachko, N. L.; Inskoe, E.; Piroyan, A.; Sokolsky, M.; Okolie, O.; Hingtgen, S. D.; Kabanov, A. V.; Batrakova, E. V. Development of Exosome-Encapsulated Paclitaxel to Overcome MDR in Cancer Cells. *Nanomedicine Nanotechnology, Biol. Med.* **2016**, *12* (3), 655–664. https://doi.org/10.1016/j.nano.2015.10.012.

(32) Soo, M.; Haney, M. J.; Zhao, Y.; Mahajan, V.; Deygen, I.; Klyachko, N. L.; Inskoe, E.; Piroyan, A.; Sokolsky, M.; Okolie, O.; Hingtgen, S. D.; Kabanov, A. V; Batrakova, E. V. Development of Exosome-Encapsulated Paclitaxel to Overcome MDR in Cancer Cells. *Nanomedicine Nanotechnology, Biol. Med.* **2016**, *12* (3), 655–664. https://doi.org/10.1016/j.nano.2015.10.012.

(33) Sun, X.; Xu, H.; Huang, T.; Zhang, C.; Wu, J.; Luo, S. Simultaneous Delivery of Anti-MiRNA and Docetaxel with Supramolecular Self-Assembled "Chitosome" for Improving Chemosensitivity of Triple Negative Breast Cancer Cells. *Drug Deliv. Transl. Res.* **2021**, *11* (1), 192–204. https://doi.org/10.1007/s13346-020-00779-4.

(34) Hernández-Vargas, H.; Palacios, J.; Moreno-Bueno, G. Molecular Profiling of Docetaxel Cytotoxicity in Breast Cancer Cells: Uncoupling of Aberrant Mitosis and Apoptosis. *Oncogene* **2007**, *26* (20), 2902–2913. https://doi.org/10.1038/sj.onc.1210102.

(35) Vakili-Ghartavol, R.; Rezayat, S. M.; Faridi-Majidi, R.; Sadri, K.; Jaafari, M. R. Optimization of Docetaxel Loading Conditions in Liposomes: Proposing Potential Products for Metastatic Breast Carcinoma Chemotherapy. *Sci. Rep.* **2020**, *10* (1), 1–14. https://doi.org/10.1038/s41598-020-62501-1.

(36) Liu, Y. L.; Chou, C. K.; Kim, M.; Vasisht, R.; Kuo, Y. A.; Ang, P.; Liu, C.; Perillo, E. P.; Chen, Y. A.; Blocher, K.; Horng, H.; Chen, Y. I.; Nguyen, D. T.; Yankeelov, T. E.; Hung, M. C.; Dunn, A. K.; Yeh, H. C. Assessing Metastatic Potential of Breast Cancer Cells Based on EGFR Dynamics. *Sci. Rep.* **2019**, *9* (1), 1–13. https://doi.org/10.1038/s41598-018-37625-0.

(37) Pimm, M. L.; Henty-Ridilla, J. L. New Twists in Actin-Microtubule Interactions. *Mol. Biol. Cell* **2021**, *32* (3), 211–217. https://doi.org/10.1091/MBC.E19-09-0491.

(38) Cenik, M.; Abas, B. I.; Kocabiyik, B.; Demirbolat, G. M.; Cevik, O. Development of a New Drug Delivery System from HELA-Derived Exosomes and the Effect of Docetaxel-Loaded Exosomes on Mitochondrial Apoptosis. *J. Pharm. Innov.* **2021**, No. 0123456789. https://doi.org/10.1007/s12247-021-09566-1.

(39) Wang, Y.; Guo, M.; Lin, D.; Liang, D.; Zhao, L.; Zhao, R.; Wang, Y. Docetaxel-Loaded Exosomes for Targeting Non-Small Cell Lung Cancer: Preparation and Evaluation in Vitro and in Vivo. *Drug Deliv.* **2021**, *28* (1), 1510–1523. https://doi.org/10.1080/10717544.2021.1951894.

(40) Haney, M. J.; Zhao, Y.; Jin, Y. S.; Li, S. M.; Bago, J. R.; Klyachko, N. L.; Kabanov, A. V.; Batrakova, E. V. Macrophage-Derived Extracellular Vesicles as Drug Delivery Systems for Triple Negative Breast Cancer (TNBC) Therapy. *J. Neuroimmune Pharmacol.* **2019**, *15* (3), 487–500. https://doi.org/10.1007/s11481-019-09884-9.

(41) Sverdlov, E. D. Amedeo Avogadro's Cry: What Is 1μg of Exosomes? *BioEssays* **2012**, *34* (10), 873–875. https://doi.org/10.1002/bies.201200045.

(42) Salarpour, S.; Forootanfar, H.; Pournamdari, M.; Ahmadi-Zeidabadi, M.; Esmaeeli, M.; Pardakhty, A. Paclitaxel Incorporated Exosomes Derived from Glioblastoma Cells: Comparative Study of Two Loading Techniques. *DARU, J. Pharm. Sci.* **2019**, *27* (2), 533–539. https://doi.org/10.1007/s40199-019-00280-5.

(43) Xu, X.; Lv, Y.; Yan, C.; Yi, J.; Ling, R. Enforced Expression of Hsa-MiR-125a-3p in Breast Cancer Cells Potentiates Docetaxel Sensitivity via Modulation of BRCA1 Signaling. *Biochem. Biophys. Res. Commun.* **2016**, *479*, 893–900. https://doi.org/10.1016/j.bbrc.2016.09.087.

(44) Yan, L.; Zhang, C. Y.; Wang, Y. B. MiR - 125a - 5p Functions as a Tumour Suppressor in Breast Cancer by Downregulating BAP1. **2018**, No. May, 8773–8783. https://doi.org/10.1002/jcb.27124.

XXXXXX

RAW Exosomes and Exosomal fragment (EF)

Chapter IV

Isolation, Preparation, Characterization and *in vitro* Evaluation of the RAW 264.7 Cell Derived Exosomes and (EF)

4.1 Introduction

The advent of exosomes for the delivery of cancer therapeutics, fulfilled the need of a cell-free biogenic nano-carrier system that can bypass the drawbacks of both polymers/lipid-based nano-formulations and cell-based therapy[1]. Among all the immune cell derived exosomes, only macrophage derived exosomes have been widely explored as a nanocarrier for anti-cancer molecules so far however, their functional duality and significance of this dual nature has been quite less explored. Murine macrophage RAW 264.7 cell-derived exosomes were reported to exhibit variable loading efficiency of small anticancer molecules (PTX and DOX) by either active or passive loading techniques. While Exo-PTX showed 25 $\mu g/10^{11}$ particles loading capacity (LC) by mild sonication technique, Exo-DOX showed LC of only 14 $\mu g/10^{11}$ particles in a pH-dependent manner. DOX loading was observed to be pH dependent; an improved LC was reported at an alkaline pH (pH=8) in the same study. The priming of source cells with DOX also exhibited variable LC depending upon the source of cells used. For example, DOX pre-treated RAW 264.7 cells derived exosomes reported a LC of 7.27 ng DOX per μg exosomes which was lower than the tumor derived exosomes (TEX); despite the lower LC, DOX loaded RAW 264.7 cell-derived exosomes, Exo-DOX showed a greater apoptotic index of 80.1% in comparison to 65.3% exhibited by TEX indicating that the immunological status of the source cell creates a significant impact in the therapeutic output as well. [2,3] Although this loading efficiency is numerically lower than the loading capacity of PTX and DOX in liposomal formulations (88.1 ± 5.8 % and 96.8 ± 1.3 %), the exosomal formulations exhibited 10 times higher uptake efficiency than the lipid/polymer-based formulations of the same.[4] Additionally, we came across just a single study wherein, RAW 264.7 cells were primed with IFN-γ to obtain M1 type macrophages from which exosomes were derived and loaded with PTX to obtain PTX-M1-Exo with 19.55 ± 2.48% drug loading. PTX-M1-Exo exhibited greater cytotoxicity in 4T1 cells within 24h in comparison to the free PTX group (IC_{50} 4.30 μg/mL vs. 17.49 μg/mL). Further, PTX-M1-Exo exhibited greater tumor volume reduction in 27 days attributed to the higher expression of IL-12/6, TNF-α and caspase 3 activity by M1 exosomes. This study demonstrated the synergistic antitumor effect of a chemotherapeutic agent loaded into M1 exosomes possessing intrinsic immune-stimulant action.[5]

Interesting outcomes have been demonstrated by the macrophage derived exosomes as a nanocarrier of chemotherapeutics as well as immunomodulatory vesicles *per se* in their naive and

polarized forms without any additional chemo or immunotherapeutic payload. The possible synergy that could result due to their immunomodulatory nature and their efficiency as a nanocarrier together still remains unexplored.

Autologous ascitic fluid (a rich source of monocytes and macrophages) from the colorectal carcinoma (CRC) patients was used to isolate exosomes, A_{ex} dose > 200 μg was found to induce superior tumor-specific cytotoxicity in the presence of GM-CSF (50 μg per immunization) than A_{ex} alone.[6] This observation led to the investigation of strategies for converting the monocyte cells into macrophages, particularly M1 specific macrophages which could be further utilized to isolate exosomes of M1 type with expected immunogenicity. In general, macrophages are heterogeneous, both the subtypes, M1 and M2 indistinctly co-exist under the physiological conditions, which can polarize and proliferate into either of two types depending on their exposure to different immunological conditions. When exposed to a specific antigen, LPS or cytokines, or a specific experimental condition, these follow the classical activation pathway to polarize into the M1 type while the M2 type predominantly proliferates upon exposure to glucocorticoid or IL-10 mediated immune-suppressant conditions. A comparative study between M1 vs M2 derived exosomes in a murine melanoma model concluded that both M1 and M2 exosomes can increase immune cell expansion. A lipid calcium phosphate (LCP) based vaccine was designed to deliver the melanoma antigen, Trp2 to trigger the Toll-like receptor 9 (TLR9). Herein, M1 exosomes were explored as an immune-potentiator adjuvant. The M1 exosomes exhibited greater cytolysis (65.4%) of antigen-specific splenocytes which was almost double the response observed with LCP alone i.e. 32.6%, clearly indicating that M1 exosomes served as an effective adjuvant in the LCP-based cancer vaccine.[7] In fact, the usage of exosome depleted FBS in the culture media of macrophages also has shown prominent effect on the immunological aspects of the macrophages. The presence of fetal bovine exosomes was reported to suppress inflammatory cytokines, TNF-α, IL-1β, and IL-6 release by macrophages in the presence and absence of LPS, although, the mechanism behind this observation remains unknown[8]. Additionally, it was also observed that EV-depleted FBS showed a reduced growth rate of different cells i.e., HEK-293T, HeLa, SY5Y human neuroblastoma cells but did not exhibit an increased sensitivity to the DNA-damaging agent etoposide and the endoplasmic reticulum stress inducing agent tunicamycin significantly[9]. The culture conditions also have a paramount role in determining the immunological and physiological alteration in the cells used for exosome procurement. Also, the nature of cells is expected to determine the

physiological alteration in the exosomes isolated from them[10]. Taking lead from the existing literature, we decided to explore RAW264.7 derived exosomes functionally along with testing its physical capability to maintain its integrity under different experimental conditions.

This chapter specifically deals with the isolation, characterization and biological implications of the RAW 264.7 cell derived exosomes on the 4T1 cells which will put some insight regarding the rationality of choosing the macrophage cells as the source of exosomes. In context of the studies mentioned here, the formulation development, validation and evaluation of the DTX loaded RAW 264.7 cell derived exosomes would be discussed in detail in **Chapter 5**. This chapter would also discuss the preparation, characterization and evaluation of the exosomal fragments from RAW exosomes. The exosomal fragments so prepared were utilized for developing a core/shell type of delivery system to co-load DTX and miR-34a (*discussed in **Chapter 6***).

4.2 Materials and Methods

4.2.1 Materials

Cells and cell culture reagents

Murine TNBC 4T1 cells and RAW 264.7 cells were procured from Regional Centre of Biotechnology (Haryana, India) and NCCS (Maharashtra, India) respectively. We are grateful to Professor Avinash Bajaj for providing the 4T1 cells. Exosome depleted FBS was prepared *in-house* by ultracentrifugation of a mixture of FBS and PBS (FBS:PBS=3:7) at 1,20,000×g and 4˚C for 18h. Dulbecco's modified Eagle's medium (Gibco™ DMEM, high glucose) and Fetal bovine serum (FBS) were purchased from GIBCO (Invitrogen Inc. Gibco BRL, USA) while, Penicillin plus streptomycin solution, 4′,6-diamidino-2-phenylindole (DAPI), and Protease inhibitor cocktail powder (#SRE 0055-1BO) were bought from Sigma-Aldrich (St. Louis, MO, USA). For the characterization purpose, Pierce™ Bicinchoninic acid (BCA) protein assay kit and PKH26 red fluorescent cell linker mini kit (MINI 26-1KT) were procured from Thermo™ Scientific (Waltham, USA).

For Western blot analysis primary antibodies used were Alix mAb (#92880), HSP 70 mAb (#4872T) and TSG101 mAb (#72312S). Secondary antibodies anti-rabbit IgG HRP linked antibody (#7074P2), anti-mouse IgG HRP linked antibody (#7076s), Caspase-3 (#9662), Cleaved caspase 3 (#9664) and β-actin (#3700) were procured from Cell Signalling Technology (Danvers, USA) and mouse CD63 (sc-365604) mAb was obtained from Santa Cruz Biotechnologies (Texas,

USA). Clarity Western ECL Substrate (#1705060), and Precision Plus Protein™ standards (#161-0394), and Immuno-Blot® PVDF membrane were procured from Bio-Rad (California, USA). Protease inhibitor cocktail powder (#SRE 0055-1BO) was bought from Sigma-Aldrich (St. Louis, MO, USA). RIPA lysis buffer (TCL 131), calcium chloride dehydrates (GRM 399) and Tris base (MB311) were procured from Himedia (Maharashtra, INDIA). Rat IFN-γ (900-M109), TNF-α (900-M73) and Mini ABTS ELISA Development kit for the ELISA assay were procured from PeproTech® (NJ, USA). For qRT-PCR, GAPDH and BCL-2 primers (sequences are mentioned below) were procured from Integrated DNA Technologies (Lowa, USA), GeneSure first strand cDNA synthesis kit was purchased from Puregene (New Delhi, INDIA), and iTaq™ Universal SYBR green Supermix was from Bio-Rad (California, USA).

Gene	Forward sequence	Reverse sequence
BCL-2	5'-CCTGTGGATGACTGAGTACC-3'	5'-GAGACAGCCAGGAGAAATCA-3'
GAPDH	5'-TGCATCCTGCACCACCAACT-3'	5'-AGCCTGCTTCACCACCTTC-3'

4.2.2 Methods

4.2.2.1 Maintenance of RAW 264.7 cells

RAW 264.7 macrophages were procured from NCCS (cell repository, Pune, India) and were cultured in DMEM, supplemented with 10% v/v exosome depleted FBS and 1% penicillin and streptomycin at 37°C and 5% CO_2. Cells were maintained in T-175 culture flasks in the complete media till 80%-90% confluent could be achieved and the conditioned media (CM) was collected twice weekly which was further processed to collect the RAW264.7 cell derived exosomes. Exosome depleted FBS was prepared *in-house* by ultracentrifugation of a mixture of FBS and PBS (FBS:PBS=3:7) at 1,20,000×g and 4˚C for 18h.

4.2.2.2 Isolation of the RAW 264.7 cell derived Exosomes

The RAW 264.7 CM was collected twice weekly from 6× T-175 culture flasks and processed by modified sequential centrifugation and ultracentrifugation technique to pellet down the exosomes. In order to deplete the CM of cells, dead cells, and cellular debris, 200 mL of the collected media was processed step-wise at 500×g, 2000×g and 13,000×g for 10 min, 15 min and 30 min respectively at 4˚C. At each step, the supernatant was collected and finally subjected to ultracentrifugation at 1,20,000×g at 4˚C for 2h. Once the exosomes were pelleted down, supernatant was discarded and the exosomes were washed with an excess of PBS (10 mM) at

1,20,000×g and 4˚C for 2 h. The final pellet was redispersed in 400 µl of PBS. The uniformly redispersed exosomes were then stored at -20˚C till further use.

4.2.2.3 Preparation of RAW 264.7 derived exosome fragment (EF)

For the preparation of the EF, RAW 264.7 cell derived exosomes were resuspended in ice-cold hypotonic solution, Tris-calcium buffer (TC buffer; 0.01 M Tris and 0.001 M calcium chloride, pH 7.4), supplemented with EDTA free protease inhibitor cocktail and stored at 4˚C overnight. This treatment would yield the ghost exosomal membrane (Exo_{TC}) only. The Exo_{TC} were further setteled down by ultracentrifugation at 1,80,000×g, 4˚C for 3h and redispersed in the modified PBS before proceeding for the EF preparation. For screening purpose, two techniques were used for further preparation of EF (a) Probe sonication wherein, the Exo_{TC} were further probe sonicated (Sonics Vibra-Cell™, USA) under low temperature at 30% amplitude, 10s on/off cycle twice, (b) Extrusion through Avanti Lipid extruder (Avanti Polar Lipids, USA) in which Exo_{TC} was further passed through a 200 nm and 100 nm pore diameter membrane (10 times).

4.2.2.4 Characterization of RAW exosomes and EF

The characterization of both RAW Exosomes and EF was carried out for particle size (nm), absolute intensity (Kcounts/s) and polydispersity index (PDI) by dynamic light scattering (DLS); surface charge (mV) and morphology were studied by Zeta-potential (ZP) and field emission scanning electron microscopy (FESEM) respectively. The surface protein content of naive exosomes and EF were quantified in terms of ≅µg protein by Pierce® BCA Kit and were characterized for exosomal positive marker proteins (Alix, TSG101, CD63) and house-keeping protein β-actin in comparison with the cell lysate (CL_N and CL_F) from RAW264.7 cells maintained in DMEM, supplemented with 10%v/v FBS and 10 %v/v exosome depleted FBS respectively. The % purity of the naive exosomes was evaluated by establishing the correlation between the absolute intensity of different concentrations of exosomes and their respective particle size and zeta-potential.

Particle size, distribution and zeta-potential

Both naive exosomes as well as EF were characterized by dynamic light scattering (DLS) using Anton Paar Litesizer 500 in backscattering mode (173° scattering angle), with 15s equilibration time, 10 runs for each analysis with 10 s for each run at 25˚C. Further, ζ-potential measurement was performed in total 50 runs, with 10s for each run, at 25˚C.

Morphology (FESEM)

The morphology of the naive exosomes, Exo_{TC}, and EF has been ascertained by FESEM analysis. For the naive exosomes and Exo_{TC}, 50µg equivalent protein was redispersed in 2% paraformaldehyde (PFA) solution (20µl) and spread onto the coverslip. For EF, 50 µg equivalent protein was smeared on the coverslip as soon as Exo_{TC} was probe sonicated at 30% amplitude for 2X sonication cycle with 10s on/off frequency. The coverslips for naive exosomes, E_{TC}, and EF were dried overnight at room temperature and sputtered with Gold-palladium coating (2-5 nm) and the analysis was carried out in 5-20 kV beam in FESEM. The comparative size, absolute intensity, zeta-potential and morphology would reflect the effect of the processes carried out on them.

Quantitative protein estimation

The quantification of exosomes is done by the equivalent protein concentration analysis using Pierce™ BCA kit wherein, BSA was used to prepare the calibration curve between 5-1000 µg/mL with R^2 value of 0.9967. The estimation of the equivalent exosomal protein content has been performed as per manufacturer's protocol. The correlation between the absolute intensity (Kcounts /s), particle size (nm) and zeta-potential (mV) of the exosomes with different equivalent protein concentration demonstrated the purity of exosomes isolated by the process. Also, it enabled characterization of the E_{TC} and EF prepared from naive exosomes.

Exosomal protein expression using Western blot technique

Exosomes (~100 µg protein) were redispersed in 50µl of RIPA buffer supplemented with protease inhibitor cocktail after being settled down by UC and probe-sonicated to release the exosomal proteins as exosome lysate (EL). Simultaneously, RAW 264.7 cells, maintained in DMEM supplemented with both normal FBS and exo-free FBS were washed thrice in PBS and then lysed to prepare the cell lysates, i.e., CL_N and CL_F by sonication (10s on/off, 2 cycles, 30% amplitude) at 15˚C. CL_N, CL_F, EL and EF (~30 µg protein) were resolved in 12.5% and 15% SDS PAGE, and transferred in polyvinylidene fluoride membrane. After blocking the blots in 3% BSA in TBST solution, the presence of exosomal marker proteins, i.e., CD63, Alix and TSG 101 and housekeeping protein β-actin was ascertained by probing the blots in CD63 (1:500) mice monoclonal antibody, rabbit- Alix (1:2000), TSG 101 (1: 2000), and β-actin (1:1000) mice monoclonal antibody overnight and then 3h incubation with secondary HRP linked anti-mouse/rabbit IgG antibody (1:1000). Thereafter, the blots were developed using Clarity Western ECL substrate in ChemiDoc™XRS+ (Bio-Rad, California, USA).

4.2.2.5 Effect of formulation process parameters on the exosomal integrity

Before optimizing the process parameters to encapsulate DTX into RAW 264.7 derived exosomes, a thorough screening of the sonication parameters, including the sonication pattern, frequency and amplitude of sonication, was carried to determine the precise impact of these parameters on the exosomal integrity by determination of particle size (nm), absolute intensity (Kcounts/s), polydispersity index (PDI), and zeta-potential (mV).

Effect of Amplitude and number of Sonication cycles

Exosomes (~100 µg protein) were dispersed in a previously optimized dispersion media (10 mM PBS + 10% v/v methanol); methanol was added in the dispersion media to mimic the same dispersion media as would be required for the formulation preparation considering the low solubility of DTX in PBS alone (12.9±0.28 µg/ml) which increases to 27.3±0.79 µg/ml in the presence of methanol and then processed as shown below in **Table 4.1**.

(1) Three identical batches, B1, B2 and B3 were prepared, wherein, **B1** was incubated at 37°C for 2 h (without sonication). **B2** and **B3** were prepared by sonicating at 20% amplitude for **4 cycles** (4X) and **12 cycles** (3*4X), 30s on/off pulses, and 2 min of intermediate cooling in ice bath after every 4 cycles) respectively. Following that, all of the batches were incubated for 2 h at 37°C.

(2) Two more batches, **B4** and **B5**, were prepared utilizing 40% sonication amplitude with one 30s on/off sonication cycle (1X) and 4X sonication cycles, respectively, to assess the impact of the sonication amplitude on the formulation. The batches were then incubated for 2 h at 37°C. Later on, all the batches were processed through ultracentrifugation to pellet down the exosomes and redispersed in 10 mM PBS.

Table 4.1
Formulations prepared for evaluating the effect of process parameters on the exosomal integrity.

Formulation	Exosomes (µg)[#]	Sonication		Incubation
		% Amplitude	**Sonication cycle**	
B1	100	-	-	37˚C, 2h
B2	100	20	4X	
B3	100	20	(3*4X)	
B4	100	40	1X	
B5	100	40	4X	

[#] Only exosomes (µg equivalent protein) without DTX are listed here.
*1X refers to one sonication cycle comprising of 30s on/off pulse.

Effect of Sonication and Extrusion processes on Exo_{TC}

After pelleting down the Exo_{TC} by ultracentrifugation at 180,000×g, 4˚C for 3h, these were redispersed in modified PBS, and quantified by Pierce™ BCA assay (as per manufacturer's protocol). The impact of the sequential processes involved in the preparation of EF by sonication and extrusion was further ascertained by comparing particle size, absolute intensity, zeta-potential and protein content.

4.2.2.6 Efficient cellular uptake of PKH 26 stained exosomes

For initial confirmation, 4T1 cells (1.0×10^4 cells/well) were seeded in a 24-well plate overnight before being treated with PKH-26 stained naive exosomes for 12h. At predetermined time-points, the cells were washed twice with PBS followed by fixing the cells with 2.0% paraformaldehyde (PFA). The nuclei of the cells were stained with DAPI and viewed under a fluorescence microscope.

4.2.2.7 Western Blot analysis

1×10^5 cells were seeded in a 6-well plate and kept overnight to allow the cells to adhere to the well before starting the experiment. Cells were treated with two different concentrations of naive exosomes, i.e., 2.5μg/mL and 5.0 μg/mL for 48h. At predetermined time-points, the cells were trypsinized and then washed with complete media and PBS twice before proceeding ahead with the cell lysate preparation.

Analysis of differential protein expression (by Western Blot assay) revealed the mode of action of different exosomal formulations on the 4T1 cells. Herein, cells from media control and exosome treated groups were lysed with Triton-X-100 lysis buffer containing a 1X protease inhibitor cocktail solution and sonicated at 30% amplitude for 10s on/off cycle twice in ice bath. The cell lysate was then centrifuged at 13,000 rpm for 10 min at 4˚C to pellet down the cellular debris. The supernatant containing the proteins was collected and stored at -20 ˚C till the next usage.

50 μg equivalent protein from each cell lysate group was resolved on a 15% gel in SDS-PAGE and transferred to a PVDF membrane by a wet transfer method. The membrane was incubated with primary antibody overnight at 4°C and secondary antibody for 1h at room temperature. Protein bands were detected using Clarity Western ECL substrate (Bio-Rad, Hercules, CA, USA). The following primary antibodies were used: Rabbit- β1-integrin, Caspase 3 and cleaved caspase-

3, and anti-rabbit HRP linked secondary antibody for probing the blots. All experiments were performed in duplicate.

4.2.2.8 Impact of EF on the inflammatory cytokine released by 4T1

1×10^5 cells were seeded in a 6-well plate and kept overnight to allow the cells to adhere before starting the treatment. Cells were treated with two different concentrations of exosomal fragments, i.e., EF1 (6 µg/mL) and EF 2 (12 µg/mL) for 48h. At predetermined time-points, the cell CM was collected and centrifuged at 5000 rpm, room temperature for 5 min to expel out the cellular debris and dead cells.

Further the cell conditioned media of media control and the EF treated groups was diluted 10 folds' and was utilized to quantify the pro-inflammatory cytokines, i.e., TNF-α and IFN-γ levels using the respective ELISA assay kits.

4.2.2.9 Impact of EF on the BCL-2 gene expression in 4T1

Following the same experimental protocol as mentioned in ***section 4.2.2.8***, the cells were trypsinized and washed thrice with sterile PBS and dispersed in 1mL of RNA-XPress™ Reahent (Himedia) and stored at -20˚C overnight. After isolating the total RNA, concentration of RNA in each sample was quantified by Nanodrop. The cDNA synthesis was carried out using GeneSure™ First Strand cDNA Synthesis Kit following manufacturer's protocol and quantified with Nanodrop. 200 ng equivalent cDNA was utilized to determine the cycle threshold (C_T) values using Real-time PCR for target gene BCL-2 and housekeeping gene GAPDH. The C_T value of the BCL-2 for each sample was normalized with respect to the C_T value of the GAPDH. Gene quantification was performed using Universal SYBR green Supermix. The folds' change of the BCL-2 expression was expressed by calculating $2^{-\Delta\Delta C_T}$ values.

4.2.2.10. Statistical Data Analysis

The data has been represented as mean ± standard deviation as processed in GraphPad Prism (Version 5.0, USA). The difference between two groups was compared using Student's *t*-test, comparison between multiple groups was carried out using one-way ANOVA followed by a Tukey's test. Value of $p < 0.05$ was considered as statistically significant.

4.3 Results

4.3.1. Isolation, characterization and % yield of RAW 264.7 cell derived exosomes

RAW 264.7 derived exosomes were isolated from the collected CM with exosomal yield of~ 172.03±28.9 µg protein per 200 mL CM. **Figure. 4.1.A** reveals hydrodynamic diameter (Z_{AVG}) of 182.40 nm with polydispersity index (PDI) of 0.256±0.03 by DLS while, the comparative size data obtained from FESEM indicated comparatively low particle size due to single particle analysis in **Table 4.2**. Lesser exosomal size measured by FESEM in comparison to that observed in DLS is possibly owing to the presence of aggregates in the DLS samples that shifted the particle size distribution towards higher end. Naive exosomes exhibited negative surface potential equivalent to -10.27±3.66 mV as indicated in **Figure 4.1.B**, attributed to the presence of phospholipids and surface proteins in the exosomal bilayer. As indicated by FESEM (**Figure 4.1.C)** naïve exosomes were found to be spherical and non-uniform in size with characteristic clumping tendency. The inherent clumping nature was more prominent in case of exosomes isolated by single UC cycle in comparison to the exosomes being washed with excess PBS and processed through additional UC cycles. Additionally, we ascertained the purity of exosomes (equivalent protein content) by plotting the absolute intensity (Kcounts/s) against the serially diluted exosomal samples (between 28-448 µg/ml equivalent protein) using particle size analyzer and observed that as the equivalent protein concentration of exosomes was increased, the absolute intensity also increased linearly (**Figure 4.1.D)** with negligible change in the particle size (% number) and zeta-potential (mV) as indicated in **Table 4.3**. This linear correlation between concentration vs. absolute intensity of exosomes proved that the samples were devoid of any contaminants.

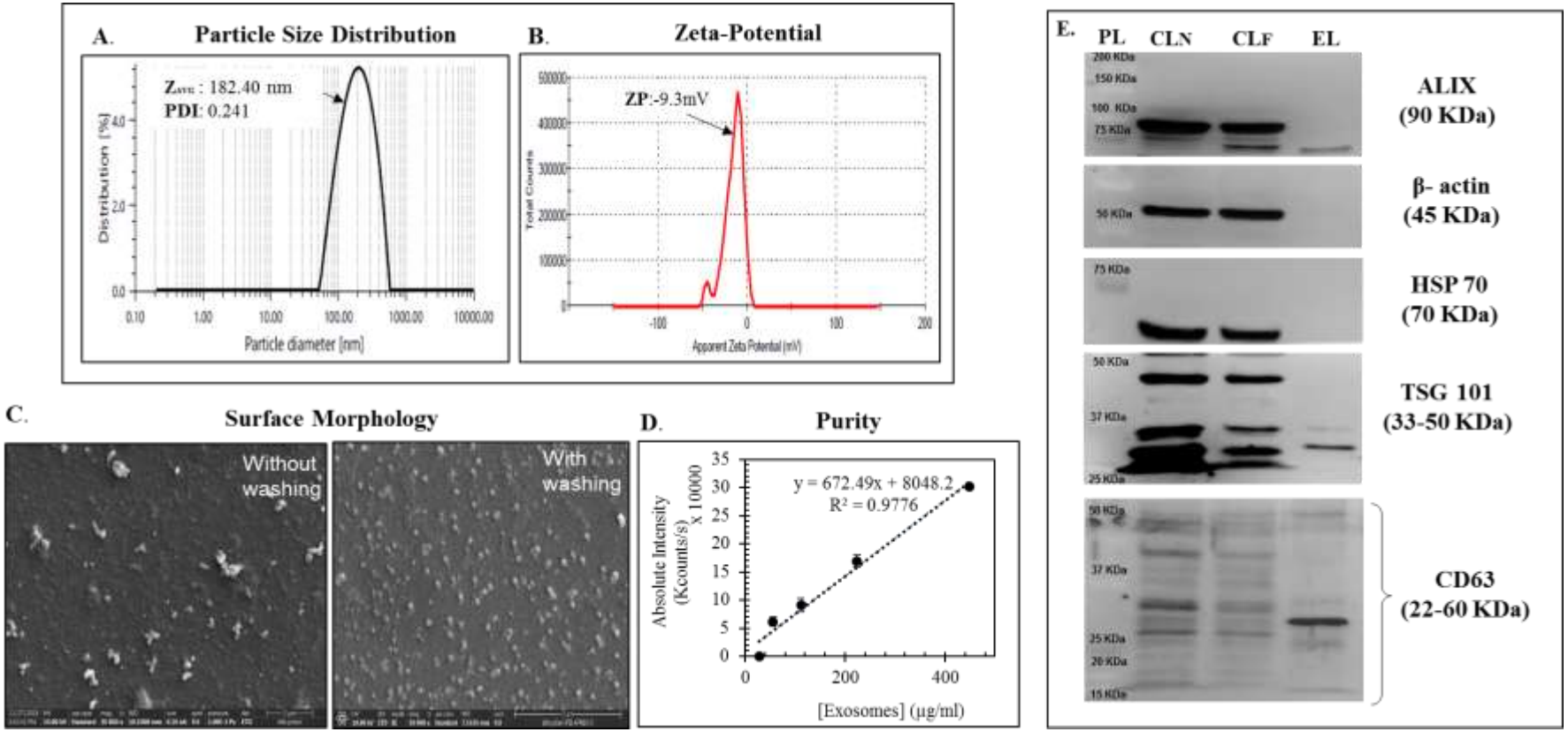

Figure 4.1. Characterization of naive RAW 264.7 cell derived exosomes isolated from cell conditioned media (CM) **(**A**)** Representative particle size distribution (B) zeta-potential graph of exosomes. (C) Characteristic change in morphology and clumping tendency of exosomes isolated from CM upon additional washing process. (D**)** Correlation between the absolute intensity (Kcounts/s) and different exosome concentration (µg equivalent protein/ml), data are presented as mean (n=3) ± SD. (E) Characterization of naive exosomes by western blot of the exosomal proteins, ALIX, TSG 101, HSP 70 and CD63 and housekeeping protein β-actin in exosome lysate (EL) in comparison to RAW264.7 cell lysates from RAW cells maintained in complete media (CL_N) and exo-depleted FBS supplemented media (CL_F).

Table 4.2
Comparative particle size (nm), PDI and zeta-potential (mV) of exosomes by DLS and FESEM.

	Particle size (nm)	PDI	ZP (mV)
DLS	208.7±36.19	0.256±0.03	-10.268±3.66
FESEM	112.5±21.48	NA	NA

Table 4.3
Effect of dilution on the physical characteristics of exosomes in a concentration dependent manner.

[Exosomes] (µg/mL)	Equivalent protein content (µg)	Particle Size* (nm)	ZP (mV)
448	26.88	113.26±2.20	-9.2±0.680
224	13.44	116.27±2.31	-10.63±1.27
112	6.72	95.34±8.08	-12.13±0.23
56	3.36	84.75±9.03	-12.76±0.95
28	1.68	113.27±13.59	-12.6±0.86

*Represents number distribution

Table 4.4
Comparative particle size (nm), absolute intensity (Kcps/s), PDI and zeta-potential (mV) of exosomes by DLS.

Batch	Specification	Particle Size (nm)	Absolute intensity (Kcps/s)	PDI	Zeta-potential (mV)
B6	Exosomes+ hypotonic environment	257.83±51.06	354769.6±82618	0.24±0.023	-20.6±0.87
B7	Ghost Exosome (Exo_{TC})	189.92±8.47	352927±11772.5	0.23±0.01	-11.7±0.57
B8	Exo_{TC} → Sonication	156.29±0.07	339743±2853.02	0.20±0.02	-11.3±0.29
B9	Exo_{TC} → Extrusion (200nm)	201.26±1.00@	144673.2±34226.53	0.26±0.06	-12.9±1.30
B10	Exo_{TC} → Extrusion (200nm→100nm)	207.3±44.05$	204523±37135.5	0.29±0.1	-13.27±0.47

@particle size with 79.7% peak intensity
$particle size with 53.5% peak intensity
Size measurements are carried under intensity distribution

The exosomes were further characterized for the expression of exosomal proteins Alix, TSG 101, CD63, and housekeeping protein β-actin and compared with RAW 264.7 cell lysates (CL_N and CL_F), as shown in **Figure 4.1.E.** We compared the exo-lysate (EL) with equivalent protein concentrations of CL_N and CL_F which clearly indicated that EL demonstrated a prominent ALIX, TSG101 and CD63 expression but absence of β-actin and HSP 70, whereas, both the CL samples showed presence of β-actin and absence of CD 63. In fact, the CL_N and CL_F showed different levels of target protein expression, while the β-actin expression was similar visually.

4.4.2 Preparation and characterization of the exosomal fragments (EF) from Exo$_{TC}$

Naïve exosomes were kept in hypotonic Tris/$CaCl_2$ buffer (TC) overnight to produce B6, which was further ultracentrifuged to pellet down the exosomal vesicles, denoted as **Exo$_{TC}$ (B7)**. Later, B7 was processed by two well-known techniques of size reduction, i.e., sonication (at 30% amplitude) and extrusion (sequentially through 200 nm and 100 nm pore diameter extruder for 10 times) to prepare B8 and B9-B10 respectively. The overall impact of the processes could be assessed from **Table 4.4** and **Figure 4.2 (A-F)**.

Comparing **Table 4.2** and **4.4**, it could be concluded that naïve exosomes swelled resulting in size increased from 208.7±36.19 nm to 257.83±51.06 nm in B6 upon being treated with hypotonic TC buffer. The osmosis of the solvent into the exosomes might be responsible for the size increment. **Figure 4.2.A** also emphasizes the fact that, sonication mediated EF preparation could not completely destroy the phospholipidic bi-layer, instead disrupted the exosomal membrane integrity and the intactness of the exosomal boundary. Also, the increased surface negativity with -20.6±0.87 mV zeta potential might have resulted due to the release of exosomal proteins upon built up of osmotic pressure causing occasional exosomal membrane rupture as seen in **Figure. 4.2.B.** The presence of ~50% of exosomal protein in the supernatant, collected after ultracentrifugation of B6 in the process of pelleting down the B7 (**Figure 4.2.B)** proved the osmotic pressure mediated release of proteins from exosomes under hypotonic conditions. Sonication definitely reduced the particle size in B8 but did not alter the absolute intensity or zeta-potential, which proves exosomal ability to withstand the harsh experimental condition. In **Figure 4.2.C**, extrusion was able to rupture the B7 to the extent that two distinct size populations could be clearly observed, and further confirmed by the increased PDI and enhanced surface negativity (attributed to the presence of the exosomal proteins). In comparison to sonication, extrusion

resulted in excessive protein release from the exosomes as indicated by **Figure 4.2.D.** This observation was further supported by the presence of multiple particle size peaks, increased PDI and enhanced surface potential negativity. The morphology determination by FESEM also revealed the enhanced particle size of individual exosomes with 257.83±51.06 nm (**Figure 4.2.E)**. Post-sonication, B8 detected ruptured exosomal boundary with uneven individual structure of exosomes, which is visibly different in shape than the Exo_{TC} (**Figure 4.2.F)**.

Further, EF were characterized by the presence of exosomal membrane proteins, i.e., TSG101, ALIX and CD63 and absence of β-actin and HSP70 in comparison to CL_F (**Figure 4.2.E)**. Interestingly, EL and EF expressed identical proteins but the EF showed a greater expression of the target proteins than the EL, and the absence of HSP 70 and β-actin in EF clearly indicated that the EF originated from the exosomes and not from the cells. Also, the identical pattern of protein expression in EF and EL proved that the process parameters employed did not destroy the physiological features of the exosomes.

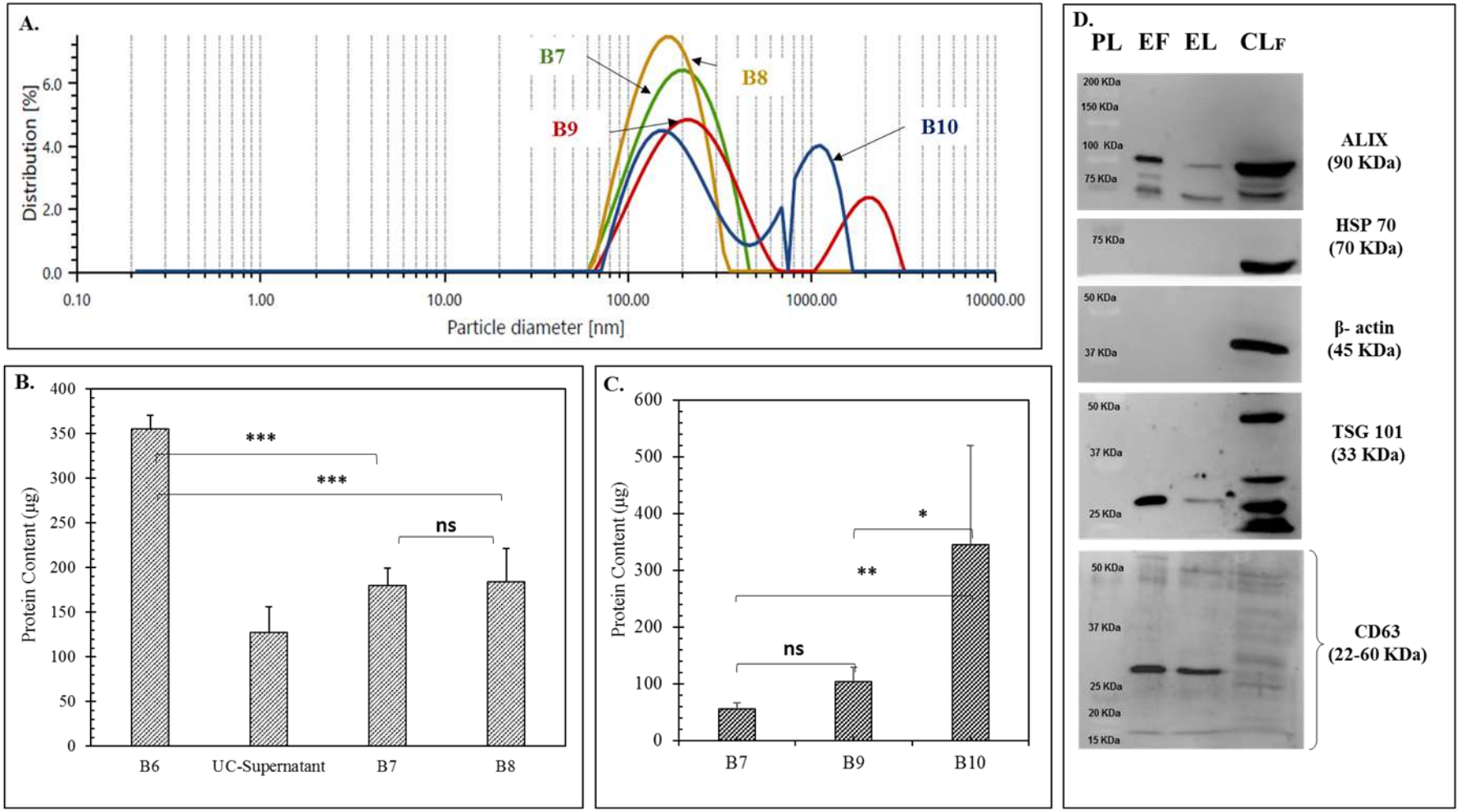

(To be continued)

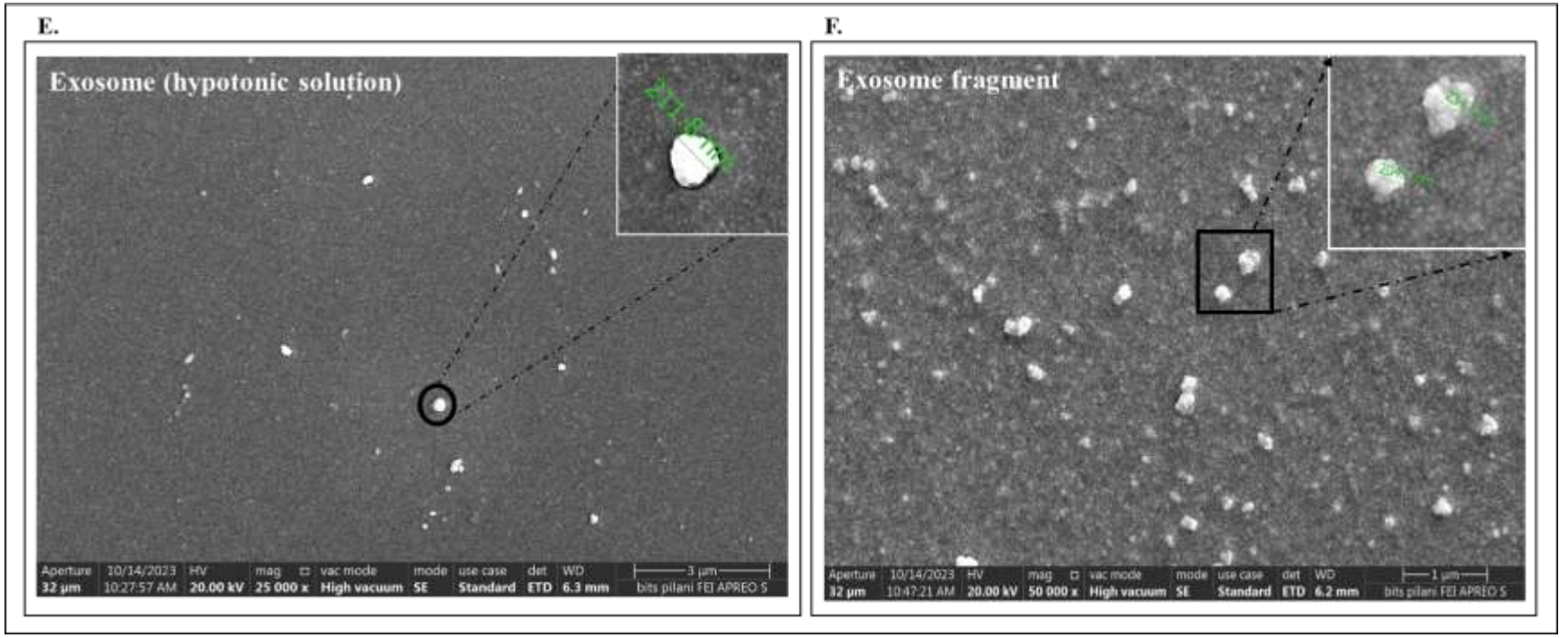

Figure 4.2: Characterization of the exosomal fragments (EF) (A) Comparative particle size distribution curve emphasizing the effect of two methods, i.e., sonication and sequential extrusion for EF preparation (B) Quantification of equivalent protein (μg) in different batches while preparing EF (**B7-B8**) using sonication method, data are represented (n=4) ±SD, (C) Quantification of equivalent protein (μg) in preparation of EF (**B9-B10**), sequential extrusion through 200nm and (200nm→100nm) pore diameter, data are represented (n=4) ±SD. (D) Characterization of exosomal protein expression in EF with respect to EL and CL_F. (E) Characteristic morphology of exosomes in hypotonic Tris/$CaCl_2$ buffer (pH 7.4), and (**F**) morphology of exosome fragments prepared by sonication.
Statistical significance was ascertained by one-way ANOVA with Tukey's comparison test, *p<0.05, **p<0.01, ***p<0.001.

4.4.3 Effect of sonication on the exosomal integrity

The impact of the sonication pattern and amplitude was assessed in batches, B1-B5 in comparison to the naive exosomes as indicated in **Table 4.1**. For batches B1-B3, exosomes were subjected to different sonication patterns at low amplitude (20%), while for batches B4 and B5 exosomes were subjected to two different sonication patterns at higher amplitude (30%). As seen in **Figure 4.3.A**, the particle size, zeta-potential, and PDI of naive exosomes and the B1 (incubation alone) formulation batch were not significantly different. But compared to B1 and naive exosomes, B2 (4X sonication cycle at 20% amplitude) and B3 (3*4X) sonication cycle at 20% amplitude) exhibited a significantly reduced surface charge and particle size as the number of sonication cycles was increased. In **Figure 4.3.B**, we compared B2 with B4 (prepared 1X sonication cycle at 30% amplitude) and B5 (prepared at 4X sonication cycle at 30% amplitude), B4 demonstrated no difference in peak (% intensity) compared to B2, but the higher sonication force resulted in drastically lowered particle size. In contrast, B5 underwent sonication at 30%
amplitude with a 4X sonication cycle resulting in two separate peaks corresponding to two different particle sizes shown as B5.1 (42%) and B5.2 (18.7%) as compared to B4 (66%).

Additionally, the absolute intensity increased almost 2 folds in case of B5 indicating rupture of exosomes upon being subjected to intense force of sonication but post-sonication incubation period assisted their resealing, resulting in two different populations of particles.

4.4.4 Efficient cellular uptake by 4T1 **cells**

This initial cellular internalization assay was planned to confirm the efficient PKH 26 staining of the exosomes and cellular uptake efficiency of PKH 26 labelled exosomes by 4T1 cells. As indicated in **Fig. 4.4**, there was no significant negative impact on the cellular morphology upon the internalization of the exosomes. Both cytoplasm and nucleus was found intact and healthy, but non-uniform cellular uptake was observed prominently even 12h post-treatment. Evidently, the exosomes accumulated in the cytoplasm of cells indicating that, exosomes can easily be explored as a promising delivery system.

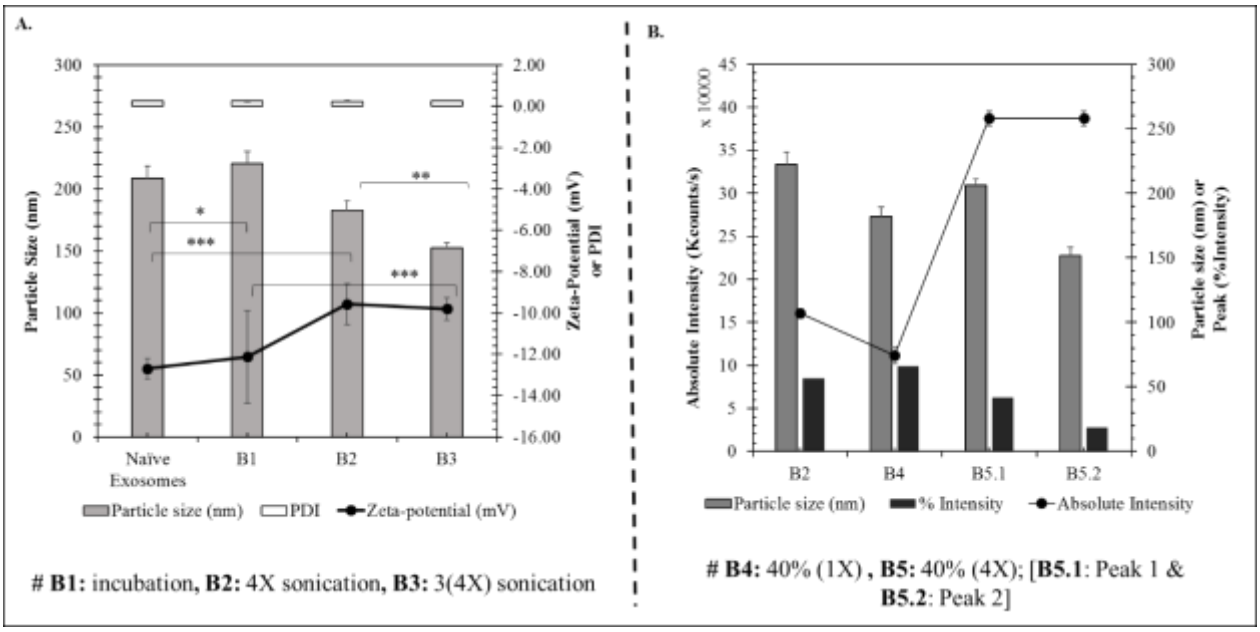

Figure 4.3: Effect of formulation process parameters on the exosomal integrity. A: Comparative characterization of naive exosomes, exosomes processed with incubation process only (B1), 4X sonication cycles (B2) and 3(4X) sonication cycles (B3) 20% amplitude. **B:** Effect of % amplitude of sonication on the exosomal integrity, where B2 is compared to B4 and B5. B4 represents exosomes processed at 40% amplitude with 1X cycle, and B5 represents exosomes processed at 40% amplitude with 4X cycle. B2 was prepared at 20% amplitude with 4X sonication cycles. All experiments were performed in triplicate (n=3, three independent experiments), statistical significance was ascertained by one-way ANOVA with Tukey's comparison test, *p<0.05, **p<0.01, ***p<0.001.

[#] [nX means 'n' number of sonication cycles comprising of 30s on/off pulse; %intensity denotes the % of light scattered by the particles under a single peak in intensity distribution graph while analyzing the particle size]

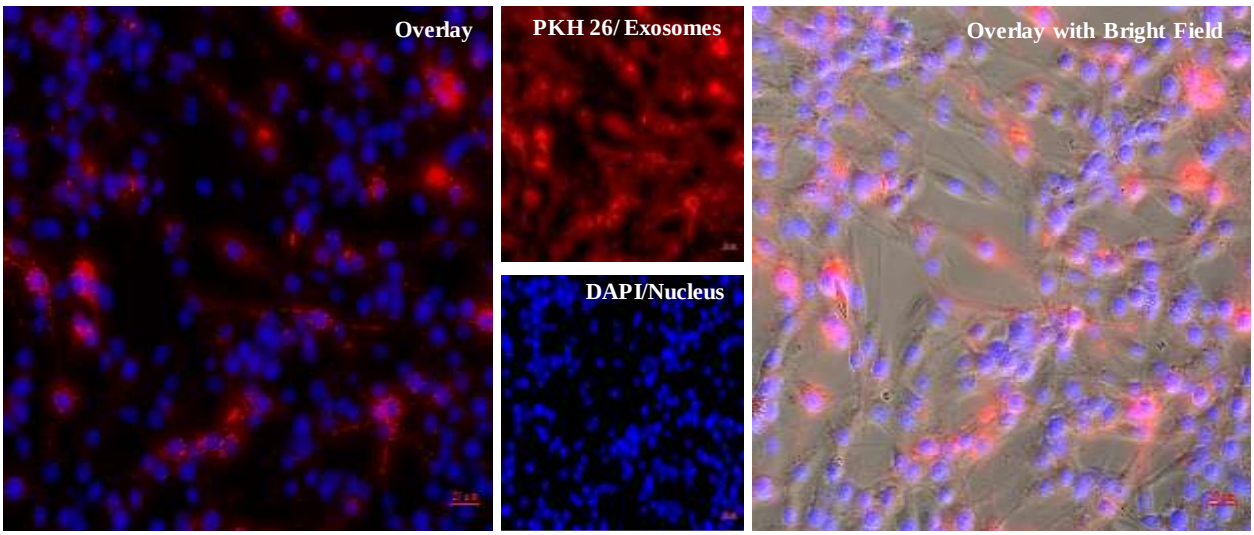

Figure 4.4: Qualitative cellular uptake of PKH 26 stained naive exosomes by 4T1 cells after 12 h of treatment.

4.4.5 Dose-dependent effect of exosomes on 4T1 cells

Figure 4.5.A and B, distinctly indicated decreased expression of β1-integrin (by almost 2.5 folds) but an increase in the ratio of CC3/C3 by 1.5 fold upon treatment with Exosome (2.5 µg/mL) in comparison to Exosome (5 µg/mL) in the 4T1 cells. This concentration dependent differential expression of apoptotic CC3/C3 ratio and metastatic marker β1-integrin, clearly indicated the inherent nature of exosomes is important to be considered. Functionally active biological nanocarrier system, exosomes originating from macrophages, exhibited a prominent anti-migratory and pro-apoptotic activity against TNBC 4T1 cells.

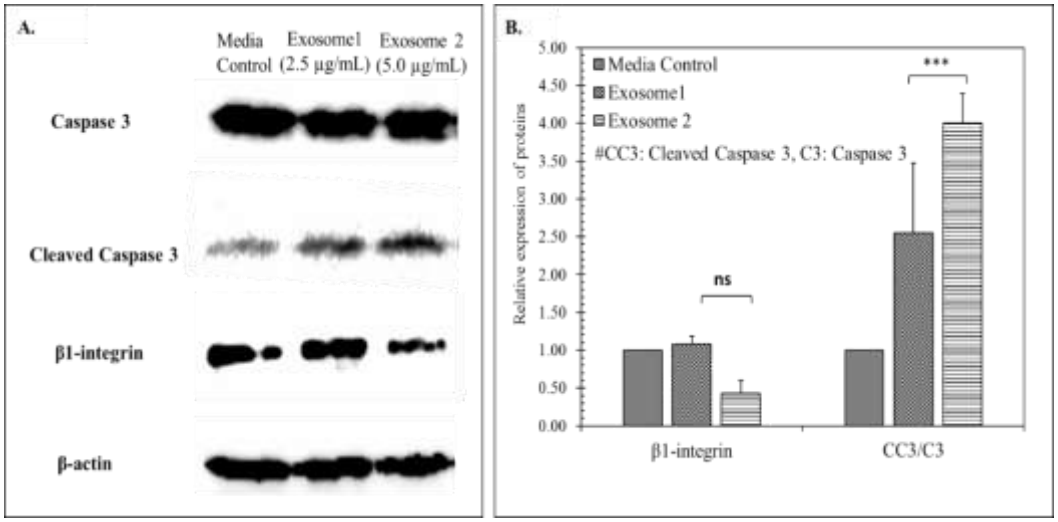

Figure 4.5: Mechanistic exploration of the naive exosomes in 4T1 cells in a dose dependent manner (A) Representative immunoblots of β-1 integrin, cleaved caspase 3/caspase 3 and housekeeping protein β-actin in 4T1 cells after being treated with different concentrations of exosomes.,(B) differential expression of mentioned proteins to evaluate the effect of exosomes in 4T1, all data are represented as mean±SD (n=3), where one way ANOVA with Tukey's test was used for the determination of the statistical significance, where *p<0.05, **p<0.01 and ***p<0.001.

4.4.6 Dose dependent effect of EF on 4T1 by ELISA of pro-inflammatory cytokines

Figure 4.6 highlights the dose dependent effect of EF on the inflammatory cytokine release in 4T1 cells. As indicated in **Figure 4.6.A**, TNF-α release by 4T1 was observed to be EF concentration dependent, but the level of IFN-γ was significantly increased in the presence of EF2 (12 µg/mL) in comparison to EF1 treated cells and the media control group. The EF1 and EF2 showed 1.89 folds and 1.58 folds increased IFN-γ release by 4T1 in comparison to the MC group.

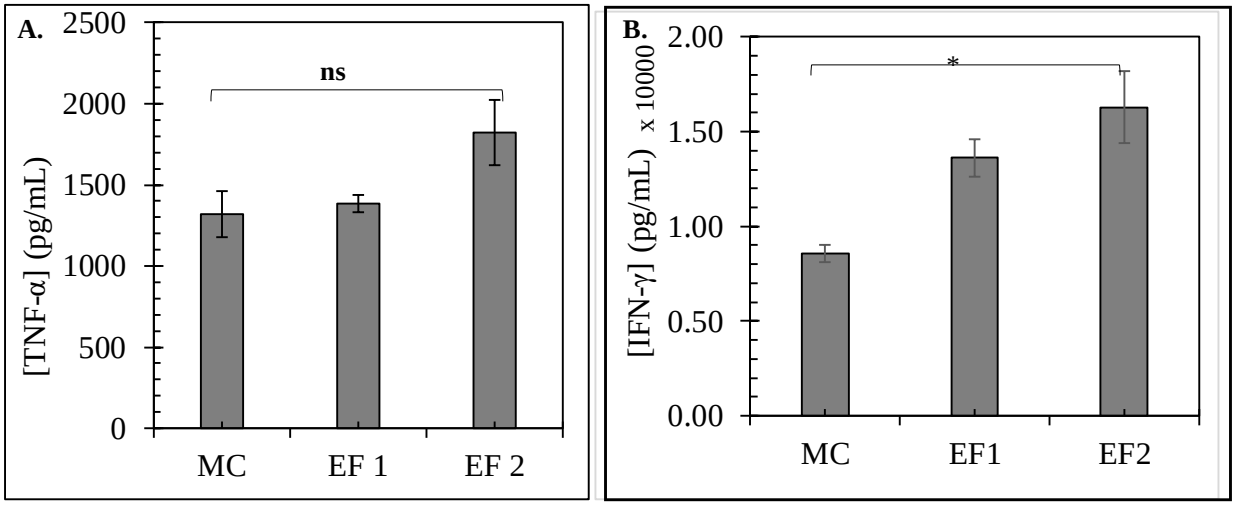

Figure 4.6. Dose dependent effect of exosomal fragments on the inflammatory cytokine (TNF-α, and IFN-γ) released by 4T1 cells, Graphical representation of the impact of EF1 (6 µg/mL) and EF2 (12 µg/mL) on the (A) TNF-α and (B) IFN-γ release by 4T1 cells. all data are represented as mean (n=3) ±SD, where one-way ANOVA with Tukey's test was used for the determination of the statistical significance, where *p<0.05, **p<0.01 and ***p<0.001.

4.4.6 Dose dependent effect on BCL-2 gene expression of EF on 4T1

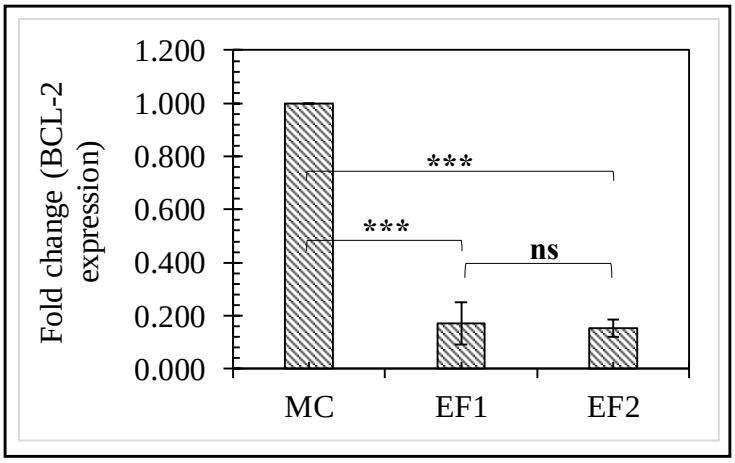

Figure 4.7. Concentration dependent *e*ffect of EF in BCL-2 gene expression. EF1 indicated ~6µg/mL protein, and EF2 indicated ~12µg/mL protein. All data are represented as mean (n=3) ±SD and statistical comparison was performed by applying one-way ANOVA with Tukey multiple comparison test. *** p-value < 0.001, **p<0.01, *p<0.05.

In **Figure 4.7,** EF1 and EF2 were observed to suppress the BCL-2 expression by 5.8 and 6.5 folds in comparison to the 4T1 cells in media control group. Although, the EF treatment has resulted significant reduction in BCL-2 expression but the impact was found to be concentration independent.

4.5. Discussion

After initial characterization of RAW264.7 cell derived exosomes for particle size (nm), absolute intensity (Kcounts/s), surface morphology, and exosomal protein expression, it was concluded that naive exosomes are nanosized, heterogeneous and pleomorphic subpopulation of EVs with an inherent tendency of forming loose aggregates (**Figure 4.1**)[11]. The comparative analysis of exosomes by DLS and FESEM supports this inference. While, DLS based characterization of naive exosomes estimated Z_{AVG} of 182.40 nm with high PDI of 0.24 and negative surface-potential, -9.3 mV; FESEM revealed a particle size 112.5±21.48 nm. This difference between the DLS and FESEM data was attributed to the presence of the exosomal aggregates responsible for the higher particle size as detected by DLS (**Figure. 4.1.C)**. Additionally, these exosomes have been utilized to prepare exosomal fragments by sonication and extrusion methods. Comparing **Table 4.2 and 4.4**, differences between the naive exosomes, Exo_{TC} and EF could be emphasized for example, Exo_{TC} showed increased particle size and PDI with higher surface negativity which is in agreement with the reported literature [5,12–15]. On the contrary, extrusion method of EF preparation resulted in invariable loss of exosomes, as indicated by the decreased absolute intensity and increased PDI in **B9-B10** resulting in two non-uniform peaks as seen in the particle size distribution curve (**Figure. 4.2.1**). The naïve exosomes and EF were also characterized for the expression of exosomal proteins (ALIX, TSG 101, CD63 and HSP 70) as seen in **Figure 4.1.D and 4.2.D**. It was observed that RAW 264.7 cells maintained in DMEM+ 10% v/v exosome depleted FBS exhibited reduced expression of target proteins, i.e., ALIX, HSP70 and TSG101 in comparison to the cells maintained in complete media containing normal FBS (**Figure. 4.1.D).** Interestingly**,** EF showed greater expression of target exosomal proteins than the exosomes isolated from the cells kept in DMEM+ 10% v/v exo-free FBS (**Figure 4.2.D).** Both CL_N and CL_F showed the expression of house-keeping protein β-actin, which was absent in EL and EF, clearly indicating that exosomes were devoid of cytoskeletal proteins. The presence of positive marker ALIX, a protein identified for selective recruitment of endosomal sorting complexes required for transport III (ESCRT III) to late endosomes [16,17]. The expression of exosomal hallmark CD 63 and truncated TSG 101 in EL and EF in comparison of the CL_F confirmed the purity of the exosome samples and also indicated that the EF preparation did not alter the biological attributes of exosomes even after fragmentation[18–22]. The purity of exosomes was further confirmed by observing a linear increase in absolute intensity with increasing exosomal concentration (equivalent protein concentration)

without any significant deviation in particle size and zeta-potential (**Figure 4.1.E and Table 4.3**) [23,24].

Post-characterization of exosomes, the effect of process parameters on exosomal integrity was evaluated wherein, it was observed to be dependent upon the sonication pattern, sonication-amplitude and the post-sonication incubation cycle. Evidently, higher sonication amplitude and more number of sonication cycles reduced the particle size significantly when compared to naïve exosomes, but post-sonication incubation at 37˚C enabled the exosomes to reseal and regain their integrity even after exposure to harsh conditions (**Figure 4.2**). Although, the main aim of preparing EF was to prepare the core/shell formulation, (discussed in detail in **Chapter 6)** the optimization of the method of preparation of EF resolved several doubts regarding the exosomal integrity. This also provided valuable insights regarding effect of incubation and mild sonication on exosomal physical characteristics and to achieve the optimum therapeutic loading capacity in the exosomes. The exosomal integrity was restored or not under different experimental conditions has been shown in **Figure 4.2 and 4.4**. Application of a 30% amplitude and a 4X sonication cycle resulted in the generation of two distinct populations of particles with different size ranges, suggesting that the 30% sonication amplitude might have caused formation of fragments. Whereas, presence of hypotonic environment along with 30% sonication amplitude and 2X sonication cycle made the exosomes swell and expel out the proteins, and distort the intactness of the exosomal membrane without completely destroying it. After thorough characterization, the physiological role of naive exosomes and EF on 4T1 cells was confirmed by mechanistic functional assay (**Fig. 4.5 and 4.6**). In **Figure 4.5**, a dose-dependent effect of naive exosomes at the concentration of 2.5 µg/ml and 5.0 µg/ml was evaluated and found to result in anti-proliferative and anti-migratory effect on 4T1 cells as demonstrated by the down-regulation of β1-integrin and reduced the CC3/C3 ratio. On the other hand, the dose-dependent effect of EF was prominent in the TNF-α and IFN-γ releasing ability of 4T1 cells (**Fig. 4.6**). Herein, enhanced inflammatory cytokine release in the presence of higher concentration of EF indicated the immune triggering response of EF in 4T1 cells. This observation could be indicative of the anti-proliferative activity of the RAW 264.7 cell derived exosomes as well. In addition to their role in release of TNF-α and IFN-γ (**Fig. 4.6**), the prominent apoptotic effect of the EF was confirmed by BCL-2 downregulation in **Figure 4.7**. It was also evident that the EF was able to retain its biological role intact even after being processed through the harsh experimental condition which would act as an add-on with the designed formulation.

References

(1) Robbins, P. D.; Morelli, A. E. Regulation of Immune Responses by Extracellular Vesicles. *Nat. Rev. Immunol.* **2014**, *14* (3), 195–208. https://doi.org/10.1038/nri3622.

(2) Haney, M. J.; Zhao, Y.; Jin, Y. S.; Li, S. M.; Bago, J. R.; Klyachko, N. L.; Kabanov, A. V.; Batrakova, E. V. Macrophage-Derived Extracellular Vesicles as Drug Delivery Systems for Triple Negative Breast Cancer (TNBC) Therapy. *J. Neuroimmune Pharmacol.* **2019**. https://doi.org/10.1007/s11481-019-09884-9.

(3) Kanchanapally, R.; Deshmukh, S. K.; Chavva, S. R.; Tyagi, N.; Srivastava, S. K.; Patel, G. K.; Singh, A. P.; Singh, S. Drug-Loaded Exosomal Preparations from Different Cell Types Exhibit Distinctive Loading Capability, Yield, and Antitumor Efficacies: A Comparative Analysis. *Int. J. Nanomedicine* **2019**, *14*, 531–541. https://doi.org/10.2147/IJN.S191313.

(4) Kim, M. S.; Haney, M. J.; Zhao, Y.; Mahajan, V.; Deygen, I.; Klyachko, N. L.; Inskoe, E.; Piroyan, A.; Sokolsky, M.; Okolie, O.; Hingtgen, S. D.; Kabanov, A. V.; Batrakova, E. V. Development of Exosome-Encapsulated Paclitaxel to Overcome MDR in Cancer Cells. *Nanomedicine Nanotechnology, Biol. Med.* **2016**, *12* (3), 655–664. https://doi.org/10.1016/j.nano.2015.10.012.

(5) Wang, P.; Wang, H.; Huang, Q.; Peng, C.; Yao, L.; Chen, H.; Qiu, Z.; Wu, Y.; Wang, L.; Chen, W. Exosomes from M1-Polarized Macrophages Enhance Paclitaxel Antitumor Activity by Activating Macrophages-Mediated Inflammation. *Theranostics* **2019**, *9* (6), 1714–1727. https://doi.org/10.7150/thno.30716.

(6) Dai, S.; Wei, D.; Wu, Z.; Zhou, X.; Wei, X.; Huang, H.; Li, G. Phase I Clinical Trial of Autologous Ascites-Derived Exosomes Combined with GM-CSF for Colorectal Cancer. *Mol. Ther.* **2008**, *16* (4), 782–790. https://doi.org/10.1038/mt.2008.1.

(7) Cheng, L.; Wang, Y.; Huang, L. Exosomes from M1-Polarized Macrophages Potentiate the Cancer Vaccine by Creating a Pro-Inflammatory Microenvironment in the Lymph Node. *Mol. Ther.* **2017**, *25* (7), 1665–1675. https://doi.org/10.1016/j.ymthe.2017.02.007.

(8) Beninson, L. A.; Fleshner, M. Exosomes in Fetal Bovine Serum Dampen Primary Macrophage IL-1β Response to Lipopolysaccharide (LPS) Challenge. *Immunol. Lett.* **2015**, *163* (2), 187–192. https://doi.org/10.1016/j.imlet.2014.10.019.

(9) Eitan, E.; Zhang, S.; Witwer, K. W.; Mattson, M. P. Extracellular Vesicle-Depleted Fetal Bovine and Human Sera Have Reduced Capacity to Support Cell Growth. *J. Extracell. Vesicles* **2015**, *4* (2015), 1–10. https://doi.org/10.3402/jev.v4.26373.

(10) Basak, M.; Sahoo, B.; Kumar, D.; Narisepalli, S.; Tiwari, S.; Chitkara, D.; Mittal, A. Human Umbilical Cord Blood-Mesenchymal Stem Cell Derived Exosomes as an Efficient Nanocarrier for Docetaxel and MiR-125a : Formulation Optimization and Anti-Metastatic Behaviour. *Life Sci.* **2023**, *322* (January), 121621. https://doi.org/10.1016/j.lfs.2023.121621.

(11) Bosch, S.; Beaurepaire, L. De; Allard, M.; Mosser, M.; Heichette, C.; Chrétien, D.; Jegou, D.; Bach, J. Trehalose Prevents Aggregation of Exosomes and Cryodamage. *Sci. Rep.* **2016**, *6* (May), 36162. https://doi.org/10.1038/srep36162.

(12) Soo, M.; Haney, M. J.; Zhao, Y.; Mahajan, V.; Deygen, I.; Klyachko, N. L.; Inskoe, E.; Piroyan, A.; Sokolsky, M.; Okolie, O.; Hingtgen, S. D.; Kabanov, A. V; Batrakova, E. V. Development of Exosome-Encapsulated Paclitaxel to Overcome MDR in Cancer Cells. *Nanomedicine Nanotechnology, Biol. Med.* **2016**, *12* (3), 655–664. https://doi.org/10.1016/j.nano.2015.10.012.

(13) Zhao, Y.; Zheng, Y.; Zhu, Y.; Li, H.; Zhu, H.; Liu, T. Docetaxel-Loaded M1 Macrophage-Derived Exosomes for a Safe and Efficient Chemoimmunotherapy of Breast Cancer. *J. Nanobiotechnology* **2022**, *20* (1), 1–12. https://doi.org/10.1186/s12951-022-01526-2.

(14) Zhao, L.; Gu, C.; Gan, Y.; Shao, L.; Chen, H.; Zhu, H. Exosome-Mediated SiRNA Delivery to Suppress Postoperative Breast Cancer Metastasis. *J. Control. Release* **2020**, *318* (May 2019), 1–15. https://doi.org/10.1016/j.jconrel.2019.12.005.

(15) Cheng, G.; Li, W.; Ha, L.; Han, X.; Hao, S.; Wan, Y.; Wang, Z.; Dong, F.; Zou, X.; Mao, Y.; Zheng,

S. Y. Self-Assembly of Extracellular Vesicle-like Metal-Organic Framework Nanoparticles for Protection and Intracellular Delivery of Biofunctional Proteins. *J. Am. Chem. Soc.* **2018**, *140* (23), 7282–7291. https://doi.org/10.1021/jacs.8b03584.

(16) Ghossoub, R.; Lembo, F.; Rubio, A.; Gaillard, C. B.; Bouchet, J.; Vitale, N.; Slavík, J.; Machala, M.; Zimmermann, P. Syntenin-ALIX Exosome Biogenesis and Budding into Multivesicular Bodies Are Controlled by ARF6 and PLD2. *Nat. Commun.* **2014**, *5*, 3477. https://doi.org/10.1038/ncomms4477.

(17) Larios, J.; Mercier, V.; Roux, A.; Gruenberg, J. ALIX- And ESCRT-III-Dependent Sorting of Tetraspanins to Exosomes. *J. Cell Biol.* **2020**, *219* (3), e201904113. https://doi.org/10.1083/jcb.201904113.

(18) Zhu, Q. J.; Zhu, M.; Xu, X. X.; Meng, X. M.; Wu, Y. G. Exosomes from High Glucose–Treated Macrophages Activate Glomerular Mesangial Cells via TGF-B1/Smad3 Pathway in Vivo and in Vitro. *FASEB J.* **2019**, *33* (8), 9279–9290. https://doi.org/10.1096/fj.201802427RRR.

(19) Tippett, E.; Cameron, P. U.; Marsh, M.; Crowe, S. M. Characterization of Tetraspanins CD9, CD53, CD63, and CD81 in Monocytes and Macrophages in HIV-1 Infection. *J. Leukoc. Biol.* **2013**, *93* (6), 913–920. https://doi.org/10.1189/jlb.0812391.

(20) Vabulas, R. M.; Ahmad-Nejad, P.; Ghose, S.; Kirschning, C. J.; Issels, R. D.; Wagner, H. HSP70 as Endogenous Stimulus of the Toll/Interleukin-1 Receptor Signal Pathway. *J. Biol. Chem.* **2002**, *277* (17), 15107–15112. https://doi.org/10.1074/jbc.M111204200.

(21) Asea, A.; Rehli, M.; Kabingu, E.; Boch, J. A.; Baré, O.; Auron, P. E.; Stevenson, M. A.; Calderwood, S. K. Novel Signal Transduction Pathway Utilized by Extracellular HSP70. Role of Toll-like Receptor (TLR) 2 and TLR4. *J. Biol. Chem.* **2002**, *277* (17), 15028–15034. https://doi.org/10.1074/jbc.M200497200.

(22) Goff, A.; Ehrlich, L. S.; Cohen, S. N.; Carter, C. A. Tsg101 Control of Human Immunodeficiency Virus Type 1 Gag Trafficking and Release. *J. Virol.* **2003**, *77* (17), 9173–9182. https://doi.org/10.1128/jvi.77.17.9173-9182.2003.

(23) Silva, A. K. A.; Morille, M.; Piffoux, M.; Arumugam, S.; Mauduit, P.; Al, E. Development of Extracellular Vesicle-Based Medicinal Products: A Position Paper of the Group "Extracellular Vesicle TranslatiOn to ClinicaL PerspectiVEs – EVOLVE France." *Adv. Drug Deliv. Rev.* **2021**, *179*, 114001. https://doi.org/10.1016/j.addr.2021.114001.

(24) Webber, J.; Clayton, A. How Pure Are Your Vesicles? *J. Extracell. Vesicles* **2013**, *1* (7), 19861. https://doi.org/10.3402/jev.v2i0.19861.

XXXXXXXXXXX

RAW Exo-DTX

Optimization, Development and Evaluation of the RAW Exo-DTX formulation

Chapter V

5.1. Introduction

As emphasized in the thesis earlier exosomes, are versatile biogenic signaling vesicles with enormous potential to be used as a nanocarrier system for both small molecules and biologicals. Among all the immune cells derived exosomes, macrophage-derived exosomes have been extensively studied as a nanocarrier for external payloads such as small anti-cancer molecules and RNAi, and they have also been functionalized for targeted cancer therapy [4–7]. The preference for macrophage derived exosomes originates from their inherent functional plasticity under different immunological conditions [8]. Also, some reports indicated that macrophages are capable of suppressing cellular migration by inducing degradation of β1-integrin and transferring miR-let 7a-5p to cancer cells, which regulates the anti-apoptotic Bcl2-like 1 protein expression [9,10]. So, it is expected that exosomes isolated from these could inherit some properties of the source cells.

Recently, the translational potential of exosomes has attracted a lot of scientific interest, as evidenced by several clinical trials being conducted worldwide wherein, exosomes are either projected as therapeutic molecules or adjuvants. Till date, there is no FDA approved exosomal formulation, but tumor antigen loaded dendritic cell derived exosomes (DEX) have completed the Phase-2 vaccination trial [NCT01159288] in non-small cell lung cancer (NSCLC), and allogenic adipose MSC derived exosomes are presently in Phase-2 trial for combating Alzheimer's disease [NCT04388982] [11,12]. The current research trends indicate a rapid progress in the field of exosomes from being mere biomarkers of pathological conditions to therapeutic aid for both regenerative purposes and cancer treatment [11,13,14]. As per the European Medicine Agency (EMA), exosomes are expected to be categorized either as "biological medicine" if they act as an active ingredient, or as "class III medical devices" if they exert an ancillary effect with some other biological molecule [11,15].

Considering the clinical applicability and commercialization potential of exosomal formulations, development and validation of the exosomal formulation is an irreplaceable step in addition to the maintenance of source cells, cell priming, exosome isolation and purification, which would be further followed by scale-up, filling, and storage. Thus, process variables and their impact on exosomal integrity must be optimized meticulously. In this context, we are reporting the application of the quality by design (QbD) approach to optimize the small anti-cancer molecule loading in murine macrophage derived exosomes for the first time. Encapsulating a small anti-

cancer molecule into exosomes is not a novel concept, but the methodological optimization and validation of anti-cancer exosomal formulation is novel and crucial in the current scenario. [16].

The QbD approach is a statistically sound method for optimizing and validating formulations in a cost-effective and efficient manner. In contrast to the "one factor at a time" approach, QbD provides a minimum number of trials with all possible combinations of process variables included as factors to evaluate the effect of the process on the formulation. For example, a "2^3- full factorial design" can investigate the effect of three factors at two levels (+1 indicates high, and -1 indicates low level) and their 2 or 3 factor interactions (2-FI or 3-FI) on the responses in a statistically relevant way from only 8 (i.e., 2^3) experiments. It also helps to achieve the target product profile (TPP) with maximal loading of the small molecule in the carrier systems. Recently, a 2-level full factorial design (DoE) has been utilized to assess the effect of the process parameters and their interactions in the development of the graphene oxide/ super para-magnetic iron oxide (GO/SPION) hybrid nanoparticles for biomedical purpose [17]. Additionally, anti-fungal ketoconazole cubosomes have also been optimized and reported utilizing the 3-level fractional factorial design by another group [18]. Despite the fact that DoE-driven nanoformulation optimization and validation is a widely explored, its application in biological origin nanocarrier like exosomes is uncommon due to the potential risk of process variability and complexity associated with the physical nature of biologicals.

The formulation reported in this work comprises of RAW264.7 derived exosomes, a biological nanocarrier with intrinsic biological activity, and the anti-cancer small molecule, DTX, known for its high hydrophobicity and low solubility (log P 2.4, BCS IV category). The incorporation of DTX in a preformed biogenic vesicular structure is indeed challenging but feasible. The initial optimization of the process parameters for development of exosomal formulation has already been reported by our group [19]. We came across several reports on passive loading techniques in exosomes, e.g., incubation, sonication, freeze-thaw, microfluidics, and electroporation as well as the active loading technique to incorporate small molecules in the exosomes wherein, the source cells were primed with the active pharmaceutical ingredient (API) prior to isolation of the exosomes [20]. We also observed a gap in the research regarding the lack of unified loading capacity of these exosomes, which clearly indicated that the optimization and validation of the loading method needs to be carried out [5,7,21,22]. However, we did not come across even a single report

exploring the application of this powerful tool to optimize and validate the exosomal formulation or any other biological formulation.

Considering the available data and the gaps in the study of exosomal formulations, we set out to systematically and statistically investigate the impact of different process parameters on modulating exosomal integrity in the final formulation and the exosomes' ability to encapsulate DTX. Herein, we utilized murine macrophage derived exosomes, as the nanocarrier for the DTX. For better understanding of the **Exo-DTX** formulation, we applied a 2-level full factorial design twice. Initially, we applied 2^3- full factorial design to confirm the suitability of the mild sonication and incubation method over only incubation technique to encapsulate DTX in exosomes. Once the method's suitability was confirmed, the process parameters were optimized to finalize the formulation and validate the same by applying 2^4- full factorial design. Furthermore, the in-vitro efficacy of the Exo-DTX was assessed in terms of cytotoxicity, cell internalization, cytoskeletal deformation and differential protein expression in murine TNBC 4T1 cells. Further we proved the translational value and relevance of Exo-DTX in comparison to the marketed formulation of DTX, Taxotere®, by investigating its pharmacokinetic profile in healthy Swiss albino mice.

5.2. Materials and Methods

5.2.1. Material

We used QSONICA sonicator (#Q125 with probe specification as- Model CL-18, Serial no. 2022030106) for the purpose of loading DTX into exosomes, and also used Ultracentrifuge (Sorvall MX 150+ micro-ultracentrifuge) from Thermo™ Scientific (Waltham, USA) with fixed angle rotor (S50-A 2185) for preparation of exo-free FBS and exosome isolation. Pierce™ Bicinchoninic acid (BCA) protein assay kit, PKH67 green fluorescent cell linker mini kit (MINI 67-1KT), 4% paraformaldehyde (#ALF-J61899-AK) and polycarbonate tubes for ultracentrifugation (75000610) were procured from Thermo™ Scientific (Waltham, USA). The study utilised 2-well culture inserts obtained from ibdi GmbH (Martinsried, Germany) and Falcon® Transwell inserts with an 8µm PET membrane designed for 24-well plate, obtained from Corning (Riverfront Plaza, USA).

Primary antibodies rabbit- β1-integrin (#4706), EGF receptor (#2232), Caspase-3 (#9662), Cleaved caspase 3 (#9664), BAX (#2722), BCl2 (#3498), β-actin (#3700), GAPDH (#2118) and secondary antibodies anti-rabbit IgG HRP linked antibody (#7074P2), anti-mouse IgG HRP linked

antibody (#7076s) were bought from Cell Signalling Technology (Danvers, USA). For SDS-PAGE and Western blot purpose, we procured N,N,N',N'-Tetramethylethylenediamine (TEMED) from Thermo™ Scientific (Waltham, USA), Tween 20 (#TC287) from Himedia laboratories (Maharashtra, India) and rest of the reagents and crystal violet (#28376) were purchased from SRL (Maharashtra, India). Ammonium Persulphate (#1610700EDU), Clarity Western ECL Substrate (#1705060) and Precision Plus Protein™ standards (#161-0394), and Immuno-Blot® PVDF membrane were procured from Bio-Rad (California, USA). All solvents of analytical grade were purchased from Merck (Darmstadt, Germany).

Cells and cell culture reagents

Murine TNBC 4T1 cells and RAW 264.7 cells were procured from Regional Centre of Biotechnology (Haryana, India) and NCCS (Maharashtra, India) respectively. We are grateful to Professor Avinash Bajaj for providing the 4T1 cells. Exosome depleted FBS was prepared *in-house* by ultracentrifugation of a mixture of FBS and PBS (FBS:PBS=3:7) at 1,20,000×g and 4˚C for 18h. Dulbecco's modified Eagle's medium (Gibco™ DMEM, high glucose) and Fetal bovine serum (FBS) were purchased from GIBCO (Invitrogen Inc. Gibco BRL, USA) while, Penicillin plus streptomycin solution and 3-(4,5-dimethylthiazol-2-yl)-2,5-diphenyltetrazolium bromide (MTT), 4′,6-diamidino-2-phenylindole (DAPI), and Protease inhibitor cocktail powder (#SRE 0055-1BO) were bought from Sigma-Aldrich (St. Louis, MO, USA). Rhodamine Phalloidin (# ab235138) was procured from Abcam (Waltham, USA).

5.2.2. Methods

5.2.2.1. RAW264.7 cell maintenance and exosome isolation

The cells were cultured and maintained as mentioned previously in Chapter 4 (*section 4.2.2*).

5.2.2.2. Animals

Female Swiss albino mice, 18-20 g were procured from the central animal facility (CPCSEA No. 417/PO/be/2001/CPCSEA), BITS Pilani, Pilani campus (India), and were used as per the approved animal protocol (IAEC/RES/31/03) for pharmacokinetic studies of Taxotere® and Exo-DTX. Animals were housed in ambient condition at a temperature of 25 ± 2 °C and relative humidity of 50−60% under 12 h light/dark cycles with sufficient supply of food and water, *ad libitum*. All the experimental conditions were maintained in accordance with guidelines of CPCSEA, India.

5.2.2.3. Methodological DoE approach for optimization and development of Exo-DTX

Herein, we optimized the Exo-DTX formulation by applying DoE twice- (a) to select an appropriate technique to formulate DTX into exosomes (**by 2^3- full factorial design**) and (b) to prepare Exo-DTX formulations with a high loading (**by 2^4- full factorial design**).

Preference of mild sonication over Incubation: 2^3-full factorial design approach

In order to find out the best technique for DTX encapsulation into exosomes, DoE with 2^3-full factorial design was adopted with three factors (parameters) wherein each factor was varied at two different levels i.e. high (+1) and low (-1). As detailed in **Table 5.1,** the three factors chosen were, (**A**) Exosome content in each batch (equivalent µg protein), (**B**) Exo: DTX ratio (w/w) and, (**C**) Number of sonication cycles. The response parameters considered here was Capacity (ng DTX/µg exosomes).

The effect of three factors (**A**, **B**, and **C**) were designated as $\mathbf{E_A}$, $\mathbf{E_B}$, and $\mathbf{E_C}$ respectively. Their 2-factors interactions (2-FI; $\mathbf{E_{AB}}$, $\mathbf{E_{BC}}$, $\mathbf{E_{AC}}$) were calculated using **Equation 1** and **2.** The statistical significance of the model in choosing mild sonication over incubation and fit statistics of the model are tabulated in **Table 5.3.** Design Expert®v11 (State-Ease, Inc. USA) was used to generate the design layout, data analysis, application of statistics, and for interpretation of data through graphical plots.

Three factors with two different levels resulted in the eight experimental runs which were carried out in a random order, the results were computed and analysed by the above-mentioned software, wherein, a p-value of 0.05 was considered statistically significant.

$$\boldsymbol{Effect} = \frac{\sum \boldsymbol{Response_{high}}}{\boldsymbol{n_{high}}} - \frac{\sum \boldsymbol{Response_{low}}}{\boldsymbol{n_{low}}} \quad \textbf{Equation 5.1}$$

(n means number of experiments at each level $Response_{high}$: 2-FI indicating (+1) level $Response_{low}$: 2-FI indicating (-1) level)

$$\mathbf{E_{AB}} = \boldsymbol{E_A} \times \boldsymbol{E_B} \quad \textbf{Equation 5.2}$$

Optimizing maximal DTX loading capacity of Exosomes: 2^4-full factorial design approach

Following the optimization of the DTX loading method in exosomes, DoE was applied once more to refine the process parameters of mild sonication technique for loading DTX. Four critical process parameters (CPPs) or independent variables were selected, including (A) the amount of

exosomes in each batch (equivalent to µg protein), (B) Exo: DTX ratio (µg: µg), (C) %Tween 80 as surfactant, and (D) the number of sonication cycles.

QbD approach was followed to investigate the impact of the aforementioned variables and their interactions on the responses or dependent variables i.e., %EE, Capacity, particle size, and PDI, Thus, we chose a 2^4-factorial design to obtain the statistically significant outcome using Design Expert® v11, (State-Ease, Inc., USA). Herein, 16 different batches were prepared by varying each factor at two levels i.e. high (+1) and low (-1) as detailed **Table 5.1** and **Figure 5**. Total 16 experiments were performed in a randomized order and p-value<0.05 was accepted as statistically significant. As particle size and PDI were discovered to be unaffected by any of these factors, we narrowed down the response parameters to only 2 factors, namely Capacity and %EE, for the optimization of the process parameters. Herein, capacity was power transformed with a λ at 0.5 (square root) to obtain a normally distributed data with minimal residual sum of squares in the transformed model. The effect of the individual factors i.e., (E_A, E_B, E_C, E_D) and the most prominent effect of interaction between **A** and **B** (**E_{AB}**) was also calculated as shown in **Table 5.4** using **Equation 1** and **2.** Also, the final fit model for √Capacity and %EE and with the coded factors is shown.

Table 5.1
DoE approach to optimize the mild sonication method to achieve maximal capacity of Exo-DTX by 2^4-full factorial design.

Factors	Factors Name	Low Level (-1)	High Level (+1)
A	Exosomes (µg)	40	200
B	Exo:DTX (µg: µg)	10:1	4:1
C	% Tween 80 (v/v)	0.02%	0.04%
D	Sonication pattern m(nX)	4X	3(4X)

Validation of Exo-DTX by Point prediction method

The software's point prediction approach was used to correlate the percentage prediction error between the experimental results and the predicted values for randomly chosen values of the factors. The randomly chosen factors would help to establish the reliability of the optimized protocol to encapsulate DTX and the batches thus prepared were applicable for the validation purpose only. The criteria were set as 200 µg of exosomes content, Exo: DTX as 7:1, 0.02 %v/v

of Tween 80, and 4X sonication cycles. The software predicted capacity was 13.07 ng DTX/µg exosomes and hence the expected limit for capacity was set at 10 to 16 ng DTX/µg exosomes. Three runs were made in a row, and the results were compared to the predicted value..

5.2.2.4. Characterization of the DTX loaded exosomes (Exo-DTX) by Capacity and %EE

A validated analytical method was developed for the quantification of DTX as already mentioned in ***Chapter 2***. To evaluate the entrapment efficiency (%EE) and capacity (ng DTX/µg exosomes) of the exosomal formulation, a 20 µL sample was disrupted in 180 µL of the mobile phase. The resulting mixture was then subjected to centrifugation at 15,000 rpm for 15 min, after which the supernatant was analysed using HPLC. %EE and capacity were calculated using **Equation 3 and 4**

$$\text{Entrapment efficiency (\%EE)} = \frac{\text{Amount of drug loaded}}{\text{Amount (drug taken)}} \times 100 \ldots\ldots \textbf{Equation 5.3}$$

$$\text{Capacity (ng DTX/µg Exosomes)} = \frac{\text{Content of drug loaded in the exosomes (ng)}}{\text{Content of exosomes (µg equivalent protein)}} \ldots\ldots \textbf{Equation 5.4}$$

5.2.2.5. *In-vitro* cellular efficacy

The murine TNBC 4T1 cells were cultured in complete culture media consisting of DMEM (high glucose) supplemented with 10% FBS and 100 IU/mL penicillin-streptomycin. The cells were maintained in a humidified atmosphere with 5% CO_2 at 37 °C in an incubator. In each study, 8-12 hours were provided for cell adhesion subsequent to seeding, prior to conducting the assay.

In-vitro cytotoxicity study

The evaluation of the cytotoxicity was performed by (1) MTT assay and, (2) morphometric analysis of the 4T1 cells 48h post-treatment. Initially, 2.5×10^3 4T1 cells/well were seeded in a 96-well plate and then time (24/48/72 h) and concentration dependent effect of free DTX (25-500 ng/ml) was screened on 4T1 cells by MTT assay.

Based upon the result of the initial experiment, incubation period and target DTX concentration range were established. In the subsequent trial, 4T1 cells underwent treatment with a narrower concentration range of free DTX, Exo-DTX (ranging from 10-250 ng/mL), and free exosomes (quantified based on optimal capacity) for a duration of 48 h. Subsequently, MTT assay was performed to assess the cytotoxicity profiles of free DTX (100 ng/ml), free exosomes (~ 5 µg/ml), and Exo-DTX (~100 ng/ml DTX). To observe the impact of DTX treatment, on the cellular

morphology cells were again treated with DTX (100 and 250 ng/ml) for 48 h and the morphology of the cells was examined using a bright field microscope at a magnification of 200X.

In-vitro cellular uptake study

Our group has already reported that exosome internalization begins within 3 h of treatment, reaches a peak in 6 h, and continues for upto 12 h [19]. In the present study, the uptake of fluorescently stained exosomes and Exo-DTX was studied for 6h. In a six-well plate, 1.0×10^4 4T1 cells were grown over a coverslip and allowed to attach and form a monolayer. PKH-67, a lipophilic dye well-known for the membrane labelling was used to prestain the exosomes (~5 µg/mL protein) and Exo-DTX formulations, the manufacturer's protocol was slightly modified for staining the unloaded and loaded exosomes. The cells were treated with free DTX, PKH67 stained exosomes and PKH-67 stained Exo-DTX (~100 ng/mL DTX) for 6h. After 6h, the cells on the coverslips were fixed with 2% PFA and cellular cytoskeleton and nuclei were stained with Rhodamine Phalloidin and DAPI respectively and analysed by confocal microscopy in a Z-stack mode.

Suppression of pro-metastatic aggression in 4T1

The pro-metastatic suppression by Exo-DTX was investigated by studying the migration capacity of cells in 2-D wound healing assay and invasion capability in 3-D by transwell assay.

In ***wound healing assay***, 4T1 cells (at a density of 2.1×10^4 cells) were seeded in a culture-insert (2-well culture inserts, ibdi, Germany) per well and allowed to adhere for 12 h. After that, the culture insert was taken out and the cells were washed to eliminate non-adherent cells. Subsequently, the cells were subjected to treatment for 48h with free DTX and Exo-DTX at a concentration of 100 ng/ml and exosomes at a concentration of 5 µg/ml in DMEM supplemented with 1% FBS. The wound area at 12, 24, and 36 h was analysed and quantified using Image J (Fiji, NIH) for comparison between the various treatment groups. Using **Equation 5,** % wound healing was calculated.

$$\%\text{Wound Healing}=\frac{(A_0-A_t)}{A_0}\times 100 \quad \ldots. \textbf{ Equation 5.5}$$

(Where A_0 represents the initial wound area at the onset of observation, while A_t denotes the wound area at a subsequent time point, t)

In ***Transwell invasion assay***, a simulated basement membrane was constructed with Corning® Matrigel® basement membrane matrix, LDEV free substance, was placed onto the uppermost

chamber of transwell (8 μm pore filter) at a concentration of 300 μg/mL, that was further placed in a 24-well plate containing DMEM. 1.0×10^5 cells were seeded onto it and allowed to condition for 12h before adding the test samples. Further, the cells were treated with free DTX (100 ng/ml), exosomes (5μg/ml) and Exo-DTX (100 ng/ml) in DMEM+1% FBS for the next 48 h. The endpoint of the experiment involved the assessment of cell invasion through the basement membrane into the lower chamber, which was filled with DMEM+10% FBS. FBS was used as a chemoattractant. The evaluation was conducted after 48 h of treatment. At the end point, the cells remaining on the Matrigel bed of the insert were removed with a cotton swab, and the cells which had traversed the membrane to the lower surface of the transwell were fixed with methanol for 5 min. The cells were stained with 0.1% crystal violet and observed under a microscope. The average number of migrated cells per field (n=3) were counted to ascertain the percentage of cell invasion.

5.2.2.6. Mechanistic exploration of underlying crosstalk

To explain the observed cytoskeletal deformation associated with triggered apoptosis, the underlying mechanism of action of Exo-DTX formulations was explored (*discussed later in section **3.5.4***). F-actin degradation assay was conducted using FESEM and confocal microscopy to investigate the cytoskeletal deformation which was further supported by the differential expression of anti-metastatic and apoptotic proteins in 4T1 upon different treatments for 48h.

For ***Cytoskeletal deformation assay***, on each coverslip placed in a 6-well plate, 1×10^5 4T1 cells were seeded and incubated for 12 h to form a cellular monolayer prior to the treatment with 100 ng/mL of both free DTX, Exo-DTX and Exosomes (equivalent to 5 μg/mL protein) for 48 h.

(a) *Disruption of F-actin by FESEM*, post-treatment the cells were washed and fixed with the help of 2% PFA and subsequently washed thrice in PBS and dehydrated by different concentrations of ethanol in ascending order (30-90% v/v). The cover-slips were air-dried overnight and gold sputtered before visualization in the electron microscopy at 3000X and 5000X magnification.

(b) *F-actin degradation by confocal microscopy* where, post- fixation of the cells, the coverslips were washed with PBS thrice. The cells were subjected to staining with Rhodamine Phalloidin dye (targeting F-actin) for a duration of 1 hat ambient temperature. Subsequently, the cellular nuclei were counterstained with DAPI and further were subjected to washing with chilled PBS thrice. The fluorescence images of the processed samples were visualized by confocal microscopy.

(c) *Differential protein expression* was studied to elucidate the mode of action of different treatment groups on the 4T1 cells. Herein, cells from different treatment groups and media control were lysed with Triton-x-100 lysis buffer containing a 1X protease inhibitor cocktail solution. 50 µg equivalent protein from each cell lysate group was resolved on a 15% gel in SDS-PAGE and transferred to a PVDF membrane by a wet transfer method. The primary antibody was incubated on the membrane overnight at a temperature of 4℃, followed by the secondary antibody for a duration of 1 h at room temperature. Protein bands were detected using Clarity Western ECL substrate (Bio-Rad, Hercules, CA, USA). The following primary antibodies were used- Rabbit-EGFR, β1-integrin, BAX, BCL2, Caspase 3 and cleaved caspase-3, GAPDH and β-actin, anti-rabbit HRP linked secondary antibody for probing the blots. All experiments were performed in duplicate.

5.2.2.7. In vivo pharmacokinetic Study

The animals were randomly distributed into two groups each containing 3 animals. The first group of animals received *in-house* formulated Taxotere® while the second group received Exo-DTX, administered via intravenous injection at a DTX dose of 1mg/kg and blood samples were withdrawn at predetermined time points. After collecting the blood samples, plasma was separated and stored at -80˚C till further processed for the bioanalytical analysis of DTX using developed LC/MS-MS method. The pharmacokinetic data of plasma concentration−time profile was analyzed by non-compartmental analysis (NCA) using Pheonix Winolin® (Version 8.0, Certara, NJ, USA). The plasma samples were analyzed utilizing the developed and validated bioanalytical method (***Chapter 2***).

5.2.2.8. Statistical Data Analysis

The statistical data has been presented as mean values accompanied by their respective standard deviations, as analysed using the GraphPad Prism software (Version 5.0, USA). The statistical analysis involved the utilisation of Student's t-test to compare the differences between two groups, while the comparison between multiple groups was conducted through one-way ANOVA, followed by a Tukey's test. Also, two-way ANOVA with Bonferroni post-test has been applied to evaluate the significant difference of multiple parameters on the treatment groups. A statistical significance level of $p < 0.05$ was deemed appropriate.

5.3. Results

5.3.1 Application of DoE for optimization of the method and process parameters for preparation of Exo-DTX

Incubation vs. mild sonication: Application of 2^3- full factorial design

Table 5.2

DoE approach to compare incubation with mild sonication technique to load DTX in exosomes: A 2^3-full factorial design with representative experimental data showing effect of different factors on capacity.

STD	Factors			Response
	A:Exosome content (µg)	**B**: (Exo:DTX)	**C**:Sonication cycle	Capacity (ng DTX/µg exosomes)
1	40	10:1	0X	4.79
2	200	10:1	0X	4.819
3	40	4:1	0X	5.66
4	200	4:1	0X	6.621
5	40	10:1	4X	5.16
6	200	10:1	4X	9.13
7	40	4:1	4X	13.55
8	200	4:1	4X	18.62

DTX can be loaded into exosomes using both incubation and sonication techniques because it is hydrophobic in nature. After understanding the impact of the process parameters on exosomal integrity, we applied *2^3 full factorial design approach* to identify the suitability of incubation vs. sonication at varying combinations of the three factors, i.e., **A**: Exosome content per batch (µg), **B**: Exo: DTX ratio and, **C**: number of sonication cycles wherein, 0X indicated incubation and 4X indicated sonication (4 cycles with each cycle comprising of 30 sec on and 30 sec off). In **Table 5.2**, **STD 1-4** indicated the batches prepared by incubation, **STD 5-8** represent batches prepared by sonication using 4 cycles (4X) followed by 2 h incubation period post-sonication).

Table 5.3

DoE based statistical analysis of the model for response capacity (ng DTX/µg exosomes) to confirm the best fit of the model while choosing between sonication and incubation in 2^3 - full factorial design.

Response	p value	R^2	Adjusted R^2	Predicted R^2	Adequate Precision
Capacity (ng DTX/µg Exosomes)	0.0083	1.000	0.99986	0.99873	248.39

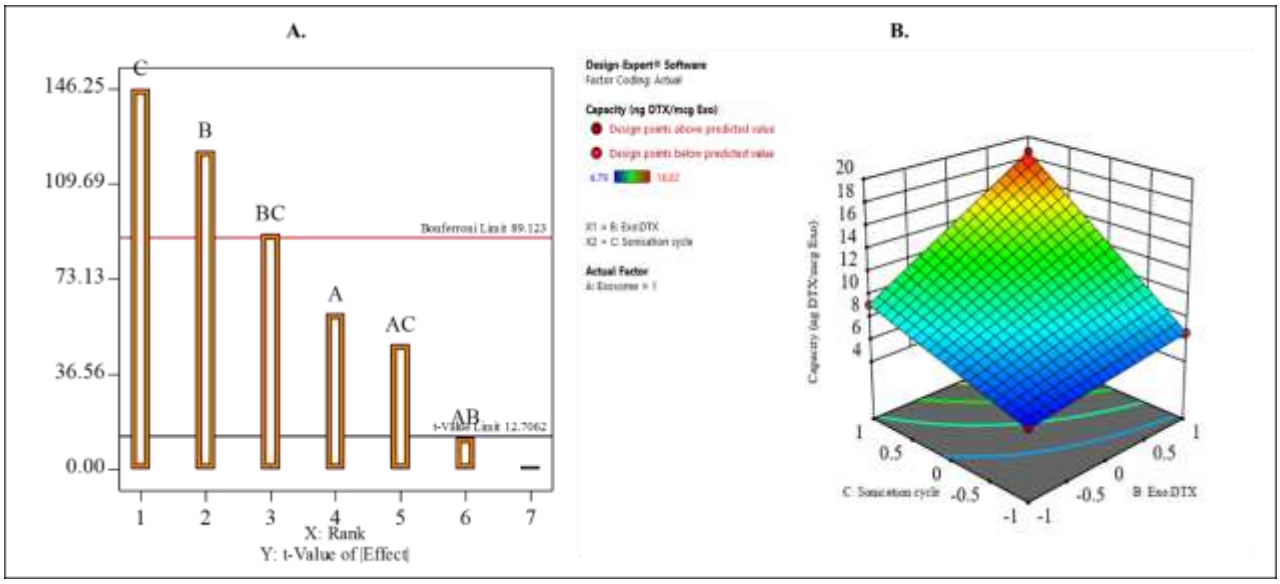

Figure 5.1: Representative plots indicating the suitability of mild sonication in combination with incubation over incubation (alone) process in encapsulating DTX into exosomes. A: Pareto chart indicating significance of factors crossing Bonferroni limit and t-limit to confirm the effect on the capacity of exosomes. B. 3D-surface plot indicating the effect of the most significant interaction term (BC) on the capacity of the exosomes in achieving the optimal capacity, while exosomes content is kept at (+1) level. Both A and B are determined by Design Expert®v11 (State-Ease, Inc. USA).

As per the observations drawn from **Table 5.1,** among the Exo-DTX prepared by incubation technique, **STD 4**, exhibited maximum capacity of 6.62 ng DTX/µg Exosomes, whereas with 4X sonication cycles and Exo: DTX ratio equivalent to 4:1, the capacity of exosomes to load DTX was increased to 18.62 ng DTX/ µg Exosomes (**STD 8).** If we compare the batches prepared by incubation i.e. STD 1-4, no significant increase in capacity could be seen even after increasing the exosome content or the Exo: DTX ratio, but application of sonication evidently enhanced the capacity in each case, for eg., STD 3 vs. STD 7 or STD 4 vs. STD 8. The detailed statistical significance of this design is provided in **Table 5.3.** In the applied design, factors B, C, and their 2FI (BC) were found highly significant since these were able to cross both the Bonferroni limit and the t-limit, as shown in **Figure 5.A**. The surface response graph in **Figure 5.B** indicated that, increasing sonication and Exo: DTX ratio enables exosomes to achieve the highest DTX payload.

Optimization of process parameters of mild sonication technique: 2^4 full factorial design approach

Further, a 2^4 -full factorial design was employed to optimize the maximum capacity of the exosomes without compromising the integrity of the same once the suitability of sonication method was established. As indicated in the **Table 5.2A,** with two levels for each factor, we prepared

Table 5.4

Representative experimental data showing effect of different factors on responses.

STD	Factors				Responses			
	(A)	(B)	(C)	(D)	%EE (Mean±SD)	Capacity (ng DTX/µg Exosomes) (Mean±SD)	Particle Size (nm)	PDI
1	-1	-1	-1	-1	4.08±0.75	4.08±0.75	187.60	0.22
2	1	-1	-1	-1	3.95±0.68	4.18±0.78	129.10	0.26
3	-1	1	-1	-1	3.46±0.41	8.64±1.06	181.09	0.25
4	1	1	-1	-1	9.44±0.62	23.60±1.54	182.40	0.24
5	-1	-1	1	-1	2.27±0.42	2.14±0.65	182.17	0.25
6	1	-1	1	-1	3.86±0.44	4.18±0.78	174.79	0.23
7	-1	1	1	-1	2.52±0.24	5.83±0.47	176.55	0.26
8	1	1	1	-1	5.38±2.85	18.5±1.85	182.88	0.25
9	-1	-1	-1	1	1.33±0.23	1.33±0.16	170.90	0.26
10	1	-1	-1	1	4.85±0.31	4.87±0.34	140.09	0.27
11	-1	1	-1	1	3.35±0.64	8.24±0.51	190.00	0.27
12	1	1	-1	1	6.45±2.93	17.16±1.59	215.55	0.26
13	-1	-1	1	1	3.87±0.38	3.86±0.37	143.57	0.22
14	1	-1	1	1	4.30±0.70	4.31±0.70	178.37	0.24
15	-1	1	1	1	3.14±0.52	7.89±1.63	187.71	0.23
16	1	1	1	1	6.51±0.13	17.12±2.06	189.40	0.26

sixteen batches (STD 1-16) in triplicate which provided different **%EE** and **Capacity** as tabulated in **Table 5.4**. Since there was no appreciable change in either particle size (nm) or PDI among the Exo-DTX formulations, these two responses were disregarded.

Capacity: When comparing **STD 4, 8, and 12**, it was concluded that the maximal capacity of the Exo-DTX formulation depended on four factors, i.e., (**A**) Exosome content, (**B**) Exo: DTX ratio,

(**C**) % T80 and, (**D**) number of sonication cycles. The maximal capacity could only be achieved when the exosome content and Exo: DTX ratio reached their highest levels with the lowest % T80 and number of sonication cycles. The corresponding Pareto chart in **Figure 5.2A** also provided the same inference for exosome capacity wherein, the effects of factors E_A, E_B, and their interaction E_{AB} were found highly significant by crossing both the t-limit and Bonferroni limit, while %Tween 80 and number of sonication cycles showed a negative impact on exosome capacity (**Table 5.4**). Additionally, it was clear from the surface response 3-D graph (**Figures 5.2.B and C**) that, increasing from 4X to 12X sonication cycle reduced exosomes' capacity. We found the model best fitted as good correlation was statistically found between R^2, adjusted R^2 and predicted R^2 value, as tabulated in **Table 5.5.** This conclusion was further supported by the ANOVA wherein, model F-value was found 31.07 implying that only 0.01% chance is possible that this F-value could have been caused by noise and $p<0.0001$ indicated that the selected model terms (A, B, AB) are highly significant.

%EE: Comparing **STD 3 and 4** wherein, only the exosomes content (A) was increased from level (-1) to (+1) keeping rest of the parameters constant, it was observed that %EE increased by ~ 3 folds. Also, **STD 9 and 10** clearly supported the above observation. As STD 9 and 10 both were processed through 3(4X) sonication cycle, only half-maximal DTX loading capacity could be achieved. In case of **STD 10**, exosome content was at +1 level which produced %EE of 4.87 ng DTX/µg exosomes, whereas %EE decreased to 1.33 ng DTX/ µg exosomes when the exosome content was reduced to -1 level. Henceforth, only **factor A** was found statistically significant for %EE. Factor **A** was determined to be significant as seen in the half-normal plot in **Figure 5.3A**, however, the addition of the AB interaction to this model increased the F-value to 10.79 and improved the projected R^2 value, as shown in **Figure 5.3B** and **Table 5.5**. Therefore, DoE revealed that exosome capacity depends upon exosome content and Exo: DTX ratio, while %EE would depend primarily on exosome content.

Table 5.5
Mathematical interpretation of the effect of factors (A, B, C, and D) and the significant interaction (E_{AB}) on √Capacity and %EE involved in DTX loading by mild sonication method.

$$E_{AB}= \left(\frac{2.02+4.85+1.46+4.30+1.15+4.14+1.96+4.13}{8}\right)-\left(\frac{2.04+2.94+2.04+2.41+2.20+2.87+2.07+2.81}{8}\right)$$

STD	Factors				Significant interaction	Responses	
	(A)	**(B)**	**(C)**	**(D)**	**E_{AB}**	**√Capacity**	**%EE**
1	-1	-1	-1	-1	1	2.02	0.75
2	1	-1	-1	-1	-1	2.04	0.68
3	-1	1	-1	-1	-1	2.94	0.41
4	1	1	-1	-1	1	4.85	0.62
5	-1	-1	1	-1	1	1.46	0.42
6	1	-1	1	-1	-1	2.04	0.44
7	-1	1	1	-1	-1	2.41	0.24
8	1	1	1	-1	1	4.30	2.85
9	-1	-1	-1	1	1	1.15	0.23
10	1	-1	-1	1	-1	2.20	0.31
11	-1	1	-1	1	-1	2.87	0.64
12	1	1	-1	1	1	4.14	2.93
13	-1	-1	1	1	1	1.96	0.38
14	1	-1	1	1	-1	2.07	0.70
15	-1	1	1	1	-1	2.81	0.52
16	1	1	1	1	1	4.13	0.13
Effect on √Capacity	1.091088	1.75	-0.0581	-0.1605	0.648		
Effect on %EE	0.63	0.52	-0.11	-0.071	0.54		

An example for calculating the effect of E_{ab} on √Capacity is shown below wherein, positive E_{AB} is coming from STD 1(-1×-1=1), 4 (1×1=1), 5 (-1×-1=1), 8 (1×1=1), 9 (-1×-1=1), 12(1×1=1), 13(-1×-1=1), 16 (1×1=1) considering Equation 4.

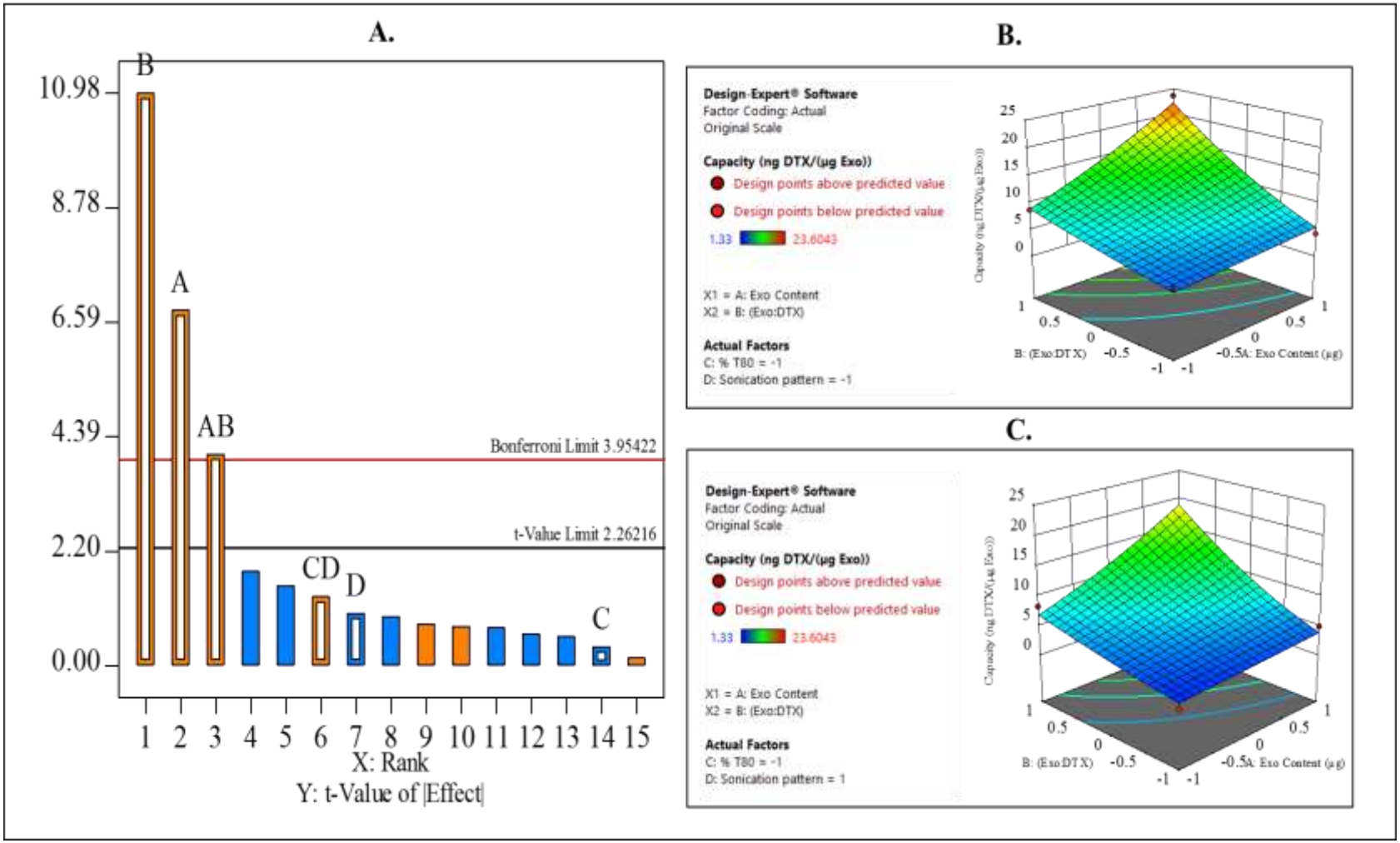

Figure 5.2: Representative plots indicating the effect of four factors and their interactions on the response 'Capacity' while optimizing the Exo-DTX by sonication method, A: Pareto chart indicating the significance of the factors crossing Bonferroni limit and t-limit to confirm the effect on the capacity and %EE of exosomes. B: 3D-surface plot indicating the effect of the most significant interaction term (AB) on the capacity of the exosomes when sonication pattern is kept at (-1) level. C: 3D-surface plot indicating the effect of the most significant interaction term (AB) on the capacity when sonication pattern is kept at (+1) level. Both 3-D plot and the Pareto chart were generated by Design Expert®v11 (State-Ease, Inc. USA).

#Herein, factors A, B, C, and D indicate Exosome content, Exo: DTX ratio, % T80 and number of sonication cycles respectively.

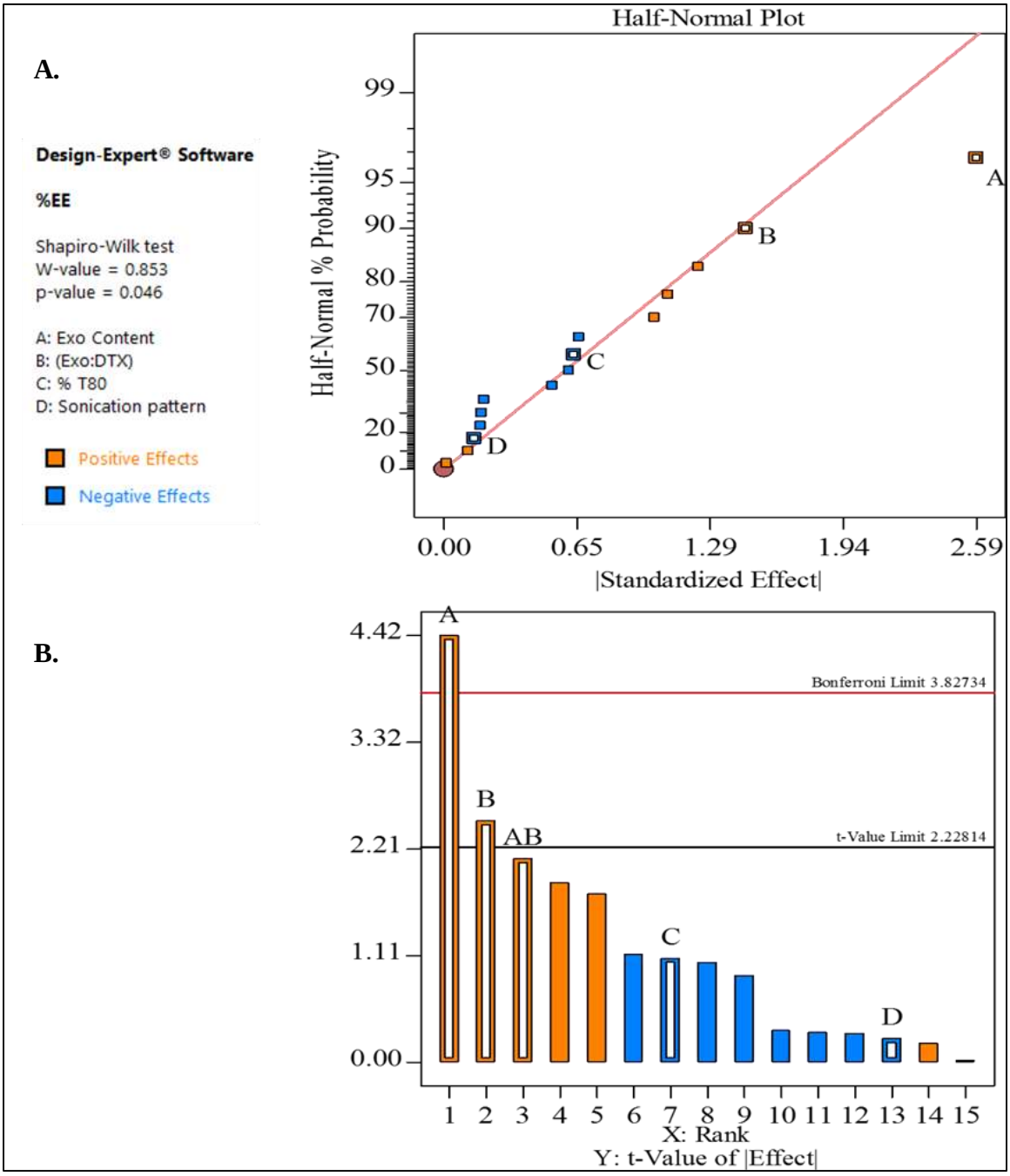

Figure 5.3: Representative plots indicating the effect of the four factors and their interactions on the response '%EE' while optimizing the Exo-DTX by sonication method. A: Half-normal plot, factors that reside away from the error line are considered as significant factors (herein, A, B, AB) using Design.Expert®v11). However, factors CD, C, and D were included in the model to improve the prediction. B. Pareto chart indicating the significance of the factors considered, where A and B showed positive effect and C and D showed negative effect.

[#]Herein, factors A, B, C, and D indicate exosome content, Exo: DTX ratio, % T80 and number of sonication cycles respectively.

Table 5.6
Representative statistical analysis of the responses √Capacity (ng DTX/µg Exosomes) and %EE to confirm DTX loading efficiency by optimized mild sonication method applying 2^4 - full factorial design.

Response	Model p value	R^2	Adjusted R^2	Predicted R^2	Adequate Precision
√Capacity (ng DTX/µg Exosomes)	<0.0001	0.9415	0.9269	0.8960	18.304
%EE	0.0010	0.7296	0.6620	0.5193	7.1622

Validation of the optimized method of DTX loading in RAW Exosomes

Considering the inferences from all the optimization studies, STD 4 (**Table 5.2B)** formulated using exosomes (200 µg equivalent protein) with 50 µg DTX (Exo: DTX =4:1) in presence of 0.02% Tween 80 was found to provide Exo-DTX formulation with a capacity of 23.6 ng DTX/µg. Exosomes were sonicated at 20% amplitude with 4X cycles followed by 2h post-sonication incubation at 37˚C. This batch was further utilized for the *in-vitro* efficacy study.

As mentioned previously, to confirm the reliability of the method optimized for DTX encapsulation in exosomes, point prediction technique was followed wherein, a random Exo: DTX ratio of 7:1 was chosen as a factor keeping other factors intact. Here, the software predicted an Exo-DTX formulation with a capacity of 13.07 ng DTX/µg exosomes when 30 µg DTX was taken with exosomes (200 µg equivalent protein) to achieve Exo: DTX ratio as 7:1. Experimentally these batches were formulated in 3 replicates wherein, a capacity of 14.5±1.67 ng DTX/µg exosomes was observed with a 9.8% prediction error. These results stated the fact that the optimized protocol was reliable with slightly modified parameters as well.

Table 5.7
Validation of the parameters selected for the optimum DTX loading capacity of Exosomes by point prediction technique.

Exosome (µg)	Exo:DTX	%Tween 80 (v/v)	Sonication pattern M (nX)	Capacity (ng DTX/µg exosomes)
200	7:1	0.02%	4X	13.07 (predicted) 14.5±1.67 (actual) 9.86% (% prediction error)

5.3.2 Characterization of the Exo-DTX

As mentioned in previous chapter, murine macrophage cell, RAW 264.7 cells wer used to isolate macrophage derived exosomes from the collected CM with exosomal yield of 172.03±28.9 µg equivalent protein per 200 mL CM. Using DLS and FESEM, unloaded and loaded exosomes were characterized for particle size (nm), zeta-potential (mV), absolute intensity (Kcounts/s), and morphology. The comparative size data obtained from DLS and FESEM indicated a higher particle size (208.7±36.19 nm) with high polydispersity index (PDI) of 0.256±0.03 by DLS as compared to that of FESEM, possibly owing to the inherent clumping nature of the exosomes (**Table 5.7**). Naive and DTX loaded exosomes exhibited negative surface potential equivalent to -10.27±3.66 and -11.03±3.09 mV, respectively, attributed to the presence of phospholipids and surface proteins embedded in the exosomal bilayer, confirming the retention of exosomal integrity after loading. As indicated by FESEM data in **Figure 5.4**, both loaded and unloaded exosomes were found spherical but non-uniform in the size visibly. Additionally, an increase in the exosomal size upto 189.2±35.93 nm by FESEM, was observed after being loaded with DTX by sonication, similar size of Exo-DTX was also demonstrated by the DLS (**Table 5.7**). The decrease in the size of Exo-DTX in comparison to that of unloaded exosomes as exhibited by DLS is possibly owing to disassembly of exosomal clumps after sonication (during formulation of Exo-DTX).

5.3.3 In-vitro efficacy of Exo-DTX formulations

Cytotoxicity Assay

Initially, the cytotoxic effect of free DTX was assessed over three time points (24/48/72 h)— at concentrations between 25-500 ng/mL. It was observed that cells treated for 48 h with DTX exhibited significantly varying cytotoxicity based on the concentration of DTX and the IC_{50} for free DTX and Exo-DTX was found to be 480.04 ng/ml and 89.77 ng/ml respectively (**Figure 5.5A)**. Based upon the IC_{50} value of free DTX, cytotoxicity assay was performed for different treatment groups, i.e., free DTX, naive exosomes and Exo-DTX within the range of 10-250 ng/ml for 48 h by MTT assay. Greater cytotoxicity of the Exo-DTX group over the free DTX group at each of the concentrations used is clearly seen in **Figure 5.5.B**. Exo-DTX exhibited an IC_{50} (89.77 ng/ml) which is approximately 5-folds lesser than that of free DTX.

Interestingly, the cytotoxicity of naïve exosomes increased with increase in their concentration (exosomal concentration increased with increase in the amount of DTX depending upon the DTX loading capacity of the exosomes). At the IC_{50} dose of Exo-DTX, the cytotoxicity of naive

exosomes was 12.36±1.62% (within acceptable range) but increased to 19.45±3.10 % at a dose of 250 ng/mL loaded DTX. The bright field microscopy of the cells shows the comparative cellular deformation upon various treatments for 48 h (**Figure 5.5C)** wherein, the Exo-DTX at 100 ng/mL and 250 ng/mL were compared with free DTX of 250 ng/mL. Evidently, Exo-DTX formulations were found to have significantly higher cytotoxicity and morphological deterioration than free DTX.

Table 5.8

Particle size (nm), PDI and zeta-potential (mV) of exosomes by dynamic light scattering (DLS) and FESEM.

	Exosomes			**Exo-DTX**		
	Particle size (nm)	PDI	ZP (mV)	Particle size (nm)	PDI	ZP(mV)
DLS	208.7±36.19	0.256±0.03	-10.268±3.66	183.11±33.93	0.25±0.0416	-11.0294±3.09
FESEM	112.5±21.48	NA	NA	189.2±35.93	NA	NA

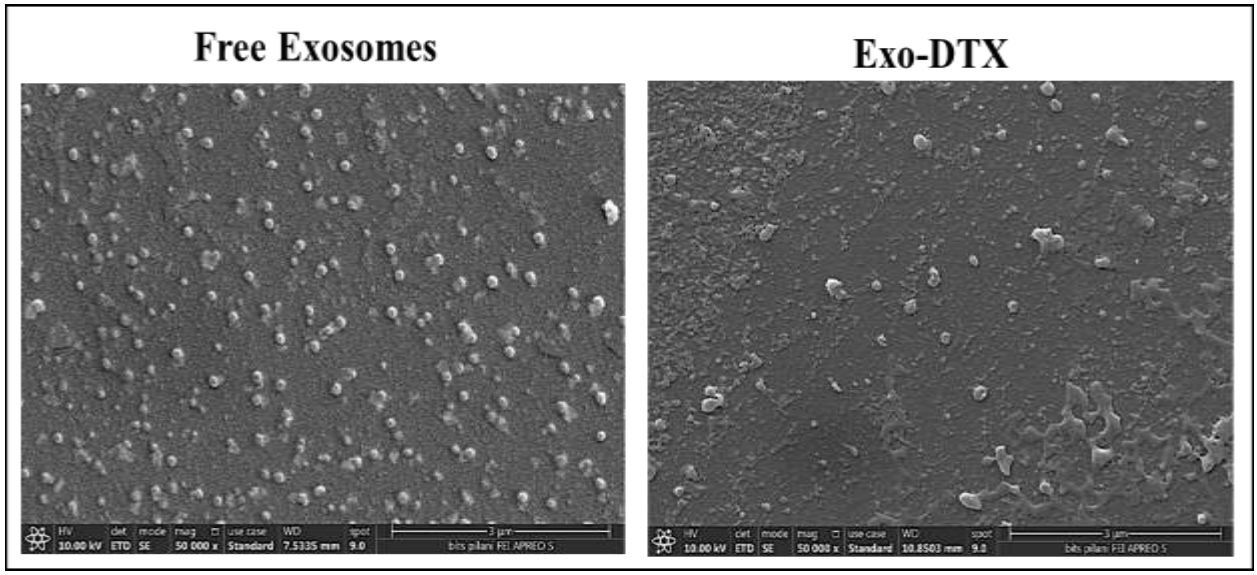

Figure 5.4 Characterization of unloaded and DTX loaded exosomes, representative surface morphology of both unloaded and DTX loaded exosomes by FESEM (Scale=3µm).

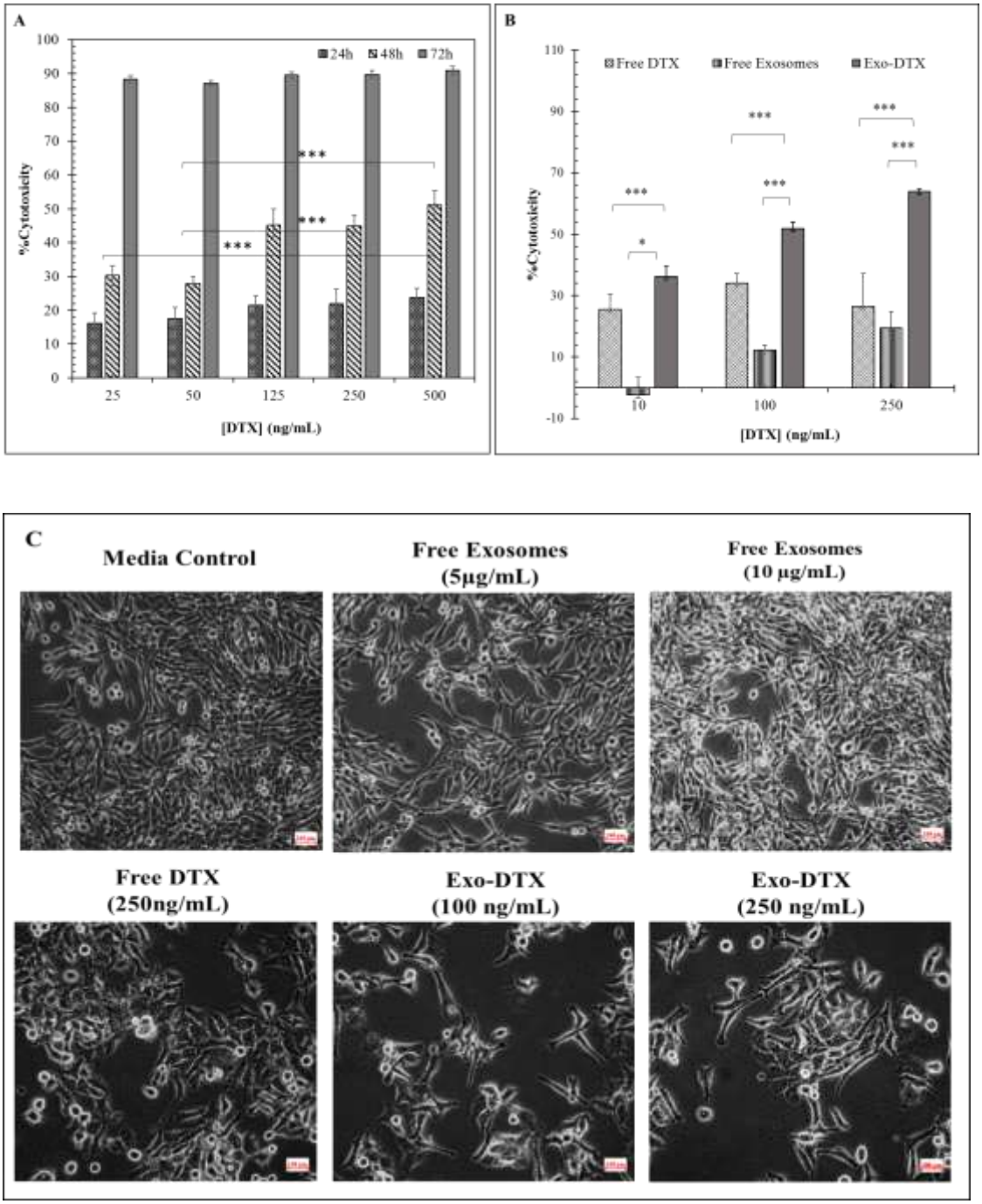

Figure 5.5: Anti-proliferative assay in 4T-1 cells by MTT and microscopy. A: Time and concentration dependent in-vitro cytotoxicity assay of free DTX. Data are represented as mean (n=5) ± SD. B: Comparative cytotoxic effect of the free DTX, naive exosomes and Exo-DTX mean (n=6) ± SD. Two-way ANOVA with Bonferroni post-test determined statistical significance. (***p<0.001, **p<0.01) C: Impact of various Exo-DTX treatments (100 and 250 ng/ml) on cellular morphology and cell density, as compared to both media control and blank exosome control groups, using brightfield microscopy (Scale=100 µm).

Cellular uptake and efficacy

The cytoskeletal structure (specifically F-actin) of the cells was stained by Rhodamine Phalloidin and the nuclei of the cells were counterstained with DAPI. As indicated in **Figure 7**, different treatment groups showed a distinct change in the cellular appearance, including cellular shrinkage and degraded appendages that resulted in loosely connected cells in case of free DTX and Exo-DTX in comparison to the control group (only media). The PKH-67 labelled naive exosomes and Exo-DTX inside the cells demonstrated that both were effectively internalized by 4T1 cells within 6h, seen as green fluorescent dots (**Figure 5.6).** In comparison to the control group (only media), F-actin degradation was evident in free DTX treated group (indicated by the **white arrows**) also revealed by the diminished intensity of Rhodamine with almost same number of cells in the selected field. Prominent F-actin degradation was also marked by the severed ends of F-actin at the cellular boundary. Likewise, in case of the Exo-DTX treated groups, cells showed similar kind of structural change with additional nuclear condensation (indicated by **red arrow**) and cytoskeletal degradation (indicated by **white arrow**), green arrows mark the PKH-67 stained Exo-DTX. This clearly proved that Exo-DTX was successfully internalized by cells wherein, they produced superior effect than free DTX group treated group even within 6h of treatment.

Pro-metastasis suppression assay

The efficacy of the Exo-DTX formulation in inhibiting pro-metastasis has been confirmed through in vitro wound healing assay and transwell invasion assay. Since the Exo-DTX formulations demonstrated some promising cytotoxic effect by producing cytoskeletal and nuclear degradation in 4T1 cells, their effect on the metastatic aggressiveness of the TNBC was also studied.

Wound healing assay

In a time-dependent manner, Exo-DTX demonstrated its superior anti-migratory effect on 4T1 cells preventing the wound closure till the end time-point of the study (36 h). As seen in **Figure 5.7.A,** wound closure or cellular migration is initiated quite early but it became prominent only after 12h of wound creation. The media control group and the free exosomes treated group displayed notable wound closure within a timeframe of 12-36 h. However, the groups treated with free DTX and Exo-DTX exhibited resistance to wound closure till 36 h, as illustrated in **Figure 5.7B**. In comparison to the free DTX treated group (50.73±10.55% wound closure within 36 h),

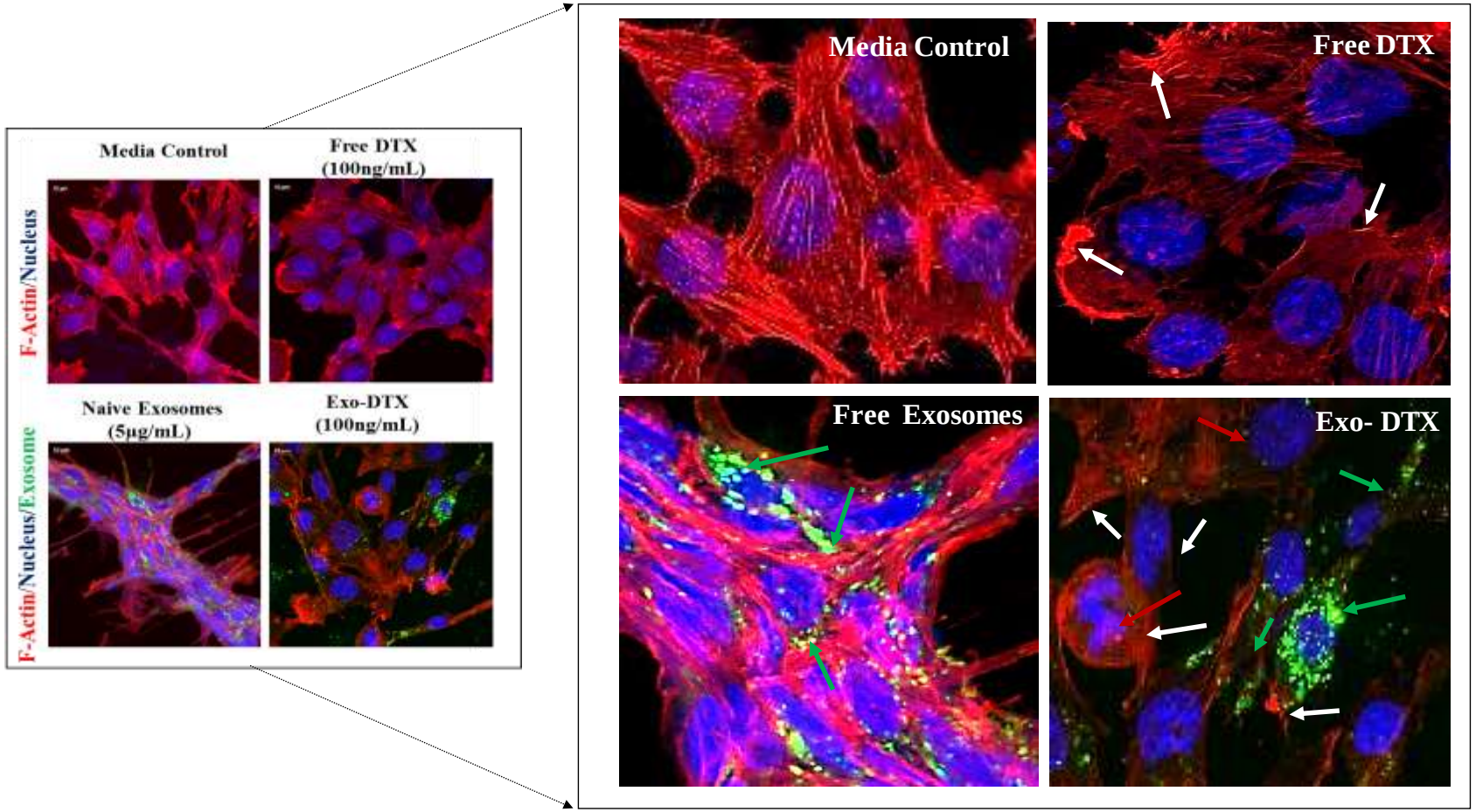

Figure 5.6. Cellular uptake in 4T-1 by confocal microscopy. Cells after 6h of treatment with PBS, free DTX (100 ng/mL), naive exosomes (5 µg/mL) and Exo-DTX (100 ng/mL). White arrow: F-actin structure degradation, Green arrow: PKH-67 stained exosomes or Exo-DTX, Red arrow: nuclear degradation.

Exo-DTX showed invariably superior anti-migratory effect (2.6±6.33% closure within 36 h of treatment). Naive exosomes exhibited similar wound closure as that of media control (83.95±0.79% and 88.85±1.2% respectively) in 36 h.

Invasion assay

Pro-metastasis involves both migration and invasion across the biological barriers hence, transwell migration assay was performed. It was expected that the cells which invade the Matrigel bed, driven by chemoattractant condition provided in the lower well, would be found adhering on the outer side of the transwell membrane (facing the bottom of the well of 24 well plate).

The group treated with Exo-DTX revealed least invasion of the 4T1 cells (**Figure 5.7 C&D)**. The anti-metastatic impact of Exo-DTX in 4T1 cells may also be partly contributed by the naïve exosomes. In comparison to the media control group, showing 99.79± 20.02% invasion, naive exosomes and Exo-DTX treatment restricted cells to 87.96±9.58% and 4.56±1.38% invasion after 48h of treatment. Free DTX alone was able to restrict the invasion to 31.74±8.6%; significantly reduced invasion by Exo-DTX might be attributed to the incorporation of DTX in the exosomes.

5.3.4 Mechanistic exploration of the underlying crosstalk

In comparison to free DTX, Exo-DTX displayed superior cytotoxicity, substantial cytoskeletal deformation followed by nuclear fragmentation, and lowered 4T1 migratory aggressiveness. Naive exosomes also affected 4T1 cells in a distinctive way. The mechanistic exploration of naive exosomes and Exo-DTX activity in 4T1 cells was corroborated through confocal microscopy analysis of F-actin degradation and morphological analysis via FESEM. Later, the findings were

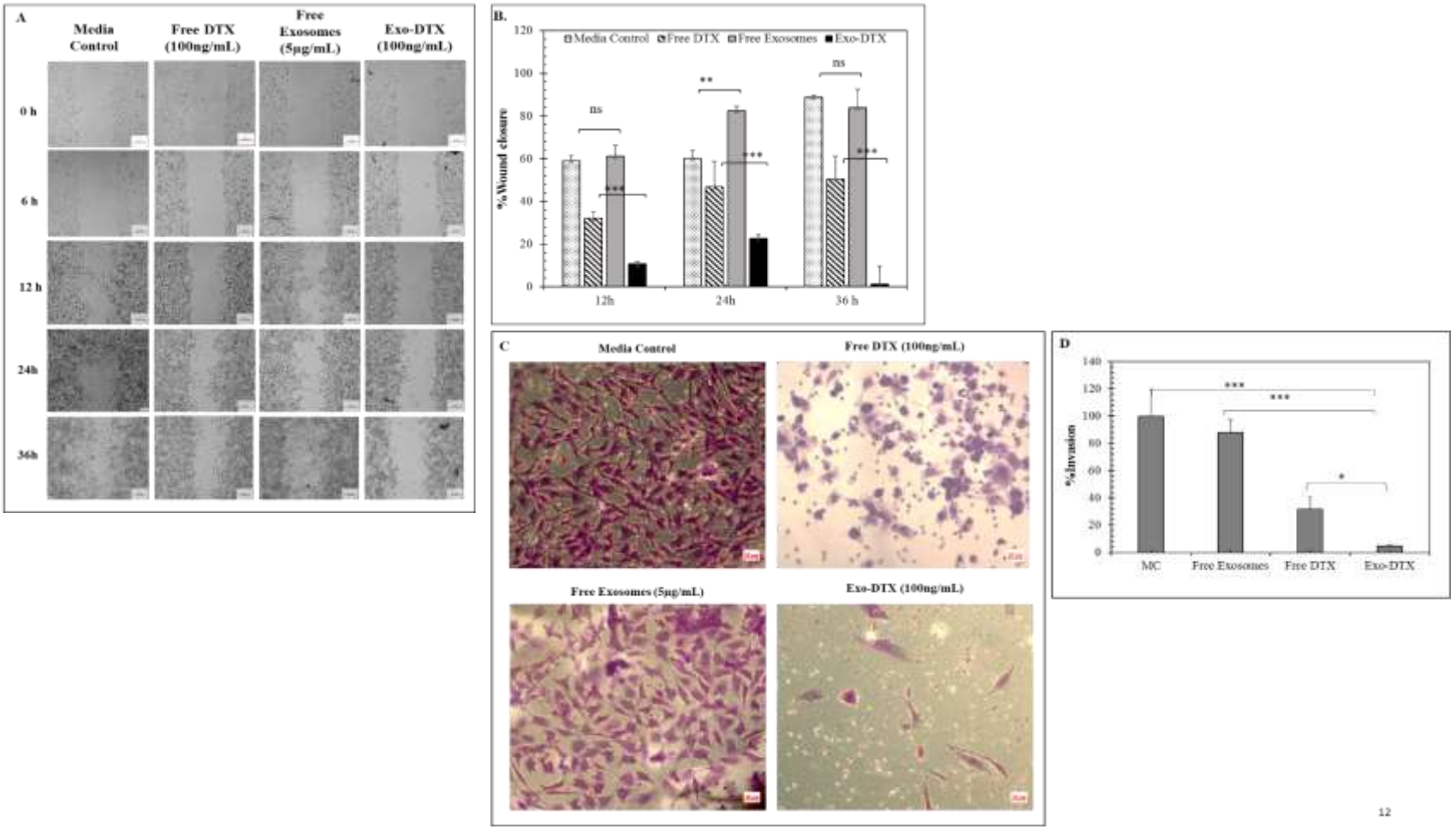

Figure 5.7 In-vitro anti-migratory wound healing (A and B) and invasion assay (C and D) in 4T-1 after being incubated with Exo-DTX. A: Time-dependent (0-36 h) migratory ability of 4T-1 cells following incubation with PBS, free DTX, naïve exosomes, and Exo-DTX (n=3) scale bar=100µm B) Graphical representation of % wound healing. The data represents mean (n=3) ± SD, two-way ANOVA with Bonferroni post-test is applied for statistical significance, where, *p<0.05, **p<0.01 and ***p<0.001. C) The invasion of metastatic cells through Matrigel® on the outer surface of the Transwell membrane (n=3) stained with crystal violet, scale bar- 20 µm D: Graphical representation of the % invasion after treatment with PBS, free DTX, naive exosomes and Exo-DTX. The dataset is presented as mean (n=3) ± SD. To determine statistical significance, a one-way ANOVA with Tukey's post-test was utilized, with significance levels denoted as *p<0.05, **p<0.01, and ***p<0.001.

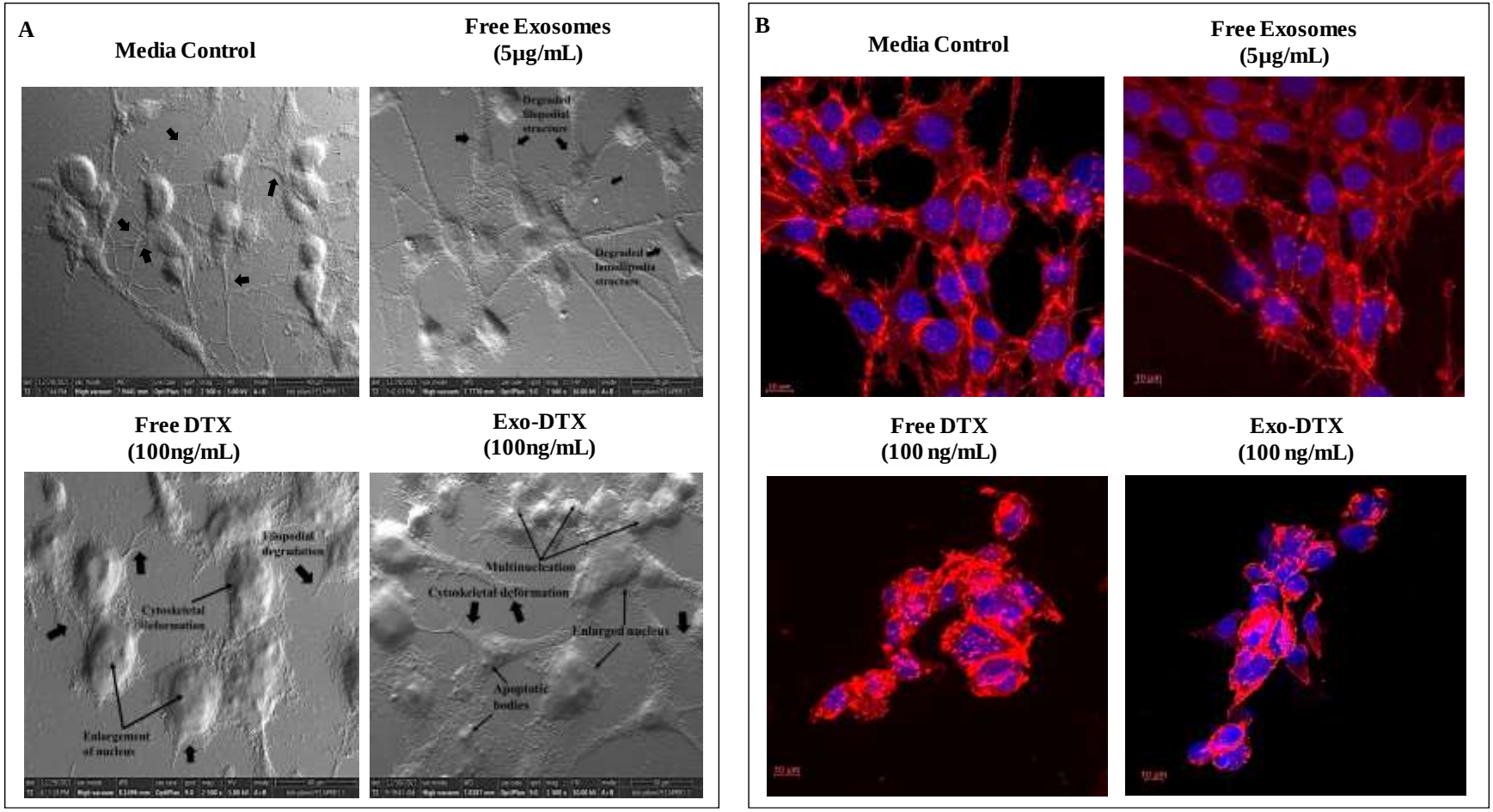

Figure 5.8 Mechanistic exploration of the effect of DTX formulation on 4T-1 cells. Effect of the DTX (free and formulation) on the cellular morphology, especially on the cytoskeletal cage and nuclei after 48 h (n=3) by, A) FESEM (magnification 2500X) and B: confocal microscopy wherein, F-actin is stained with Rhodamine phalloidin (red) and nuclei with DAPI (blue) (n=3), scale bar=10 µm.

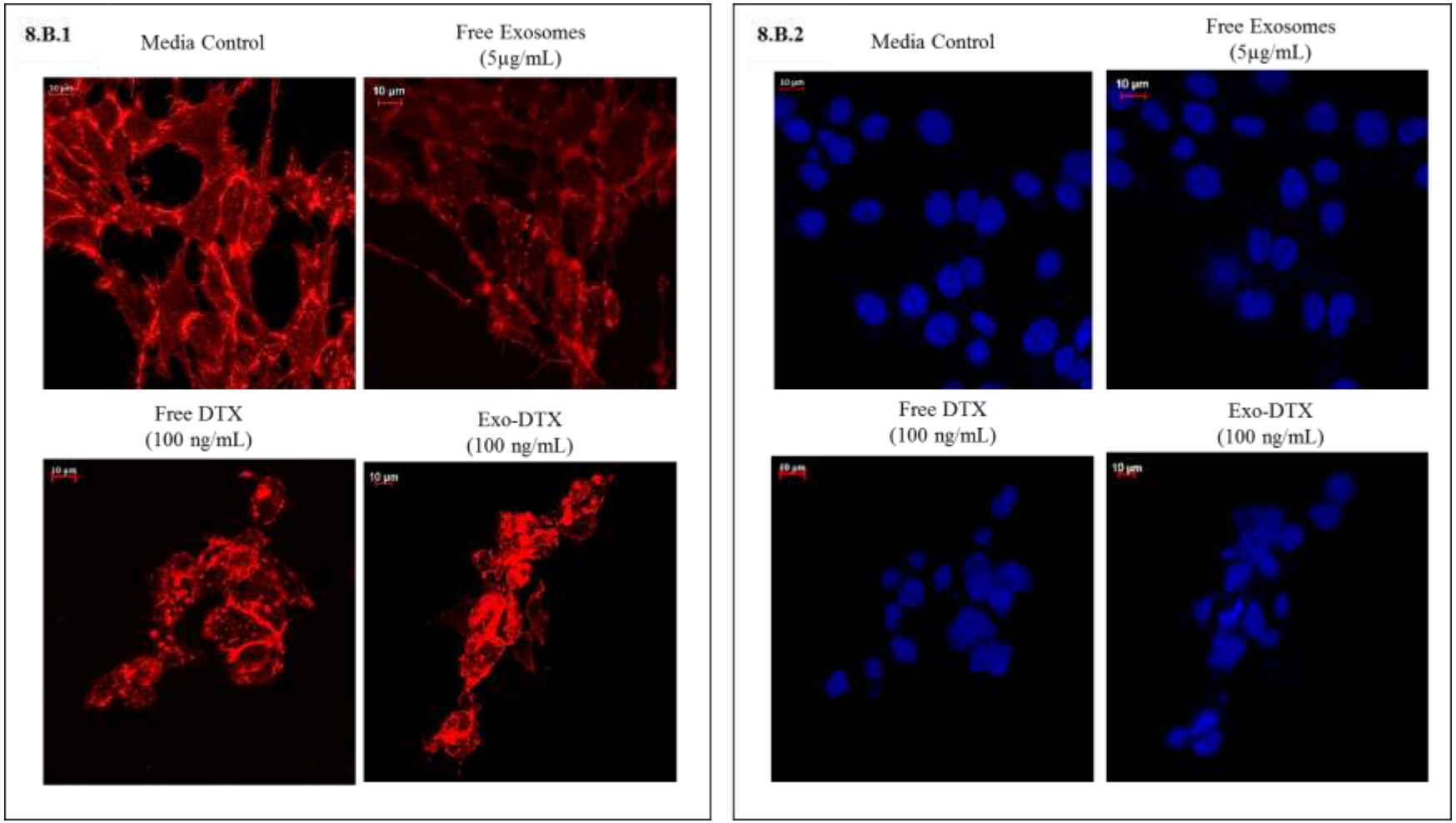

Figure 5.8.B Cytoskeletal disorganization and nuclear degradation in 4T-1 cells after incubation with Exo-DTX for 48 h visualised using confocal microscopy (split diagram of Figure 5.8B). B1: Cytoskeleton of the cells stained with Rhodamine Phalloidin (red) and, B2: Nuclei stained with DAPI (blue) (n=3), scale bar=10µm.

also linked to the differential protein expression in 4T1 cells (both apoptotic and anti-metastatic) following treatment with different formulations.

Both **Figure 5.8A and 5.9** indicated close intercellular connection among the 4T1 cells in the media control group via their healthy appendages *(as indicated by the black arrow).* When compared with media control, it was observed that naive exosomes exhibited a minor distortion of invadopodia, specifically filopodia and lamellipodia. Evidently, free DTX regressed the cellular morphology by distorted filopodia, lamellipodia, an enlarged nucleus, and the presence of cellular debris and apoptotic bodies. Exo-DTX caused more pronounced cytoskeletal deformation and nuclear degradation compared to free DTX. The enlargement of nucleus indicates the cell-cycle arrest in G_2/M phase while multinucleation indicated incomplete cell division. The same observations were resonated by F-actin degradation assay by confocal microscopy (**Figure 5.8B).** Herein, the reduced intensity of the Rhodamine clearly indicated the degradation of F-actin filaments in Free DTX and Exo-DTX treated groups. Also, in both Free DTX and Exo-DTX group, presence of the F-actin foci on the periphery of the cells clearly indicated that the cell is being restricted in the mitotic phase. Exo-DTX showed significantly higher distortion of intercellular connection, nuclear degradation, and multi-nucleation than free DTX.

While correlating both **Figure 5.8A and B,** a clear indication of apoptotic and anti-migratory effect of Exo-DTX in 4T1 cells was observed wherein, Exo-DTX degraded the cytoskeletal network more efficiently and induced significant apoptosis in comparison to the free DTX. The results were in line with FESEM data of treatment group. At a higher magnification level in confocal microscopy (**Figure 5.8 B1& B2**), massive F-actin degradation, nuclear condensation and fragmentation could be clearly seen.

Mechanistic exploration by Western blot for apoptotic and anti-metastatic protein expression

In this final study of mechanistic exploration, we tried to explore the mechanisms behind the observations made so far. **Figure 5.10** illustrates the impact of free DTX (100 ng/mL), naive exosomes (5 µg/mL), and Exo-DTX (100 ng/mL) on the distinct protein expression of 4T1 cells. Considering the differential expression of the apoptotic markers in **Figure 10A & C**, Exo-DTX resulted in increased ratio of cleaved caspase 3 and caspase 3 (CC3/C3) and BAX/BCL-2 by 2.9 and 2.05 folds in comparison to the free DTX in comparison to the media control. Also, EGFR expression was found downregulated in the order, free DTX <naive exosomes < Exo-DTX, while β1-integrin was found decreased in free DTX and Exo-DTX group only. Free DTX decreased the

EGFR and β1-integrin expression in 4T1 cells by 1.32 and 1.99 folds respectively. In comparison to free DTX, naive exosomes and Exo-DTX exhibited 2.2 and 2.9 folds' decrease in the expression of EGFR respectively (**Figure 10.D**).

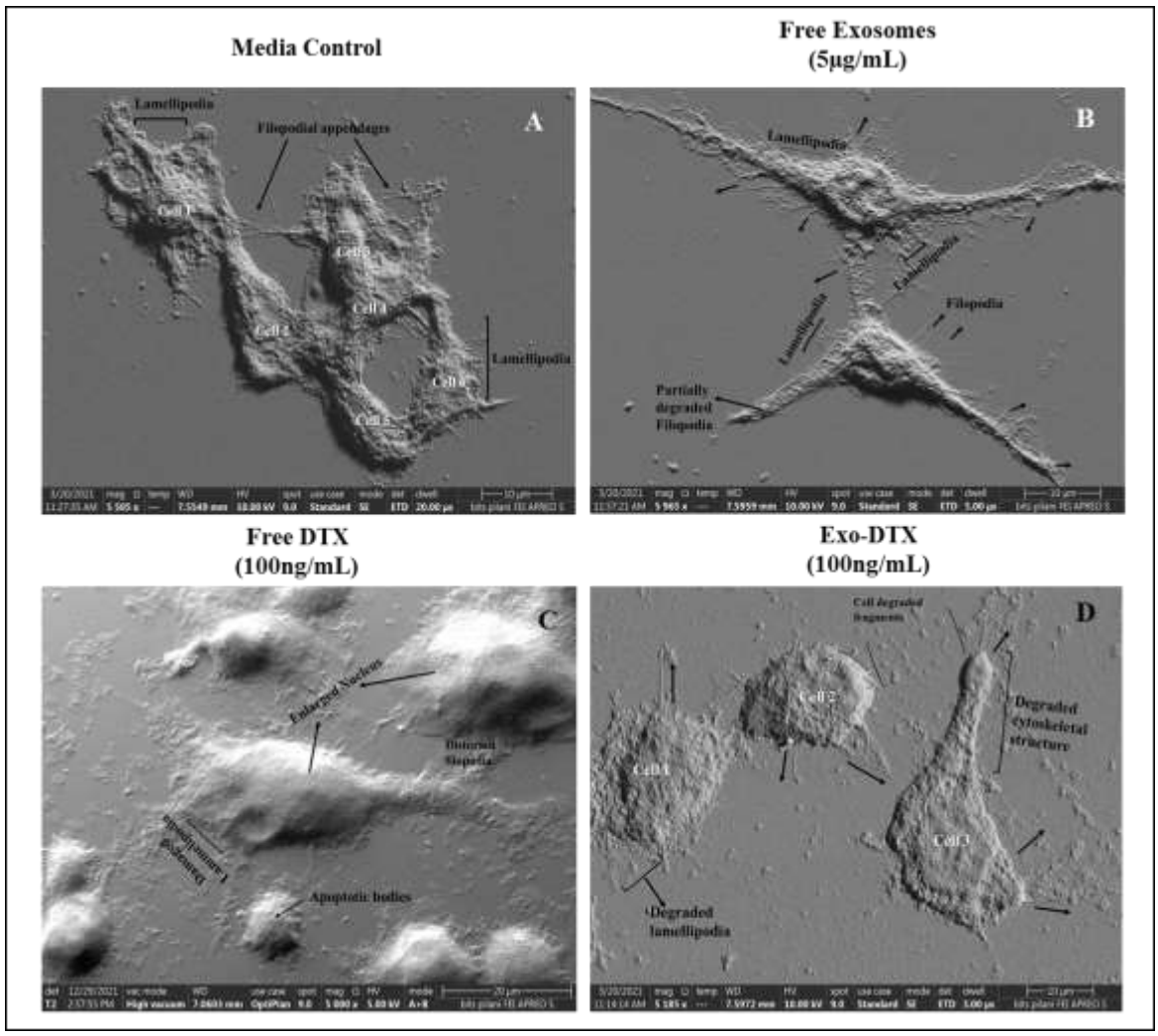

Figure 5.9: Cytoskeletal disorganization in 4T-1 cells after incubation with Exo-DTX by FESEM assay. The damage of the invadopodia (filopodia and lamellipodia) is more prominent in A than B, whereas the damaged invadopodia with enlarged nucleus is evident in C and D. Cellular debris and cytoskeletal deformation are more prominent in D.

Figure 10.B and E, distinctly indicated decreased expression of β1-integrin (by almost 2.5 folds) but an increase in the ratio of CC3/C3 by 1.5 fold upon treatment with Exosomes (2.5 µg/mL) in comparison to Exosomes (5 µg/mL) in the 4T1 cells. This concentration dependent differential expression of apoptotic CC3/C3 ratio and metastatic marker β1-integrin, clearly indicate that the inherent nature of exosomes is undoubtedly important to be considered. In our case, we considered

exosomes at 5 µg/mL as the blank formulation keeping in mind the optimum capacity of Exo-DTX formulation. All the studies provided a clear evidence that Exo-DTX exhibited enhanced anti-cancer effect in comparison to free DTX in terms of both apoptosis induction as well as anti-metastatic function, attributed to the loading of DTX in the functionally active biological origin nanocarrier system, exosomes originating from macrophages, known to possess prominent anti-cancer activity against TNBC 4T1 cells.

5.3.6. In vivo pharmacokinetic study

The time dependent plasma concentration profiles of DTX from Taxotere® and the Exo-DTX have been shown in **Figure 5.11** and the comparative pharmacokinetic parameters have been tabulated in **Table 5.8**.

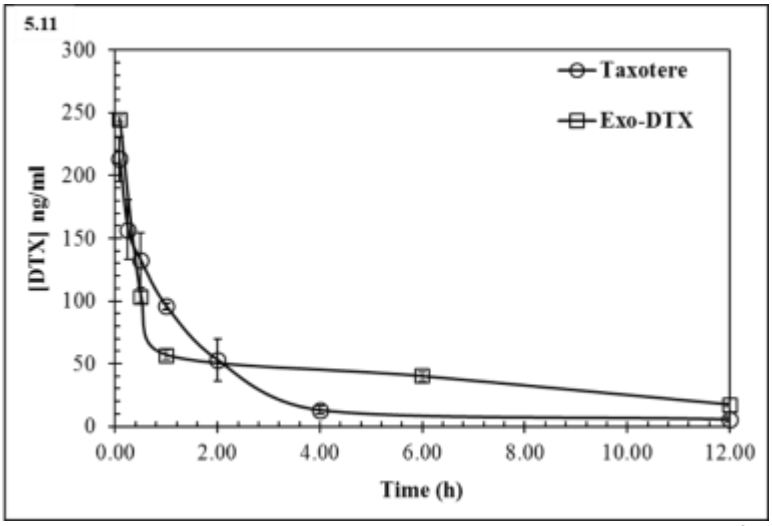

Figure 5.11. Representative plasma concentration-time profile of Taxotere® and Exo-DTX in in vivo pharmacokinetic study. The dataset is presented as mean (n=3) ± SEM.

Table 5.9
Comparative pharmacokinetic parameters for Taxotere and Exo-DTX.

Parameter	Unit	Taxotere (1mg/kg, i.v bolus)	Exo-DTX[@] (1mg/kg, i.v bolus)
C_{max}	ng/mL	213.19±17.77	244.90±2.54
T_{max}	h	0.083	0.083
$t_{1/2}$	h	1.045±0.169	6.328±0.04
$AUC_{(0-\alpha)}$	h×(ng/mL)	339.43±27.04	675.52±11.55
MRT	h	2.83±0.465	8.23±0.198
V_d	mL/kg	4434.00±587.47	13516.42±143.90
Cl	mL/h/kg	2958.37±230.7	1480.6±25.07

[@]all values are mentioned as mean (n=3) ± SD.

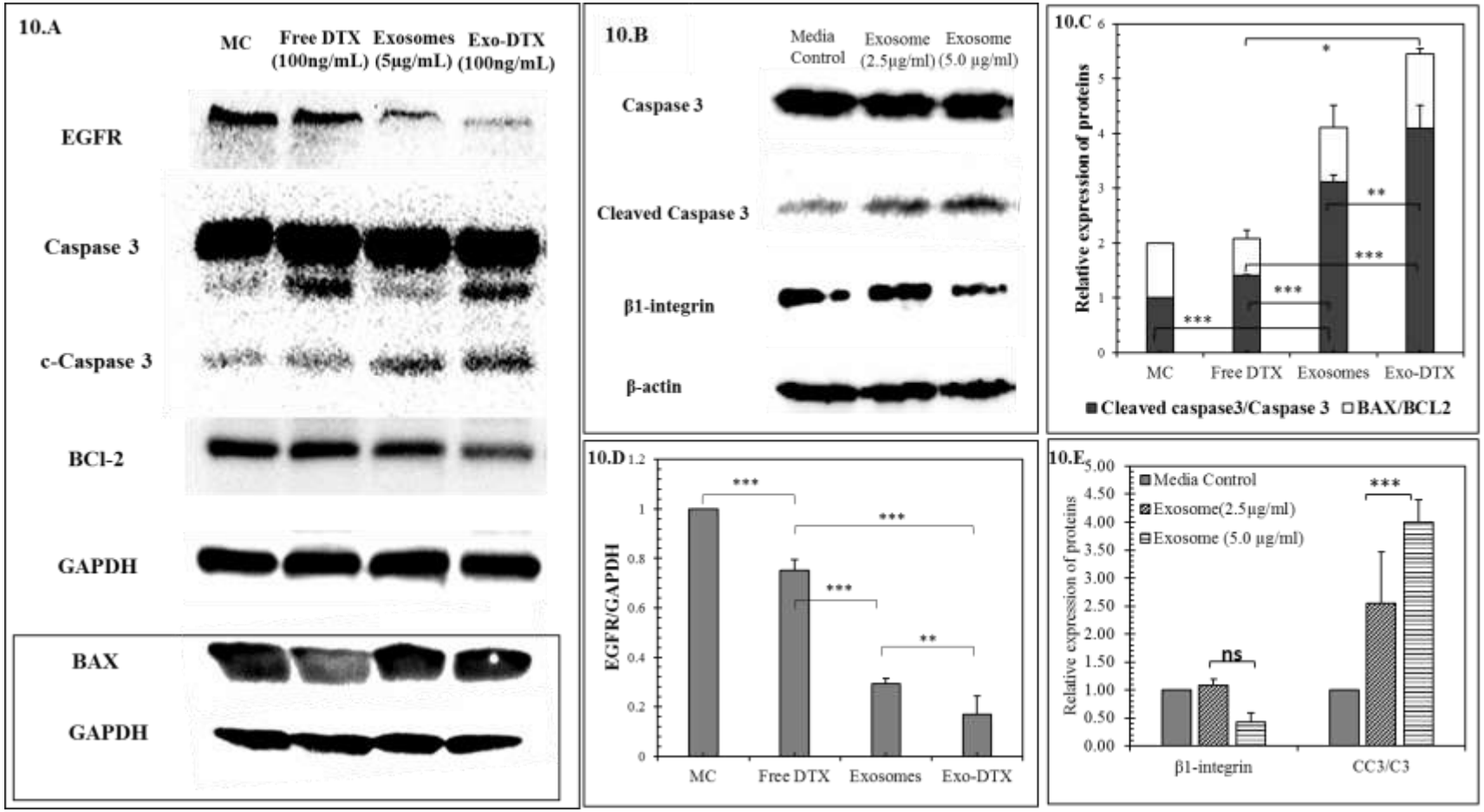

Figure 5.10: Mechanistic exploration of the anti-apoptotic and anti-metastatic protein expression in 4T-1 cells upon incubation with different samples. A: Representative immunoblots of the different anti-metastatic proteins (EGFR and β1-Integrin) and anti-apoptotic proteins (BAX, BCL-2, Caspase-3; C3, cleaved caspase-3; CC3) and housekeeping protein GAPDH. B: Representative immunoblots of β-1 integrin, CC3, C3 and housekeeping protein β-actin in 4T1 cells after being treated with different concentration of exosomes. C. Graphical representation of ratio of cleaved caspase-3 and caspase-3 (CC3/C3) and BAX and BCL-2 (BAX/BCL-2). In both the cases, the individual protein expression was first normalized and quantified with respect to the housekeeping protein GAPDH followed by calculating respective ratios. D: Differential expression of EGFR upon different treatments. E: Differential expression of mentioned proteins to evaluate the effect of exosomes in cells, all data are represented as mean (n=3) ± SD, where one-way ANOVA with Tukey's test was used for the determination of the statistical significance, where *p<0.05, **p<0.01 and ***p<0.001.

Exo-DTX exhibited significant decline in the plasma DTX concentration within 1h of administration, it maintained almost steady state concentration 56.8-39.8 ng/ml till 6h however, Taxotere® showed gradual elimination, reaching upto 13.07±3.45 ng/ml within 4h of the treatment (**Fig. 5.11**). The initial rapid decline in the concentration of DTX after administering Exo-DTX in vivo has also been reported earlier wherein, half-life of RAW 264.7 derived exosomes was found to be $t_{0.5}$= 2.77±0.28 min with MRT of 0.261±0.024 h after a dosing of 5 µg gLuc /LA labelled exosomes in BALB/c mice [23,24]. In the present study, 6-folds' and 3.04-folds' improvement in $t_{0.5}$ and V_d of the Exo-DTX in comparison to the Taxotere® in a statistically significant manner ($p<0.001$ and <0.01 respectively) was observed; clearly indicating its rapid tissue distribution owing to the easy uptake of the Exo-DTX. Exo-DTX also showed significantly improved MRT and AUC with decreased Cl when compared with the Taxotere.

All the studies provided a clear evidence that Exo-DTX exhibited enhanced anti-cancer effect in comparison to free DTX in terms of both apoptosis induction as well as pro-metastasis suppression in *in vitro* assays, attributed to the loading of DTX in the functionally active biological nanocarrier system that is exosomes of macrophages origin, known to possess prominent anti-cancer activity against TNBC 4T1 cells. Additionally, the improved PK profile of Exo-DTX in comparison to the marketed formulation of DTX, Taxotere®, highlights the translational value of the exosomes for the anti-cancer formulation development in near future wherein, exosomes could be projected as a promising biogenic replacement of synthetic nanocarriers.

5.4 Discussion

Cell derived exosomes as efficient nanocarrier of anti-cancer small molecules have been well explored both in-vitro and in-vivo [25–27]. However, there is a lack of unified report on the methodological optimization and validation of exosomal formulations and this is unquestionably a gap in exosomal research [28]. Literature reports, RAW 264.7 cell-derived exosomes with a loading capacity (% LC) of 28.29%, 5.30%, and 1.44% for PTX when prepared using sonication, electroporation, and incubation techniques respectively [29]. Further, polarization of RAW 264.7 cells (M_0) to M_1, mediated by interferon-γ (IFN-γ), resulted in %LC of PTX of 19.55% and 4.88% with sonication and incubation respectively in M1 cells derived exosomes [7]. PC-3 cell-derived

exosomes revealed 9.20% loading of PTX, whereas milk-derived exosomes demonstrated only 7.90% practical loading capability [21,30]. The drug loading (% DL) of gemcitabine in PANC-1 exosomes was found to be 11.68% by sonication and 2.79% by incubation [31]. It was also evident that sonication was more effective for encapsulating small molecules into exosomes than incubation, however, as evident from the above examples, % LC differed from one research group to another. Since the % LC varied, so did the estimated number/ amount (equivalent protein) of exosomes required to achieve a given dose equivalent, which influenced their inherent biological effect on the cells or in animal model. As exosomes are not merely preformed vesicles, but rather biogenic with certain intrinsic biological functions, the choice of source cells for exosomes and their encapsulating capacity must also be evaluated [19,21,32–34]. In this context, our research is relevant as we have not only optimised the formulation development methodology of Exo-DTX but also evaluated the contribution of the naïve RAW264.7 derived exosomes in Exo-DTX formulation development and anti-cancer attributes in TNBC cells.

The overall formulation optimization was achieved utilizing the QbD-based approach. **Figure 5.1** shows that exosomes can only efficiently encapsulate DTX through diffusion with an efficiency range of 4.79–6.62 ng DTX/µg of exosomes without sonication, even when the exosome content and Exo: DTX ratio are increased. However, mild sonication increased DTX encapsulating capacity of exosomes by threefold, clearly demonstrating that re-organization of the exosomal membrane during mild sonication loosens the tightly packed bilayer and certainly facilitates the maximum encapsulation of DTX (**Table 5.2**) [35]. QbD based approach was again applied to ensure the maximal DTX loading capacity of exosomes using mild sonication/incubation technique. **Table 5.4** indicates that exosome content and Exo: DTX were two positive factors, whereas %Tween 80 and sonication cycles were the two negative factors. With increasing exosome content and Exo: DTX ratio, maximal %EE was obtained with batches that contained minimal %Tween 80 and were subjected to only 4 cycles of sonication. The most effective batch was **STD 4** (**Table 5.4)** with DTX encapsulating capacity of 23.60±1.54 ng DTX/ µg exosomes, which also indicated that reducing the exosome content by 5 folds would decrease the capacity by nearly 3 folds in **STD 3** (with 8.64±1.06 ng DTX/ µg exosomes), considering all other factors remain constant. The negative impact of % Tween 80 and sonication cycle could be also seen upon comparing **STD 4** vs. **STD 8** vs. **STD 12.** Also, Exo-DTX with a capacity ranging from 17.16-23.60 ng DTX/µg

exosomes was obtained from these three formulations employing 200 µg of exosomes and an Exo: DTX ratio of 4:1 while adjusting all other parameters.

DTX is a well-known anti-cancer small molecule from Taxane family which results in distinct cytoskeletal deformation by inducing "dynamic instability" and "mitotic slippage" in a concentration dependent manner [36,37]. It is well reported that DTX at 100nM concentration arrests, most of the TNBC cells get arrested in G_2/M phase within 24h of treatment [38]. Also it is evident that, DTX, activates some mitotic checkpoints that delay the separation of chromosomes and results in the formation of daughter cells with replicated pair of sister chromatids. This mitotic arrest would result in the cellular death or abnormal exit from the mitosis itself giving rise to tetraploids, well known as the mitotic slippage, followed by some cellular anomalies [39]. DTX has also been reported to alter the mechanical properties of the ovarian cancer cells, SKOV 3 wherein, at 100 ng/ml, the cellular roughness, and rigidity increased but area decreased significantly. This was correlated to the reduced migratory and invasive potential of the cancer cells [40]. As indicated by MTT assay in **Figure 5.5B**, Exo-DTX showed an IC_{50} value of 89.77 ng/ml, which is around 5.3 folds' lesser than the IC_{50} of free DTX along with prominent cytoskeletal deformation (**Figure 5.5C).** The cytoskeletal deformation of Exo-DTX treated 4T-1 cells was more prominent than free DTX even within 6h of treatment (**Figure 5.6**) indicating the superior uptake of DTX upon encapsulation into the exosomes. This is further supported by the inherent antifouling effect of exosomal membranes owing to the presence of zwitter-ionic phospholipids, i.e., phosphatidylcholine (PC) and sphingomyelin (SP) in the lipid bilayer structure, which provide zwitterion neutralization, resulting in super hydration by forming dipole-ion interaction between the membrane and the water molecule. This resulted in an efficient uptake and significantly higher biocompatibility of exosomes [41–43]. Cytoskeletal deformation and metastatic potential are inversely correlated and the same was also confirmed in case of Exo-DTX. **Figure 5.7B** shows only 2.6±6.33% wound closure in 36h, indicating the efficient anti-metastatic effect of Exo-DTX. Further, **Figure 5.7D** exhibits only 4.56±1.38% invasion of 4T1 cells treated with Exo-DTX for 48 h. This significant anti-metastatic effect confirms an efficient cellular uptake and resultant apoptosis [44].

After confirming the anti-migratory potential, a mechanistic exploration was carried out to ensure the efficacy of Exo-DTX in 4T1 cells. Herein, we evaluated the in-vitro pro-metastatic suppression

and apoptotic efficacy of Exo-DTX in cells, particularly its impact on the **F-actin;** a polymeric G-actin structure degradation, a cytoskeletal component essential for microfilament organization, maintenance of cell morphology, proliferative attributes and regulation of the cellular motility [45–47]. Invasion of cancer cells from the primary tumor site to the distant organs required epithelial-mesenchymal transition (EMT), a closely co-ordinated mechanism wherein, the role of the phenotypic and subcellular structure invadopodia (filopodia and lamellipodia) is important [48,49]. F-actin-mediated membrane protrusions called "invadopodia" transport receptors and proteolytic proteins that contribute to metastasis. Cytoskeletal remodelling during the invadopodia formation involves some proteins, i.e., epidermal growth factor receptor (EGFR) and β1-integrin [50–52]. The process of pro-metastasis is characterised by the upregulation of EGFR expression, which leads to increased phosphorylation of cortactin and consequent facilitation of invadopodia formation. Moreover, invadopodia are characterised by the presence of β1-integrin, which facilitates ECM remodelling. [49]. DTX, on the contrary is responsible for the 'dynamic instability' by excessive polymerization of the microtubule which results in anti-apoptotic BCL-2 phosphorylation and thus increased Caspase-3 related apoptotic activity [38]. Incorporation of DTX in macrophage derived exosomes is thus expected to produce synergistic effect attributed to the immune-regulatory feature of the exosomes and anti-cancer activity of DTX together. This synergistic effect is further enhanced by the more efficient uptake of DTX as Exo-DTX. As per our observation from morphometric assay by FESEM and CSLM, induction of apoptosis and superior cytoskeletal deformation in 4T1 cells upon being treated with Exo-DTX formulations was clear (**Figure 5.8. and 9**). Further, the western blot analysis in **Figure 5.10** confirmed that the Exo-DTX showed prominent anti-metastatic effect with significantly decreased EGFR expression and significantly high apoptotic effect with increased expression ratio of BAX/BCL-2 and CC3/C3 in comparison to the free DTX. The underlying cause of this observation was explained by the distinct cytotoxic effect of naive exosomes, which included a 2.5 folds' decrease in β1-integrin and a 1.5 folds' increase in CC3/C3 ratio.

Understanding the pharmacokinetics of the Exo-DTX is essential to elucidate the behaviour of the formulation in the biological milieu especially considering that the exosomes are themselves biogenic and well reported to possess paracrine signalling property. Irrespective of the source cells, exosomes tend to distribute more to the highly perfused organs (especially liver, spleen, lungs, tumor etc.) almost instantaneously (within 1h) upon i.v bolus injection as observed in case of

gLuc/Lac labelled B16-BL6 or RAW264.7 or NIH3T3 cells derived exosomes[23]. In the present study also, similar observation was made wherein, a drastic decline in DTX concentration was observed in case of Exo-DTX treated group within initial 1h, followed by sustained DTX level in plasma till 12h post administration (**Fig. 5.11).** In another study, the radiolabelled (Indium 111) PC-3 derived exosomes exhibited rapid plasma clearance within 1 h however, 24-h post-injection bio-distribution study revealed accumulation of the same in liver>spleen>kidney>tumor in descending order[53]. In fact, RAW 264.7 derived exosomes loaded with PTX (exoPTX) have been compared with Taxol, 18 days post-treatment of Luc/mCherry-3LL-M27 lung metastases in C57BL/6 mice, clearly indicated better suppression of metastasis in the lung slides of exoPTX treated animals in comparison to the Taxol treated animals [54]. Based upon these reported studies, it was concluded that the massive tissue distribution and long duration tissue sustenance of exosomes would benefit the formulation of Exo-DTX which would eventually help to reduce the dose, dosing frequency and thus increase the efficacy of chemotherapeutic agents and would help to overcome the organ toxicities attributed to the high dosing regimen as compared to the conventional therapy.

5.5 References

(1) Théry, C.; Witwer, K. W.; Aikawa, E.; Alcaraz, M. J.; Anderson, J. D.; Andriantsitohaina, R.; Antoniou, A.; Arab, T.; Archer, F.; Atkin-Smith, G. K. et al. Minimal Information for Studies of Extracellular Vesicles 2018 (MISEV2018): A Position Statement of the International Society for Extracellular Vesicles and Update of the MISEV2014 Guidelines. *J. Extracell. Vesicles* **2018**, *7*, 1535750. https://doi.org/10.1080/20013078.2018.1535750.

(2) Mathieu, M.; Martin-Jaular, L.; Lavieu, G.; Théry, C. Specificities of Secretion and Uptake of Exosomes and Other Extracellular Vesicles for Cell-to-Cell Communication. *Nat. Cell Biol.* **2019**, *21* (1), 9–17. https://doi.org/10.1038/s41556-018-0250-9.

(3) Caponnetto, F.; Manini, I.; Skrap, M.; Palmai-Pallag, T.; Di Loreto, C.; Beltrami, A. P.; Cesselli, D.; Ferrari, E. Size-Dependent Cellular Uptake of Exosomes. *Nanomedicine Nanotechnology, Biol. Med.* **2017**, *13* (3), 1011–1020. https://doi.org/10.1016/j.nano.2016.12.009.

(4) Rayamajhi, S.; Nguyen, T. D. T.; Marasini, R.; Aryal, S. Macrophage-Derived Exosome-Mimetic Hybrid Vesicles for Tumor Targeted Drug Delivery. *Acta Biomater.* **2019**, *94*, 482–494. https://doi.org/10.1016/j.actbio.2019.05.054.

(5) Kim, M. S.; Haney, M. J.; Zhao, Y.; Yuan, D.; Deygen, I.; Klyachko, N. L.; Kabanov, A. V.; Batrakova, E. V. Engineering Macrophage-Derived Exosomes for Targeted Paclitaxel Delivery to Pulmonary Metastases: In Vitro and in Vivo Evaluations. *Nanomedicine Nanotechnology, Biol. Med.* **2018**, *14* (1), 195–204. https://doi.org/10.1016/j.nano.2017.09.011.

(6) Li, S.; Wu, Y.; Ding, F.; Yang, J.; Li, J.; Gao, X.; Zhang, C.; Feng, J. Engineering Macrophage-Derived Exosomes for Targeted Chemotherapy of Triple-Negative Breast Cancer. *Nanoscale* **2020**, *12* (19), 10854–10862. https://doi.org/10.1039/d0nr00523a.

(7) Wang, P.; Wang, H.; Huang, Q.; Peng, C.; Yao, L.; Chen, H.; Qiu, Z.; Wu, Y.; Wang, L.; Chen, W. Exosomes from M1-Polarized Macrophages Enhance Paclitaxel Antitumor Activity by Activating Macrophages-Mediated Inflammation. *Theranostics* **2019**, *9* (6), 1714–1727. https://doi.org/10.7150/thno.30716.

(8) Cianciaruso, C.; Beltraminelli, T.; Duval, F.; Nassiri, S.; Hamelin, R.; Mozes, A.; Gallart-Ayala, H.; Ceada Torres, G.; Torchia, B.; Ries, C. H.; Ivanisevic, J.; De Palma, M. Molecular Profiling and Functional Analysis of Macrophage-Derived Tumor Extracellular Vesicles. *Cell Rep.* **2019**, *27* (10), 3062-3080.e11. https://doi.org/10.1016/j.celrep.2019.05.008.

(9) Lee, H. D.; Kim, Y. H.; Kim, D. S. Exosomes Derived from Human Macrophages Suppress Endothelial Cell Migration by Controlling Integrin Trafficking. *Eur. J. Immunol.* **2014**, *44* (4), 1156–1169. https://doi.org/10.1002/eji.201343660.

(10) Duan, S.; Yu, S.; Yuan, T.; Yao, S.; Zhang, L. Exogenous Let-7a-5p Induces A549 Lung Cancer Cell Death through BCL2L1-Mediated PI3Kγ Signaling Pathway. *Front. Oncol.* **2019**, *9* (AUG), 1–14. https://doi.org/10.3389/fonc.2019.00808.

(11) Silva, A. K. A.; Morille, M.; Piffoux, M.; Arumugam, S.; Mauduit, P.; Al, E. Development of Extracellular Vesicle-Based Medicinal Products: A Position Paper of the Group "Extracellular Vesicle TranslatiOn to ClinicaL PerspectiVEs – EVOLVE France." *Adv. Drug Deliv. Rev.* **2021**, *179*, 114001. https://doi.org/10.1016/j.addr.2021.114001.

(12) Besse, B.; Charrier, M.; Lapierre, V.; Dansin, E.; Lantz, O.; Planchard, D.; Le Chevalier, T.; Livartoski, A.; Barlesi, F.; Laplanche, A.; Al, E. Dendritic Cell-Derived Exosomes as Maintenance Immunotherapy after First Line Chemotherapy in NSCLC. *Oncoimmunology* **2016**, *5* (4), e1071008. https://doi.org/10.1080/2162402X.2015.1071008.

(13) Zhang, M.; Zang, X.; Wang, M.; Li, Z.; Qiao, M.; Hu, H.; Chen, D. Exosome-Based Nanocarriers as Bio-Inspired and Versatile Vehicles for Drug Delivery: Recent Advances and Challenges. *J. Mater. Chem. B* **2019**, *7* (15), 2421–2433. https://doi.org/10.1039/C9TB00170K.

(14) LeBleu, V. S.; Kalluri, R. Exosomes as a Multicomponent Biomarker Platform in Cancer. *Trends in Cancer* **2020**, *6* (9), 767–774. https://doi.org/10.1016/j.trecan.2020.03.007.

(15) EMA. Scientific Recommendation on Classification of Advanced Therapy Medicinal Products.

Reflect. Pap. **2018**, *44* (June), 1–2.

(16) Cancer, I.; Srivastava, A.; Babu, A.; Filant, J.; Moxley, K. M.; Ruskin, R.; Dhanasekaran, D.; Sood, A. K.; Mcmeekin, S.; Ramesh, R. Exploitation of Exosomes as Nanocarriers for Gene-, Chemo-, and Immune-Therapy of Cancer. **2016**, *12* (6), 1159–1173. https://doi.org/10.1166/jbn.2016.2205.

(17) Mei, K. C.; Guo, Y.; Bai, J.; Costa, P. M.; Kafa, H.; Protti, A.; Hider, R. C.; Al-Jamal, K. T. Organic Solvent-Free, One-Step Engineering of Graphene-Based Magnetic-Responsive Hybrids Using Design of Experiment-Driven Mechanochemistry. *ACS Appl. Mater. Interfaces* **2015**, *7* (26), 14176–14181. https://doi.org/10.1021/acsami.5b03577.

(18) Rapalli, V. K.; Banerjee, S.; Khan, S.; Jha, P. N.; Gupta, G.; Dua, K.; Hasnain, M. S.; Nayak, A. K.; Dubey, S. K.; Singhvi, G. QbD-Driven Formulation Development and Evaluation of Topical Hydrogel Containing Ketoconazole Loaded Cubosomes. *Mater. Sci. Eng. C* **2021**, *119* (September 2020). https://doi.org/10.1016/j.msec.2020.111548.

(19) Basak, M.; Sahoo, B.; Kumar, D.; Narisepalli, S.; Tiwari, S.; Chitkara, D.; Mittal, A. Human Umbilical Cord Blood-Mesenchymal Stem Cell Derived Exosomes as an Efficient Nanocarrier for Docetaxel and MiR-125a : Formulation Optimization and Anti-Metastatic Behaviour. *Life Sci.* **2023**, *322* (January), 121621. https://doi.org/10.1016/j.lfs.2023.121621.

(20) Batrakova, E. V.; Kim, M. S. Using Exosomes, Naturally-Equipped Nanocarriers, for Drug Delivery. *J. Control. Release* **2015**, *219*, 396–405. https://doi.org/10.1016/j.jconrel.2015.07.030.

(21) Agrawal, A. K.; Aqil, F.; Jeyabalan, J.; Spencer, W. A.; Beck, J.; Gachuki, B. W.; Alhakeem, S. S.; Oben, K.; Munagala, R.; Bondada, S.; Gupta, R. C. Milk-Derived Exosomes for Oral Delivery of Paclitaxel. *Nanomedicine Nanotechnology, Biol. Med.* **2017**, *13* (5), 1627–1636. https://doi.org/10.1016/j.nano.2017.03.001.

(22) Salarpour, S.; Forootanfar, H.; Pournamdari, M.; Ahmadi-Zeidabadi, M.; Esmaeeli, M.; Pardakhty, A. Paclitaxel Incorporated Exosomes Derived from Glioblastoma Cells: Comparative Study of Two Loading Techniques. *DARU, J. Pharm. Sci.* **2019**, *27* (2), 533–539. https://doi.org/10.1007/s40199-019-00280-5.

(23) Charoenviriyakul, C.; Takahashi, Y.; Morishita, M.; Matsumoto, A.; Nishikawa, M.; Takakura, Y. Cell Type-Specific and Common Characteristics of Exosomes Derived from Mouse Cell Lines: Yield, Physicochemical Properties, and Pharmacokinetics. *Eur. J. Pharm. Sci.* **2017**, *96*, 316–322. https://doi.org/10.1016/j.ejps.2016.10.009.

(24) Morishita, M.; Takahashi, Y.; Nishikawa, M.; Takakura, Y. Pharmacokinetics of Exosomes—An Important Factor for Elucidating the Biological Roles of Exosomes and for the Development of Exosome-Based Therapeutics. *J. Pharm. Sci.* **2017**, *106* (9), 2265–2269. https://doi.org/10.1016/j.xphs.2017.02.030.

(25) Saari, H.; Lázaro-ibáñez, E.; Viitala, T.; Vuorimaa-laukkanen, E.; Siljander, P.; Yliperttula, M. Microvesicle- and Exosome-Mediated Drug Delivery Enhances the Cytotoxicity of Paclitaxel in Autologous Prostate Cancer Cells. *J. Control. Release* **2015**, *220*, 727–737. https://doi.org/10.1016/j.jconrel.2015.09.031.

(26) Kim, M. S.; Haney, M. J.; Zhao, Y.; Mahajan, V.; Deygen, I.; Klyachko, N. L.; Inskoe, E.; Piroyan, A.; Sokolsky, M.; Okolie, O.; Hingtgen, S. D.; Kabanov, A. V.; Batrakova, E. V. Development of Exosome-Encapsulated Paclitaxel to Overcome MDR in Cancer Cells. *Nanomedicine Nanotechnology, Biol. Med.* **2016**, *12* (3), 655–664. https://doi.org/10.1016/j.nano.2015.10.012.

(27) Kim, M. S.; Haney, M. J.; Zhao, Y.; Yuan, D.; Deygen, I.; Klyachko, N. L.; Kabanov, A. V; Batrakova, E. V. Engineering Macrophage-Derived Exosomes for Targeted Paclitaxel Delivery to Pulmonary Metastases : In Vitro and in Vivo Evaluations. *Nanomedicine Nanotechnology, Biol. Med.* **2018**, *14* (1), 195–204. https://doi.org/10.1016/j.nano.2017.09.011.

(28) Rankin-Turner, S.; Vader, P.; O'Driscoll, L.; Giebel, B.; Heaney, L. M.; Davies, O. G. A Call for the Standardised Reporting of Factors Affecting the Exogenous Loading of Extracellular Vesicles with Therapeutic Cargos. *Adv. Drug Deliv. Rev.* **2021**, *173*, 479–491. https://doi.org/10.1016/j.addr.2021.04.012.

(29) Soo, M.; Haney, M. J.; Zhao, Y.; Mahajan, V.; Deygen, I.; Klyachko, N. L.; Inskoe, E.; Piroyan, A.;

Sokolsky, M.; Okolie, O.; Hingtgen, S. D.; Kabanov, A. V; Batrakova, E. V. Development of Exosome-Encapsulated Paclitaxel to Overcome MDR in Cancer Cells. *Nanomedicine Nanotechnology, Biol. Med.* **2016**, *12* (3), 655–664. https://doi.org/10.1016/j.nano.2015.10.012.

(30) Saari, H.; Lázaro-Ibáñez, E.; Viitala, T.; Vuorimaa-Laukkanen, E.; Siljander, P.; Yliperttula, M. Microvesicle- and Exosome-Mediated Drug Delivery Enhances the Cytotoxicity of Paclitaxel in Autologous Prostate Cancer Cells. *J. Control. Release* **2015**, *220*, 727–737. https://doi.org/10.1016/j.jconrel.2015.09.031.

(31) Li, Y. J.; Wu, J. Y.; Wang, J. M.; Hu, X. Bin; Cai, J. X.; Xiang, D. X. Gemcitabine Loaded Autologous Exosomes for Effective and Safe Chemotherapy of Pancreatic Cancer. *Acta Biomater.* **2020**, *101*, 519–530. https://doi.org/10.1016/j.actbio.2019.10.022.

(32) Liu, J.; Wu, F.; Zhou, H. Macrophage-Derived Exosomes in Cancers: Biogenesis, Functions and Therapeutic Applications. *Immunol. Lett.* **2020**, *227* (14), 102–108. https://doi.org/10.1016/j.imlet.2020.08.003.

(33) Basak, M.; Chaudhary, D. K.; Takahashi, R. U.; Yamamoto, Y.; Tiwari, S.; Tahara, H.; Mittal, A. Immunocyte Derived Exosomes: Insight into the Potential Chemo-Immunotherapeutic Nanocarrier Targeting the Tumor Microenvironment. *ACS Biomater. Sci. Eng.* **2023**, *9* (1), 20–39. https://doi.org/10.1021/acsbiomaterials.2c00893.

(34) Wiklander, O. P. B.; Nordin, J. Z.; O'Loughlin, A.; Gustafsson, Y.; Corso, G.; Mäger, I.; Vader, P.; Lee, Y.; Sork, H.; Seow, Y.; Heldring, N.; Alvarez-Erviti, L.; Edvard Smith, C. I.; Le Blanc, K.; Macchiarini, P.; Jungebluth, P.; Wood, M. J. A.; El Andaloussi, S. Extracellular Vesicle in Vivo Biodistribution Is Determined by Cell Source, Route of Administration and Targeting. *J. Extracell. Vesicles* **2015**, *4* (2015), 1–13. https://doi.org/10.3402/jev.v4.26316.

(35) Kim, M. S.; Haney, M. J.; Zhao, Y.; Mahajan, V.; Deygen, I.; Klyachko, N. L.; Inskoe, E.; Piroyan, A.; Sokolsky, M.; Okolie, O.; Hingtgen, S. D.; Kabanov, A. V.; Batrakova, E. V. Development of Exosome-Encapsulated Paclitaxel to Overcome MDR in Cancer Cells. *Nanomedicine Nanotechnology, Biol. Med.* **2016**, *12* (3), 655–664. https://doi.org/10.1016/j.nano.2015.10.012.

(36) Hernández-Vargas, H.; Palacios, J.; Moreno-Bueno, G. Molecular Profiling of Docetaxel Cytotoxicity in Breast Cancer Cells: Uncoupling of Aberrant Mitosis and Apoptosis. *Oncogene* **2007**, *26* (20), 2902–2913. https://doi.org/10.1038/sj.onc.1210102.

(37) Pimm, M. L.; Henty-Ridilla, J. L. New Twists in Actin-Microtubule Interactions. *Mol. Biol. Cell* **2021**, *32* (3), 211–217. https://doi.org/10.1091/MBC.E19-09-0491.

(38) Palacios, J. Molecular Profiling of Docetaxel Cytotoxicity in Breast Cancer Cells : Uncoupling of Aberrant Mitosis and Apoptosis. **2007**, No. November 2006, 2902–2913. https://doi.org/10.1038/sj.onc.1210102.

(39) Weaver, B. A. How Taxol/Paclitaxel Kills Cancer Cells. *Mol. Biol. Cell* **2014**, *25* (18), 2677–2681. https://doi.org/10.1091/mbc.E14-04-0916.

(40) Hou, Y.; Zhao, C.; Xu, B.; Huang, Y.; Liu, C. Effect of Docetaxel on Mechanical Properties of Ovarian Cancer Cells. *Exp. Cell Res.* **2021**, *408* (2021), 112853. https://doi.org/10.1016/j.yexcr.2021.112853.

(41) He, M.; Gao, K.; Zhou, L.; Jiao, Z.; Wu, M.; Cao, J.; You, X.; Cai, Z.; Su, Y.; Jiang, Z. Zwitterionic Materials for Antifouling Membrane Surface Construction. *Acta Biomater.* **2016**, *40* (92), 142–152. https://doi.org/10.1016/j.actbio.2016.03.038.

(42) Dang, Y.; Quan, M.; Xing, C. M.; Wang, Y. B.; Gong, Y. K. Biocompatible and Antifouling Coating of Cell Membrane Phosphorylcholine and Mussel Catechol Modified Multi-Arm PEGs. *J. Mater. Chem. B* **2015**, *3* (11), 2350–2361. https://doi.org/10.1039/c4tb02140a.

(43) Skotland, T.; Hessvik, N. P.; Sandvig, K.; Llorente, A. Exosomal Lipid Composition and the Role of Ether Lipids and Phosphoinositides in Exosome Biology. *J. Lipid Res.* **2019**, *60* (1), 9–18. https://doi.org/10.1194/jlr.R084343.

(44) Zhou, L. Y.; Zhu, Y. H.; Wang, X. Y.; Shen, C.; Wei, X. W.; Xu, T.; He, Z. Y. Novel Zwitterionic Vectors: Multi-Functional Delivery Systems for Therapeutic Genes and Drugs. *Comput. Struct. Biotechnol. J.* **2020**, *18* (37), 1980–1999. https://doi.org/10.1016/j.csbj.2020.07.015.

(45) Murrell, M. P.; Gardel, M. L. F-Actin Buckling Coordinates Contractility and Severing in a Biomimetic Actomyosin Cortex. *Proc. Natl. Acad. Sci. U. S. A.* **2012**, *109* (51), 20820–20825. https://doi.org/10.1073/pnas.1214753109.

(46) De La Cruz, E. M.; Gardel, M. L. Actin Mechanics and Fragmentation. *J. Biol. Chem.* **2015**, *290* (28), 17137–17144. https://doi.org/10.1074/jbc.R115.636472.

(47) Dugina, V. B.; Shagieva, G. S.; Kopnin, P. B. Biological Role of Actin Isoforms in Mammalian Cells. *Biochem.* **2019**, *84* (6), 583–592. https://doi.org/10.1134/S0006297919060014.

(48) Rao, J. Y.; Hurst, R. E.; Jones, P. L.; Bass, R. A.; Hemstreet, G. P.; Bales, W. D.; Archer, L. T.; Bell, P. B. Cellular F-Actin Levels as a Marker for Cellular Transformation: Relationship to Cell Division and Differentiation. *Cancer Res.* **1990**, *50* (8), 2215–2220.

(49) Williams, K. C.; Coppolino, M. G. SNARE-Dependent Interaction of Src, EGFR and SS1 Integrin Regulates Invadopodia Formation and Tumor Cell Invasion. *J. Cell Sci.* **2014**, *127* (8), 1712–1725. https://doi.org/10.1242/jcs.134734.

(50) Parvani, J. G.; Galliher-Beckley, A. J.; Schiemann, B. J.; Schiemann, W. P. Targeted Inactivation of B1 Integrin Induces B3 Integrin Switching, Which Drives Breast Cancer Metastasis by TGF-β. *Mol. Biol. Cell* **2013**, *24* (21), 3449–3459. https://doi.org/10.1091/mbc.E12-10-0776.

(51) Sheng, W.; Chen, C.; Dong, M.; Wang, G.; Zhou, J.; Song, H.; Li, Y.; Zhang, J.; Ding, S. Calreticulin Promotes Egf-Induced Emt in Pancreatic Cancer Cells via Integrin/Egfr-Erk/Mapk Signaling Pathway. *Cell Death Dis.* **2017**, *8* (10), 1–14. https://doi.org/10.1038/cddis.2017.547.

(52) Lahlou, H.; Muller, W. J. B1-Integrins Signaling and Mammary Tumor Progression in Transgenic Mouse Models: Implications for Human Breast Cancer. *Breast Cancer Res.* **2011**, *13* (6), 1–10. https://doi.org/10.1186/bcr2905.

(53) Smyth, T.; Kullberg, M.; Malik, N.; Smith-Jones, P.; Graner, M. W.; Anchordoquy, T. J. Biodistribution and Delivery Efficiency of Unmodified Tumor-Derived Exosomes. *J. Control. Release* **2015**, *199*, 145–155. https://doi.org/10.1016/j.jconrel.2014.12.013.

(54) Kim, M. S.; Haney, M. J.; Zhao, Y.; Yuan, D.; Deygen, I.; Klyachko, N. L.; Kabanov, A. V.; Batrakova, E. V. Engineering Macrophage-Derived Exosomes for Targeted Paclitaxel Delivery to Pulmonary Metastases: In Vitro and in Vivo Evaluations. *Nanomedicine Nanotechnology, Biol. Med.* **2018**, *14* (1), 195–204. https://doi.org/10.1016/j.nano.2017.09.011.

XXXXXXX

Exo(PAN$_{34a+DTX}$)

Exploring Exosomal Fragment Enclosed Polyamine-salt Nanocomplex of DTX & miR-34a as a Novel Co-delivery Strategy in Breast Cancer

Chapter VI

6.1. Introduction

Conventional cancer monotherapies elicit non-selective cytotoxicity accompanied by their immunosuppressive and myelosuppressive activity which leads to adverse effects, secondary cancer induction, metastasis, chemo resistance and cancer recurrence [1]. These inevitable drawbacks could be managed by combination therapy wherein, different pathways could be targeted simultaneously at a significantly lesser dose than recommended for monotherapy regimen of individual drug [2]. Currently, combination therapy with chemotherapeutics and RNA interference (RNAi) has been widely projected as a potential alternative to monotherapy and combination therapy of the chemotherapeutics. Among the RNAi, microRNAs (miRNAs) are classified as the non-coding RNAs responsible for regulation of gene expression by posttranscriptional modifications. The primary miRNA duplex (pri-miRNA) is transcribed from DNA sequences in the nucleus and converted to the pre-miRNA which is exported to cytoplasm to regulate the respective mRNA translation[3]. As, miRNAs regulate multiple pathways in cancer development and progression, these prove beneficial in maintaining the sensitivity of tumor towards chemotherapeutics either by restoring tumor suppressor activity (by TS miRNA mimic) or suppression of oncogenic dominance (by miRNA inhibitor) [3–5]. MRX 34a, the first miRNA mimic to reach phase I clinical trial in 2013, clearly proved that, even at a suboptimal dose, miRNA can turn on the cellular threshold of tumor suppression[6]. Interestingly, miR-34a is a well reported TS miRNA, which is found suppressed in various types of cancer including both solid tumors and blood cancers. miR-34a is reported to induce apoptosis, cell cycle arrest and growth inhibition by downregulating the target genes including CDK4/6, silent information regulator 1 (SIRT1), BCL-2, MYC and MET, and is considered as the transcriptional target of p53[7,8]. Recently, miR-34a has also proven to sensitize the resistant breast cancer cells towards DTX giving impetus to the field of combination delivery of miRNA and chemotherapeutic[9].

Exogenous miRNA delivery faces critical hurdles, including poor cellular uptake (due to negative charge), off target effects, short half-life and limited stability in blood stream[10–13]. Encapsulation of miRNAs in nanoparticles by nanoprecipitation or emulsion techniques results in low encapsulation efficiency, attributed to the quick diffusion of miRNA into the water phase because of its high affinity towards water , although nanoparticles improve the tissue distribution and site-specific localization of miRNA[14]. The importance of efficient delivery of DTX and miR-34a in breast cancer is exemplified by same literature reports. A folate conjugated cationic lipo-polymer

has been reported to form NC with miRNA at N/P ratio of 8:1 with 94.8% DTX payload. This system showed improved cytotoxicity (~5 folds), and apoptosis (~2.0 folds) when compared to the free DTX in breast cancer cells[15]. Another novel core-shell nanoformulation was reported for the co delivery of miR-34a and DTX in breast cancer wherein, 83.46±2.36% DTX was encapsulated in the lipidic core and 13.91±0.39% miR-34a was electrostatically complexed in the cationic BSA shell of the nanoformulation. The resultant system delivered the payload in the cytoplasm as indicated by appearance of a yellow fluorescence emerging from the overlay of Cy5-RNA (red fluorescence) and Coumarin 6 (C6, green fluorescence) as the model replacements of the miRNA and DTX in 4T1 cells. Further, the *in vivo* efficacy study confirmed ~1.74 fold higher tumor volume reduction by combination therapy in comparison to the free DTX in 4T1 tumor bearing animals[16]. In an interesting study carried out to explore the application of exosomes for the RNAi delivery, cationic BSA (cBSA) was synthesized to prepare the cBSA/siRNA nanoplexes which were further serially extruded with exosomes (redispersed in hypotonic buffer) 100 times to entrap the cBSA/siRNA nanoplexes within the exosomal layer. In a time-dependent biodistribution study, cBSA/siRNA@Exo showed 2.9 times improved uptake in lung tumor in comparison to the cBSA/siRNA@liposomes[17].

In this context, "Tandem self-assembly" is considered as one of the relatively less explored **core-shell** delivery systems in which cationic polyamines form a nanosized **core** structure (polyamine-salt aggregates or PSA) in the presence of the multivalent anionic salts, and the **shell** material (either nanoparticles, polymer, or biomolecules) of reverse ionic charge form the capsule surrounding the core by means of electrostatic interaction[18]. Apart from electrostatic interaction, hydrophobic interaction and hydrogen bonding are also observed playing important role in PSA formation[19]. Interestingly, a wide variety of cargo molecules have already been delivered using PSA including, small dye molecules, small drugs, contrast agents, siRNA, enzymes and proteins [20–23]. In 2010, Wong *et al.* reported a PSA system to encapsulate the imaging molecule indocyanin green (ICG) in the Polyallylamine (PAH)-phosphate spherical aggregate, which was further coated with anti-EGFR antibodies to selectively target the EGFR overexpressing malignant tumor in three carcinoma cell lines, 1483 (human head and neck squamous cell), SiHa (human cervical squamous cell), and 435 (cancerous human breast cell) depicting variable expression of EGFR [21]. Almost a decade later, Andreozzi P et al. reported application of PSA for siRNA delivery wherein, they developed a pH responsive polyamine phosphate nanocarrier (PAN) by leveraging the electrostatic

interaction between amine groups of PAH (pK_a: 8.8) and the phosphate group of the optimized phosphate buffer (PB) to complex the negatively charged siRNA. They also proved that PAN remained stable at physiological pH but dissembled only when pH of dispersant media attained a value below pH 6 or above pH 9. Although they successfully delivered the GFP siRNA through PAN in the GFP-A549 cells; the cellular viability was found compromised within 16-72 h, when 6.6×10^{-5}mM monomers were used for PAN formation, possibly, due to high positive charge of the nanoparticles [23,24]. This system has never been explored for delivery of DTX. DTX possesses one hydroxyl group at C-10 and forms hydrogen bond with tertiary amine group of Dipalmitoylphosphatidylcholine (DPPC)[25] and thus offers a high possibility of hydrophobic interaction between the primary amine of Polyallyamine and DTX but it has not been explored so far.

Considering these facts, we aimed to explore the phosphate driven PSA to co-load DTX and miR-34a in the core designated as $PAN_{34a+DTX}$. Phosphate buffer saline (PBS) acts as a source of phosphate ions required to crosslink Poly(allylamine) hydrochloride (PAH, pKa=8.8); its composition was optimized for co-loading DTX by hydrophobic interaction and miR-34a by electrostatic interaction in the noncomplex. RAW 264.7 cell derived exosomes were utilized to prepare exosomal fragments to form the shell of the core, $PAN_{34a+DTX}$ and yield the final formulation Exo($PAN_{34a+DTX}$). It was hypothesized that the presence of exosomal layer would improve the cellular uptake of the $PAN_{34a+DTX}$ along with protecting the cells from the toxicity resulting from the cationic noncomplex. Additionally, the "proton sponge" effect of the polyamines (due to their characteristic cationic nature) in the acidic environment of endosomes would help the formulation to burst open and release the payload in cytoplasm[26]. The main aim of this work was to explore and optimize this novel strategy to co-deliver DTX and miR-34a, characterize the formulation and evaluate its efficacy in TNBC 4T1 cells.

6.2. Materials & Methods

6.2.1 Materials

Polyallylamine hydrochloride (PAH, MW: 1.75 $\times10^4$ g/mol), sodium phosphate dibasic (Na_2HPO_4), potassium phosphate monobasic (KH_2PO_4), hydrochloric acid (HCl), sodium hydroxide (NaOH), sodium chloride (NaCl), and DEPC (diethylpyrocarbonate, molecular grade) were obtained from CDH (New Delhi, INDIA). Polyelectrolyte stock solutions and all the subsequent diluted precursor solutions were prepared in Milli-Q deionized water (dI).

Formulations were prepared in the DEPC containing dI water. FAM-siRNA was obtained from GeneCust, Europe, while, hsa-miRNA-34a-5p mimic, mirVana miRNA mimic negative control, Lipofectamine-2000® and CellTracker™ CM-DiI, Pierce™ Bicinchoninic acid (BCA) protein assay kit and 4% paraformaldehyde (#ALF-J61899-AK) were purchased from ThermoFisher Scientific (USA). For, agarose gel electrophoresis, Agarose (RM6249), RNA loading dye (R1386-5VL), TBE buffer 10X (T4415) were purchased from Sigma Aldrich (USA). Ethidium bromide (RM 813) and Heparin sodium salt (TC138) were procured from Himedia (INDIA) and Ribonuclear low range RNA ladder (SM1831) was procured from Thermo Fischer (USA). For qRT-PCR, GAPDH and BCL-2 primers (sequences are mentioned below) were procured from Integrated DNA Technologies (Lowa, USA), GeneSure first strand cDNA synthesis kit was purchased from Puregene (New Delhi, INDIA), and iTaq™ Universal SYBR green Supermix was from Bio-Rad (California, USA). Additionally, Rat IFNγ (900-M109) and TNFα (900-M73) Mini ABTS ELISA Development kit for the ELISA assay were procured from Pepro Tech® (NJ, USA).

Gene	Forward sequence	Reverse sequence
BCL-2	5'-CCTGTGGATGACTGAGTACC-3'	5'-GAGACAGCCAGGAGAAATCA-3'
GAPDH	5'-TGCATCCTGCACCACCAACT-3'	5'-AGCCTGCTTCACCACCTTC-3'

6.2.2 Cell culture

Murine TNBC 4T1 cells and RAW 264.7 cells were procured from Regional Centre of Biotechnology (Haryana, India) and NCCS (Maharashtra, India) respectively. We are grateful to Professor Avinash Bajaj for providing the 4T1 cells. Exosome depleted FBS was prepared *in-house* by ultracentrifugation of a mixture of FBS and PBS (FBS:PBS=3:7) at 1,20,000×g and 4˚C for 18h. Dulbecco's modified Eagle's medium (Gibco™ DMEM, high glucose) and Fetal bovine serum (FBS) were purchased from GIBCO (Invitrogen Inc. Gibco BRL, USA). Both DMEM and MEM incomplete media, Penicillin plus streptomycin solution, 4′,6-diamidino-2-phenylindole (DAPI), and 3-(4,5-dimethylthiazol-2-yl)-2,5-diphenyltetrazolium bromide (MTT) were bought from Sigma-Aldrich (St. Louis, MO, USA).

6.2.3 Methods

6.2.3.1. Optimization and development of formulations

Fabrication of Exo($PAN_{34a+DTX}$) was carried out in three major steps, involving the preparation of (I) $PAN_{34a+DTX}$ (II) exosomal fragments (EF) followed by, (III) Exo($PAN_{34a+DTX}$) (**Figure 6.1)**.

6.2.3.1.1 Development and optimization of $PAN_{34a+DTX}$

PAN_{34+DTX} was prepared by adding miR-34a (~ 0.5 µg) and DTX (400 ng from 12 µg/mL aqueous solution) together into PBS (containing 5 mM Na_2HPO_4, 3 mM KH_2PO_4 and 10 mM NaCl). Next, 3µl of PAH (from 10 mg/mL solution) was added to the reaction mixture to achieve an effective concentration of 1 mg/mL PAH. Appearance of spontaneous cloudiness indicated the formation of $PAN_{34a+DTX}$ wherein, it was hypothesized that miR-34a would be encapsulated within the particles by electrostatic interaction and DTX would be loaded by hydrophobic interaction with the polymeric backbone containing primary amines. The reaction mixture was allowed to stand at room temperature for 10 min for aging and then centrifuged at 5000 rpm for 5 min to remove the particles with higher particle size. The supernatant with small sized particles was further processed for exosomal layering.

In this process, the composition of PBS (molar ratio of Na_2HPO_4: KH_2PO_4 and amount of NaCl), PAH concentration (1-0.01mg/ml) and effect of dilution on the properties of PAN were optimized to achieve an appropriate R value (ratio of total negative charges from the multivalent salt to the total positive charge of the polyamine) as indicated in **Equation 6.1**. Two important factors i.e, the composition of PBS and PAH concentration were screened as detailed in **Table 6.1**, which was further followed by understanding the pH dependency of PAN_{DTX} formation. For the optimization of PAN_{RNA} formulation, total RNA isolated from RAW 264.7 cells was quantified and utilized as a replacement of miR-34a. Further, the complexation of miR-34a in PAN_{34a} was confirmed by agarose gel electrophoresis. PAN_{34+DTX} used for all further experiments was prepared with the optimized process parameters and material attributes.

$$R=\frac{[Phosphate\ ]\times n^{-}}{[PAH]\times n^{+}} \qquad \ldots\textbf{Equation 6.1}$$

Table 6.1
Representative batches of the blank PAN to optimize the R ratio.

S. No.	PAH as polyamine (mg/mL)	Phosphate ion (cross-linker)		Ratio of Na_2HPO_4 and KH_2PO_4	R ratio
		$[Na_2HPO_4]$ (mM)	$[KH_2PO_4]$ (mM)		
B1	1.0	5	1	5:1	0.93
B2	1.0	5	2	5:2	1.12
B3	1.0	5	3	5:3	1.214
B4	0.1	5	3	5:3	12.14
B5	0.01	5	3	5:3	121.4

6.2.3.1.2 Isolation and preparation of RAW 264.7 cell derived Exosomal Fragments (EF)

2.3.1.2.1 Isolation of the RAW 264.7 cell derived exosomes

RAW 264.7 cell derived exosomes were isolated by differential centrifugation of 200 mL of RAW 264.7 conditioned media (CM) collected from the 175 cm^2 flask. The CM was processed step-wise 500×g, 2000×g and 13,000×g for 10 min, 15 min and 30 min respectively at 4˚C. At each step, the supernatant was collected and finally subjected to ultracentrifugation at 120,000×g at 4˚C for 2h. Once the exosomes were pelleted down, supernatant was discarded and the exosomes were washed with an excess of PBS (10 mM) at 120,000×g and 4˚C for 2 h. The final pellet was redispersed in 400 µl of PBS. The uniformly redispersed exosomes were then processed for EF preparation.

2.3.1.2.2 Preparation of EF

This part of the formulation has already been discussed in detail in **Chapter 4, (*section 4.2.2.3).***

6.2.3.1.3 Preparation of Exo($PAN_{34a+DTX}$) and Exo($PAN_{FAM+DTX}$)

Exo($PAN_{34a+DTX}$) was prepared by vortexing freshly prepared EF from ~12 µg equivalent Exo_{TC} with $PAN_{34a+DTX}$ (containing 0.5µg miR-34a and 400 ng of DTX; as mentioned in ***Section 6.2.3.1.1*** for 5 min at RT and the volume of the formulation was made upto 100 µL with RNAse free water. The exosomal layering was confirmed by reduced haziness of the final formulation and was allowed to stand at 4˚C for 1h to allow efficient layering of the particles by EF. The protocol as discussed for the preparation of Exo($PAN_{34a+DTX}$) was followed for the preparation of Exo($PAN_{FAM+DTX}$) formulation only by replacing miR-34a with 0.5 µg FAM-siRNA.

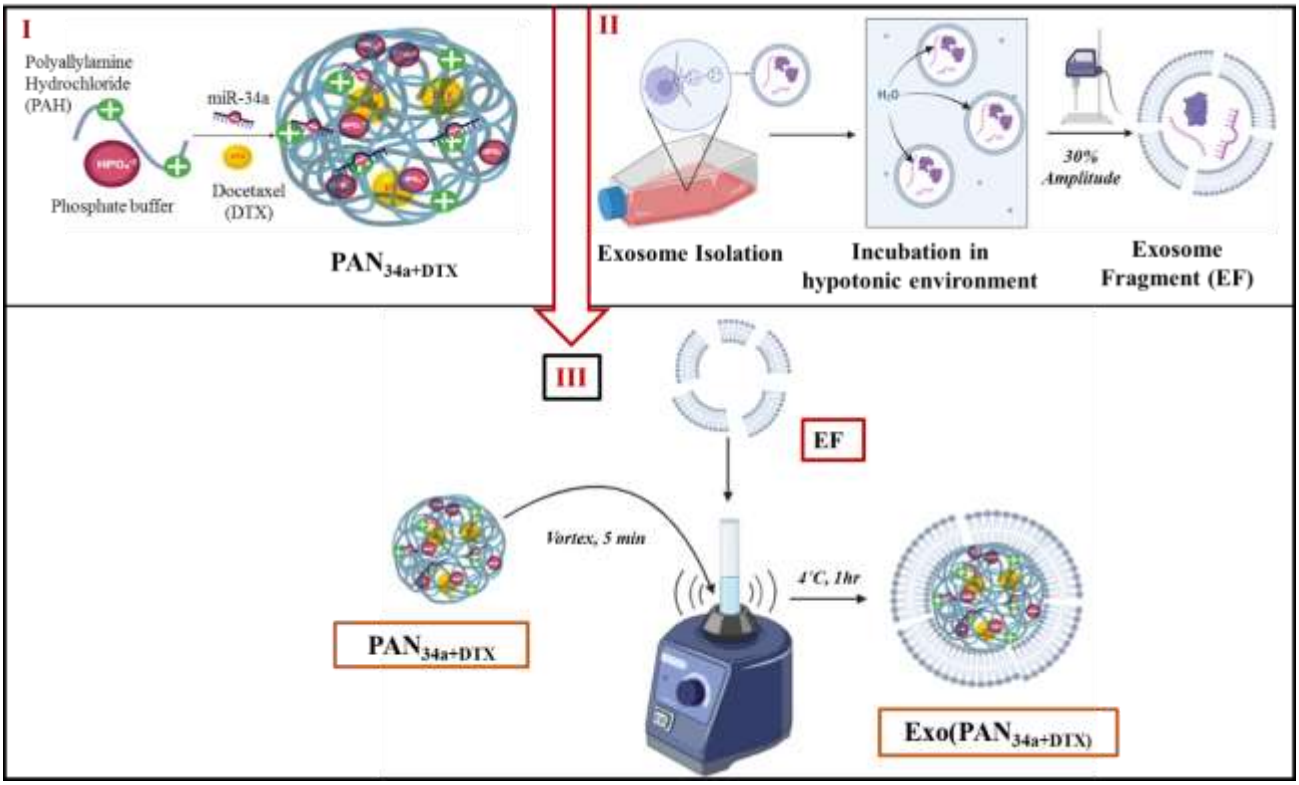

Figure 6.1. Schematic diagram for the preparation of Exo($PAN_{34a+DTX}$). Step I: Preparation of PAN_{34+DTX}, step II: Preparation of exosomal fragments (EF) and, step III: preparation of Exo($PAN_{34a+DTX}$).

6.2.3.2 Characterization of the formulations

All the formulations were characterized for particle size (nm), absolute intensity (Kcounts/s) and zeta-potential (mV).

6.2.3.2.1 Particle size distribution, absolute intensity, and zeta-potential

All the formulations were characterized by DLS using Anton Paar Litesizer 500 using backscattering mode (173° scattering angle), with 15s equilibration time, 10 runs for each analysis with 10 s for each run at 25˚C. The absolute intensity indicated the light scattering capacity of the particles which is directly proportional to the number of particles. Absolute intensity (Kcounts/s) is generated by the instrument depending upon the sample concentration. Further, zeta-potential measurements were performed in total 50 runs with 10s for each run at 25˚C.

6.2.3.2.2 Characterization of EF by Western Blot

This part of the formulation has already been discussed in detail in **Chapter 4, (*section 4.2.2.4*).**

6.*2.3.2.3 Morphology (FESEM)*

The morphology of the naive exosomes, Exo_{TC}, EF, $PAN_{34a+DTX,}$ and Exo($PAN_{34a+DTX}$) was ascertained by FESEM. For the naive exosomes and E_{TC}, the detailed procedure is mentioned in **Chapter 4, (*section 4.2.2.4).*** . FESEM sample for $PAN_{34a+DTX}$ was prepared one-day prior to analysis by putting a drop of the formulation on a clean coverslip and air drying overnight. FESEM samples Exo($PAN_{34a+DTX}$) was also processed same as EF. The sample smears were washed with dI water thrice and air-dried overnight at RT. Next day, all samples were gold-sputtered (2-5nm) and analyzed using 20 kV beam in FESEM. Alongside the morphology, the individual particles from each sample (n=50) were also analyzed for size and expressed as mean ± SD for the characterization of particle size.

6.2.3.2.4 Functional characterization of PAN_{DTX}

2.3.2.4.A In-vitro stability study

In this seven-day long stability study of PAN_{DTX}, 5 mL formulation was prepared in triplicate and stored at 4˚C and stability samples were withdrawn at pre-determined time-points, i.e., 0.5, 1, 4, 7, 12, 24, 48, 72, 96, and 144 h. The samples were analyzed for the particle size, zeta-potential and %EE using DLS and HPLC to check the stability of the PAN_{DTX} formulation.

2.3.2.4.B In-vitro release study

The release pattern of DTX from the PAN_{DTX} formulation was determined using dialysis bag method. In this method, free DTX and PAN_{DTX} containing 40 µg of the DTX were dispersed in dI water and transferred to a regenerated cellulose dialysis tube bag (Snakeskin™ dialysis tubing, Thermo Fisher, MWCO3500 Da). The dialysis bag was immersed in 5 mL of release media (PBS+0.1% Tween 80) at two different pH values (7.2 and 5.5), and at each time-point, 2mL of release media was withdrawn and replaced with fresh media. The amount of DTX released from PAN_{DTX} at each time-point in both the release media was analyzed using a validated HPLC/UV method.

2.3.2.4.C In-vitro hemocompatibility study

PAN_{DTX} was tested for its hemocompatibility as PAH is a synthetic and cationic polymer. For this assay, blood was collected from the Wistar rats in a collection tube containing 10% w/v EDTA solution as the anti-coagulant and centrifuged at 2500 rpm at RT for 5 min. The RBC pellets were washed with excess PBS till the supernatant became colorless. Next, the RBC were redispersed in

PBS (250 µL) and incubated with different samples, including PBS (negative control), 0.1% Triton-X-100 (positive control), Free DTX (~100 ng/mL), blank PAN particles and PAN_{DTX} (100 ng/mL DTX) for 30 min. Thereafter, the samples were centrifuged to pellet down the RBCs and the supernatants were analyzed using Epoch ELISA plate reader at 540 nm. The % hemolysis was calculated using **Equation 6.2.**

$$\text{Hemolysis (\%)}: \frac{OD_{sample} - OD_{negative\ control}}{OD_{positive\ control} - OD_{negative\ control}} \times 100 \qquad \text{…….. } \mathbf{Equation\ 6.2}$$

6.2.3.2.5 Characterization of miR-34a complexation by gel retardation assay

The miR-34a complexation capacity of the $PAN_{34a+DTX}$ and Exo($PAN_{34a+DTX}$) has been evaluated by gel retardation assay wherein, the miR-34a content (0.05-0.5 µg) and PAH concentration (0.01-1 mg/mL) were varied. Additionally, the complete complexation of miR-34a was confirmed by performing the heparin competition assay. Herein, different PAN formulations containing 0.2 µg miR-34a and 0.01-1 mg/mL PAH, were prepared and incubated with heparin (2 I.U.) for 1h at RT. Formulations (in the presence and absence of heparin) were electrophoresed simultaneously in 2% agarose gel containing 0.5 µg/mL ethidium bromide (EtBr). The electrophoresis was carried out in 0.5× Tris- Borate-EDTA buffer at 100V for 20 min. The run was further followed by visualization on ChemiDoc™XRS+.

6.2.3.3 In vitro efficacy studies

TNBC 4T1 cells were cultured in DMEM (high glucose), supplemented with 10% FBS, and penicillin-streptomycin (100 IU/mL) in complete culture media in an incubator at 37 ℃ in a humidified atmosphere with 5% CO_2. Cells were kept for 12h to adhere post seeding in each study before performing the experiment.

6.2.3.3.1 Transfection and uptake efficiency

4T1 cells (1.5×10^4 cells/well) were seeded over a coverslip in a 6-well plate and allowed to attach and form a monolayer. The culture media was replaced with Opti-MEM media 1h prior to the treatment and the cells were further incubated with FAM-siRNA Lipofectamine® 2000 (positive control), PAN_{FAM}, Exo(PAN_{FAM}), and Exo($PAN_{FAM+DTX}$) for 6h. In the final formulation, $PAN_{FAM+DTX}$ was prepared containing 40 ng/mL DTX and 50 nM FAM-siRNA.

CM-DiI (red fluorescence) stained EF were prepared by incubating exosomes (~100 µg protein) with CM-DiI for 1h at 4˚C and ultracentrifuged at 180,000×g for 2h to pellet down CM-DiI stained exosomes. These CM-DiI stained exosomes were further redispersed in the hypotonic solution and processed for preparing the CM-DiI stained EFs.

Post treatment, the cells were washed with PBS thrice, fixed with 2% PFA for 15 min at RT followed by staining with DAPI. The samples were further washed with PBS and analyzed by confocal microscopy.

6.2.3.3.2 In-vitro cytotoxicity study

2.5×10^3 cells were seeded in 96-well plate and allowed to adhere for 12h before being treated with different formulations. Cells were treated with free DTX (100 ng/mL), miR-34a (50 nM; with Lipofectamine 2000®), and combination of DTX (100 ng/mL) and miR-34a (10 nM, 25nM, and 50 nM) in the presence of Lipofectamine 2000®. In another set of experiment, the cells were treated with formulations i.e, Blank PAN, free DTX, free miR-34a, EF, PAN_{DTX}, PAN_{34a}, Exo(PAN_{DTX}), Exo(PAN_{34a}), and Exo($PAN_{34a+DTX}$). All the formulations were loaded with 40 ng/mL DTX and 50 nM miR-34a. The cells were treated for 48h and then were subjected to MTT assay.

6.2.3.3.3 Inflammatory cytokine release

Briefly, 4T1 cells (2×10^6 cells/well) were seeded in 6-well cell culture plate and allowed to adhere overnight and different treatments, i.e., free DTX, blank PAN, EF (~6 µg and ~12 µg protein), PAN_{DTX}, PAN_{34a}, $PAN_{34a+DTX}$, Exo(PAN_{DTX}), Exo(PAN_{34a}), and Exo($PAN_{34a+DTX}$) containing 40 ng/mL DTX and 50 nM miR-34a were given for 48 h. At the end of 48h, the CM from cells was collected and centrifuged to expel out the dead cells and cellular debris at 3500 rpm, 4˚C for 5 min. The supernatants were collected and ELISA assay of TNF-α IFN-γ was carried out.

6.2.3.3.4 Gene Expression analysis

Following the same experimental protocol as mentioned in *section 2.3.2.3*, the cells were trypsinized and washed thrice with sterile PBS and dispersed in 1mL of RNA-XPress™ Reahent (Himedia) and stored at -20˚C overnight. After isolating the total RNA, concentration of RNA in each sample was quantified by Nanodrop. The cDNA synthesis was carried out using GeneSure™ First Strand cDNA Synthesis Kit following manufacturer's protocol and quantified with Nanodrop. 200 ng equivalent cDNA was utilized to determine the cycle threshold (C_T) values using Real-time PCR for target gene BCL-2 and housekeeping gene GAPDH. The C_T value of the

BCL-2 for each sample was normalized with respect to the C_T value of the GAPDH. Gene quantification was performed using Universal SYBR green Supermix. The fold change of the BCL-2 expression was expressed by calculating $2^{-\Delta\Delta C_T}$ values.

6.2.3.4 Statistical analysis

The data has been represented as mean ± standard deviation as processed in GraphPad Prism (Version 5.0, USA). The difference between two groups was compared using Student's *t*-test, comparison between multiple groups was carried out using one-way ANOVA followed by a Tukey's test. Value of $p < 0.05$ was considered as statistically significant.

6.3. Results

6.3.1 Development & optimization of PAN formulations

6.3.1.1 Determination of the suitable R ratio for blank PAN formation

It is well reported in literature that PSA formation and its meta-stable condition is regulated by the molecular weight of polyamine, R-ratio, ageing time, storage temperature and dilution[18]. Taking clues from the literature, the buffer composition, polyamine concentration, and dilution were further optimized in this work to obtain the R ratio at which the formed PAN particles would remain stable for a sufficient duration of time to enable further processing following 'single parameter change at once' method. The parameters were varied as mentioned in **Table 6.1** and the effect is depicted in **Figure 6.1.**

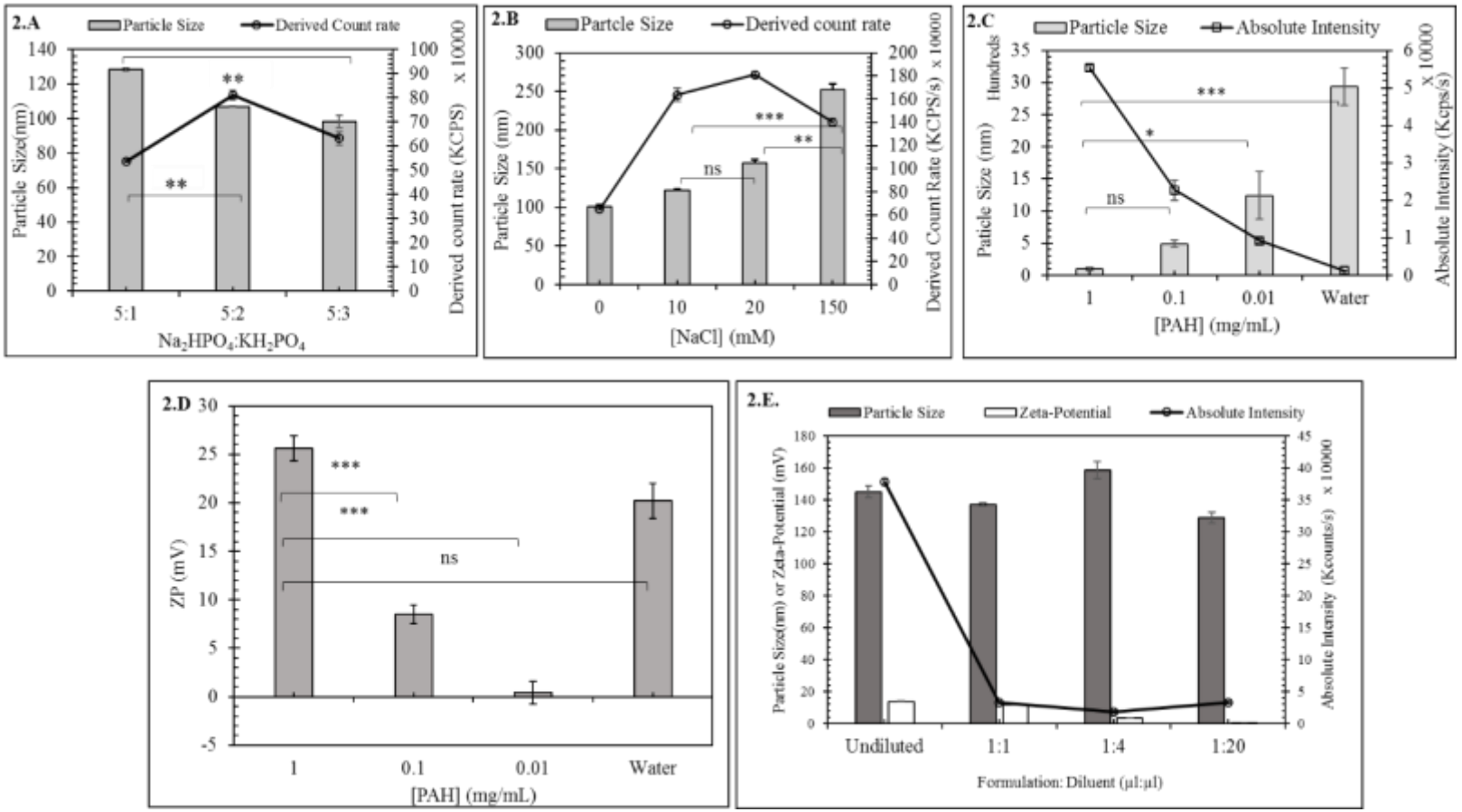

Figure 6.2. Optimization of blank PAN based on particle size, zeta-potential and absolute intensity (Kcounts/s). (**A**) Effect of molar ratio of Na_2HPO_4:KH_2PO_4 (varied from 5:1 to 5:3) at 10 mM sodium chloride. (**B**) Effect of concentration of sodium chloride (0/ 10/ 20/ 150 mM) with optimized Na_2HPO_4:KH_2PO_4 =5:3 (**C**) Effect of PAH concentration (0.01-1 mg/mL) in optimized PBS (Na_2HPO_4:KH_2PO_4: NaCl: 5:3:10). The PAN particles thus formed were compared to PAH (1 mg/mL) in water. (**D**) Effect of PAH concentration on the zeta-potential of the blank PAN when the concentration was varied between 0.01-1mg/mL in modified PBS and compared with PAH (1mg/mL) in dI water (**E**) Effect of dilution. All experiments were performed in n=3 (three independent experiments), statistical significance was ascertained by one-way ANOVA with Tukey's comparison test, *p<0.05, **p<0.01, ***p<0.001.

As given in **Table 6.1**, Batches# B1-B3 demonstrated a significant role of phosphate ion as a cross-linker as also seen in **Figure 6.2.A** wherein, R≈1.21 resulted in PAN formation in 10 mM NaCl with minimum particle size, i.e., 98.135±3.75 nm and ~ 1.75 folds more derived count rate than the particles formed with same R ratio in absence of NaCl. PAN formed in the presence of NaCl (10-150 mM) compared to the PAN particles formed in absence of NaCl showed gradual enhancement in the derived count rate in a concentration dependent manner (**Figure 6.2.B)** wherein, addition of NaCl contributed additional ionic strength to the media thus stabilizing the particles[27]. A slight increase in the size of PAN particle i.e., 122.25±0.96 nm with ~2.5 folds' more derived count rate (KCPS) after the incorporation of 10 mM NaCl in the modified PBS favored the presence of NaCl in PBS giving the optimized PBS composition as Na_2HPO_4: KH_2PO_4: NaCl::5:3:10. Further, varying PAH concentration in the range of 1.0-0.01 mg/mL (5.74×10^{-5} M-0.057×10^{-5} M) resulted in 10 and 100 folds increased R ratio (**Table 6.1**, #**B3-B5**) and was found to have a significant impact on the particle size, absolute intensity and zeta-potential of the blank PAN; herein the optimized composition of PBS has been used as the dispersant media. As indicated in **Figure 6.2.C**, with increasing R ratio and decreasing polyanion concentration the particle size drastically increased and absolute intensity decreased. But, the observed intensity of PAN prepared with 0.01mg/mL PAH in optimized PBS was higher than the absolute intensity observed when the same amount of PAH was added in deionized water. This clearly proved that the formation of PAN particles required the presence of phosphate ions as a cross-linker for PAH wherein, the molar ratio of the phosphate ions and amines (PAH) not only determine the tendency to form aggregates spontaneously but also the stability and physical characteristics of the PAN particles. Interestingly, PAN showed increase in zeta-potential value from 0.44±1.16 mV to 25.6±1.27 mV when PAH concentration was increased from 0.01 and 1.0 mg/mL in optimized PBS at same R ratio. (**Figure 6.2.D**) After the formation of blank PAN, effect of dilution was evaluated as indicated in **Figure 6.2.E.** It was observed that dilution of blank PAN particles by increasing the volume of the diluent (dI water) resulted in same particle size with drastically decreased absolute intensity as expected. Interestingly, particles diluted in 1:1 v/v ratio were found equivalent in size to the undiluted PAN particles (except for the decrease in absolute intensity) and hence 1:1 v/v ratio was considered best suited among all the dilution ratios. This indicated that particles remained stable even after dilution and inspite of their metastable nature did not exhibit self-aggregation.

6.3.1.2 PAN_{DTX}

The formation and the %EE of DTX in PAN_{DTX} was found pH dependent (**Figure 6.3.A and 6.3.B).** PAN_{DTX} formed at pH 7.2 showed particle size of 158.3±9.19 nm, zeta-potential of 29.1±1.13 mV (**Figure 6.2.E**) with 77.5% EE. It was also observed that at pH 5.5 and 9.4, PAN_{DTX} exhibited very high particle size with significantly lowered zeta-potential values (**Figure 6.3.A).** This might be attributed to inefficient PAN_{DTX} formation at these two pH values, as also supported by the significant reduction in the derived count rate (KCPS) at these two pH values (**Figure 6.3.B).** The observed pH dependency was further correlated with the %EE of DTX in the presence of different concentrations of NaCl. Previously, it was demonstrated that presence of NaCl facilitated the PAN particle formation (**Fig. 6.2.B**) however, it was also anticipated that increasing NaCl might alter the DTX entrapment efficiency significantly. Experimentally, %EE was found maximum at pH 7.2 and was not significantly affected by NaCl concentration. The minimum %EE was seen at pH 9.4 and this could be attributed to the formation of large sized particles (Fig. 3.A), which were later removed during centrifugation at 5000 rpm. The efficient entrapment of DTX in PAN_{DTX} formed at pH 7.2 was proved by dialyzing PAN_{DTX} into 30 mL of water for 1h to expel out the dissolved but unentrapped DTX. As indicated in **Figure 6.3.D,** DTX unentrapped in the formulation was found to be 5.9±6.0 % and ~18.79±5.3 % before and after dialysis. Further, PAN_{DTX} were found to be spherical but not very compact particles when viewed under FESEM (**Figure 6.3.F)**. 50 such individual particles gave mean size of 163.3± 42.64 nm by FESEM which was in agreement with the size estimated by DLS.

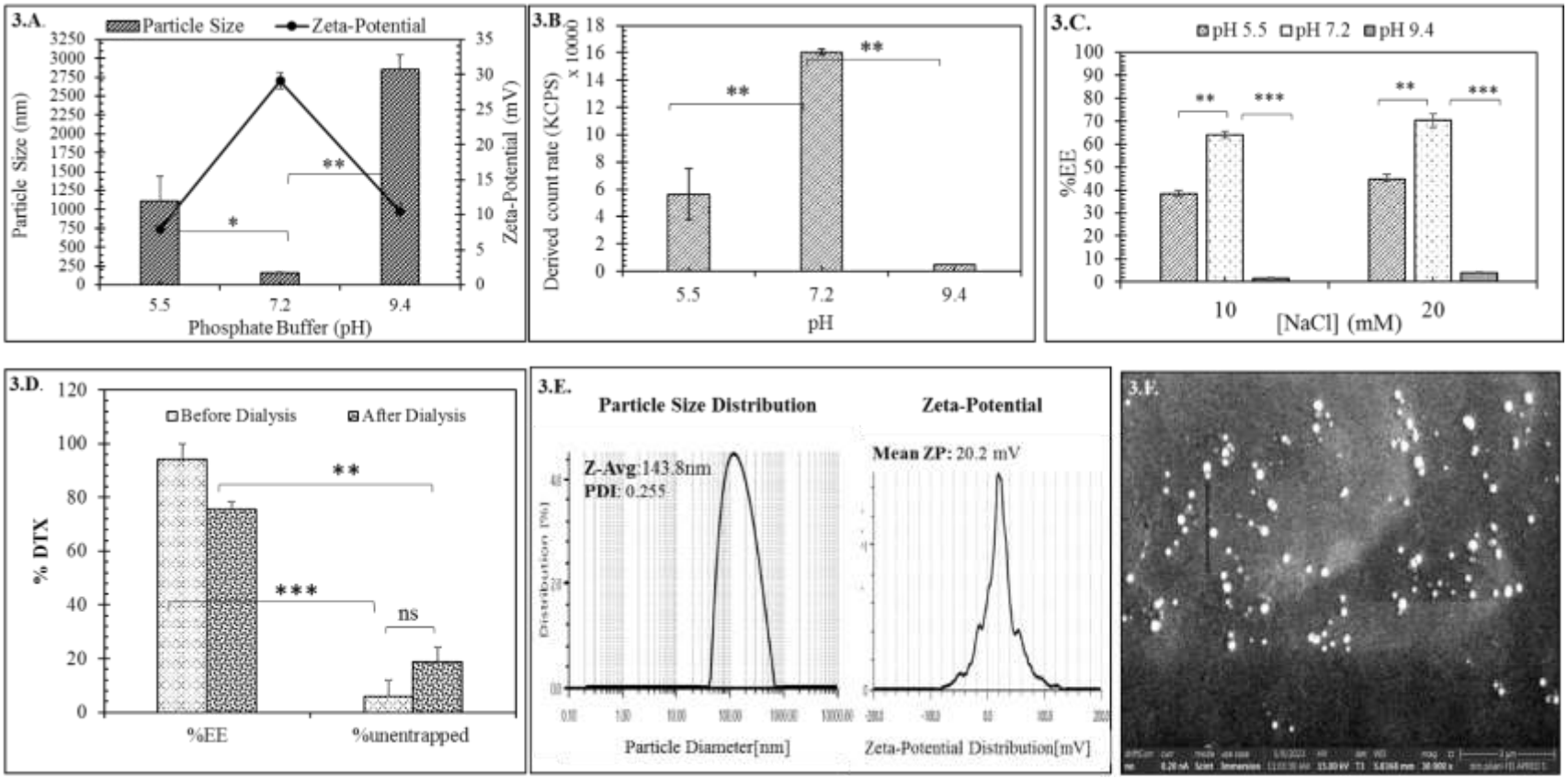

Figure 6.3. Optimization and characterization of PAN_{DTX} formulation**.** Effect of pH (5.5, 7.2, and 9.4) of reaction medium on, (**A**) particle size (nm) and zeta-potential (mV) and, (**B**) derived count rate (KCPS). (**C**) Effect of pH and concentration of NaCl on %EE of DTX, (**D**) DTX quantified in the formulations before and after dialysis, (**E**) representative particle size distribution and zeta-potential graphs and, (**F**) Representative morphology of the PAN_{DTX} using FESEM at magnification 30,000X, scale bar 3µm.

Data are represented as mean(n=3) ± SD, where one-way ANOVA with Tukey's test was used for determination of the statistical significance; *p<0.05, **p<0.01 and ***p<0.001.

6.3.1.3 PAN_{RNA} and $PAN_{DTX+RNA}$

The formation of PAN_{RNA} and $PAN_{RNA+DTX}$ was confirmed by an increase in particle size and decrease in zeta-potential values as compared to the blank PAN (**Figure 6.4.A and 6.4.B).** The successful exosomal layering of $PAN_{DTX+RNA}$ was also confirmed by the zeta potential values wherein, Exo($PAN_{RNA+DTX}$) demonstrated zeta potential of -11.4 mV, which is the characteristic surface charge of the EFs (**Fig. 6.4.B**). It was also observed that increasing amount of RNA (0.1-2 μg) resulted in formation of PAN_{RNA} with varied particle size at constant R ratio wherein, the larger particles were formed with the higher amount of RNA (**Fig. 6.4.C**). Unlike the particle size, the surface potential of PAN_{RNA} was not found dependent on the content of RNA used (**Fig. 6.4.D**). As indicated in **Figure 6.4.E,** $PAN_{RNA+DTX}$ did not exhibit significantly different particle size than the blank PAN but exhibited significantly higher absolute intensity than the blank PAN and PAN_{RNA}. **Figure 6.4.F** proved the complexation of RNA and encapsulation of DTX in the PAN particles as seen by drastic change in the zeta-potential. While, RNA exhibited zeta-potential of -5.54±0.219 mV, upon complexation to form PAN_{RNA} and $PAN_{DTX+RNA,}$ the zeta-potential values increased to 24.35±0.64 mV and 19.25±3.04 mV; clearly proving the efficient encapsulation of DTX and RNA in the PAN particles (26.05±3.6 mV).

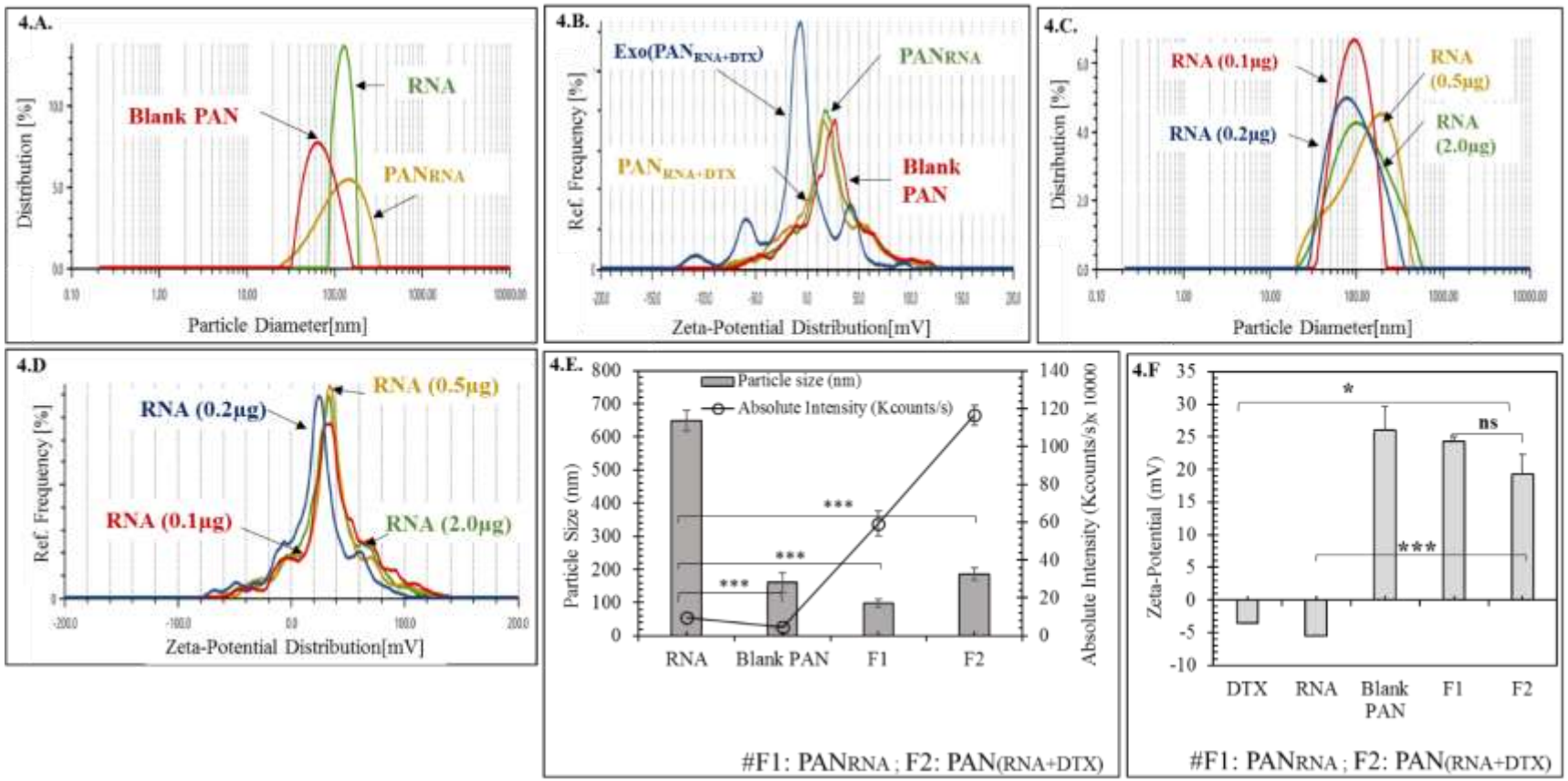

Figure 6.4: Characterization of PAN_{RNA} formulation by particle size and zeta-potential measurement (**A**) Particle size of blank PAN, RNA (2 µg) and PAN_{RNA} at R ratio of 1.214 in modified PBS. (**B**) Zeta-potential of blank PAN, PAN_{RNA}, $PAN_{RNA+DTX}$, and Exo ($PAN_{RNA+DTX}$) indicating efficient formulation development leveraging electrostatic interaction. Effect of varying the content of RNA on (**C**) particle size (nm) and (**D**) zeta-potential (mV) of the PAN_{RNA} at R ratio 1.214 in modified PBS. Representative (**E**) particle size and absolute intensity and, (**F**) zeta-potential (mV) confirming the formation of PAN_{RNA} and $PAN_{RNA+DTX}$. All data are represented as mean (n=3) ± SD, where one-way ANOVA with Tukey's test was used for the determination of the statistical significance, where *p<0.05, **p<0.01 and ***p<0.001.

3.1.4 $PAN_{34a+DTX}$ and $PAN_{FAM+DTX}$

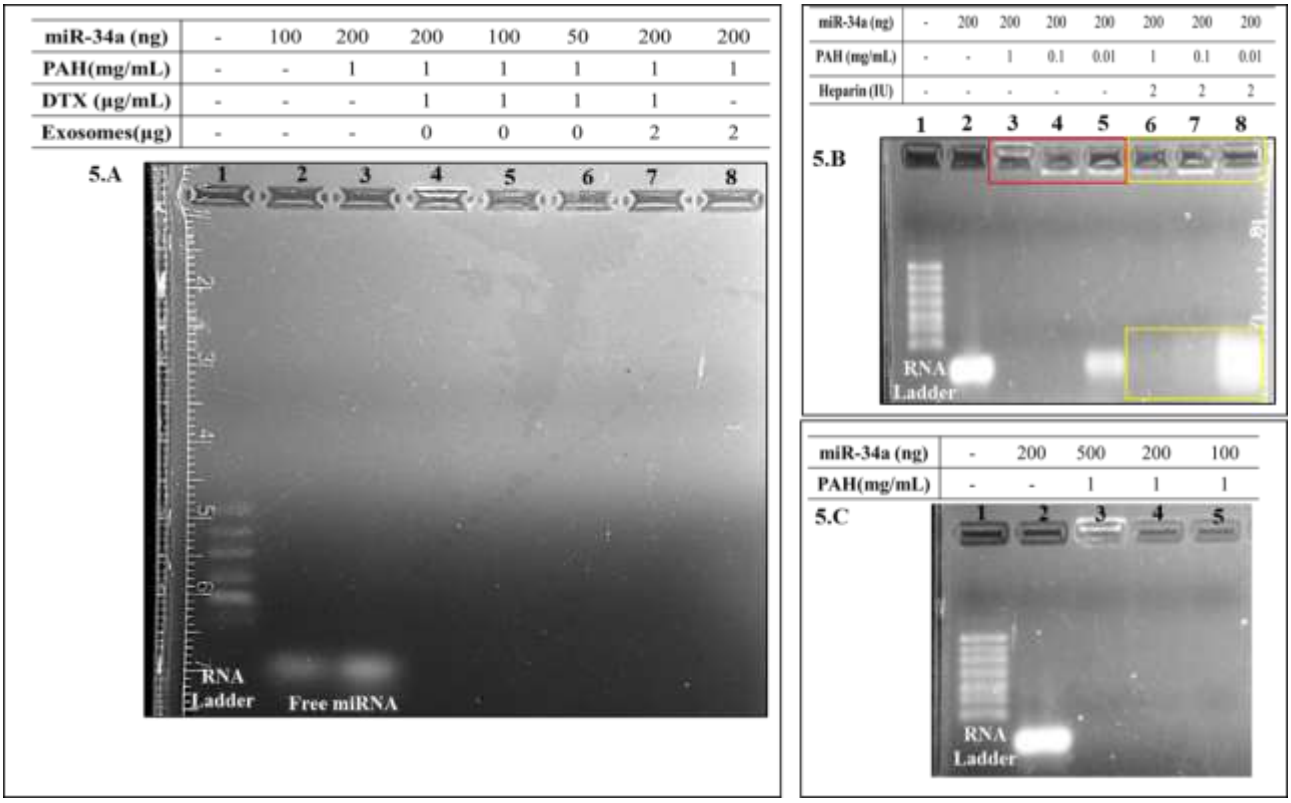

Figure 6.5. Characterization of $PAN_{34a+DTX}$ and Exo ($PAN_{34a+DTX}$). (A) Complexation of miRNA demonstrated by gel retardation assay. (B) Effect of the PAH concentration on miRNA complexation in the absence (lanes 3-5) and presence of heparin (lanes 6-8). (C) Effect of varying the amount of miR-34a (100-500 ng) on the formation of PAN-miR34a at R≈1.2.

After initial optimization of ***PAN_{RNA}***, RNA was replaced by the miRNA of our interest i.e., miR-34a. Using the gel retardation assay (**Fig. 6.5.A**), the complexation efficiency of PAN particles (R≈1.2) with 50-200 ng miR-34a in $PAN_{34a+DTX}$ and Exo($PAN_{34a+DTX}$) was evaluated. All the formulations were found retarded in the well and showed no migration of miRNA unlike free miRNA (100-200 ng) in lane 2 and 3 of **Figure 6.5.A**. Surprisingly, the fluorescence intensity of retarded miR-34a was only visible in the **lane 4** but not in **lane 5-6** which presumably might be attributed to a stronger interaction between miR-34a and the PAN particles (as miRNA amount was decreased from 200 to 50 ng in lanes 4, 5 and 6 respectively) which hindered free access of the miRNA to EtBr mediated intercalation[28]. Further, formulation prepared using higher amount of miRNA (200 ng) was seen clearly retarded in the well (Lane 4) as indicated by the faint fluorescence observed in the well, but was not prominently visible for the formulations prepared with lower amount of miRNA (50 and 100 ng in lane 5 and 6).

However, the heparin treatment clearly indicated that the interaction between miR-34a and PAN particles was strong enough to hinder miRNA release in presence of its competitor polyanion heparin **(Fig 6.5.B)**. Also, it indicated that R ratio (~1.214) of the formulation had an important role in the complexation of miR-34a especially as indicated in lane 3 vs. lane 5. With increasing R ratio (by decreasing the polyanion concentration), the miR-34a complexation was found compromised in **lane 5** (R=121.4) in comparison to **lane 3** (R=1.21). The inference was further confirmed by heparin treatment of the same formulation which resulted in the release of highest amount of miR-34a in lane 8. In **Figure 6.5.C,** it was further confirmed that the R ratio (followed throughout the formulation development) was able to completely complex even higher amount of miR-34a (500 ng) as visualized in **lane 3** as well. Further, miR-34a was replaced with FAM-siRNA to prepare PAN_{FAM} and $PAN_{FAM+DTX}$ which were further used for transfection and uptake assays.

6.3.2 Characterization of the EF

This part of the study has already been incorporated in detail in **Chapter 4, (*section 4.2.2 and Table 4.4).***

6.3.3 Characterization of Exo($PAN_{34a+DTX}$)

Exo(PAN_{34+DTX}) formulations were formed by electrostatic interaction between the positively chargedPAN_{34+DTX} and negatively charged EF. The final formulation was characterized by the particle size, zeta-potential and FESEM for morphology analysis. As indicated in **Figure 6.4.A**, miR-34a was seen retarded in well of the **lane 4** but fluorescence could not be observed in lane 7 and 8 containing Exo(PAN_{34+DTX}) and Exo(PAN_{34}), which is only possible if EtBr could not access the miRNA complexed in the final formulation, as the particles were layered with the exosomal fragments. Later on, the final formulation was characterized for the morphological changes before and after exosomal layering that is; $PAN_{34a+DTX}$ and Exo(PAN_{34+DTX}). Morphologically, $PAN_{34a+DTX}$ were spherical shaped but not very compact particles, whereas the EF showed non-uniform particle size and shape, which together resulted in formation of non-uniform but compact Exo(PAN_{34+DTX}). **Table 6.3** shows that the core/shell strategy resulted in Exo(PAN_{34+DTX}), with zeta potential value of -7.23±2.75mV, which is similar to that of EF i.e., -8.40±1.79 mV, since EF form the shell of the core-shell formulation. In comparison to the positive charge of $PAN_{34a+DTX}$ (17.53±5.10 mV), the negative zeta potential of Exo(PAN_{34+DTX}) indicates the successful layering of EF on $PAN_{34a+DTX}$ formulation. In fact, considering the particle size of different groups (**Table**

6.3, and **Figure 6.6),** it could be concluded that, Exo(PAN_{34+DTX}) are non-spherical, and heterogeneous and possibly enclosed several PAN_{34+DTX} particles resulting in high particle size (393.87±127.89 nm) in comparison to $PAN_{34a+DTX}$ formulation.

As indicated in **Figure 6.7.A**, a seven-day long stability study at 4˚C was performed which indicated slight increase in the particle size of PAN_{DTX} within initial 12 h from 116.5±0.70 nm to 156.5±9.19 nm and then the size remained stable till 144 h. Unlike the particle size, the zeta-potential and the %EE of the PAN_{DTX} remained constant throughout the study.

Figure 6.7.B indicates the most important property of PAN_{DTX}, i.e., pH dependent release of DTX from the formulation. It is seen that free DTX showed 26.05±2.63% and 72.41±2.57% release within 30 min and 4h respectively, thereafter a plateau phase persisted till 24h followed by an insignificant decrease to 63.31±1.70% at 145 h. In comparison to free DTX, PAN_{DTX} at pH 7.4 showed only 10.35±0.39% and 21.79±1.45% of DTX release within 30 min and 4 h respectively. PAN_{DTX} demonstrated overall constant release till the end of the study with a cumulative drug release of 33.55±2.12% within 145 h. With the change in pH from 7.4 to 5.5, an initial burst release was observed within first 4h, wherein 17.75±0.44% and 52.33±0.17% DTX was released within 30 min and 4h respectively and maximum 75.21±1.8% DTX was released within 145 h. This clearly indicated that, PAN_{DTX} would remain intact at physiological pH (pH 7.2) and would only release DTX in endo-lysosomal compartment and acidic tumor microenvironment.

Figure 6.7.C highlights the physiological safety of the formulation upon coming in contact with blood components. This study revealed that, PAN_{DTX} was less hemotoxic than the free DTX wherein, free DTX exhibited 17.69±0.69% and PAN_{DTX} 5.93±1.2% hemolysis in comparison to the positive control (RBCs treated with 0.1% Triton-X-100).

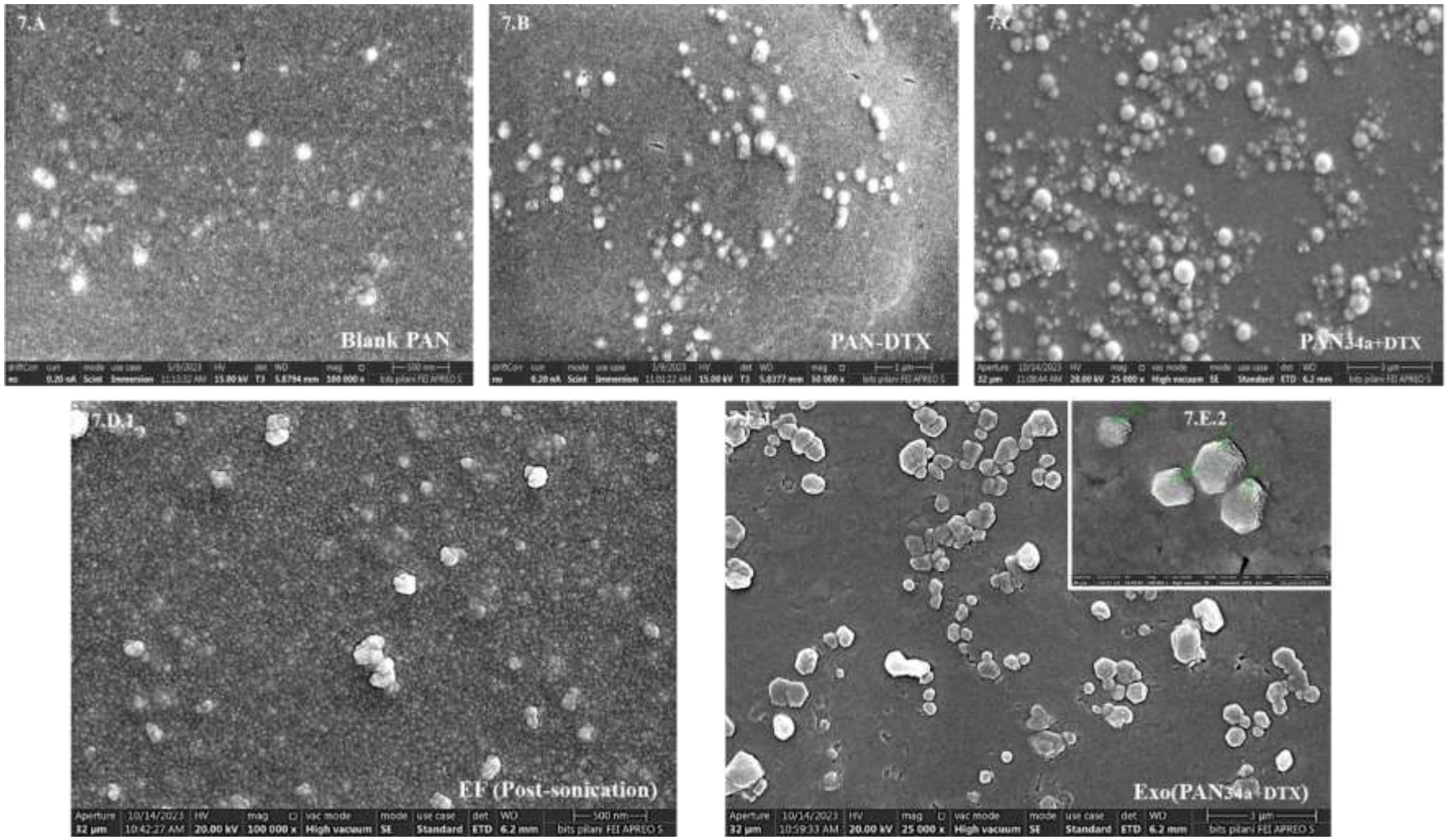

Figure 6.6: Comparative morphological characterization of the formulations by FESEM. (**A**) Blank PAN, (**B**) PAN_{DTX}, (**C**) $PAN_{34a+DTX}$ and (**D**) EF, (**E1**) Exo ($PAN_{34a+DTX}$), scale bar: 3µm. (**Inset E2**) Single particle analysis was carried out at 200,000 X. Scale bar 400 nm for Exo ($PAN_{34a+DTX}$) inset.

Interestingly, PAN_{DTX} (**Figure 6.6.B**) and $PAN_{34a+DTX}$ (**Figure 6.6.C**) were formed as spherical particles with relatively higher compactness than the blank PAN particles (**Figure 6.6.A**). In comparison to the spherical core, EF (**Figure 6.6.D**) demonstrated a non-uniform structure. After the exosomal layering of the core formulation, a characteristic morphological change is clearly evident (**Figure 6.6.E**) when compared to both PAN particles and the EF.

Table 6.3
Comparative particle size, PDI and zeta-potential of $PAN_{34a+DTX}$ and Exo (PAN_{34+DTX}).

Formulation	Blank PAN	$PAN_{34a+DTX}$	EF	Exo(PAN_{34+DTX})
Particle size (nm)	116.73±28.62	163.86±12.89	180.73±127.71	393.87±127.89
Zeta-potential (mV)	24±4.35	17.53±5.10	-8.40±1.79	-7.23±2.75

6.3.4 In vitro functional assays

6.3.4.1 Functional studies for PAN_{DTX}

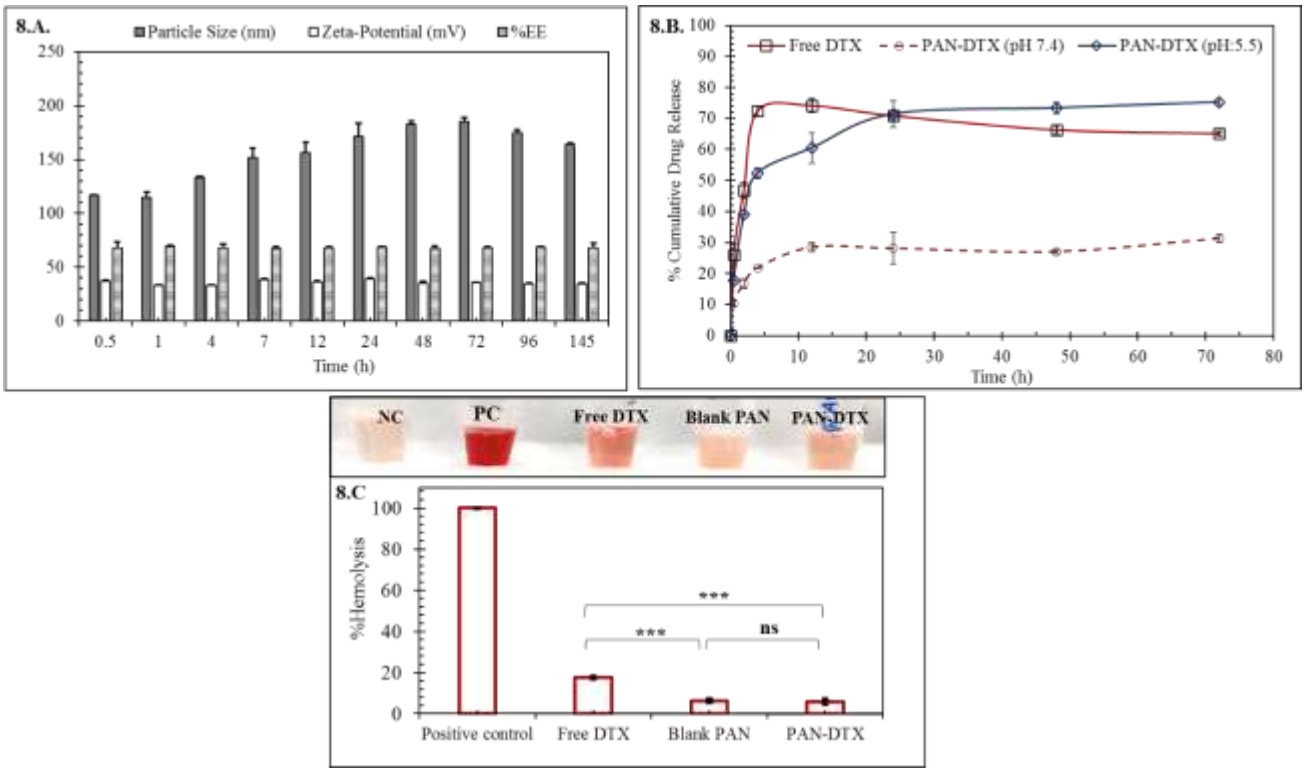

Figure 6.7. In vitro functional studies of PAN_{DTX} formulation. (A) Seven-day long stability study at 4˚C. All data are represented as mean (n=3) ± SD, (B) *in vitro* pH dependent release of DTX at pH=5.5 and 7.4. % Cumulative drug release is expressed as mean (n=3) ± SD, (C) *in vitro* hemocompatibility study wherein, % haemolysis was evaluated for free DTX (100 ng/mL), Blank PAN, PAN_{DTX} (100 ng/mL) and expressed as mean (n=3)± SD, one-way ANOVA with Tukey's test was used for determination of the statistical significance, where *p<0.05, **p<0.01 and ***p<0.001.

6.3.4.2 Functional studies for Exo(PAN_{34+DTX})

6.3.4.2.1 In vitro transfection efficiency and Uptake

In vitro transfection efficiency and uptake of FAM-siRNA using commercially available transfecting agent Lipofectamine 2000® was compared qualitatively with the designed PAN particles (**Figure 6.8.A and 6.8.B).** Greater green fluorescence and superior transfection efficiency of PAN_{FAM} in comparison to the FAM-siRNA/Lipofectamine in 4T1 cells was clearly evident within 6 h post-treatment. Additionally, the PAN_{FAM} caused morphological deformation of 4T1 cells (**Figure 6.8.B)** which might be attributed to the cationic nature of the PAN particles.

The transfection efficiency was further confirmed by uptake study of the formulations, Exo(PAN_{FAM}) and Exo($PAN_{FAM+DTX}$) to closely evaluate the effect of each component of the formulation. Being labeled with CM-DiI (red fluorescence probe) EF formulations, Exo($PAN_{FAM\text{-}siRNA}$) and Exo($PAN_{FAM+DTX}$) exhibited co-localized yellow signal inside the cells after cellular uptake, which provided an additional proof that FAM-siRNA is encapsulated inside the PAN (**Figure 6.8.C and 6.8.D)**. Also, the green fluorescence if not co-localized with the red fluorescence of the exosomes would indicate the release of FAM-siRNA from both the formulations, Exo($PAN_{FAM\text{-}siRNA}$) and Exo($PAN_{FAM+DTX}$). Interestingly, Exo($PAN_{FAM\text{-}siRNA}$) and Exo($PAN_{FAM+DTX}$) treated cells showed lesser fluorescence intensity than the PAN_{FAM}, possibly due to delayed release of the payload caused by layering of the PAN particles with the EF. Further, the EF layering of PAN_{FAM} proved beneficial in maintaining the cellular morphology as evident upon comparison of **Figure 6.8.B** and **6.8.C**. This is attributed to the protection of cells by EF in Exo(PAN_{FAM}) from the cationic nature of the $PAN_{FAM.}$ Lastly, it was also observed that the cells treated with Exo(PAN_{FAM}) showing yellow fluorescence in their cytoplasm were healthier and retained their morphology and nuclear integrity in comparison to the cells treated with Exo($PAN_{FAM+DTX}$) (**Figure 6.8.C vs. Figure 6.8.D)** owing to the anti-tumor effect of DTX present in the formulation. It indicated cytoskeletal deformation and multinucleation in the 4T1 cells (as indicated by red arrow) attributed to the presence of DTX as has already been reported in our previous work[29].

6.3.4.2.2 In vitro cytotoxicity assay

It has already been reported by our group that cells treated for 48 h with DTX exhibited significant cytotoxicity based on the concentration of DTX and the IC_{50} of free DTX was found to be 480.04 ng/ml[29]. Herein, **Figure 6.9.A** indicated that free DTX (100 ng/ml) and free miR-34a (50 nM) exhibited 17.65±3.40% and 17.54±0.84% cytotoxicity in 4T1 cells respectively, 48h post-treatment and 23.76±7.06% cytotoxicity in combination. **Figure 6.9.B,** further confirmed that PAN_{DTX} (40 ng/ml, designated as **A** in the figure), PAN_{34a} (50nM, designated as **C** in the figure) and their respective combination $PAN_{34a+DTX}$ (designated as **E** in the figure) resulted in 31.20±7.21%, 14.36±3.48 % and 8.74±5.93% cytotoxicity respectively, whereas free PAN showed 27.51±2.63% cytotoxicity.

It was also evident that complexation with miR-34a and miR-34a+DTX resulted in reduction of the positive charge of PAN which lowered the cytotoxicity of the formulations as compared to the PAN particles alone. The observed toxicity of PAN_{DTX} was further reduced to 13.76±11.28 % after getting layered with EF wherein, EF itself induced only 6.82±8.08% cell death, which can considered negligible. In comparison to Exo(PAN_{DTX}), superior cytotoxicity was exhibited by Exo (PAN_{34a}) and Exo(PAN_{34a}+DTX) with 25.06±4.78% and 48.20±4.59% after 48h of the treatment.

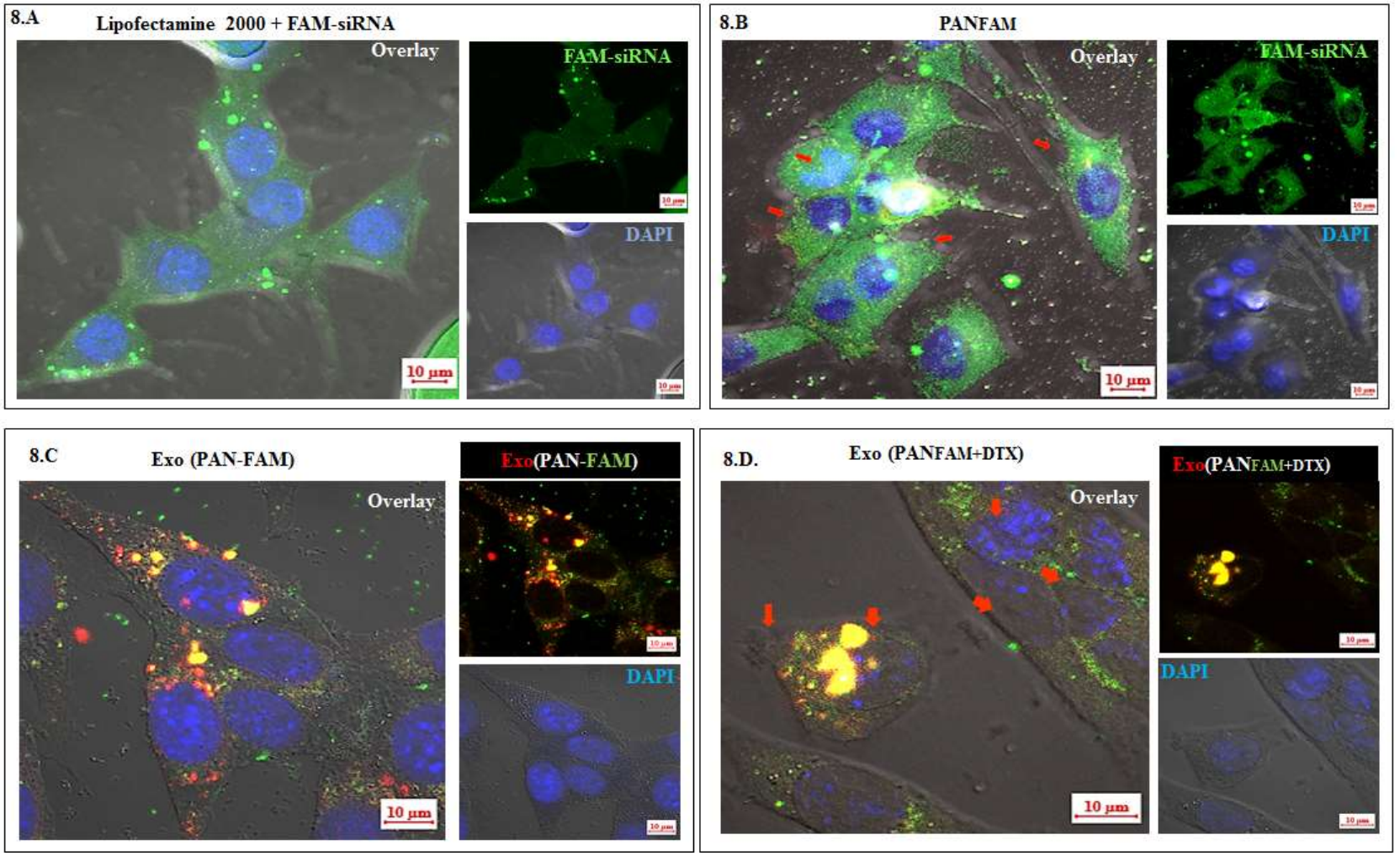

Figure 6.8: In vitro transfection efficiency and uptake of different formulations in 4T1 cells. FAM siRNA transfection mediated by, (**A**) Lipofectamine 2000® (A, as positive control) and, (**B**) PAN particles. (**C**) Representative uptake efficiency of FAM-siRNA by Exo(PAN_{FAM}) wherein, CM-DiI stained exosomes were utilized to prepare EF and used for formulation development. The overlay of red (CM-DiI) and green (FAM siRNA) fluorescence produced yellow fluorescence within the cells indicating successful uptake of the formulation by 4T1 cells. (**D**) The CM-DiI stained Exo($PAN_{FAM+DTX}$) showed both uptake (as indicated by yellow fluorescence) and cytoskeletal deformation (due to DTX) in 4T1 cells. Magnification 630X and scale bar 10µm

6.3.4.2.3 Inflammatory cytokine release study

As indicated in **Figure 6.10.A and B**, 4T1 cells treated with free DTX showed elevated release of inflammatory cytokines, TNF-α and IFN-γ in comparison to the normal cells (without any treatment). Evidently, Blank PAN had non-significant impact on the 4T1 cells but blank EF exhibited immune-stimulant effect which was further highlighted in **Figure 6.10.C and D**. While comparing the effect of the different formulations on the cytokine release, Exo($PAN_{34a+DTX}$) showed prominent impact on 4T1 cells by releasing highest amount of TNF-α and IFN-γ with 1.20±1.83 ng/mL and 11.8±1.84 ng/mL respectively which was significantly higher in comparison to Exo(PAN_{DTX}) and Exo(PAN_{miR34a}). Interestingly, EF demonstrated immune-stimulant effect by increasing the release of both TNF-α and IFN-γ as indicated in **Figure 6.10.C and D** in a concentration dependent manner**.**

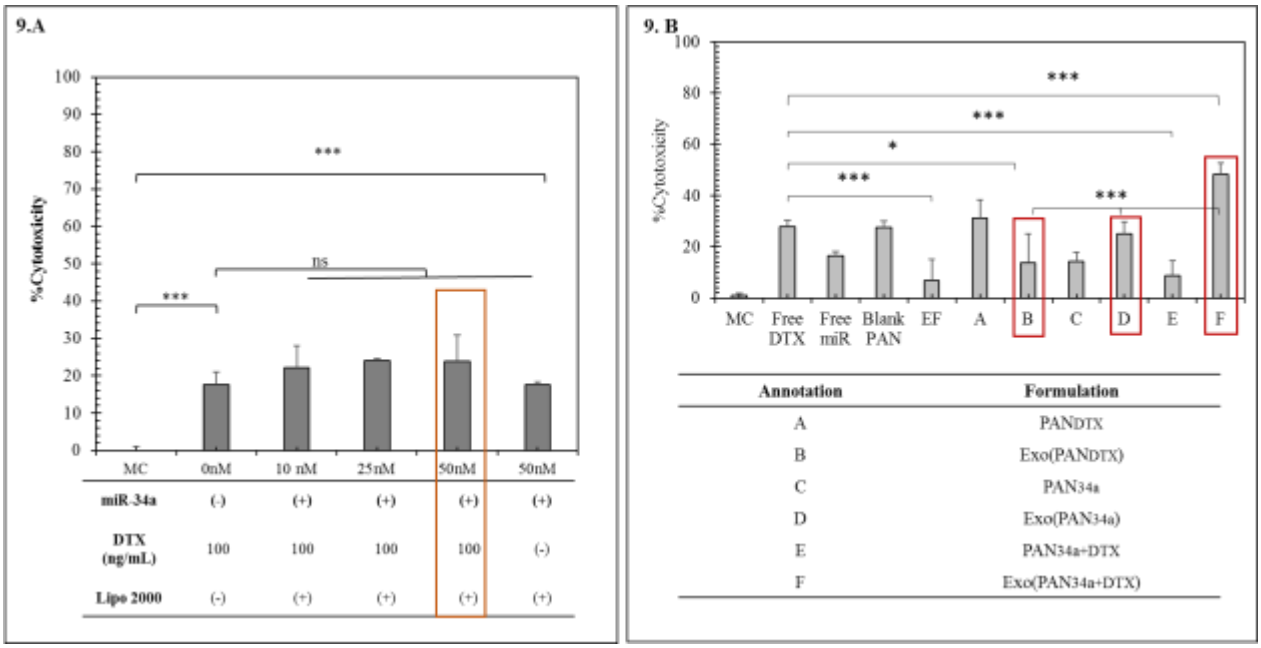

Figure 6.9: Anti-proliferative assay in 4T1 cells after 48 h. (A) Cytotoxic effect of free DTX (100 ng/mL), DTX in combination with miR-34a (10-50 nM), and free miR-34a (50 nM). Herein, the data are represented as mean(n=6) ±SD, (B) The cytotoxic effect of formulations A-F (as annotated) in comparison to the free DTX (40 ng/mL), free miR-34a (50 nM), free PAN, and EF (~12 µg) on 4T1 cells after being treated for 48h. All data represented here is mean(n=6) ±SD. One-way ANOVA with Tukey's test was used for the determination of the statistical significance, where *p<0.05, **p<0.01 and ***p<0.001

Although, elevated release of TNF-α is non-significant in **Figure 6.10.C**, elevation in IFN-γ was found significantly higher than the media control group in 4T1 cells. In comparison to EF1 (6

µg/mL), EF2 with 12µg/mL equivalent protein resulted in 1.31 fold and 1.19 fold elevated TNF-α and IFN-γ release by the cells.

6.3.4.2.4 Gene expression analysis

As indicated in **Figure 6.11**, the overall effect of the formulations on the expression level of BCL-2 was ascertained. **Figure 6.11.A** indicated that free DTX (40 ng/mL) elevated BCL-2 expression level in 4T1 cells, but the expression was decreased after treatment with blank PAN and EF by 1.7 and 6.5 fold respectively. Interestingly, Exo(PAN_{DTX}) reduced the BCL-2 expression by 3.20 fold as compared to free DTX, but did not behave significantly different from that of the blank PAN. Whereas, Exo(PAN-miR34a) and Exo($PAN_{34a+DTX}$) significantly reduced the BCL-2 expression in 4T1 cells in comparison to free DTX. As indicated by **Figure 6.11.B,** EF was also observed to suppress the BCL-2 expression significantly in 4T1 cells in a concentration independent manner.

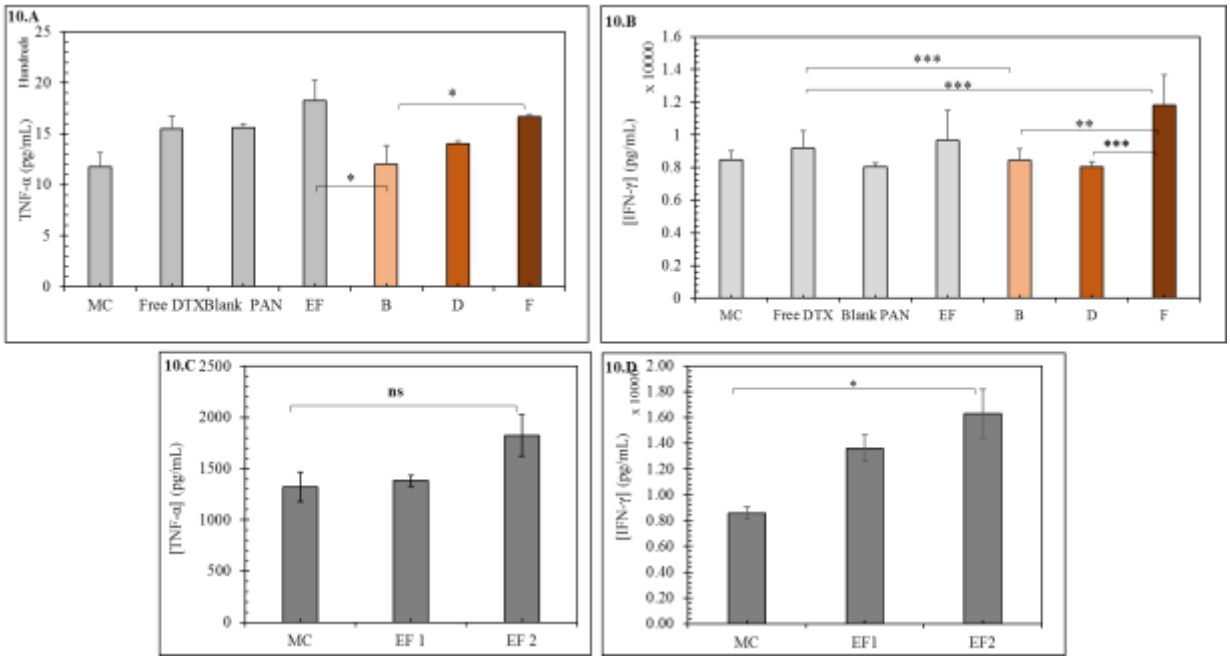

Figure 6.10: Effect of formulations B, D, and F and EF on the inflammatory soluble cytokine release by 4T1 cells, herein, formulation **B**, **D**, and **F** denote Exo(PAN_{DTX}), Exo(PAN-miR34a) and Exo($PAN_{34a+DTX}$) respectively **(A) TNF-α and (B)** IFN-γ in the conditioned media of the cells treated with free DTX (40 ng/mL), blank PAN, EF, and formulations B, D, and F for 48h. The release of (**C**) TNF-α and (D) IFN-γ by EF treatment in a concentration dependent manner in 4T1Effect of EF1(6 µg/mL) and EF2 (12 µg/mL) indicated the biological role of EF in 4T1 cells. All data represented here in (n=6) ±SD, One-way ANOVA with Tukey's test was used for the determination of the statistical significance, where *p<0.05, **p<0.01 and ***p<0.001.

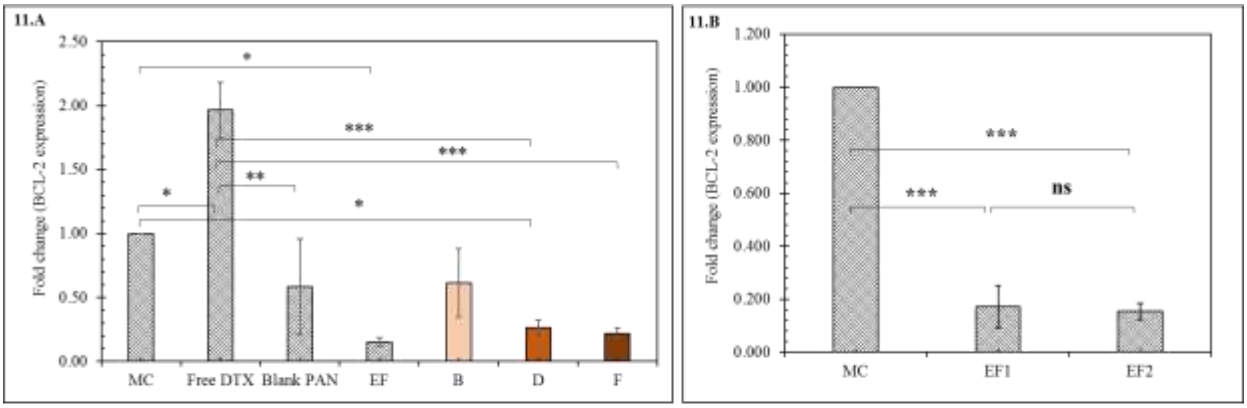

Annotation	Formulation
B	Exo(PAN-DTX)
D	Exo(PAN-miR 34a)
F	Exo(PAN34a+DTX)

Figure 6.11. **qRT-PCR analysis of 4T1 cells for the expression of miR-34a target gene BCL-2**. (A) Effect of different formulations and, (B) effect of EF in a concentration dependent manner wherein, EF1 indicated ~6µg/mL protein, and EF2 indicated ~12µg/mL protein. All data are represented as mean (n=3) ±SD and statistical comparison was performed by applying one-way ANOVA with Tukey multiple comparison test. *** p-value < 0.001, **p<0.01, *p<0.05.

6.4. Discussion

The formation of PSA based core/shell nanoparticles involved assembly of the poly-cationic polymer, poly-allylamine hydrochloride, PAH by ionic crosslinking with multivalent anionic salts (e.g., HPO_4^{-2} and $H_2PO_4^{-1}$) into a metastable template to encapsulate the cargo (herein, DTX and miR-34a) to form the core, and then the shell material (exosomal fragment, EF) was deposited on the core by leveraging the electrostatic interaction between the reverse surface charges of the core and shell material[18]. After initial optimization of the buffer composition (Na_2HPO_4: KH_2PO_4=5:3 with [NaCl]=10mM), PAH concentration, and dilution, PAN particles prepared with a suitable R ratio (~1.21) provided desired size (122.25±0.96 nm) and zeta-potential values (24±4.35mV) with characteristic loosely bound structure which is in alignment with the existing literature[24]. Recently, Doxorubicin (DOX) has been reported to self-associate in water upon increasing its concentration (0.1-100 µM) or concentration of polyanion like polystyrene sulphonate, PSS (0.48-48 mM) and formed complexes wherein, PSS acted as a template for concentrating DOX. In our study, DTX in its supersaturated aqueous solution (log P 2.4, solubility ~12.4 µg/mL) carried slightly negative charge (-3.5±0.176 mV) at physiological pH along with the presence of a hydroxyl group at C-10 which aided its encapsulation by hydrophobic interaction into the polycationic polymeric

backbone of PAH resulting in 77.5 % EE at pH 7.4. The efficient encapsulation of DTX in PAN was confirmed after dialysis of the formulation in water to allow the expulsion of the dissolved unentrapped DTX from the PAN_{DTX} particles (**Figure 6.3.D)**. Further, the functional characterization by in-vitro release study of PAN_{DTX} supported the efficient encapsulation of DTX by showing a pH dependent release at pH 5.5 and at 7.4 (**Figure 6.7.B**). This characteristic release pattern observed at pH 5.5 is attributed to the fact that PAN dissembles at pH<6 and pH>9 to release the entrapped DTX since PAH (pKa 8.8) becomes deprotonated [24,30]. During the formulation development, it was evident that these PAN_{DTX} particles were stable at physiological pH (pH 7.2) since PAN_{DTX} was formed with reproducible %EE and maximum absolute intensity at pH 7.2, both of which decreased at pH 5.5 and almost diminished at pH 9.4 (**Figure 6.3.B and 6.3.C).** Literature supports this observation wherein, Indocyanin green (ICG) with only one negative charge has been reported to be encapsulated in PAH-phosphate PSA with the help of hydrophobic interaction (~29%)[18,21].

PAN has been well reported for efficient delivery of GFP siRNA in stably expressing GFP transfected A549 cells and provided endosomal (pH 6.5-4.5) release of GFP siRNA in the cells resulting in 60-65% inhibition of the GFP fluorescence in GFP-A549 [24]. Based on the available reports, miR-34a was incorporated into PAN_{DTX} with slight modification in the protocol to utilize these PAN particles for co-loading the DTX and miRNA. For initial optimization, we utilized the cellular RNA as the cargo, wherein, we observed a constant surface potential of the PAN_{RNA} as the amount of RNA was varied (**Figure 6.4.C and 6.4.D**). Increase in derived count rate along with decreased zeta-potential upon incorporation of RNA and DTX into the reaction mixture confirmed encapsulation of DTX and complexation of RNA to form $PAN_{(RNA+DTX)}$ (**Figure 6.3.E and 6.3.F)** Further, RNA was replaced with miR-34a and FAM-siRNA to form $PAN_{34a+DTX}$ and $PAN_{FAM+DTX}$ using the optimized method. While literature reports no significant change in particle size after complexation of siRNA with the PAN particles[23]), our result indicated an increase in particle size with 163.86±12.89 nm and 164.85±22.12 nm as compared to blank PAN (124.8±30.61 nm) in $PAN_{34a+DTX}$ and $PAN_{FAM+DTX}$ respectively[24]. The efficient complexation of 0.5 µg miR-34a (~3.6 µM) in $PAN_{34a+DTX}$ was evident as indicated in **Figure 6.5.C** at the optimized R ratio. This amount of miR-34a was used for all the further experiments for characterization and functional evaluation mentioned in this work. Also, the strong interaction between the miR-34a and PAH could be estimated by the observation made in the gel retardation assay in presence of

the heparin (**Figure 6.5.B).** At R~1.21 and ~0.2 µg miR-34 (1.45 µM), the complexation in PAN-miR 34a was found strong enough to resist the release the miRNA even after heparin treatment. Interestingly, PAN-miR 34a, prepared with compromised R~121.4, resulted in inefficient complexation of miRNA (uncomplexed miRNA seen in lane 5; **Figure 6.5.B),** which further released the most of the miRNA upon heparin treatment (lane 8 in the same gel; **Figure 6.5.B)**. This clearly indicated the efficiency of the PAN particles forming the core of the system that was designed to co-deliver both small molecule drug, DTX and miRNA. Once the core of the formulation was optimized, the preparation and characterization of the shell was undertaken.

As the shell, the RAW 264.7 cell derived EF were prepared and characterized for particle size, zeta-potential and morphology. Exosomal extrusion and sonication methods for preparing EF are well reported in literature along with reports of an enhanced particle size of EF in one of the studies (351 ± 58.33 nm with high PDI 0.29±0.01) which could be correlated well with our observation as well[31]. The single particle analysis by FESEM (n=100) indicated heterogeneous size distribution of the EF with an average diameter of 180.73±127.71 nm and DLS analysis of the same indicated 0.26±0.06 PDI and -11.3 mV zeta-potential. The prepared Exo($PAN_{34a+DTX}$), formulation demonstrated surface-potential equivalent to the EF, i.e., -7.23±2.75 mV, which is in line with the previous reports[31–34]. The change in the surface potential was in accordance with the reported literature but the particle size observed significantly differed from reported studies with the observed high particle size in FESEM and polydispersity by DLS. The final core/shell formulation, Exo($PAN_{34a+DTX}$) was significantly different from EF as well as $PAN_{34a+DTX}$ as indicated by **Figure 6.6**. The distinct change in morphology and compactness of formulation in comparison to blank PAN and EF as observed in FESEM is similar to that reported for ICG containing nanoparticle assembled capsule (NAC) further layered with the SiO_2 nanoparticles [19].

Once the final formulation was optimized, the Exo($PAN_{34a+DTX}$) was further evaluated for transfection efficiency and uptake in 4T1 cells. Both Exo($PAN_{FAM+DTX}$) and Exo (PAN_{FAM}) were prepared and investigated in the studies. The co-localization study exhibited yellow fluorescence in the cells owing to the localization of CM-DiI (red) labeled EF and FAM-siRNA (green), confirming their being present in the same formulation. A similar co-localization study has been reported for the encapsulation of GFP-siRNA in the Rhodamine green labeled PAN particles[24] and DiI (red) labeled exosome enclosed PLGA nanoparticles wherein, PLGA has been stained with

DiO (green)[35]. Additionally, the observation was further supported by reduced green fluorescence in Exo($PAN_{FAM-siRNA}$) and Exo($PAN_{FAM+DTX}$) treated cells than the PAN_{FAM}, possibly due to delayed release of the payload caused by the layering of the PAN_{FAM} particles with the EF (**Fig. 6.8)**. The efficiency of the formulations was further evaluated by *in vitro* anti-proliferative assay and anti-inflammatory cytokine release. Exo($PAN_{34a+DTX}$) containing 40 ng/mL DTX and 50 nM miR-34a was able to produce ~2.4 folds' greater cytotoxicity than the combination of DTX (100 ng/mL) and miR-34a (50 nM) with Lipofectamine 2000®) (**Figure 6.9.A** and **6.9.B)** in 4T1 cells. Exo($PAN_{34a+DTX}$) also proved to enhance the inflammation in cells as indicated by the released TNF-α and IFN-γ in the media in comparison to the normal cells in media, although the difference was not significant in case of TNF-α. TNF-α is an inflammatory cytokine and is expected to be increased by immune stimulation, but the functional duality of TNF-α only could be confirmed by the receptors present in the vicinity[36–38]. DTX has been reported to initially enhance the TNF-α release from breast cancer cells in a time-dependent manner but reduces the TNF-α release in a concentration dependent manner within 48h[39]. On the contrary, IFN-γ release was profoundly significant in case of Exo($PAN_{34a+DTX}$) in comparison to the Exo(PAN_{DTX}), Exo (PAN-miR 34a) and free DTX which indicated the efficiency of the formulation towards immune stimulation which could trigger the T-cell responses (TCR) to mediate the cancer cell cytotoxicity. The possibility could be hypothesized but can be only confirmed with more detailed studies. The final formulation evidently was able to produce anti-cancer effect and the novel approach utilized here successfully overcame the limitation of cytotoxicity triggered by the cationic nature of the PAN formulations by layering them with EF owing to their distinct immune-stimulant nature and high uptake efficiency. Comparing **Figure 6.9.B** and **6.10.A**, it can be concluded that the Exo($PAN_{34a+DTX}$) showed superior cytotoxic and immune-stimulant effect than the Exo(PAN_{DTX}) and Exo (PAN-miR 34a) formulations. Additionally, the observed suppression of BCL-2 expression by Exo(PAN-miR34a) and Exo($PAN_{34a+DTX}$) could be correlated with the individual effect of the DTX and miR34a, as reported in the literature[40–42]. While, DTX has shown to regulate BAX/BCL-2 ratio instead only suppressing the BCL-2 expression in a dose and time-dependent manner, miR-34a is well reported to downregulate the BCL-2 translation in cancer as well as neurodegenerative diseases[9,43–45]. In fact, a cationic BSA (CBSA) coated nanocarrier of miR-34a and DTX has already been reported to deliver the payload in cytosol in a caveolae mediated pathway which was able to suppress the BCL-2 expression in both *in vitro* and *in vivo* TNBC model[46]. miR-34a

mediated BCL-2 suppression aided in the chemo-sensitivity of DTX, which was also observed in our case. As indicated in **Figure 6.11.A,** the BCL-2 expression in Exo(PAN-miR34a) and Exo($PAN_{34a+DTX}$) showed significant downregulation in comparison to both Exo(PAN_{DTX}) and free DTX. In addition to their role in release of TNF-α and IFN-γ (**Fig. 6.10.B and C**), the prominent effect of the EF in BCL-2 downregulation (**Fig. 6.11.B**) is also evident, but the detailed mechanism is yet to be investigated. Hence, exosomal membrane enclosed PAN particles could be utilized to co-deliver both the small molecule and macromolecule.

6.5 References

(1) Nurgali, K.; Jagoe, R. T.; Abalo, R. Editorial: Adverse Effects of Cancer Chemotherapy: Anything New to Improve Tolerance and Reduce Sequelae? *Front. Pharmacol.* **2018**, *9* (MAR), 1–3. https://doi.org/10.3389/fphar.2018.00245.

(2) Mokhtari, R. B.; Homayouni, T. S.; Baluch, N.; Morgatskaya, E.; Kumar, S.; Das, B.; Yeger, H. COMBINATION THERAPY IN COMBATING CANCER. *Oncotarget* **2017**, *8* (23), 38022–38043.

(3) O'Brien, J.; Hayder, H.; Zayed, Y.; Peng, C. Overview of MicroRNA Biogenesis, Mechanisms of Actions, and Circulation. *Front. Endocrinol. (Lausanne).* **2018**, *9* (AUG), 1–12. https://doi.org/10.3389/fendo.2018.00402.

(4) Dai, X.; Tan, C. Combination of MicroRNA Therapeutics with Small-Molecule Anticancer Drugs: Mechanism of Action and Co-Delivery Nanocarriers. *Adv. Drug Deliv. Rev.* **2015**, *81*, 184–197. https://doi.org/10.1016/j.addr.2014.09.010.

(5) Bravo-Vázquez, L. A.; Méndez-García, A.; Rodríguez, A. L.; Sahare, P.; Pathak, S.; Banerjee, A.; Duttaroy, A. K.; Paul, S. Applications of Nanotechnologies for MiRNA-Based Cancer Therapeutics: Current Advances and Future Perspectives. *Front. Bioeng. Biotechnol.* **2023**, *11* (July). https://doi.org/10.3389/fbioe.2023.1208547.

(6) Bouchie, A. First MicroRNA Mimic Enters Clinic. *Nat. Biotechnol.* **2013**, *31* (7), 577. https://doi.org/10.1038/nbt0713-577.

(7) He, L.; He, X.; Lowe, S. W.; Hannon, G. J. MicroRNAs Join the P53 Network — Another Piece in the Tumour- Suppression Puzzle Lin. *Nat. Rev. Cancer* **2007**, *7* (November), 1–4.

(8) Ji, Q.; Hao, X.; Zhang, M.; Tang, W.; Meng, Y.; Li, L.; Xiang, D.; DeSano, J. T.; Bommer, G. T.; Fan, D.; Fearon, E. R.; Lawrence, T. S.; Xu, L. MicroRNA MiR-34 Inhibits Human Pancreatic Cancer Tumor-Initiating Cells. *PLoS One* **2009**, *4* (8). https://doi.org/10.1371/journal.pone.0006816.

(9) Kastl, L.; Brown, I.; Schofield, A. C. MiRNA-34a Is Associated with Docetaxel Resistance in Human Breast Cancer Cells. *Breast Cancer Res. Treat.* **2012**, *131* (2), 445–454. https://doi.org/10.1007/s10549-011-1424-3.

(10) Raemdonck, K.; Vandenbroucke, R. E.; Demeester, J.; Sanders, N. N.; De Smedt, S. C. Maintaining the Silence: Reflections on Long-Term RNAi. *Drug Discov. Today* **2008**, *13* (21–22), 917–931. https://doi.org/10.1016/j.drudis.2008.06.008.

(11) Loinger, A.; Shemla, Y.; Simon, I.; Margalit, H.; Biham, O. Competition between Small RNAs: A Quantitative View. *Biophys. J.* **2012**, *102* (8), 1712–1721. https://doi.org/10.1016/j.bpj.2012.01.058.

(12) van Dongen, S.; Abreu-Goodger, C.; Enright, A. J. Detecting MicroRNA Binding and SiRNA Off-Target Effects from Expression Data. *Nat. Methods* **2008**, *5* (12), 1023–1025. https://doi.org/10.1038/nmeth.1267.

(13) Gray, G. D.; Basu, S.; Wickstrom, E. Transformed and Immortalized Cellular Uptake of Oligodeoxynucleoside Phosphorothioates, 3'-Alkylamino Oligodeoxynudeotides, 2'-O-Methyl Oligoribonucleotides, Oligodeoxynucleoside Methylphosphonates, and Peptide Nucleic Acids. *Biochem. Pharmacol.* **1997**, *53* (10), 1465–1476. https://doi.org/10.1016/S0006-2952(97)82440-9.

(14) Cun, D.; Jensen, D. K.; Maltesen, M. J.; Bunker, M.; Whiteside, P.; Scurr, D.; Foged, C.; Nielsen, H. M. High Loading Efficiency and Sustained Release of SiRNA Encapsulated in PLGA Nanoparticles: Quality by Design Optimization and Characterization. *Eur. J. Pharm. Biopharm.* **2011**, *77* (1), 26–35. https://doi.org/10.1016/j.ejpb.2010.11.008.

(15) Sharma, S.; Pukale, S.; Sahel, D. K.; Singh, P.; Mittal, A.; Chitkara, D. Folate Targeted Hybrid Lipo-Polymeric Nanoplexes Containing Docetaxel and MiRNA-34a for Breast Cancer Treatment. *Mater. Sci. Eng. C* **2021**, *128* (July), 112305. https://doi.org/10.1016/j.msec.2021.112305.

(16) Zhang, L.; Yang, X.; Lv, Y.; Xin, X.; Qin, C.; Han, X.; Yang, L.; He, W.; Yin, L. Cytosolic Co-

Delivery of MiRNA-34a and Docetaxel with Core-Shell Nanocarriers via Caveolae-Mediated Pathway for the Treatment of Metastatic Breast Cancer. *Sci. Rep.* **2017**, *7* (March), 1–16. https://doi.org/10.1038/srep46186.

(17) Han, J.; Wang, Q.; Zhang, Z.; Gong, T.; Sun, X. Cationic Bovine Serum Albumin Based Self-Assembled Nanoparticles as SiRNA Delivery Vector for Treating Lung Metastatic Cancer. *Small* **2014**, *10* (3), 524–535. https://doi.org/10.1002/smll.201301992.

(18) Bagaria, H. G.; Wong, M. S. Polyamine-Salt Aggregate Assembly of Capsules as Responsive Drug Delivery Vehicles. *J. Mater. Chem.* **2011**, *21* (26), 9454–9466. https://doi.org/10.1039/c1jm10712g.

(19) Yu, J.; Yaseen, M. A.; Anvari, B.; Wong, M. S.; Chemical, D.; Engineering, B.; V, R. U.; September, R. V; Re, V.; Recei, M.; December, V. Synthesis of Near-Infrared-Absorbing Nanoparticle-Assembled Capsules. **2007**, No. 8, 1476–1483.

(20) Murthy, V. S.; Wong, M. S. Enzyme Encapsulation Using Nanoparticle-Assembled Capsules. *ACS Symp. Ser.* **2008**, *986*, 214–232. https://doi.org/10.1021/bk-2008-0986.ch013.

(21) Yu, J.; Javier, D.; Yaseen, M. A.; Nitin, N.; Richards-Kortum, R.; Anvari, B.; Wong, M. S. Self-Assembly Synthesis, Tumor Cell Targeting, and Photothermal Capabilities of Antibody-Coated Indocyanine Green Nanocapsules. *J. Am. Chem. Soc.* **2010**, *132* (6), 1929–1938. https://doi.org/10.1021/ja908139y.

(22) Su, J.; Sun, H.; Meng, Q.; Yin, Q.; Zhang, P.; Zhang, Z.; Yu, H.; Li, Y. Bioinspired Nanoparticles with NIR-Controlled Drug Release for Synergetic Chemophotothermal Therapy of Metastatic Breast Cancer. *Adv. Funct. Mater.* **2016**, *26* (41), 7495–7506. https://doi.org/10.1002/adfm.201603381.

(23) Di Silvio, D.; Martínez-Moro, M.; Salvador, C.; de los Angeles Ramirez, M.; Caceres-Velez, P. R.; Ortore, M. G.; Dupin, D.; Andreozzi, P.; Moya, S. E. Self-Assembly of Poly(Allylamine)/SiRNA Nanoparticles, Their Intracellular Fate and SiRNA Delivery. *J. Colloid Interface Sci.* **2019**, *557*, 757–766. https://doi.org/10.1016/j.jcis.2019.09.082.

(24) Andreozzi, P.; Diamanti, E.; Py-Daniel, K. R.; Cáceres-Vélez, P. R.; Martinelli, C.; Politakos, N.; Escobar, A.; Muzi-Falconi, M.; Azevedo, R.; Moya, S. E. Exploring the PH Sensitivity of Poly(Allylamine) Phosphate Supramolecular Nanocarriers for Intracellular SiRNA Delivery. *ACS Appl. Mater. Interfaces* **2017**, *9* (44), 38242–38254. https://doi.org/10.1021/acsami.7b11132.

(25) Aranda, E.; Teruel, J. A.; Ortiz, A.; Pérez-Cárceles, M. D.; Aranda, F. J. Interaction of Docetaxel with Phosphatidylcholine Membranes: A Combined Experimental and Computational Study. *J. Membr. Biol.* **2022**, *255* (2–3), 277–291. https://doi.org/10.1007/s00232-022-00219-z.

(26) Singha, K.; Namgung, R.; Kim, W. J. Polymers in Small-Interfering RNA Delivery. *Nucleic Acid Ther.* **2011**, *21* (3), 133–147. https://doi.org/10.1089/nat.2011.0293.

(27) Di, D.; Martínez-moro, M.; Salvador, C.; Angeles, M. D. L.; Caceres-velez, P. R.; Grazia, M.; Dupin, D.; Andreozzi, P.; Moya, S. E. Journal of Colloid and Interface Science Self-Assembly of Poly (Allylamine)/ SiRNA Nanoparticles , Their Intracellular Fate and SiRNA Delivery. **2019**, *557*, 757–766. https://doi.org/10.1016/j.jcis.2019.09.082.

(28) Yasar, H.; Biehl, A.; De Rossi, C.; Koch, M.; Murgia, X.; Loretz, B.; Lehr, C. M. Kinetics of MRNA Delivery and Protein Translation in Dendritic Cells Using Lipid-Coated PLGA Nanoparticles. *J. Nanobiotechnology* **2018**, *16* (1), 1–19. https://doi.org/10.1186/s12951-018-0401-y.

(29) Basak, M.; Sahoo, B.; Kumar, D.; Narisepalli, S.; Tiwari, S.; Chitkara, D.; Mittal, A. Human Umbilical Cord Blood-Mesenchymal Stem Cell Derived Exosomes as an Efficient Nanocarrier for Docetaxel and MiR-125a : Formulation Optimization and Anti-Metastatic Behaviour. *Life Sci.* **2023**, *322* (January), 121621. https://doi.org/10.1016/j.lfs.2023.121621.

(30) Cuenca, V. E.; Martinelli, H.; Ramirez, M. D. L. A.; Ritacco, H. A.; Andreozzi, P.; Moya, S. E. Polyphosphate Poly(Amine) Nanoparticles: Self-Assembly, Thermodynamics, and Stability Studies. *Langmuir* **2019**, *35* (44), 14300–14309. https://doi.org/10.1021/acs.langmuir.9b02636.

(31) Zhao, L.; Gu, C.; Gan, Y.; Shao, L.; Chen, H.; Zhu, H. Exosome-Mediated SiRNA Delivery to Suppress Postoperative Breast Cancer Metastasis. *J. Control. Release* **2020**, *318* (May 2019), 1–15. https://doi.org/10.1016/j.jconrel.2019.12.005.

(32) Dehaini, D.; Wei, X.; Fang, R. H.; Masson, S.; Angsantikul, P.; Luk, B. T.; Zhang, Y.; Ying, M.; Jiang, Y.; Kroll, A. V.; Gao, W.; Zhang, L. Erythrocyte–Platelet Hybrid Membrane Coating for Enhanced Nanoparticle Functionalization. *Adv. Mater.* **2017**, *29* (16), 1–8. https://doi.org/10.1002/adma.201606209.

(33) Hu, C. M. J.; Zhang, L.; Aryal, S.; Cheung, C.; Fang, R. H.; Zhang, L. Erythrocyte Membrane-Camouflaged Polymeric Nanoparticles as a Biomimetic Delivery Platform. *Proc. Natl. Acad. Sci. U. S. A.* **2011**, *108* (27), 10980–10985. https://doi.org/10.1073/pnas.1106634108.

(34) Han, Z.; Lv, W.; Li, Y.; Chang, J.; Zhang, W.; Liu, C.; Sun, J. Improving Tumor Targeting of Exosomal Membrane-Coated Polymeric Nanoparticles by Conjugation with Aptamers. *ACS Appl. Bio Mater.* **2020**, *3* (5), 2666–2673. https://doi.org/10.1021/acsabm.0c00181.

(35) Li, S.; Wu, Y.; Ding, F.; Yang, J.; Li, J.; Gao, X.; Zhang, C.; Feng, J. Engineering Macrophage-Derived Exosomes for Targeted Chemotherapy of Triple-Negative Breast Cancer. *Nanoscale* **2020**, *12* (19), 10854–10862. https://doi.org/10.1039/d0nr00523a.

(36) Sprowl, J. A.; Reed, K.; Armstrong, S. R.; Lanner, C.; Guo, B.; Kalatskaya, I.; Stein, L.; Hembruff, S. L.; Tam, A.; Parissenti, A. M. Alterations in Tumor Necrosis Factor Signaling Pathways Are Associated with Cytotoxicity and Resistance to Taxanes : A Study in Isogenic Resistant Tumor Cells. *Breast Cancer Res.* **2012**, *14* (1), R2. https://doi.org/10.1186/bcr3083.

(37) Wang, L.; Chiou, J.; Lee, Y.; Chang, L. Docetaxel-Triggered SIDT2 / NOX4 / JNK / HuR Signaling Axis Is Associated with TNF- α -Mediated Apoptosis of Cancer Cells. *Biochem. Pharmacol.* **2022**, *195* (November 2021), 114865. https://doi.org/10.1016/j.bcp.2021.114865.

(38) Slabáková, E.; Culig, Z.; Remšík, J.; Souček, K. Alternative Mechanisms of MIR-34a Regulation in Cancer. *Cell Death Dis.* **2017**, *8* (10), 1–10. https://doi.org/10.1038/cddis.2017.495.

(39) Edwardson, D. W.; Boudreau, J.; Mapletoft, J.; Lanner, C.; Kovala, A. T.; Parissenti, A. M. *Inflammatory Cytokine Production in Tumor Cells upon Chemotherapy Drug Exposure or upon Selection for Drug Resistance*; 2017.

(40) Sharma, S.; Pukale, S.; Sahel, D. K.; Singh, P.; Mittal, A.; Chitkara, D. Folate Targeted Hybrid Lipo-Polymeric Nanoplexes Containing Docetaxel and MiRNA-34a for Breast Cancer Treatment. *Mater. Sci. Eng. C* **2021**, *128* (March), 112305. https://doi.org/10.1016/j.msec.2021.112305.

(41) Li, L.; Yuan, L.; Luo, J. MiR-34a Inhibits Proliferation and Migration of Breast Cancer through down-Regulation of Bcl-2 and SIRT1. **2013**, 109–117. https://doi.org/10.1007/s10238-012-0186-5.

(42) Sun, X.; Xu, H.; Huang, T.; Zhang, C.; Wu, J.; Luo, S. Simultaneous Delivery of Anti-MiRNA and Docetaxel with Supramolecular Self-Assembled " Chitosome " for Improving Chemosensitivity of Triple Negative Breast Cancer Cells. **2021**, *21*, 192–204.

(43) Su, C. C.; Lin, J. W.; Chang, K. Y.; Wu, C. T.; Liu, S. H.; Chang, K. C.; Liu, J. M.; Lee, K. I.; Fang, K. M.; Chen, Y. W. Involvement of AMPKα and MAPK-ERK/-JNK Signals in Docetaxel-Induced Human Tongue Squamous Cell Carcinoma Cell Apoptosis. *Int. J. Mol. Sci.* **2022**, *23* (22), 1–17. https://doi.org/10.3390/ijms232213857.

(44) Yuan, Z.; Jiang, H.; Zhu, X.; Liu, X.; Li, J. Ginsenoside Rg3 Promotes Cytotoxicity of Paclitaxel through Inhibiting NF-KB Signaling and Regulating Bax/Bcl-2 Expression on Triple-Negative Breast Cancer. *Biomed. Pharmacother.* **2017**, *89*, 227–232. https://doi.org/10.1016/j.biopha.2017.02.038.

(45) Wang, X.; Liu, P.; Zhu, H.; Xu, Y.; Ma, C.; Dai, X.; Huang, L.; Liu, Y.; Zhang, L.; Qin, C. MiR-34a, a MicroRNA up-Regulated in a Double Transgenic Mouse Model of Alzheimer's Disease, Inhibits Bcl2 Translation. *Brain Res. Bull.* **2009**, *80* (4–5), 268–273. https://doi.org/10.1016/j.brainresbull.2009.08.006.

(46) Zhang, L.; Yang, X.; Lv, Y.; Xin, X.; Qin, C.; Han, X.; Yang, L. Cytosolic Co-Delivery of MiRNA-34a and Docetaxel with Core-Shell Nanocarriers via Caveolae-Mediated Pathway for the Treatment of Metastatic Breast Cancer. *Nat. Publ. Gr.* **2017**, No. March, 1–16. https://doi.org/10.1038/srep46186.

XXXXXXX

Chapter VII

Conclusions & Future Perspectives

7.1 Conclusion

The thesis work entitled, "**Cell derived exosomes as the co-delivery nanocarrier for anticancer small molecule and tumor suppressor miRNA**" focused upon 2 major aspects of exosomal delivery- (i) development of strategic approach for co-loading miRNA and DTX in the exosomal formulations to obtain an optimum LC and evaluation of their anti-cancer efficacy in TNBC 4T1 cells and, (ii) to understand the role of the intrinsic biological nature of the exosomes in the efficacy of exosomal anti-cancer formulations *in vitro*.

Hence, we primarily emphasized on the comparative characterization of various Exo-DTX formulations to highlight the role of the optimised DTX encapsulation process on exosomal integrity while formulating Exo-DTX from exosomes isolated from two different sources cells using two different strategies (**Table 7.1)**. While, hUCBMSC and miR-125a exosomes were isolated from untransfected and miR-125a transfected hUCBMSC derived exosomes, RAW Exo-DTX was developed using RAW 264.7 cell derived exosomes using the same mild sonication method as reported for hUCBMSC derived exosomes. In case of Exo($PAN_{34a+DTX}$), PAN particles were developed to co-load DTX and miR-34a exogenously and the RAW 264.7 cell derived exosomal fragments (EF) were utilized to layer the particles to form an outer shell. As indicated in **Table 7.1,** there was no significant change in particle size (nm) and zeta-potential (mV) before and after the Exo-DTX formulation development among the different exosomal formulations but they significantly differed from each other in terms of capacity.

RAW Exo-DTX exhibited maximum DTX encapsulation capacity (23.60±1.54 ng DTX/ μg exosomes) which was 1.5 folds and 2.6 folds greater than the hUCBMSC Exo-DTX and miR-125a Exo-DTX formulations. This also indicated the limited DTX loading capacity of the exosomes. On the other hand, EF layering of the $PAN_{34a+DTX}$ resulted in final Exo($PAN_{34a+DTX}$) formulation (as mentioned in ***Chapter 6, section 6.3.1***) improved the theoretical DTX loading capacity to 33.34±2.82 ng DTX/ μg exosomes with ~77.5% DTX encapsulation capacity in PAN particles. Interestingly, miR-125a Exo-DTX was able to retain 12.31±5.73% miRNA after DTX loading by mild sonication method. Consequently, elimination of sonication step in Exo($PAN_{34a+DTX}$) development resulted in efficient complexation of 3.6 μM miR-34a in the $PAN_{34a+DTX}$, prior the EF layering.

With inclusion of exosomes from 2 different sources, a detailed understanding of the biological role of exosomes was also developed (**Figure 7.1**) which further guided us to further improvise our formulation development strategies.

Table 7.1
Comparative characterization of different exosomal formulations of DTX fabricated in this thesis work.

S.No.	Exo-DTX	Before loading/ EF layering			After Loading/ EF layering			Capacity (ng DTX/ µg exosomes)
		Particle Size (nm)	Zeta-potential (mV)	PDI	Particle Size (nm)	Zeta-potential (mV)	PDI	
1	hUCBMSC Exo	187.57±4.55	-10.62±4.05	0.36	217.6±16.88	-9.61±1.07	0.28	14.96±1.84
2	miR-125a hUCBMSC Exo	183.64 ±0.33	-6.65±1.90	0.26	232.5±12.9	-3.6±1.97	0.27	8.86±1.97
3	RAW Exo	208.7±36.19	-10.27±3.66	0.24	183.11±33.93	-11.03±3.1	0.25	23.60±1.54
4	Exo($PAN_{34a+DTX}$)	163.86±12.89	17.53±5.10	NA	393.87±127.89	-7.23±2.75	NA	33.34±2.82

As indicated by **Figure 7.1.A,** hUCBMSC derived exosomes demonstrated a concentration dependent cell proliferative activity which was suppressed upon miR-125a transfection. On the contrary, RAW 264.7 cell derived exosomes were anti-proliferative in nature and induced 12.32±1.32% cytotoxicity in 4T1 cells. Additionally, RAW Exo-DTX elicited 2.20 and 1.29 folds' greater cytotoxicity in cells in comparison to hUCBMSC Exo-DTX and miR-125a Exo-DTX respectively at a dose of 100 ng/ml (**Fig. 7.1.B**). Evidently, the nature of the exosomes plays an important role in overall cytotoxic effect of Exo-DTX formulations. While, miR-125a transfection lowered IC_{50} value of miR-125a Exo-DTX by 3 folds' than the hUCBMSC Exo-DTX; RAW Exo-DTX achieved the IC_{50} at 89.77 ng/ml which was further 3.4 and 2.15 folds' lesser than hUCBMSC Exo-DTX and miR-125a Exo-DTX respectively. Contrary to the proliferative nature of hUCBMSC exosomes, RAW exosomes demonstrated anti-proliferative and anti-migratory activity in 4T1 cells in a dose dependent manner as inferred by the increased CC3/C3 level with decreased expression of β1-integrin (***Chapter 5, Figure 5.10***).

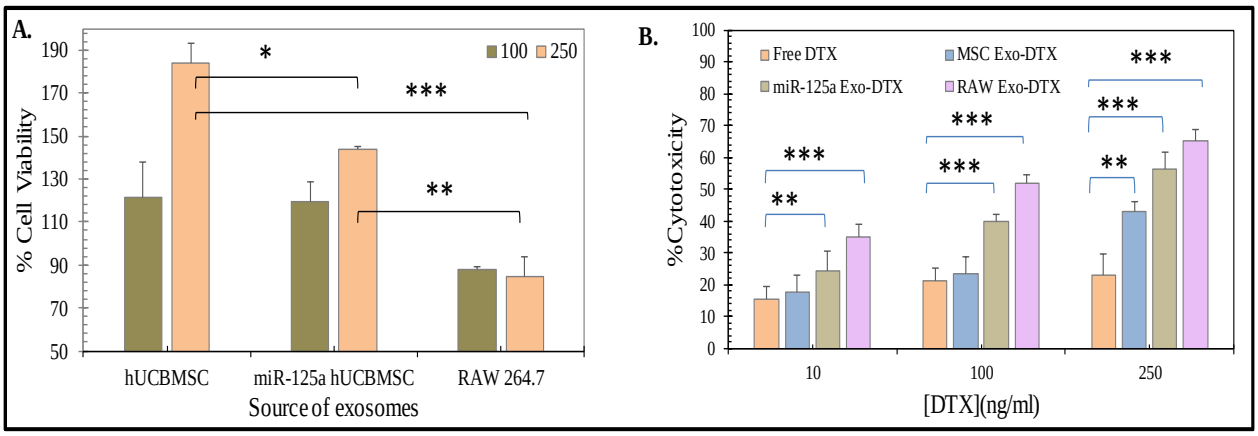

Figure 7.1. Effect of the source of exosomes on the cell viability of 4T1 cells. (**A**) The effect of hUCBMSC, miR-125a transfected hUCBMSC, and RAW 264.7 cell derived exosomes indicated by % cell viability (the amount of exosomes used here were equivalent to that required to load 100 and 250 ng/mL DTX to account for the different loading capacities of the exosomes from different sources). (**B**) Concentration dependent cytotoxic effect of different Exo-DTX formulations was compared to free DTX. All data is represented here as mean (n=6) ±SD. One-way ANOVA with Tukey's test was used for the determination of the statistical significance, where *p<0.05, **p<0.01 and ***p<0.001.

The biological role of exosomes derived from RAW 264.7 was also exhibited by the EF; MTT assay confirmed that RAW exosomes (~5 µg/mL protein) and EF (~12 µg/mL protein) exhibited 12.36±1.62% and 6.92±8.08% respectively. The release of immune-stimulant cytokines (TNF-α and IFN-γ) with suppressed expression of BCL-2 by EF in 4T1 cells also proved its anti-proliferative activity.

Next, we utilized the functionally active RAW EF to develop Exo($PAN_{34a+DTX}$), exosomal membrane enclosed miR-34a and DTX co-loaded PAN particles. While comparing the RAW Exo-DTX with Exo($PAN_{34a+DTX}$), the former killed ~48% of the cell population at a concentration of 100 ng/mL and the latter demonstrated the same effect at 40 ng/mL. The superior *in vitro* efficacy of the Exo($PAN_{34a+DTX}$) might be attributed to the additional incorporation of miR-34a and the ability of the PAN particles to release the payload by proton-sponge effect in a pH dependent manner. In fact, the Exo($PAN_{34a+DTX}$) formulation exhibited greater cytotoxicity in 4T1 cells in comparison to Exo(PAN-DTX) and Exo (PAN-miR 34a); 48.20±4.59% *vs.* 13.76±11.28 % and 25.06±4.78%, indicating the synergistic effect of the miR-34a and DTX. The synergistic anticancer effect was also observed in case of miR-125a Exo-DTX wherein, miR-125a exosomes were found cell proliferative but miR-125a Exo-DTX produced 56.5±1.76% cell death at 250 ng/mL. This indicated that DTX encapsulation in the both hUCBMSC and RAW exosomes proved beneficial in producing the desired anticancer effect wherein, their biological make-up plays an

important role in dictating efficacy of the different Exo-DTX formulations. The shift in formulation strategy from directly using exosomes to exosomal layering in the co-loaded polymeric nanoformulation revealed the beneficial effect of the RAW EF with its characteristic anti-proliferative activity and easy uptake of the $PAN_{34a+DTX}$ wherein, PAN released its payload in the pH dependent manner as supported by literature as well.

Thus in this work, we investigated the application of the exosomes and the exosomal fragments (EF) in a systematic manner with their characteristic functionality for the development of the co-loaded formulation of DTX and TS miRNA and proved its efficacy in TNBC cells.

7.2 Future Perspective

Like other biologicals, exosomes need more aggressive approach and newer strategies to explore its possibilities as a nanocarrier of the therapeutics. Exosomal research spans across different aspects, including 'exosomes as biomarker', 'exosomes in drug delivery, 'exosomes in targeted delivery', 'exosomes and their omics' and many more, however, the knowledge emerging from each of these sectors need to be unified to propel the success in this field and enable clinical translation.

1. Two strategies were applied to develop and evaluate the DTX and miRNA co-loaded formulations i.e, miR-125a Exo-DTX and Exo($PAN_{34a+DTX}$), which were characterized and evaluated individually for their anticancer effect in 4T1 cells. A direct comparison of both the formulations by *in vitro* and *in vivo* experiments would yield deeper insights into their anticancer potential.
2. *In vivo* biodistribution and efficacy study was not feasible owing to the limited yield of RAW exosomes (~172.03±28.9 µg protein per 200 mL CM), limited availability of the miR-125a hUCBMSC derived exosomes and limited LC of the exosomes (23.60±1.54 ng DTX/ µg exosomes). Hence, techniques for large scale production of exosomes need to be devised to conduct *in vivo* studies and establish the *in vitro* and *in vivo* correlation (IVIVC).
3. Chemical modification of the Polyallylamine hydrochloride (PAH) using some hydrophobic moiety would impart the required amphiphilicity to the polymer which would help to form self-assembled compact particles and might aid more efficient drug encapsulation and miRNA complexation.

4. In case of the Exo($PAN_{34a+DTX}$), the miRNA and DTX formed a complex together in presence of the phosphate driven polyamine which encapsulated the miRNA. miRNA encapsulation is more beneficial than complexation, hence a detailed study could be undertaken to elucidate the exact mechanism of the miRNA loading into the formulation.
5. The inclusion of the homing strategy with the EF by click chemistry or layer by layer (L-b-L) or by hydrogel technique would be beneficial to target the formulation to the desired site of action.
6. Macrophages can be polarized to either M1 and M2 type by chemical induction, the use of M1 type exosomes and EF from these M1 exosomes to prepare Exo-DTX and Exo($PAN_{34a+DTX}$) might yield potent drug delivery vehicles bearing additional immunotherapeutic attributes.

XXXXXXX

.

Achievements & Biography

APPENDIX

A1.1 List of Publications

From Thesis

1.**Basak M**, Narisepalli S, Salunkhe S, Tiwari S, Chitkara D, Mittal A. Macrophage derived Exosomal Docetaxel (Exo-DTX) for Pro-metastasis suppression: QbD driven formulation development, validation, in vitro and pharmacokinetic investigation, Eur. J. Pharm. Biopharm. 195 (2024) 114175.

2. **Basak M**, Sahoo B, Chaudhary DK, Narisepalli S, Tiwari S, Chitkara D, Mittal A. Human umbilical cord blood-mesenchymal stem cell derived exosomes as an efficient nanocarrier for Docetaxel and miR-125a: Formulation optimization and anti-metastatic behaviour. Life Sci. 2023, 30, 322, 121621.

3. **Basak M**, Chaudhary DK, Takahashi RU, Yamamoto Y, Tiwari S, Tahara H, Mittal A. Immunocyte Derived Exosomes: Insight into the Potential Chemo-immunotherapeutic Nanocarrier Targeting the Tumor Microenvironment. ACS Biomater Sci Eng. 2023, 9, 9(1), 20-39.

4. **Basak M**, Kulkarni M, Narisepalli S, Chitkara D, Mittal A. Exploring exosomal membrane enclosed Polyamine-salt nano-complex for co-delivery of Docetaxel and miR-34a: Formulation development and anti-cancer evaluation in 4T1. (*Communicated*)

Allied

1. Salunkhe S, Dheeraj, **Basak M**, Chitkara D, Mittal A. Surface functionalization of exosomes for target-specific delivery and in vivo imaging & tracking: Strategies and significance. J Control Release. 2020 10, 326, 599-614.

2. Italiya KS, **Basak M**, Mazumdar S, Sahel DK, Shrivastava R, Chitkara D, Mittal A. Scalable Self-Assembling Micellar System for Enhanced Oral Bioavailability and Efficacy of Lisofylline for Treatment of Type-I Diabetes. Mol Pharm. 2019, 16, 12, 4954-4967.

A.1.2 Achievements

A.1.2.1 Conferences

1.Poster presentation on "**hUCBMSCs derived exosomes as nanocarriers of mir-125a and docetaxel inhibit metastasis causing cell apoptosis**" in 3rd National Biomedical Research Compeition (NBRCOM 2021) arranged by Society of Young Bio-medical Scientists (SYBS); 6th-10th December, 2021.

2.Poster presentation on "**Systematic Development and In-Vitro Evaluation of Docetaxel Loaded RAW 264.7 Derived Exosomes for Anti-Migratory Effect in Breast Cancer**" in Advances in Technology and Business Potential of New Drug Delivery Systems arranged by CRS India Chapter; 24th -26th February, 2022.

3.Abstract Selection for poster presentation on "**New Edge" Anti-cancer Therapy of Macrophage derived Exosomal Docetaxel (Exo-DTX): Formulation Development, Validation and Evaluation**" in Select Science® Biopharma Summit; 5th Sept 2023.

4. Abstract selection for poster presentation on "**Origin of Exosomes is equally vital as their exogenous payloads": An in-vitro Case study on Exosomal Docetaxel**" at AAEV,2023; 27th-28th October 2023.

A.1.2.2 Awards

1. Received ***DST INSPIRE Fellowship (2019-2024)*** for pursuing PhD from Department of Science &Technology (DST), India.

2. Received '***ICMR-Financial Support***' for attending '8th Nano Today Conference, San Diego, California' (*Not claimed*)

A.2. Biographies

A.2.1. Biography of Prof. Anupama Mittal

BIOGRAPHICAL SKETCH

ANUPAMA MITTAL, Ph.D.
Associate Professor, Department of Pharmacy,
Birla Institute of Technology and Science (BITS), Pilani, Vidya Vihar Campus, 333031
Rajasthan, INDIA

Professional Experience

Positions held	Duration	Institute
Associate Professor	June 2021-till date	BITS-Pilani, Pilani, Rajasthan
Assistant professor	2014-May 2021	BITS-Pilani, Pilani, Rajasthan
Visiting Research Scholar	Oct 2012- May 2013	University of Tennessee Health Science Center (UTHSC), Memphis, TN, USA
Post-Doctoral Research Associate	May 2013- June 2014	University of Nebraska Medical Center (UNMC), Omaha, NE, USA

Education

Degree	Institute	Field	Year
B.PHARMACY	Delhi Institute of Pharmaceutical Sciences & Research, Delhi University	Pharmacy	2001-2005
M. S.(Pharm)	National Institute of Pharmaceutical Sciences and Research (NIPER), SAS Nagar, Punjab.	Pharmaceutics	2005-2007
Ph.D.	NIPER, S.A.S. Nagar	Pharmaceutical Sciences	2007-2012

Personal Statement

Prof. Anupama Mittal currently working as an Associate Professor in Department of Pharmacy, BITS, Pilani, Pilani campus is an established researcher and scientist in the field of Nanomedicine. She has been involved actively in teaching (on campus as well as industry professionals from various pharmaceutical industries) and independent research since nearly last 10 years. Her research interests and expertise primarily focus upon generating nanotechnology based solutions for diseases like cancer and diabetes. Her lab has been engaged in research activities in the areas of polymer/fatty acid drug conjugates for effective treatment of cancer & diabetes, stem cells and exosomes as biogenic carriers of miRNA & proteins in cancer, nanoparticles & polymeric micelles for site-specific drug delivery, and growth factor and peptide based therapeutics for wound healing and diabetes. She has published more than 60 research and review articles in peer reviewed international journals and edited 01 book (CRC press), and filed 10 Indian/PCT patent applications among which 04 have been successfully granted. She has been the recipient of prestigious Young scientist award-2015 (SERB-DST) and Ranbaxy Science Scholar award-2011 (Ranbaxy Science Foundation) in Pharmaceutical Sciences. She has also received several awards for best papers presented at National/International conferences. Her lab is generously funded by several extramural research grants from SERB-DST, DST-Rajasthan, DST-Nanomission, ICMR and DBT. She has guided 2 PhD students, several M. Pharm and B. Pharm students and is currently supervising 07 Ph.D. students. She also serves as one of the founding directors of start-up company, Nanobrid Innovations Pvt. Ltd. aimed towards the translation of nanotechnology based products.

A.2.2. Biography of Moumita Basak

Ms. Moumita Basak has completed his Bachelor of Pharmacy from Gurunanak Institute of Pharmaceutical Science and Technology (GNIPST, Kolkata) in the year of 2015 and M. Pharm in Pharmacology from GNIPST in 2017 with University Gold medal. Initially, she joined BITS Pilani as the JRF in DST Nanomission project (SR/NM/NB-1025/2016) and then joined the Department of Pharmacy at BITS Pilani, Pilani campus in Sept 2018 for pursuing Ph.D. She has received DST INSPIRE fellowship for pursuing doctoral study from 2019-2024. Her areas of interests include exploring the formulation aspects of the cell derived exosomes as the co-delivery nanocarrier system for small anticancer drug molecule and miRNA. She has published 7 research/review articles in renowned international journals, her research work got recognized by international conferences and participated in various National conferences.

XXXXXXX